Experimental and Numerical Evaluation of Flow Beneath Mini Disc Infiltrometer for Estimating Wetting Characteristics of Soils

Thesis submitted in partial fulfilment of the requirements

for the award of the degree of

Doctor of Philosophy

in

Civil Engineering

by

Aparimita Priyadarshini Naik

[Roll No. 166104016]

under the supervision of

Dr. Sreeja Pekkat

Department of Civil Engineering

Indian Institute of Technology Guwahati

Guwahati – 781039, Assam, India

February, 2023

Dedicated To

My Father & Mother

Declaration

I do hereby declare that the matter embodied in this thesis is the result of investigations carried out by me in the Department of Civil Engineering, Indian Institute of Technology Guwahati, Assam, India. In keeping with the general practice of reporting scientific observations, due acknowledgements have been made wherever the work described is based on the findings of other investigators. The work presented here is free from plagiarism to the best of my knowledge, and I take the responsibility for any issues. I also affirm that my thesis supervisor is not responsible for any possible instance of plagiarism within this submitted work.

Aparimita Priyadarshini Naik

[166104016]

Date: 20th February, 2023

Place: IIT Guwahati

Indian Institute of Technology Guwahati
Department of Civil Engineering,
Guwahati, Assam 781039

Certificate

This is to certify that this thesis entitled "**Experimental and Numerical Evaluation of Flow Beneath Mini Disc Infiltrometer for Estimating Wetting Characteristics of Soils**" submitted by **Aparimita Priyadarshini Naik**, in partial fulfilment of the requirements for the award of the degree of Doctor of Philosophy, to the Indian Institute of Technology Guwahati, Assam, India, is a record of the bonafide research work carried out by her under my guidance and supervision at the Department of Civil Engineering, Indian Institute of Technology Guwahati, Assam, India. To the best of my knowledge, no part of the work reported in this thesis has been presented for the award of any degree at any other institution.

Date: 20th February, 2023

Place: IIT Guwahati

Dr. Sreeja Pekkat
Associate Professor
Department of Civil Engineering
IIT Guwahati
Assam, India-781039
Email: sreeja@iitg.ac.in

Acknowledgements

The completion of this thesis would not have been possible without the participation and assistance of so many individuals whose names cannot all be listed. I am indebted to everyone who helped me directly or indirectly in completing my research work and making this Ph.D. journey possible.

I express my first and foremost gratitude to my supervisor, Dr. Sreeja Pekkat, for her diligent supervision, insightful suggestions, and persistent commitment and perseverance throughout the research work. I am deeply indebted to her for her advice and assistance in keeping my progress on schedule. Her kindness and interest in originality have inspired and fostered my intellectual abilities, which will serve me for a long time to come. I feel privileged to have received the opportunity to work under her and benefit from her research competence, academic knowledge, and wisdom of life. I express my utmost reverence to my Doctoral Committee's chair, Prof. Arup K. Sarma, and members, Prof. Rajib K. Bhattacharjya and Dr. Ravi K., for their insightful comments, constant support, and prompt assistance during the course of my research and thesis compilation. I would also like to express my sincere gratitude to Prof. Sreedeep S., Civil Engineering Department, IIT Guwahati, for his valuable suggestions and timely assistance.

I am obliged to my seniors, Dr. Biplab Ghosh, Dr. Anjaneyulu Akkimi., Dr. Vinay Chembolu, and Dr. B. G. Rajeev Gandhi for all the motivation, direction, and advices they have provided, throughout this journey of mine. Their timely assistance and positive attitude have helped me overcome many challenges during this journey. I am glad to have worked with Gangadhar, Shabeeb, and Tsering, my M. Tech juniors, who have not only assisted me in carrying out the experiments but also instilled in me a sense of teamwork. Discussing ideas with them and getting their invaluable feedback have always helped to accelerate my research progress. I also thank my Ph.D juniors, Priya and Abdul, for always being supportive and creating a welcoming environment at workplace. Further, I owe my thanks to Ms. Jonali, the scientific officer, Civil Engineering Department, IITG, for assisting me with the instruments. I also extend my thanks to other staffs, Mr. Bazal, Mr. Susanta, Mrs Juri, Mr. Soroj, Mr. Priyananda, Mr. Tapan, and Mr. Tinku for their timely support and help.

It will be incomplete without expressing my heartfelt thanks to my dearest friends and colleagues, Amrutha, Chandan, Sushree, and Geetanjali, without whom it is difficult to envisage this journey. My utmost gratitude to them for being there at the time of my need, for providing me all the moral and emotional support, motivation, and unconditional care. My special thanks to my close friends Jyoti, Venu, Shivani, Mrunalini, and Ketan for their friendly affection and care. I also express my deepest appreciations for my dear friends, Dr. Ashutosh S. and Dr. Suvin P. V., for their motivation and concern.

Finally, it goes without saying that this journey would not have been possible without the unwavering support, unconditional love, financial assistance, and heartfelt encouragement of my parents, my sister, and my brother. They have never questioned my motives and have supported me wholeheartedly in all my endeavours. I thank them deep heartedly for their moral support, motivation, and inspiration throughout my journey.

Aparimita Priyadarshini Naik

******

Abstract

Infiltration, or the entry of water at the soil surface, and re-distribution of infiltrated water within the sub-surface, are generally complex processes to comprehend. Characterizing infiltration measurements is essential for developing soil management strategies to lower the risk of ground water pollution, for various flow and solute modelling processes to prevent contaminant transport in the vadose zone, as well as for various flood and drought management studies. Moreover, the knowledge of infiltration is essential for water balance estimation, watershed modelling, estimating plant water availability in the root zone of soil, and controlled irrigation.

Over the last few decades, the disc infiltrometers have become a popular choice for characterizing wetting hydraulic characteristics of soils, namely the near-surface near-saturated soil hydraulic conductivity (K_0) and sorptivity (S_0), the wetting water retention characteristics curves (WWRCC), and the soil hydraulic conductivity functions (SHCF). In this context, the miniature version of disc infiltrometer, known as mini disc infiltrometer (MDI) appears to be a potential option owing to its small size, compact design, and easy operation process. These features make MDI particularly suitable for laboratory scale studies using soil column setups while also allowing multiple replications of its measurements. However, not many studies have critically evaluated the potential of MDI for characterizing the above properties using laboratory measurements. This study presents a comprehensive analysis for evaluating MDI measurements to determine wetting soil hydraulic characteristics employing both laboratory and field measurements and using various soil textures.

The MDI test results obtained for a silty clay loam soil texture by applying various suctions were evaluated using three different transient methods to determine parameters, K_0 and S_0. A comparison among the results revealed existence of evaluation method related bias on the estimated parameters. The results also demonstrated that the influence of tension head on the estimated parameters were not significant. The investigation carried out using controlled laboratory measurements for the same soil, to verify the influence of initial soil conditions on the estimated parameters from MDI, showed that the initial water content was the most influential parameter compared to the tension head and dry density of soil.

This study has also performed systematic assessments for investigating the time dependence on the transient analysis of MDI measurements for accurate quantification of

parameters K_0 and S_0. Measurements carried on six different soil textures in the field and laboratory were analysed using two linearization methods (cumulative linearization and differentiated linearization) and time fractionation approach to identify the adequate measurement duration for MDI tests. Based on this investigation, the adequate MDI measurement durations were suggested for the six soil textures. Further, this study has evaluated the saturated hydraulic conductivity estimates from MDI with the measurements from other established devices like rainfall simulator and permeameter for gaining more confidence in MDI measurements.

Additionally, soil column setups in laboratory instrumented with sensor measurements were employed to conduct MDI infiltration tests for three different soil textures. The results were then analysed using existing methods as well as inverse modelling technique to evaluate the SHCF measurements. Similar investigation for WWRCC measurements were also carried using MDI measurements for two fine textured soils. Using various input parameters recorded during MDI infiltration tests and by varying the initial conditions, extensive numerical analysis was carried out to propose the optimized van Genuchten retention parameters α and n for the two soil textures, loam and silt loam.

This study has conducted an extensive evaluation to contribute to the knowledge of soil hydraulic characterization from MDI and its use as an ideal infiltrometer for both laboratory and field applications. The investigations conducted and the findings reported in this study can be highlighted as follows. It examined the time-dependence and proposed appropriate measurement durations for accurate soil hydraulic characterization using MDI. It established that the impact of imposed tension head on estimated soil hydraulic parameters from MDI measurements were negligible. It demonstrated MDI's application to determine saturated hydraulic conductivity by employing numerical inversion technique. In addition, with the help of independent measurements and inverse modelling, it demonstrated the utility of MDI for rapidly and effectively characterizing the soil hydraulic properties (WWRCC and SHCF) in a non-intrusive and non-invasive way, and also with adequate repetitions. However, further evaluations by including broader range of soil types need to be conducted for generalizing the findings and popularizing the MDI technique.

Keywords: *Infiltration*, *Mini disc infiltrometer*, *Hydraulic conductivity*, *Transient analysis*, *Inverse modelling*, *Parameter estimation*, *Wetting water retention characteristics*, *Soil hydraulic conductivity function*

Table of Contents

List of Figures

List of Tables

List of Symbols

Symbol	Description
A_1	Dimensionless coefficient
A_2	Dimensionless coefficient
b	Constant
C_1	Fitting coefficient in two-term infiltration equation
C_2	Fitting coefficient in two-term infiltration equation
f	Correction factor
G	Specific gravity
H	Total head
h_o	Imposed pressure head at the soil surface
I	Cumulative infiltration
i_s	Steady-state infiltration rate
$K(\psi)$	Soil hydraulic conductivity function
$K(h)$	Soil hydraulic conductivity function
K_0	Soil hydraulic conductivity at the imposed pressure head
K_s	Saturated hydraulic conductivity
l	Tortuosity parameter
m	Constant
n	van Genuchten shape parameter
P	Transmissivity factor
q	Variable used during inverse modelling
q_{WF}	Water flux wetting front advance zone
r	Correlation coefficient
R	Radial coordinate
r_0	Disc radius
R^2	Coefficient of determination
R_i	Rainfall intensity
S_0	Soil sorptivity at pressure head h_0
S_e	Effective saturation
t	time

T_{CL}	Duration calculated using Cumulative linearization method
T_{DL}	Duration calculated using Differentiated linearization method
T_m	Duration calculated using time fractionation approach, based on Zhangs method
t_m	Geometric meantime
v_{WF}	Wetting front advancing velocity
w	Gravimetric water content
w_f	Final gravimetric water content
w_i	Initial gravimetric water content
z	Vertical coordinate, Datum head
z	Vertical coordinate
α	van Genuchten shape parameter
β	Constant
γ	Constant
γ_b	Bulk density of soil
γ_d	Dry density of soil
γ_w	Density of water
η	Porosity
θ	Volumetric soil water content
$\theta(h)$	Soil water retention function
θ_0	Volumetric soil water content corresponding to a given pressure head
θ_f	Final volumetric water content
θ_i	Initial volumetric water content
θ_m	Digital indicator of volumetric water content in wetting front advancing method
θ_r	Residual volumetric water content
θrs	Maximum volumetric water content in rising phase
θs	Saturated volumetric water content
λ	Macroscopic capillary length
ξ	Hydraulic gradient
Φ	Objective function for inverse simulation
ψ	Soil matric suction

List of Abbreviations

Terms	Description
ANOVA	Analysis of variance
AS	Agricultural soil
ASTM	American Society for Testing and Materials
BAp	Bland-Altman plot
BC	Boundary conditions
BEST	Beerkan Estimation of Soil Transfer parameters
CI	Cumulative infiltration
CL	Cumulative Linearization method
CP	Carsel and Parrish
CR	Capillary rise
CV	Coefficient of variation
DH	Dohnal method
DL	Differentiated Linearization method
DRI	Double ring infiltrometer
GA	Green-Ampt method
GP	Guelph Permeameter
HSD	Honest Significant Difference
HV	Haverkamp method
IC	Initial conditions
IPM	Instantaneous profile method
IS:2720	Indian Standards on methods of test for soils
IS	Inverse simulation
IS-CI	Inverse simulation using CI data only
IS-CI+θ_f	Inverse simulation using CI and final VWC
LM	Levenberg-Marquardt
LoA	Limits of agreement
LSD	Least significant difference
MAE	Mean absolute error
MDI	Mini disc Infiltrometer

MDI-emp	MDI results analysed using empirical method
MDI-inv	MDI results analysed using inverse modelling
M-EQ	Mathematical formulations
MF	Measurement footprint
NRMSE	Normalized root mean square error
PH	Philips method
PM	Laboratory falling-head permeameter
RD	Relative difference
RE	Relative error
RMSE	Root mean square error
RS	Rainfall simulator
SD	Standard deviation
SE	Standard error
SHCF	Soil hydraulic conductivity function
SRI	Single ring infiltrometer
SSE	Sum of squared errors
SWP	Soil water potential
TI	Tension disc infiltrometer
USDA	United States Department of Agriculture
vG	van Genuchten
VGM	van Genuchten-Mualem
VWC	Volumetric water content
WFAM	Wetting front advancing method
WRCC	Water retention characteristic curve
WWRCC	Wetting water retention characteristic curve
ZH	Zhang method
1-D	One-dimensional
2-D	Two-dimensional
3-D	Three-dimensional

Chapter 1

Introduction

1.1. General

The process of water entering the soil at the natural ground surface is known as infiltration. Gravity and capillarity are the factors that drive water into the soil or porous media. Further, the re-distribution of water through the subsurface zone depends on soil texture, soil structure, pore size and pore distribution, connectivity among pores, compaction state defined by soil density and soil moisture content, state of unsaturation, presence of preferential flow paths and other secondary factors (Mein and Larson, 1973; Romano et al., 1998; Alaoui et al., 2011; Dagadu and Nimbalka, 2012; Assouline, 2013; Ma et al., 2017; Ghosh and Pekkat, 2019). All of these factors combinedly make the process of infiltration and re-distribution complex and sometimes difficult to comprehend. Furthermore, some of the inherent features, such as preferential flow paths within the subsurface, are difficult to comprehend and remain as a source of uncertainty while studying the flow through porous media (Nimmo, 2012; Guo et al., 2014; Ma et al., 2017).

Increasing municipal, industrial, and agricultural operations have all led to subsurface environment degradation. Thus, researchers from a variety of disciplines have shifted their attention to soil water infiltration and sub-surface water movement in order to develop soil management practices that can minimize the risk of groundwater pollution from land-based pollutants (Ankeny et al., 1991). The quantitative description of water and solute movement into and across these unsaturated zones of the soil relies on the characterization of soil hydraulic properties (namely, soil infiltration, near-surface hydraulic conductivity, and water retention characteristics). Further, for reliable hydraulic and hydrologic modelling (related to flood, drought, irrigation, and contaminant transport), estimation of infiltration rate, near-surface near-saturated hydraulic conductivity, and water retention characteristics is mandatory.

Several ring infiltrometers (double ring and single ring) and tension disc infiltrometers (TI) are currently available for in-situ and laboratory soil hydraulic characterization. The disc infiltrometers impede the macro pore flow by applying a negative head at the surface during the infiltration measurements (Minasny and George, 1999). Thus, the disc infiltrometers reflect

the flow through the soil matrix, unlike the ring infiltrometers, where the flow into macro pores is inevitable. Furthermore, the ring infiltrometers have the drawbacks of being heavy, cumbersome, less portable, and time-consuming to use, as well as requiring a large volume of water. This restricts its application to large-scale infiltration measurements with sufficient repetitions over difficult terrain. On the other hand, the disc infiltrometers are handy, require relatively less water, and offer spatial-temporal infiltration measurements with adequate repetitions over a large area (Smettem and Ross, 1992; Warrick, 1992; Haverkamp et al., 1994; Smettem et al., 1994; Angulo-Jaramillo et al., 2000).

Among various disc infiltrometers, the Mini disc infiltrometer (MDI) has emerged as a popular choice among researchers for infiltration characterization. Its extensive use for more than two decades can be ascribed to its small size, portability, ease of operation, rapid measurement, and low water need (Angulo-Jaramillo et al., 2016; Gadi et al., 2017; Nestingen et l., 2018; Ghosh & Pekkat, 2019). Furthermore, its non-intrusive and non-destructive measurement procedure causes minimal soil disturbance and also enables the user to undertake extensive spatial-temporal measurements with adequate replications for field measurements.

1.2. Motivation of the research

The systemic influence of soil and infiltrometer-related parameters for MDI measurements needs further study. Although MDI is a disc infiltrometer, it differs from the conventional tension infiltrometer (TI) in many ways, including its measurement footprint (disc diameter), installation process, water requirement, and, most importantly, its evaluation methodologies. While the literature offers an extensive evaluation for TI (Bagarello & Iovino, 2003; Vandervaere et al., 2000a; Angulo-Jaramillo et al., 2016), the same is missing for MDI even after several years of its deployment. A comprehensive literature survey of this device revealed the following key points.

- MDI, due to its small size and portable nature, was preferred over other instruments for infiltration measurements. However, despite its extensive use in literature, there is still a lack of standard operating procedures to analyse its measurements. As a consequence, the MDI measurements may suffer from non-unique soil hydraulic parameterization when analysed using different available methodologies.
- Some of the past works point out the measurement time dependency of soil hydraulic properties from disc infiltrometer measurements. However, the same is not studied in detail for MDI. A guideline related to adequate measurement time for MDI would

alleviate the uncertainty in estimated parameters associated with measurement time dependency.

- Most previous studies have used MDI only for limited purposes, including estimating soil hydraulic properties, namely, near-surface near-saturated hydraulic conductivity and sorptivity, corresponding to a given tension pressure head. However, not many studies exist
    a) to understand the relationship between the supplied pressure head in the device and the resulting hydraulic parameters.
    b) for analysing the hydraulics of flow beneath the MDI in the sub-surface zone.
    c) for exploring the efficacy of MDI to determine water retention characteristics and soil hydraulic conductivity functions.

It is worth mentioning that a detailed evaluation using both short-term and long-term measurements of MDI is required to gain confidence in the infiltration measurements from this device. The role of the applied negative boundary pressure head in MDI on the measured infiltration characteristics needs to be assessed in detail. Moreover, to evaluate whether the infiltration characteristics obtained using MDI relate to the prediction from infiltration models reported in the literature, it is crucial to compare its measurements with established methods like rainfall simulators. Apart from the above, there is also a need to investigate the relationship between MDI infiltration and soil-specific characteristics. For instance, the variation in moisture status and water potential of the soil that occurs during the wetting process of infiltration is crucial to comprehend the subsurface moisture dynamics of a particular soil. Such assessments are also critical for verifying the accuracy of the model parameters used during the numerical modelling of flow in variably saturated soils.

A comprehensive study including all the above aspects is essential to investigate the potential of the MDI, which in turn would help in further establishing the usefulness of the device. Such a study would help to formulate guidelines required for standardizing disc infiltrometer measuring methodology. A need for such studies has motivated to conduct this research.

1.3. Research objectives

Motivated by the above discussion and considering the research gaps, the main aim of this study is to appraise the wetting characteristics of soils by evaluating the flow beneath the MDI, both experimentally and numerically. The objectives of the current work are defined as follows.

1. Understanding the relationship between the imposed tensions on the soil surface by MDI and the resulting hydraulic parameters.
2. Experimental evaluation of near-surface wetting hydraulic characteristics and understanding their time-dependence.
3. Evaluating and analyzing the saturated hydraulic conductivity from MDI measurements by comparing with other head-based and flux-based approaches.
4. Investigating the utility of MDI to obtain soil hydraulic conductivity function (SHCF) in the laboratory using soil column study.
5. Investigating the utility of MDI to generate wetting water retention characteristics curve (WWRCC) using laboratory measurements and numerical modeling.

It may be noted that MDI has the potential to replace conventional ring infiltrometers and TIs, as it offers several advantages over these devices. Hence, there is a critical need to popularize the MDI for the benefit of the user community. As discussed earlier, the use of MDI currently is limited to infiltration measurements and soil parameters (K_0 and S_0) estimation only. The main purpose of this study was to explore the utility of MDI beyond infiltration measurements, which, as far as our knowledge is concerned, is missing in the existing literature. With the help of extensive evaluations, this study attempted to assess the performance and approve MDI's efficacy beyond its traditional role as an infiltrometer.

1.4. Organisation of the thesis

The thesis is organized into the following chapters:

Chapter 1: introduces the topic of the research and the motivation behind it. The objectives and structure of the thesis are provided in this chapter.

Chapter 2: reports the review of literature pertinent to the current research, followed by a summary of the review and gaps in research.

Chapter 3: describes various instruments used in this study for soil hydraulic characterization based on infiltration measurements. The experimental measurement methodologies and the numerical modelling technique adopted in this study are also presented.

Chapter 4: investigates the relationship between imposed tension in MDI and the resulting soil hydraulic parameters using transient infiltration measurements from both laboratory and field tests of MDI.

Chapter 5: critically analyses the time dependence of wetting hydraulic characteristics from transient analysis of MDI measurements. It also provides adequate measurement durations for accurately quantifying soil hydraulic properties from MDI for six different soil textures.

Chapter 6: presents controlled laboratory investigation, numerical modelling, and statistical analysis for evaluating the saturated hydraulic conductivity measurements from MDI by comparing with other flux-based and head-based methods, namely rainfall simulator, SATURO infiltrometer, and falling-head permeameter.

Chapter 7: demonstrates the utility of MDI for determining soil hydraulic conductivity function (SHCF) with the help of experimental analysis using instrumented soil column setups in the laboratory and numerical investigation.

Chapter 8: investigates the utility of MDI for generating the wetting water retention characteristics curve (WWRCC) using controlled laboratory measurements. This chapter rigorously analyses the flow from MDI for precise quantification of soil hydraulic model parameters by inverse analysis and proposes the parameter values for two fine-textured soils.

Chapter 9: enlists the summary and major contributions from this research and highlights the future scope of this study.

Chapter 2

Literature Review

2.1. General

Infiltration, or the flow of water from the ground to the subsurface, represents an important component of the earth's hydrologic cycle. Its dependency on the vadose zone soil characteristics and atmospheric factors makes it a complex process to comprehend. The non-linearity of soil-air-water interaction within the pores, hysteretic behaviour of the soil water interaction, and variability in soil's initial and boundary conditions further increase the intricacies of the infiltration process. Hence, attempts were made by researchers and scientists to comprehend and enhance the knowledge of the physics and mechanics of this soil-water-atmosphere interaction at the soil boundary and also within the subsurface zone. As a consequence of such rigorous efforts over last few decades, new developments in infiltration measurement philosophies and techniques were established. Following sections presents a summary of methods used for infiltration characterization.

2.2. Review of existing mathematical models and instruments for infiltration analysis

The literature shows existence of several mathematical models for determining infiltration and soil hydraulic properties. These models differ primarily in their mathematical representation and the parameters involved. Initially, in the year 1856, Darcy has formulated expressions for soil hydraulic characterization from infiltration measurements in saturated soils (Darcy, 1856), which was later extended for interpreting flow in unsaturated soils by Buckingham (1907) and Richards (1931). It was reported that determining the solutions of the unsaturated problems required additional information of soil hydrological properties like water retention characteristics, and hydraulic conductivity. By performing a large number of soil-column experiments, Buckingham observed that in case of unsaturated soils, the moisture content and hydraulic conductivity are strongly dependent on the capillary/matric potential of the soil. In 1931, Richards gave the analytical expression that governs the flow in variably saturated porous media (Richards, 1931; Chow et al., 1988), and provided the physical basis for infiltration process. His equation was derived based on Darcy's flow equation and the mass

conservation equation. The Richard's flow equation is highly nonlinear in nature, and thus requires simplifying assumptions for deriving its analytical solutions (Narasimhan, 2007).

Over years, several theoretical (Green and Ampt, 1911; Philips,1969) and empirical (Kostiakov, 1932; Horton, 1933; Mezencev, 1948) expressions were formulated to analyse infiltration measurements and determine soil hydraulic parameters (Chow et al., 1988). By assuming a sharp wetting front boundary during soil moisture migration within the subsurface, Green and Ampt derived an exact analytical expression for infiltration measurements, based on Darcy's law (Green and Ampt, 1911; Chow et al., 1988). Philips (1969) provided a two-term infiltration equation to analyse infiltration characteristics of soils by solving Richards expression. Philip's method was based on fitting of the two-term equation to the cumulative infiltration measurements from various infiltrometers to determine the infiltration coefficients and the soil hydraulic parameters, sorptivity and hydraulic conductivity. Among the empirical methods, Kostiakov (1932) proposed a simple power equation based on curve fitting from field measurements. This method was later modified by Mezencev (1948) by adding a constant term to the expression. The empirical expression of Horton (1933) was based on the observation that the infiltration for a soil begins at some maximum rate (infiltration capacity) and then exponentially decreases until it reaches a constant rate or steady-state condition. The Horton's expression is one of the earliest and most widely used expression for infiltration analysis (Chow et al., 1988).

Simultaneously, several instruments were developed by researchers for characterizing soil hydraulic properties from infiltration measurements. The literature review shows an extensive evaluation using these devices which include the single ring infiltrometer (SRI) and double ring infiltrometer (DRI) (Bouwer, 1986; Bodhinayake, et al.,2004; Fatehnia, et al., 2016; Ghosh and Pekkat, 2019a; Ghosh et al., 2019), rainfall simulators (Gupta et al., 1993; Holden and Burt, 2002; Pérez-Latorre et al., 2010; Aksoy et al., 2012; Morbidelli et al., 2017), disc or tension infiltrometers (Warrick, 1992; Logsdon and Jaynes, 1993; Angulo-Jaramillo, et al. 2000; Vandervaere, et al., 2000a, b; Madsen and Chandler 2007; Alagna et al., 2013; Gadi et al., 2017; Ghosh and Pekkat, 2019a; Ghosh et al., 2019), Beerkan estimation of soil transfer parameters (BEST) method (Lassabatère, et al., 2006; Mubarak, et al. 2009; Yilmaz, et al. 2010; Bagarello, et al. 2014b; Di Prima, et al. 2018; Alagna, et al. 2019a).

The ring infiltrometers like DRI and SRI measure the flow under ponded or saturated conditions, where preferential flows may dominate and overestimate the measured parameters (Minasny and George, 1999; Köhne etal 2011). Hence, disc infiltrometers were designed to create negative or tension head at the infiltrating surface so as to avoid overestimation due to

preferential flows. This would reduce the macropores from the flow process and would only measure the flow of the soil matrix (Minasny and George, 1999; Kohne et al., 2011; Angulo-Jaramillo et al., 2016). Moreover, the disc infiltrometers have three-dimensional geometry of infiltration that allows steady state to be reached quicker than in the case of one-dimensional experiments (Elrick et al., 1990). The portability and the need of relatively small volume of water in the disc infiltrometers also make them suitable particularly for spatial variability studies (Mohanty et al., 1994; Jarvis and Messing, 1995). The rainfall simulators allow to manage and control the amount, intensity and, duration of rainfall depending on the requirement of the research, and thus, are highly useful for simulating natural rainfall events for infiltration related studies (Holden and Burt, 2002; Adams et al., 2005; Aksoy et al., 2012; Verbist et al., 2013). However, the bulkier size, high water demand, and limitation of replications for the rainfall simulators, often make them inconvenient for regular use, especially for field studies (Aksoy et al., 2012; Verbist et al., 2013). The BEST method (Lassabatère, et al., 2006) allows simultaneous determination of the water retention curve, and the hydraulic conductivity curve facilitated by shape and scale parameters. The scale parameters are estimated from infiltration studies at zero pressure head, while the shape parameters are estimated through particle size distribution analyses using pedo-transfer functions. This method was further revised (Yilmaz et al., 2010; Bagarello et al., 2014b), and widely adopted in the literature (Di Prima et al., 2018; Lassabatere et al., 2019; Alagna et al., 2019a).

2.3. Historical development of various disc infiltrometers and mathematical models for disc infiltrometer analysis

Tension infiltrometry is a reliable technique for determining soil hydraulic properties such as near-surface hydraulic conductivity, sorptivity, and macro porosity (Reynolds and Elrick, 1991; Zhang, 1997a; Madsen and Chandler, 2007). Thus, disc infiltrometers are becoming increasingly popular for soil hydraulic characterization since they offer relatively simple, quick, and inexpensive test procedures. Several designs of these disc infiltrometers have been proposed (e.g., Perroux and White, 1988) and are commercially available.

The first innovation in this field can be dated back to the early nineteen hundred when Gardner (1937) developed a negative head permeameter based on the capillary potential concept of Buckingham (1907). Later, Talsma (1969) developed a technique for the in-situ determination of sorptivity, but it was restricted to a positive water supply pressure. Thus, it suffered from the disadvantage that the water supply potential decreased during the measurement. Dirksen (1974) showed that from the measurements of steady, spherically

symmetric flows from a cavity at a series of steady, negative pressure heads, hydraulic conductivity's dependence upon the pressure head could be obtained. It required only one controlled boundary without having to impose one-dimensionality upon the flow system. No measurements were required within the soil, thereby making this method attractive for in-situ measurements. The major disadvantage of this method was the time required to reach steady state at lower soil water contents which were quite high. Dirksen (1975) specifically designed a permeameter to measure sorptivity at a range of negative water supply potentials to estimate soil-water diffusivity. Although the permeameter was a simple device with a membrane to supply water, it appeared not to have been used much in the field. Dixon (1975) developed a closed-top single-ring infiltrometer to study preferential flow in macropores. Water in it was applied to the closed-top system to allow the imposition of negative pressure on the ponded water surface. This device allowed for a supply of water potential in the range of -3 to 1 cm of water. However, it was not convenient for field measurements.

A simpler and more convenient sorptivity tube for the field was developed by Clothier and White (1981), which could provide a constant tension head on the soil surface based on the sorptivity apparatus design given by Dirksen (1975). Their sorptivity tube was essentially a Mariotte bottle in which the supply water potential was determined by the bubbling pressure of a capillary or the radius of the hypodermic needle through which air enters the water reservoir. The water supply to the soil was accomplished via a sintered glass plate of appropriate bubbling pressure, and the practical range of supply potentials achieved was -10 to 0 cm of water. However, the sorptivity tube had many shortcomings, which were later overcome by Perroux and White (1988). Chong and Green (1983) gave a water supply plate design by modifying the sorptivity apparatus design of Dirksen (1975). However, it was restricted to an even narrower range of supply potential because of its smaller bubbling pressure. Topp and Zebchuk (1985) simplified the closed top single ring infiltrometer developed by Dixon (1975). However, the limitation of this device was that infiltration had to be started by ponding the closed-top infiltrometer, i.e., by applying a positive head and then adjusting it to a negative pressure.

Perroux and White (1988) modified the design given by Clothier and White (1981). They developed a disc permeameter or tension infiltrometer, which could be used for both positive and negative supply pressure heads. It comprised of a nylon mesh supply membrane with a very small diameter (suitable for a wide range of supply potential up to -20 cm), a water reservoir, and a bubbling tower. The bubbling tower was connected to the reservoir at one end and open to air at the other. By adjusting the water height in the air-inlet tube, the supply

potential in the membrane could be regulated. Now the pores in the soil needed to have an energy level equivalent to that of the supply potential to overcome water which was held under tension in the reservoir. This device was used to supply water potential ranging from -20 cm to 0 cm, effectively excluding pores with a diameter bigger than 0.75 cm. However, the noting down of water level drop visually for measuring the infiltration rates was tedious and acted as a drawback to this method. Hence, its automation was tried by a few researchers with the help of pressure transducers (Ankeny et al., 1988; Casey and Derby, 2002). The disc infiltrometers also required establishing a proper hydraulic contact between the infiltrometer chamber and the soil surface (Latorre et al., 2015; Angulo-Jaramillo et al., 2016). To overcome this issue, a special type of tension infiltrometer, known as the hood infiltrometer, was developed (Schwarzel et al., 2006) based on the closed-top infiltrometer design of Dixon (1975). The hood infiltrometer can determine saturated and unsaturated hydraulic conductivity in situ. However, it allows for the measurement of hydraulic conductivity, including flow in macropores, from saturation till the soil's bubble point, which might restrict its application to a small pressure head range (Patra et al., 2019).

The mini disc infiltrometer (MDI) was developed by METER Group, USA (formerly known as Decagon devices) based on the design of the tension disc infiltrometer of Perroux and White (1988). It is a miniaturized tension disc infiltrometer that allows simple and rapid determination of soil hydrodynamic parameters (Wallage et al., 2011; Angulo-Jaramillo et al., 2016). Unlike tension infiltrometer, it has a simple design, and it can be transported to remote locations. Additionally, its features allow easy installation in difficult terrains, which are generally inaccessible for larger tension infiltrometers (Madsen and Chandler, 2007; Murray et al., 2007; Ravi et al., 2007).

Most of the early research studies on estimating soil hydraulic properties from tension infiltrometers (Perroux and White, 1988; White et al., 1992; Logsdon and Jaynes, 1993; Simunek et al., 1999) were based on the frequently used steady-state approximation of Wooding equation (Wooding, 1968). Wooding's equation is a partial numerical and analytical approximation (Weir, 1987) to study the flow from a shallow, ponded, circular disc at steady-state conditions by the method of linearization. Both the multiple disc approach (Smettem and Clothier, 1989) and the multiple head approach (Ankeny et al., 1991; Reynolds and Elrick, 1991) can be used to estimate the soil hydraulic properties using Wooding's equation. However, the steady-state methods require the assumption of uniform initial water content and homogeneity of the soil, which may be unlikely for large volumes of sampled soil. Additionally, the duration needed to reach the steady-state flow may impose constraints on its

application in field conditions (Vandervaere et al., 2000). Owing to numerous limitations associated with the steady-state method, research was focused on the analysis of transient flow data to estimate the soil hydraulic properties (Warrick, 1992; Haverkamp et al., 1994; Smettem et al., 1994; Zhang, 1997a, b; Simunek et al., 1998; Vandervaere, 2000a, b). Due to shorter experiment durations and smaller sampled volumes of soil, the transient analysis technique conformed more with the assumptions of homogeneity and initial water uniformity (Angulo-Jaramillo et al., 2000). Consequently, there was a rise in the application and evaluation of the transient methods of disc infiltrometer measurements during the mid-2000s and thereafter, as reported in the literature (Ferraris et al., 2003; Lichner et al., 2007; Ronayne et al., 2012; Taiwo et al., 2016; Ruwanza, 2017; Ghosh and Pekkat, 2019a).

The transient analysis of disc infiltration measurements needs to ascertain the adequacy of the measured data. For this purpose, two linearization methods, namely cumulative linearization (CL) (Smiles & Knight, 1976) and differentiated linearization (DL) (Vandervaere et al., 2000a; Angulo-Jaramillo et al., 2016), were proposed. Depending on the presence or absence of the contact layer during infiltration measurements, several researchers evaluated the CL and DL methods extensively for measurements from TI (Bagarello and Iovino, 2003, 2004; Bagarello et al., 2004; Vandervaere et al., 2000a). Alagna et al. (2019b) conducted a field study where both the CL and DL methods were applied to evaluate the adequacy of MDI measurements obtained for three soil textures. Additionally, a few studies were reported that identified the adequate measurement duration needed for transient analysis of TI measurements to accurately predict the soil hydraulic parameters (Bagarello and Iovino, 2003; Bagarello et al., 2004).

2.4. Mini disc infiltrometer application and its comparative analysis with other devices

The MDI has been used extensively for studying infiltration measurements and characterizing soil hydraulic properties. In an attempt to sustain the productivity of a native forest in New Zealand, Kirkaham and Clothier (2000) conducted infiltration studies using MDI. Li et al. (2004) used MDI in the laboratory to measure the steady-state infiltration rate of soil crust under tension. The experiments were performed at three different water pressure heads of -0.5 cm, -2 cm, and -6 cm on the soil crust samples removed from the field in Tabernas Desert Badlands. The results showed the adequacy of MDI for infiltration measurement in soil crusts. Lewis et al. (2004, 2006) used MDI along with remote sensing to test the surface water repellence and assess the burn severity of the soil suffered from fire. The results of the water repellence test with soil burn severity using MDI were in greater agreement in these studies.

Lincher et al. (2007) made use of MDI to carry out infiltration experiments for studying the impact of vegetation on the hydraulic conductivity of a sandy soil. The automation of two models of MDI was attempted by Madsen and Chandler (2007). Murray et al. (2007) investigated the hydrogeological properties of clastic dikes to model the flow and transport through dikes by characterizing the hydraulic conductivity of these dikes and their enclosing matrix. They reported that MDI could be used conveniently to get the infiltration measurements from certain narrow sites due to its relatively small size.

Ravi et al. (2007) studied the effect of differential rates of soil deposition and removal by aeolian process on infiltration and runoff like hydrogeological processes in the arid landscapes of the northern Chihuahua desert. More than 100 infiltration experiments were conducted with MDI in the study area. Robichaud et al. (2008, 2013) used MDI tests to obtain relative infiltration rates to classify soil water repellency and compare the infiltration capacities of tested sites. Boxell et al. (2009) used MDI to determine surface hydraulic conductivity to assess the differences in physical and hydrological properties of soil in two different habitats. Moody et al. (2009) conducted both laboratory and field infiltration experiments with MDI to find sorptivity and near-saturated hydraulic conductivity as a function of initial soil moisture content ranging from extremely dry to near-saturated conditions. Glenn and Finley (2010) and Gonzalez-Pelayo et al. (2010) used MDI to study the effect of fire and vegetation cover on infiltration and hydrological characteristics of soils. Rice and Grismer (2010), to study the hydrological responses to repellency, preferred MDI along with the rainfall simulator to carry out infiltration experiments.

Wallage et al. (2011) used MDI along with dip wells to study the impact of blanket peat land management on water tables, near-surface macro pore flow, and saturated hydraulic conductivity. In a study to measure the hydrodynamic properties of soil crust, MDI was used by Alagna et al. (2013). Bhave and Pekkat (2013) investigated the influence of initial soil condition (soil moisture content and dry density) on the infiltration characteristics of locally available sandy soil using MDI. Elbl et al. (2014) carried out studies to investigate the impact of mineral nitrogen and organic carbon addition on the hydrophobicity of soil affected by rainfall variations, for which MDI was used to measure saturated hydraulic conductivity. In a study to understand the effect of liquid humus and calcium sulphate on soil aggregation, MDI was used for carrying out micro-infiltration measurements by Norambuena et al. (2014). In situ infiltration measurements with the help of MDI were carried out by Schacht et al. (2014) to study the impact of treated wastewater irrigation on the water repellency of Mediterranean soils. Fatehnia et al. (2014) analysed MDI measurements in the laboratory to obtain the cumulative

infiltration curve of the poorly graded sand for various suction rates. The results were analysed using eight different methods to determine the saturated and unsaturated hydraulic conductivity values.

Schacht et al. (2015) conducted in-situ infiltration measurements using MDI to compare the hydraulic conductivity of fresh water irrigated sites and treated wastewater irrigated sites in the long-term agricultural experimental orchards in northern Israel. For spatial analysis of soil hydraulic properties at different points of an alfisol in Nigeria, MDI was preferred by Taiwo et al. (2016). In an attempt to study the soil physicochemical changes in the abandoned agricultural fields and natural sites in Eastern Cape, South Africa, Ruwanza (2017) made use of MDI to measure the infiltration rate on all soil collection points and determined hydraulic conductivity from its measurements. Gadi et al. (2017), in a study to understand the spatial and temporal variation of hydraulic conductivity in green infrastructures, used MDI to conduct the infiltration measurements. In order to evaluate the relative performance of various interpolation methods for predicting spatial variability of hydraulic conductivity, Ghosh and Pekkat (2019d) used MDI to conduct in-situ infiltration tests at two different locations in India. In a recent study by Fajardo-Cantos et al. (2022), MDI was used to assess hydraulic conductivity and water repellency of soil after conducting prescribed burning in Ayna, Spain. Their study was intended to understand the ecological effects of late prescribed burning treatments under mixed trees.

Similar to tension infiltrometers (TI), macropore flow is prevented in the case of MDI due to the application of negative head during infiltration tests (Minasny and George, 1999; Fodor et al., 2011; Bordoloi et al., 2018; Radinja et al., 2019). A comparison of MDI's measurements with TI has shown statistically comparable estimates of hydraulic conductivity (Alagna et al., 2016; Ghosh et al., 2019) and soil water repellency index (Hunter et al., 2011). When compared with other head-based methods like SRI and DRI, MDI has produced contradictory results. The sorptivity and hydraulic conductivity estimates from field measurements using MDI were lower than that of SRI (Gonzalez-Sosa et al., 2010), while the saturated hydraulic conductivity (at tension close to saturation) from MDI was reported to be higher yet statistically comparable with that of SRI measurements (Alagna et al., 2016). Compared with DRI measurements, the saturated hydraulic conductivity estimates from MDI were either higher (Radinja et al., 2019) or lower (Ronayne et al., 2012; Ghosh et al., 2019). Literature also reports a comparison of MDI measurements with various other devices such as SATURO (Radinja et al., 2019) and Guelph permeameter (Ghosh et al., 2019; Nestingen et al., 2018; Ronayne et al., 2012). The results from these cases indicated both higher and lower values from MDI.

The literature review shows the application of MDI in numerous studies both in the field and laboratory. Most of these applications include determining the infiltration rates (Kirkaham and Clothier, 2000; Li et al., 2004; Ravi et al., 2007; Rice and Grismer, 2010), estimating the hydraulic properties, like sorptivity, and unsaturated and saturated hydraulic conductivity, of sediment and soils (e.g., Lichner et al. 2007; Moody et al., 2009; Boxell et al., 2009; Wallage et al., 2011; Elbl et al., 2014), and investigating the soil water repellency induced by fire or vegetation cover (Lewis et al. 2006; Glenn and Finley, 2010; Gonzalez-Pelayo et al., 2010; Fajardo-Cantos et al., 2022). MDI has also been successfully used to evaluate the influence of initial soil conditions on soil hydraulic characterization (Bhave and Pekkat, 2013) and to conduct spatial-temporal analysis of soil hydraulic properties (Taiwo et al., 2016; Gadi et al., 2017; Ghosh and Pekkat, 2019d). Similarly, in many other studies, estimates from MDI's measurements were evaluated with various other devices. The results from these studies, however, were contradictory and inconclusive, thereby indicating the need for further evaluations.

2.5. Numerical studies related to infiltration characterization

In the recent two decades, inverse modelling techniques have become increasingly popular for estimating soil hydraulic parameters, which are quite essential for the physical modelling of transient water flow in the vadose zone (Sprenger et al., 2015). Although many analytical solutions were suggested by researchers (Cho, 1971; Wagenet et al., 1976; van Genuchten, 1980), for complex situations like transient analysis of flow, such analytical solutions are not available. In such situations, numerical modelling and inverse analysis play significant roles. In the following sections, some of the works using numerical modelling of infiltration measurements and inverse parameter estimation of soil hydraulic properties are reviewed.

Ogawa et al. (1992), using a numerical analysis based on a one-dimensional infiltration model, evaluated the infiltration and discharge of rainwater and water movement in the soil. The numerical analyses were carried out for a range of precipitation intensities, initial soil moisture conditions, and soil characteristics. Skaggs et al. (2004) conducted the simulations (HYDRUS-2D) of water infiltration and redistribution under drip irrigation for a sandy loam soil and compared the simulation results with the field data. The results were in good agreement with each other, and the numerical simulation method was successful in investigating and designing drip irrigation management practices. Vasudeo et al. (2005) developed a numerical model to predict the transient position of the water table in response to recharge from a

rectangular basin. The method was based on the Finite Difference Method with an explicit scheme. An infiltration model based on the numerical resolution of Richard's equation was developed by Herrada et al. (2014) to simulate infiltration into heterogeneous soils. They considered arbitrary initial moisture content distributions, unsteady rainfall, and free drainage conditions in their study. Ramos et al. (2011) used numerical model (HYDRUS-1D) to simulate water movement and solute transport in two experiments carried out under field conditions in which water with different salinities and nitrogen concentrations was used. Latorre et al. (2015) proposed a numerical method based on the analysis of Haverkamp et al. (1994) to estimate the soil hydraulic properties (sorptivity and hydraulic conductivity) known as the NSH (Numerical solution of the Haverkamp equation) method. Using HYDRUS-3D, the NSH method was validated for 12 synthetic soils. They reported that infiltration time was an essential factor to estimate hydraulic conductivity.

Kool et al. (1985) evaluated the feasibility of simultaneously determining the water retention and hydraulic conductivity functions from transient flow data by parameter estimation method using two hypothetical soils and van Genuchten's model (van Genuchten, 1980). Russo (1988) used the parameter estimation method to find the soil hydraulic properties for two different soils using three different models, van Genuchten (1980), Brooks and Corey (1964), and Gardener (1958). Using Mualem's (1976) model for related soil hydraulic conductivity, hydraulic conductivity and soil water pressure head relationship are developed for all the above three models. Simunek et al. (1998) reviewed three field methods (data collected from tension disc permeameter, modified cone penetrometer, and a multiple-step field extraction device) for estimating the soil hydraulic properties by inverse analysis of Richards' equation. The soil hydraulic parameters for all three methods were estimated by coupling the numerical solution of Richard's equation with the Levenberg- Marquardt parameter estimation algorithm.

Simunek et al. (1999) analysed laboratory experiment results from tension disc infiltrometer to determine the unsaturated soil hydraulic properties using Wooding's analytical solution and numerical inversion. Goncalves et al. (2006) used HYDRUS-1D to analyse water flow, and solute transport in three soil lysimeters irrigated using different quality water. Provenzano (2007) conducted numerical modelling (HYDRUS-2D) to assess the infiltration process around a buried emitter in a sandy loam soil and evaluated the same using experimental observations. This study helped to evaluate the duration of irrigation and as well as the emitter spacing needed to be followed during subsurface drip irrigation. Sprenger et al. (2015) employed inverse modelling, using pore water stable isotopes, to analyse soil hydraulic parameters in the unsaturated zone. Three study sites with distinct soil properties and

vegetation cover were selected for the analysis. The Richards equation was numerically solved using the finite element code of HYDRUS-1D to simulate the transient unsaturated water flow.

2.6. Water retention characteristics and hydraulic conductivity function from infiltration measurements

The determination of wetting water retention characteristics curve (WWRCC) and soil hydraulic conductivity functions (SHCF) are extremely crucial while modelling various flow and transport problems in unsaturated soils (Cai et al., 2022; Milatz et al., 2018; Li et al., 2009; Watson, 1966). The WWRCCs from direct infiltration measurements are more reliable compared to measurements from steady-state methods (Šimůnek et al., 1999). Several previous works were noted where WWRCCs were evaluated directly from the wetting process simulated using infiltrometers. Some of these studies involved conducting direct measurements in the field and laboratory using infiltration tests from the tension disc infiltrometer (Ramos et al., 2006; Rashid et al., 2015; Schwartz & Evett, 2003; Šimůnek et al., 1998; Wang et al., 1998; Šimůnek et al., 1999), while, in some cases, WWRCC measurements were carried indirectly using numerical modelling (Šimůnek et al., 1999; Šimůnek & van Genuchten, 1996; Šimůnek & Van Genuchten, 1997). Similarly, the SHCFs have also been evaluated numerically using inverse simulation and parameter estimation techniques from infiltration measurements in some of the studies (Simunek et al., 1998; Ventrella et al., 2005).

It should be emphasised that all the above discussed evaluations are limited to the large-sized tension disc infiltrometer, TI. There were no similar studies reported in the literature for MDI. The accurate estimation of WWRCC is crucial for MDI, particularly because the evaluation of soil hydraulic parameters from MDI using the transient analysis method of Zhang (Zhang, 1997a, b) requires the van Genuchten model parameters, α, and n (van Genuchten, 1980). Any uncertainty in these parameters will directly influence the soil hydraulic characterization from MDI (Fodor et al., 2011; Ronayne et al., 2012). Moreover, the reliability of using the parameters measured from WWRCC for SHCF measurement in the case of MDI has already been questioned by Fodor et al. (2011). Further investigations incorporating WWRCC and SHCF measurements from MDI are needed to bridge such gaps in the literature and broaden existing knowledge.

2.7. Summary of literature review

The following findings were obtained from the reviewed literature:

- An extensive study has been carried out from the early 1900s to date in the field of infiltration, and several analytical and empirical methods have been proposed to measure flow rate and other soil hydraulic properties.
- Several improvements in disc infiltrometers were witnessed, starting from tension disc infiltrometer (TI) to mini disc infiltrometer (MDI) to advance the soil hydraulic characterization from its measurements.
- The infiltration measurements from the disc infiltrometer can be evaluated using both steady-state and early-time transient flow analysis methods. However, the latter method was preferred, mainly to avoid time constraints and simplifying assumptions of the former method.
- The data adequacy check (required during transient flow analysis) using the proposed linearization methods, DL and CL, was evaluated extensively for TI measurements. A few studies also reported recommended measurement duration for TI. However, similar studies for MDI measurements for varying soil textures are scarce.
- A large number of infiltration experiments were conducted both in the field and the laboratories to estimate the soil hydraulic parameters and other measurements using MDI. It was noted that due to its small size and portable nature, MDI was preferred over other instruments for infiltration characterization.
- Most of the evaluations for MDI data were carried out using the transient analysis method of Zhang (1997). Although van Genuchten retention parameters are directly involved in such analysis, the previous studies resorted to using these values from existing literature or pedo-transfer functions. The direct evaluation of retention parameters for MDI measurements was missing in the literature.
- Comparison of MDI measurements with various other infiltrometers and permeameters were inconclusive and presented contradictory reports, thus indicating the need for more evaluations.
- Numerical modelling and inverse analysis employing parameter optimization are useful and convenient tools to analyse and estimate soil hydraulic characteristics from infiltration measurement. However, only limited studies report such assessments for MDI measurements.

2.8. Gaps in the literature

The following gaps in literature was noted based on the literature review:

- Different from TI, MDI can offer a very small range of tension head (0.5 to 6 cm equal to 0.05 to 0.6 kPa). However, the implications of such negligible tension head on soil hydraulic characterization were not addressed in the literature.
- There are no recommendations in the literature for checking the data adequacy and/ or measurement duration for transient analysis of MDI measurements. Moreover, a comparative assessment of the recommended measurement time with the time obtained from the adequacy of the data check (from linearization methods) was also missing in the literature.
- While many head-based and flux-based methods have been compared for saturated hydraulic conductivity analysis from MDI, a critical evaluation to determine which factor (measurement footprint or mathematical equation) primarily influences such variations in its estimates were not reported.
- There are no studies that carried out extensive numerical investigation for determining wetting soil hydraulic characteristics from MDI measurements.
- Moreover, the utility of this handy device for determining wetting soil hydraulic characteristics and hydraulic conductivity function using instrumented soil column measurements in the laboratory was not adequately examined before.

Chapter 3

Materials Used and Methodology

3.1. General

The details of all the instruments used for conducting experiments in this study and their evaluation methodologies are provided in this chapter. Besides, the measurement methodologies for soil physical properties and hydraulic characteristics determination are also discussed. Finally, the inverse analysis using the numerical modelling technique is presented in the last part of this chapter.

3.2. Soil characterization and specification

Soils of various textures were used to carry out this study. Each soil was characterized for its basic index properties like grain-size distribution (ASTM D2487-11; IS 2720), specific gravity (G), moisture content (w), and bulk density (γ_b). As per IS: 2720 (part-4) – 1985, the grain size analysis of soil can be done by using dry or wet sieve analysis. For coarse and large-sized particles (> 0.075mm), the best method is dry sieve analysis, and for soils with more fine content (< 0.075mm), wet sieve analysis and hydrometer analysis should be conducted. The reagents used for wet sieve analysis are sodium hexametaphosphate or sodium carbonate and sodium hydroxide mixture per one liter of water solution. Based on the results of the sieve analysis and hydrometer, the texture of each soil was identified with the help of the soil triangle classification of USDA (United States Department of Agriculture).

3.2.1. Specific Gravity (G) Determination

Specific Gravity is defined as the ratio of weight in air of a given volume of soil solids at a stated temperature to the weight in air of an equal volume of distilled water at that temperature. The standard temperature for its determination is 27^0 C ± 2^0 C. As per IS:2720 (part- 3/sec-2) – 1980, the G of coarse-grained soil is determined using the Pycnometer, and for fine soils, it is determined using the density bottle method. G is calculated using the following formula.

$$G = \frac{m_2 - m_1}{(m_4 - m_1) - (m_3 - m_2)} \tag{3.1}$$

where m_1 represents the mass of the empty bottle with stopper, m_2 represents the mass of the bottle and soil, m_3 is the mass of the bottle filled with water and soil, and m_4 is the mass of the bottle filled with water. Specific gravity tests for all the soil samples were repeated 4-5 times, and the close values were averaged.

3.2.2. Determination of Density of Soil

The infiltration characteristics are significantly affected by the density and water content of the soil. Therefore, determining the bulk density and dry density is essential for characterizing infiltration. Bulk density (γ_b) is defined as the weight (W) per unit volume (V) of the existing soil.

$$\gamma_b = \frac{W}{V} \tag{3.2}$$

The soil consists of solids and voids. The voids can be filled with water and air. Ideally, when the voids are completely filled with water, it is called saturated condition, and if the voids are completely filled with air, it is called dry condition. The dry density of a soil represents the density of the soil in its dry condition and is given by

$$\gamma_d = \frac{\gamma_b}{1+w} \tag{3.3}$$

Where γ_d *is* the dry density of soil, and w is the gravimetric water content.

3.2.3. Determination of gravimetric water content (*w*)

As per IS: 2720 (part2) – 1973, the standard method for finding the gravimetric water content of the soil is the oven drying method. In this method, the water content of the soil is expressed as a percentage of oven-dried weight. The percentage of gravimetric soil moisture content can be calculated as follows

$$w = \frac{w_2 - w_3}{w_3 - w_1} \tag{3.4}$$

Where w is the gravimetric water content, w_1 is the weight of the empty pan; w_2 is the weight of the pan plus the weight of wet soil, and w_3 is the weight of the pan plus the weight of dry soil. Before carrying out every experiment, at least three samples of soil are stored in small pans, and the initial gravimetric moisture content is calculated by using the above procedure. Similarly, wherever needed, the final w values are also calculated by collecting samples after the termination of the experiments.

3.2.4. Determination of volumetric water content (VWC)

The volumetric water content is the ratio of the volume of water (V_w) present in the soil to the volume of wet soil (V). The measured gravimetric moisture contents (w) can be converted to VWC values using the following expression (Eq. 3.5). Here, m_w is the mass of water present in the soil; m_s is the mass of soil; γ_w is the density of water (1gm/cc), and γ_d is the dry density of soil. Alternately, VWC was measured directly using the appropriate sensors, which is discussed in the later part of this chapter.

$$VWC = \frac{V_w}{V} = \frac{m_w \gamma_b}{m_s \gamma_w} = w\frac{\gamma_d}{\gamma_w} \tag{3.5}$$

The results of particle size fractions, specific gravity values, soil classification, and dry densities used for the experiments corresponding to each soil are described in their respective chapters.

3.3. Instruments used for various experiments

3.3.1. Mini disc infiltrometer (MDI)

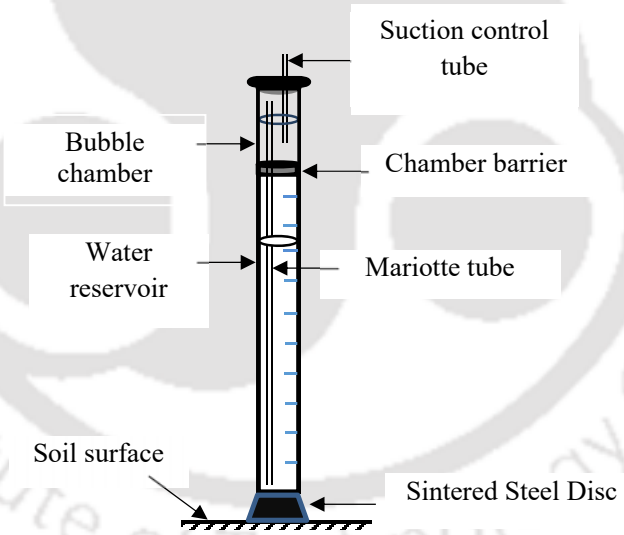

Figure 3.1 Schematic diagram of Mini Disc Infiltrometer

The MDI (METER Group Inc., USA) is a compact, portable tension disc infiltrometer with a disc diameter of 4.5 cm (schematic diagram in Figure 3.1). The total height of MDI is 32.7 cm, divided into two chambers and separated by a chamber barrier. The upper chamber (bubble chamber) has provision for maintaining a constant suction head (h_0) that can be adjusted in the range of -0.5 cm to -6 cm, at which water infiltrates into the soil. The lower chamber (reservoir chamber) stores water, wherein the drop in the water level is noted with

respect to time during infiltration measurements, which are further used to calculate the corresponding cumulative infiltration (CI) measurements. At the base of the MDI, a porous sintered stainless-steel disc of diameter 4.5 cm and thickness of 0.3 cm is provided for water entry into the soil. MDI enables the measurement of near surface-near saturated hydraulic conductivity (K_0) and sorptivity (S_0) corresponding to the supplied tension, h_0, in the field or laboratory.

3.3.1.1. Transient analysis of infiltration response from MDI

Transient infiltration rates corresponding to the three-dimensional infiltration process beneath the infiltrometer disc can be approximated by the first two terms of the following equation (Eq. 3.6) (Dohnal et al., 2010) given by Philip (Philip, 1957, 1969).

$$I = C_1\sqrt{t} + C_2 t \tag{3.6}$$

Where I is the cumulative infiltration rate (m), t is time (s), and C_1 (m/s$^{1/2}$) and C_2 (m/s) are coefficients that can be determined by fitting Eq. (3.6) to the measured cumulative infiltration vs. time data. This method involves plotting the square root of time values (for a given duration) along the x-axis and its corresponding CI values along the y-axis. Eq. 3.6 is then fitted to the data using a quadratic polynomial fit to obtain the coefficients C_1 and C_2 (METER Group, USA). Figure 3.2 provides a sample plot showing the fitting of the equation and the coefficients C_1 and C_2.

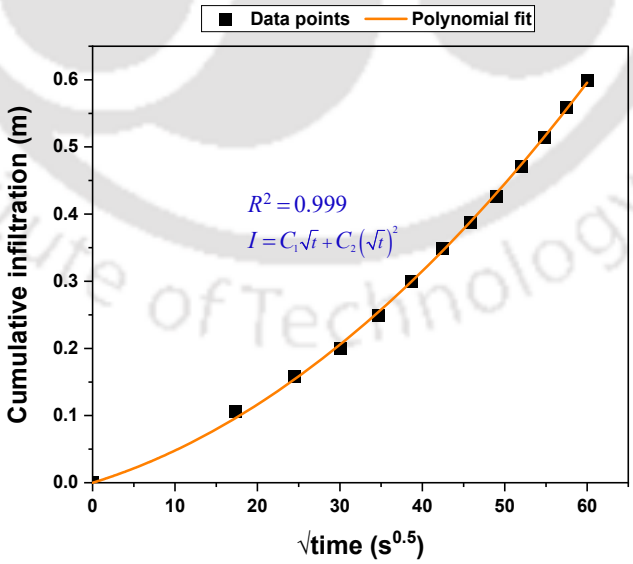

Figure 3.2 Cumulative infiltration vs. square root of time plot fitted to two term infiltration equation to determine coefficients C_1 and C_2

Haverkamp et al. (1994) have proposed a physically based method for determining the parameters S_0 and K_0 from disc infiltrometer measurements, valid for short to medium times and accounting for the lateral flux at the edge of the circular infiltration surface. In their approach, the infiltration coefficients C_1 and C_2 are related to S_0 and K_0 through the following expressions:

$$C_1 = S_0 \tag{3.7}$$

$$C_2 = \left(\frac{2-\beta}{3}\right)K_0 + \left(\frac{\gamma}{r(\theta_0 - \theta_i)}\right)S_0^2 \tag{3.8}$$

Where θ_0 (m^3/m^3) is the volumetric soil water content corresponding to h_0 and θ_i (m^3/m^3) is the initial volumetric soil water content; β is a parameter depending on the capillary diffusivity function that lies in the interval [0, 1] and γ is a constant approximately equal to 0.75. An average value of β= 0.60 can be assumed for most soils initially in dry conditions (Smettem et al. 1994; Haverkamp et al. 1994). Substituting Eq. (3.7) and (3.8) into Eq. (3.6) yields:

$$I = S_0\sqrt{t} + \left[\left(\frac{2-\beta}{3}\right)K_0 + \left(\frac{\gamma}{r(\theta_0 - \theta_i)}\right)S_0^2\right]t \tag{3.9}$$

The three terms on the right-hand side of Eq. 3.9 correspond to the vertical capillary flow, gravity-driven vertical flow, and lateral capillary flow, respectively. The first term dominates infiltration during its early stage and the third term, as shown by Smettem et al. (1994), is linear with time. Although the Haverkamp method has been extensively used for analysing infiltration measurements of large diameter tension disc infiltrometers (TI) (Vandervaere 2000a, b; Bagarello and Iovino, 2003; Bagarello et al., 2004, Angulo-Jaramillo et al., 2016), its application to MDI is limited (Ghosh and Pekkat, 2019b, c; Dohnal et al., 2010).

Zhang (1997a, b), in his studies, has suggested the two following simple linear expressions (Eq. 3.10 and 3.11) to relate coefficients C_1 and C_2 to capillary forces and gravity forces, respectively, which, when substituted in Eq. 3.6 make the final expression, Eq. 3.12.

$$S_0 = \frac{C_1}{A_1} \tag{3.10}$$

$$K_0 = \frac{C_2}{A_2} \tag{3.11}$$

$$I = S_0 A_1 \sqrt{t} + K_0 A_2 t \tag{3.12}$$

Here, A_1 and A_2 are dimensionless coefficients determined by the following empirical equations obtained based on numerous numerical experiments (Zhang, 1997a, b).

$$A_1 = \frac{1.4 b^{0.5} \left(\theta_0 - \theta_i\right)^{0.25} \exp\left[3\left(n-1.9\right)\alpha h_0\right]}{\left(\alpha r_0\right)^{0.15}} \tag{3.13}$$

$$A_2 = \frac{11.65\left(n^{0.1}-1\right)\exp\left[2.92\left(n-1.9\right)\alpha h_0\right]}{\left(\alpha r_0\right)^{0.91}}; n \geq 1.9 \tag{3.14}$$

$$A_2 = \frac{11.65\left(n^{0.1}-1\right)\exp\left[7.5\left(n-1.9\right)\alpha h_0\right]}{\left(\alpha r_0\right)^{0.91}}; n < 1.9 \tag{3.15}$$

Where n (dimensionless) and α (m^{-1}) are the van Genuchten (van Genuchten, 1980) water retention parameters, and b = 0.55 (Warrick and Broad bridge, 1992). The values of n and α parameters as a function of soil texture (Carsel and Parrish, 1988) are provided in the manual of MDI (METER Group, USA, 2020). Zhang's method is considered to be a simple procedure that works well for initially dry soil (Dohnal et al., 2010; Ghosh et al., 2019). The manufacturer of MDI, METER Group Inc., USA, has recommended using Zhang's method for evaluating soil hydraulic parameters from MDI measurements.

Dohnal et al. (2010) noticed that Zhang's method was invalid, particularly for soils with van Genuchten parameter n < 1.35. For such soils, they provided the modified expression by retaining the original functional formulation of Zhang (Eq. 3.11 and 3.15) and deriving the new fitting parameters through non-linear optimization. Specifically, for small-diameter discs like MDI and a limited range of suction (-0.5 to -6 cm), the following expression for K_0 was proposed. All the terms here bear the same meaning as that of Zhang's expression.

$$K_0 = \frac{C_2 \left(\alpha r\right)^{0.6}}{11.65\left(n^{0.82}-1\right)\exp\left[34.65\left(n-1.19\right)\alpha h_0\right]} \tag{3.16}$$

The use of the three methods discussed above is limited to the determination of unsaturated or near-saturated soil hydraulic parameters from MDI measurements. To determine saturated hydraulic conductivity (K_s) using MDI recordings, a formulation given by Kutilek and Nielsen (Kutilek and Nielsen, 1994; Radinja et al., 2019) was adopted, as given in Eq. 3.17. This method has functional similarity with Zhang's method (Eq. 3.12). Comparing the

two expressions, the equation for K_s is given as in Eq. 3.18. The recommended value of parameter m is equal to 0.667 based on the literature (Fodor et al., 2011; Radinja et al., 2019).

$$I \approx C_1\sqrt{t} + mK_s t \tag{3.17}$$

$$K_s = \frac{AK_0}{m} \tag{3.18}$$

3.3.2. SATURO infiltrometer

The SATURO (METER Group, USA) is a recently developed fully automated dual-head infiltrometer to measure infiltration rates and K_s. Its components include an infiltrometer head, a control unit, and a tank for storing and supplying water (Figure 3.3). Its inner diameter is 14.4 cm, its insertion depth is 5cm, and it can produce infiltration in the wide range of 0.038 –1150 mm/h. SATURO is similar to a single-ring infiltrometer that calculates K_s using a modified two-ponding head approach (Reynolds & Elrick, 1990).

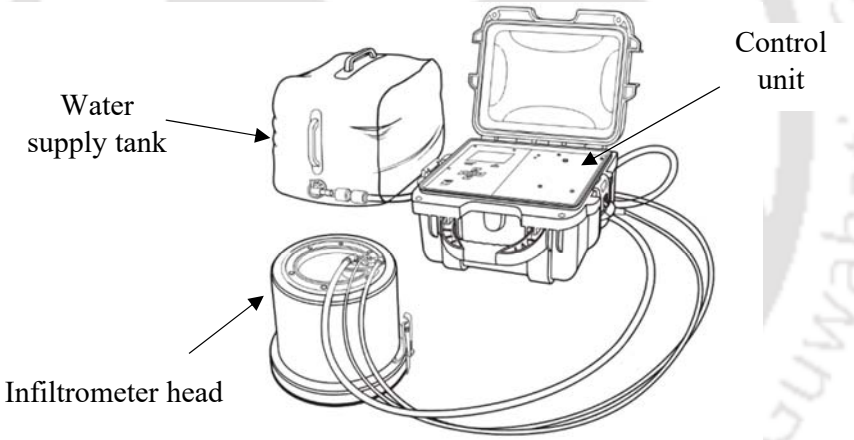

Figure 3.3 Schematic diagram of SATURO infiltrometer (Source: METER Group, USA)

For determining K_s using SATURO, the infiltration rate is measured at two different pressure heads created using air pressure without varying the steady ponding water depth (≈ 5 cm). The K_s value is calculated from the average of infiltration rates observed from the two complete pressure head cycles by using the equations given by Nimmo et al. (2009) as presented below:

$$K_s = \frac{i_s}{f} \tag{3.19}$$

Where i_s is the steady (final) infiltration rate, and f is the function that corrects for sorptivity and geometric effects. The correction factor f is given by Eq. (3.20), which takes into account the insertion depth of the infiltrometer (d), the radius of the infiltrometer (b_r), the water depth (D), and macroscopic capillary length of soil (λ or the reciprocal of the Gardner α_G (Wooding, 1968)).

$$f = 1 + \frac{\lambda + D}{L_1 d + L_2 b_r} = 1 + \frac{\lambda + D}{\Delta} \tag{3.20}$$

The correction factor takes care of the lateral divergence of the 3-dimensional flow and thus provides K_s corresponding to the 1-D flow condition (Nimmo et al., 2009; Reynolds and Elrick, 1990; METER Group, USA). Here Δ is a constant for given infiltrometer geometry (given by $L_1 d + L_2 b_r$) where L_1 and L_2 are equal to 0.993 and 0.578, respectively (Reynolds & Elrick, 1990). For two ponding depths, the Eqs. 3.19 and 3.20 can be combined and represented as Eq. 3.21, which can be further re-arranged to give Eq. 3.22. D_1 and D_2 refer to the high-pressure and low-pressure heads, respectively, and i_{s1} and i_{s2} are the corresponding infiltration rates. For SATURO, the flux values are recorded by its automated control unit.

$$K_s = \frac{i_{s_1}\Delta}{\Delta + \lambda + D_1} = \frac{i_{s_2}\Delta}{\Delta + \lambda + D_2} \tag{3.21}$$

$$K_s = \frac{\Delta(i_{s_1} - i_{s_2})}{D_1 - D_2} \tag{3.22}$$

3.3.3. Rainfall simulator (RS)

The rainfall simulator (RS) (Norwood instrument Ltd., Great Britain) is a flux-based method for determining the flow characteristics of soil under simulated rainfall conditions. The laboratory RS used in this study (shown in Figure 3.4) has a rectangular tank of an area of 1.82 m^2 and a depth of 0.25 m. The area of RS is sufficient to determine the average K_s value from the surface runoff under the ponding condition (Morbidelli et al., 2017). The other major components of RS include a storage chamber for supplying rainfall water, sprinkler-type nozzles for spreading rainfall, valves for regulating the flow, and a flowmeter to measure the supplied flow (Figure 3.4).

For RS experiments, the soil is first placed within the tank to the required level, followed by a supply of rainfall at the desired intensity. The RS used for the current study is

equipped with eight sprinkler-type nozzles, which allow the rainfall intensity to be simulated consistently across the whole soil surface. The simulated rainfall from the nozzles gradually saturates the soil, initiating runoff. For runoff collection, two tanks are provided on either side of the RS. The collected runoff is measured and used for further analysis. Water that infiltrates during the experiments is collected in a gravel drainage layer placed at the bottom of the tank.

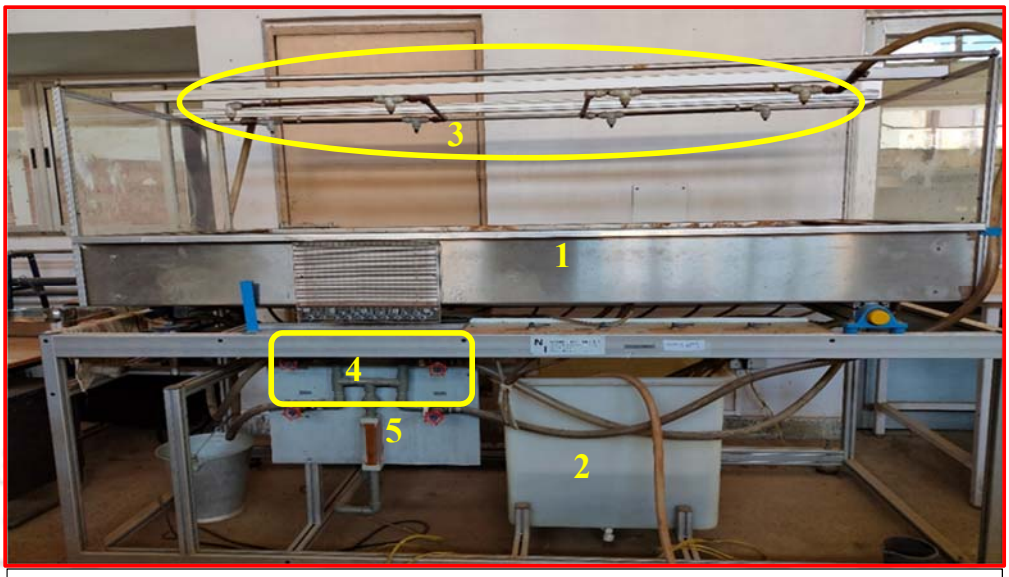

1- Tank for packing soil bed; 2- water storage chamber for rainfall; 3- eight nozzles for simulating rainfall; 4- valves for flow regulation; 5- flow meter for flow measurement

Figure 3.4 The laboratory rainfall simulator and its components

The infiltration measurements for RS are obtained by subtracting the runoff response from the applied rainfall (Gupta et al., 1993; Holden and Burt, 2002). The K_s values are determined with the help of two different methods, the Green-Ampt method (Green and Ampt, 1911) given by Eq. 3.23 and Philips method (Philip, 1957, 1969; Gupta et al., 1993) represented by Eq. 3.24 (Chow et al., 1988). Equations 3.23 and 3.24 are fitted to the measured CI versus time data from RS to obtain the best fit values of K_s.

$$K_s = \frac{1}{t}\left\{ I - \psi \Delta\theta \ln\left[1 + \frac{I}{\psi \Delta\theta}\right]\right\} \tag{3.23}$$

$$I = Pt + St^{\frac{1}{2}} \tag{3.24}$$

Here I is the cumulative infiltration obtained from RS measurements, ψ is the wetting front soil suction head, $\Delta\theta$ is the moisture deficit (difference between porosity η and initial

moisture content θ_i), parameter P is called the transmissivity factor, and S is the soil sorptivity. The K_s values are calculated from P using a multiplication factor of 3/2 (Youngs, 1968).

3.3.4. Laboratory falling-head permeameter (PM)

The laboratory falling-head permeameter (PM) test is a well-established method for determining K_s of soils based on the bulk flow of water through the soil mass. This method is simple and relatively inexpensive for the independent determination of K_s for various soil textures. These tests can be used to determine K_s for both fine-grained and coarse-grained soils using the standard procedures given in ASTM D5084. The soil sample is first saturated under a specific head condition (Figure 3.5). The water is then allowed to flow through the soil without adding more water, so the pressure head declines as water passes through the specimen. At different time intervals, the fall in the head of water is noted down. The calculation of K_s under the falling-head method is carried out using the following equation

$$K_s = \frac{a_p L_s}{a_s t_d} \ln\left(\frac{H}{H'}\right) \tag{3.25}$$

Where L_s is the length of the soil column, a_p and a_s are the cross-sectional areas of the standpipe and the soil column, respectively, t_d is the time interval to head drop, H is the total head before the test, and H' is the total head after the test. Cylinders of diameter 10 cm and height 18 cm are used in this study to carry out PM tests for various soils.

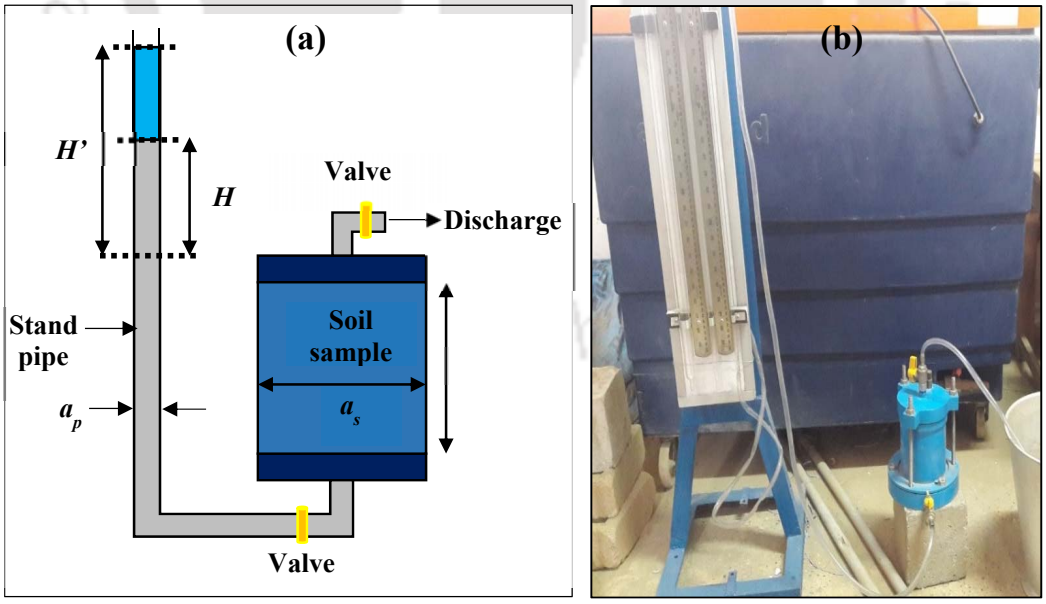

Figure 3.5 Falling head method (a) Schematic diagram and (b) Experimental Set up in laboratory

3.3.5. Soil moisture and soil water potential sensors

The initial soil suction (or soil water potential) and soil moisture content are important factors influencing infiltration measurements. The soil water potential (SWP) is measured using either TEROS 21 or tensiometer, depending on the soil type, and the volumetric water content (VWC) is measured using 5TM sensor.

3.3.5.1. TEROS 21

The TEROS 21 (Figure 3.6) used for the current study are made available by METER Group, USA. It is a dielectric water potential sensor that can measure soil water potentials in the range of -9 to -10^5 kPa (resolution of 0.1kPa) and temperature in the range of -40 to +60 °C (resolution 1°C, and accuracy ±1°C). TEROS 21 provides an accuracy of ± (10% of reading + 2 kPa) for SWP measurements in the range of -9 to -100 kPa. These sensors require very less power and are designed for a continuous and long-term recording of SWP for both field and laboratory measurements. During the experiments, the sensor's cable needs to be connected to a data logger (EM50, METER Group, USA) for continuous monitoring of its data.

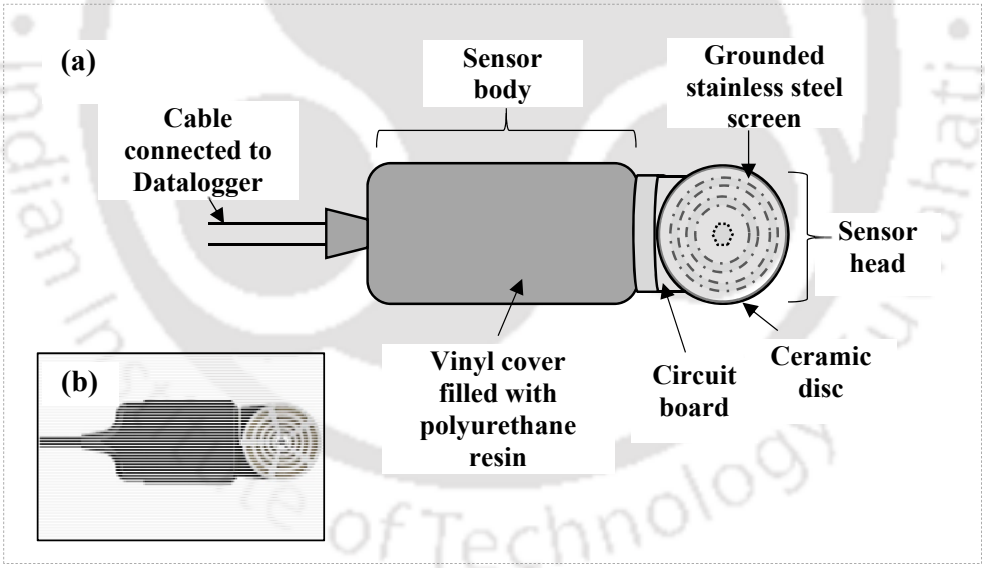

Figure 3.6 TEROS 21 sensor used for soil water potential measurements (a) Schematic diagram showing components and (b) actual image

TEROS 21 contains two porous ceramic discs sandwiched between stainless steel screens and the circuit board (Figure 3.6). These ceramic discs measure the water potential of soil. When TEROS 21 sensor is introduced into the soil, its ceramic discs come into hydraulic equilibrium with that of the water potential of the soil. Once in equilibrium,

measuring the water potential of ceramic discs gives the water potential of the soil. Originally, the TEROS 21 sensor measures the dielectric permittivity of its solid matrix (i.e., porous ceramic disc) depending on the water content of soil during the equilibration process. The dielectric permittivity value ranges from 1 for air to 80 for water. Based on this measured value, the water content is known, which is then converted to the corresponding SWP by using the soil moisture characteristics curve unique to the porous ceramic disc.

3.3.5.2. Tensiometer (T5)

The T5 Tensiometer (UMS, Munchen, Germany) works within a suction range of +100 to -85 kPa (accuracy ±0.5 kPa). Its working principle is similar to that of TEROS 21. The Tensiometer consists of a high air–entry, porous ceramic cup connected to a pressure measuring device through a small plastic tube. This water-permeable ceramic creates an ideal pore/water interface between the soil water and Tensiometer water. The soil water potential or the pore water pressure in the soil comes to equilibrium with the ceramic cup, and this is then directly translated from the ceramic cup to the pressure transducer, which offers a continuous signal. The Tensiometer runs out of water if the soil dries out and needs to be refilled as soon as the soil is adequately moist again.

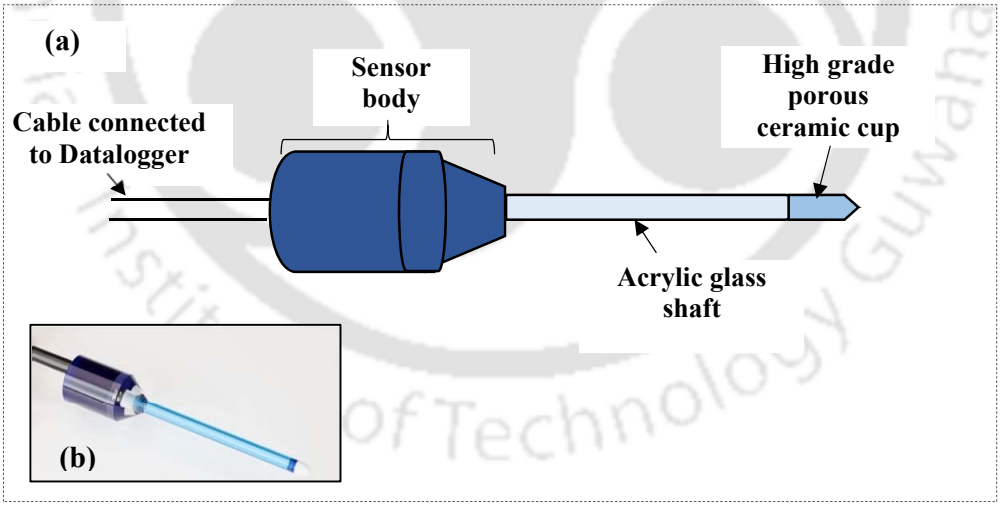

Figure 3.7 T5 tensiometer used for soil water potential measurements (a) Schematic diagram with components and (b) actual image

The sensor body (Figure 3.7) of the Tensiometer is made of acrylic glass. It consists of the pressure transducer and all electronic parts. The Tensiometer has a body made of acrylic glass (Figure 3.7), which contains all the electronic parts and the pressure transducer. The ceramic tip in the T5 tensiometer has an active surface of only 0.5 cm^2 and

a diameter of 0.5 cm. Due to its small dimensions, it offers quick response, minimal soil disturbance, and can be easily used for laboratory soil column measurements. Similar to TEROS 21, the T5 tensiometer needs to be connected to a data logger (DL6-te, UMS, Munchen, Germany) for continuous measuring of its readings.

3.3.5.3. 5TM sensor

The 5TM sensor (METER Group, USA) measures the volumetric water content of the soil by measuring its dielectric constant or permittivity using capacitance and frequency domain reflectometry technology. It uses an inbuilt oscillator running at 70 MHz and supplies the wave to the sensor prongs (dielectric sensor in Figure 3.8), which then charge according to the dielectric of the soil media or the stored VWC of soil. The stored charge is measured by the 5TM microprocessor, and the dielectric permittivity is produced as output. The polyurethane coating on the 5TM circuit board guards it against water damage and extends the sensor's life. The thermistor is provided for soil temperature measurements. The equilibrium time of the 5TM sensor is Instantaneous. It can measure VWC in the range of 0.0 to 1.0 m^3/m^3 with an overall general accuracy of ± 0.03 m^3/m^3. Data from 5TM can be continuously monitored with the help of EM50 (METER Group, USA) datalogger.

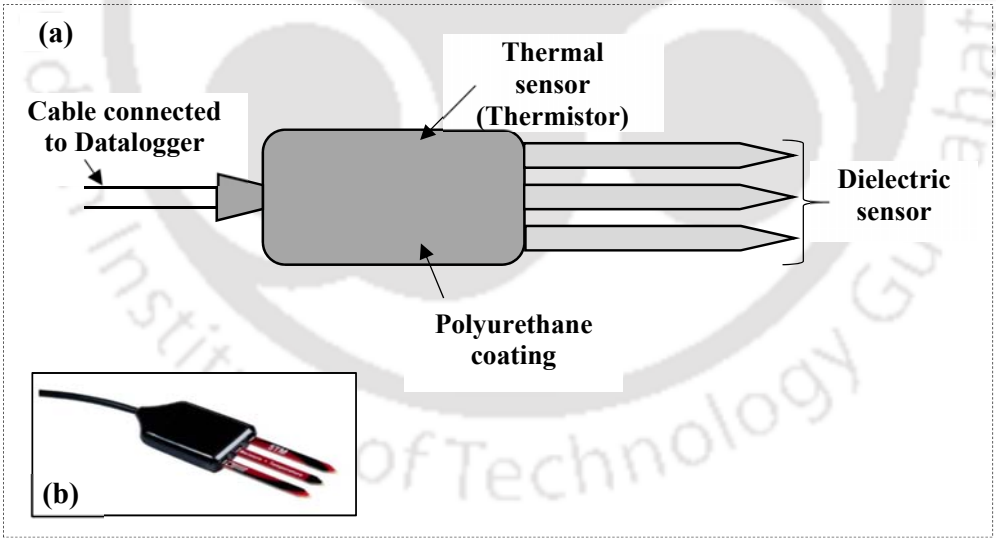

Figure 3.8 5TM sensor used for volumetric water content measurements (a) Schematic diagram showing components and (b) actual image

3.3.5.4. Calibration of the sensors

The T5 mini-tensiometers measure at an accuracy level of ± 0.5 kPa (≈ 0.05 m). These sensors are originally pre-calibrated with an offset of 0 kPa (when in a horizontal position) and

a linear response. This offset in the pressure transducer varies very little over time. The manufacturer (METER Group, USA) recommends inspecting the sensor once a year and recalibrating it once every two years. Before using, the tensiometers were checked for the offset of 0 kPa by using the procedure recommended in the user manual.

The TEROS 21 sensor was evaluated in the laboratory by Saha et al. (2020) to evaluate its accuracy. According to this study, TEROS 21 performed accurately for SWP measurements within the range of approximately 0.9 to 170 m. Beyond 170 m, some fluctuations were reported. This observation is in line with the manufacturer's (METER Group, USA) observation that TEROS 21 performed accurately with low sensor-to-sensor variability at least up to 150 m using laboratory evaluations and up to 200 m using field evaluations. It may be noted that in TEROS 21 sensor, the ceramic component used to measure SWP is factory calibrated. According to the manufacturer, the sensor is factory calibrated for an air-dry state corresponding to 10000 kPa (≈ 1000m). The measurement of SWP by TEROS 21 is dependent on the water retention characteristics and electrical properties of the ceramic component. Hence, its measurements are entirely dependent on the ceramic and are not soil-specific (METER Group, USA). As its measurement is not affected by the type of soil, hence, no soil-specific calibration is necessary.

The 5TM sensors have an overall accuracy of ± 0.03 m^3/m^3. However, the manufacturer (METER Group Inc., USA) recommends soil-specific calibration to improve its accuracy further. It may be noted that unlike TEROS 21, the calibration of 5TM sensors is entirely dependent on the soil in which it is inserted. The calibration equation is regulated by the electrical properties of the soil. Therefore, to maintain the accuracy of VWC sensors, it is ideal to perform soil-specific calibration. The 5TM sensors were calibrated for the various soils used in this study. The soils in which VWC measurements were made using 5TM sensors had different physical properties and were identified as sand, loam, silt loam, and silty clay loam textures. The details of the physical properties and particle size fractions of these soils are provided in the respective chapters.

A 5-point calibration (i.e., using five different target water content between 0% to 40%) was performed in the laboratory for the four discussed soils according to the procedure described in the literature (Shaikh et al., 2019). The computed VWC values from the measured gravimetric water content (w) (Eq. 3.5) were correlated to the sensor output (raw count). A scatter plot with the raw count on the x-axis and computed VWC on the y-axis was plotted to establish a mathematical calibration equation. Figure 3.9 depicts the measured data, the best-fit calibration equation, and the calibrated data for all the 5TM sensors and the four soils used

in this study. Depending on the soil, the calibrated equation obtained was later used to convert the measured raw count from 5TM sensors to the corresponding VWC.

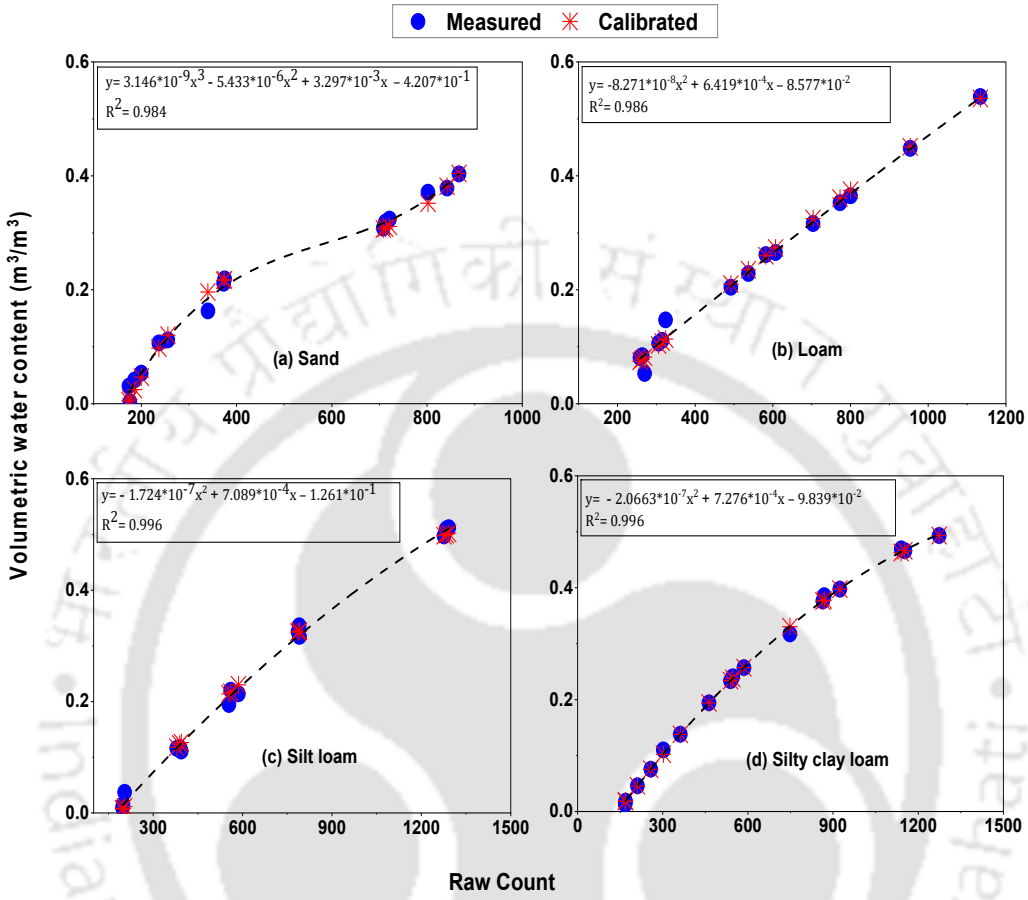

Figure 3.9 Soil specific calibration for the 5TM sensors for a) sand, b) loam, c) silt loam, and d) silty clay loam

3.4. Inverse flow modelling during infiltration

In addition to experimental evaluation, the current study investigates the soil water flow during infiltration inversely by employing numerical modelling technique. The inverse flow modelling was performed with the well-known HYDRUS 3D (version 3.01; Simunek et al., 2018) software. HYDRUS solves the following modified form of Richards' equation (Richard, 1931) given by Warrick (1992)

$$\frac{\partial\theta(h)}{\partial t}=\frac{1}{R}\frac{\partial}{\partial R}\left(RK(h)\frac{\partial h}{\partial R}\right)+\frac{\partial}{\partial z}\left(K(h)\frac{\partial h}{\partial z}\right)-\frac{\partial K(h)}{\partial z} \tag{3.26}$$

where h is the pressure head; $\theta(h)$ and $K(h)$ represent, respectively, the VWC and hydraulic conductivity as a function of h; z is the vertical coordinate (positive downward) and

R is the radial coordinate. The simulations require the use of soil water retention function, *θ(h),* and soil hydraulic conductivity function, *K(h)*, which are expressed using the popular van Genuchten-Mualem (VGM) constitutive relationships (Mualem, 1976; van Genuchten, 1980) (Eqs. 3.27 to 3.30).

$$\theta(h) = \begin{cases} \theta_r + \dfrac{\theta_s - \theta_r}{\left[1 + |ah|^n\right]^m} & h < 0 \\ \theta_s & h \geq 0 \end{cases} \tag{3.27}$$

$$K(h) = K_s S_e^l \left[1 - \left(1 - S_e^{1/m}\right)^m\right]^2 \tag{3.28}$$

$$m = 1 - \frac{1}{n}, \quad n > 1 \tag{3.29}$$

$$S_e = \frac{\theta - \theta_r}{\theta_s - \theta_r} \tag{3.30}$$

Where θ_s and θ_r are the saturated and residual VWC, respectively, *l* is the tortuosity parameter, *α,* and *n*, as mentioned previously (section 3.3.1.1), are the van Genuchten parameters that determine the shape of the retention curves, and S_e is the effective saturation. The parameter *α* is inversely related to air-entry suction, and *n* is inversely related to pore size distribution (Šimůnek et al., 2012). The VGM soil hydraulic models consist of six different parameters; θ_s, θ_r, *α, n, l,* and K_s. Depending on the requirement of the user, either all six parameters or any combination of the parameters can be fitted during the inverse simulation process to produce optimized model outputs.

The inverse parameter estimation involves minimizing an appropriate objective function, which expresses the discrepancy between the measured and estimated values (Kool & Parker, 1987; Nakhaei & Šimůnek, 2014; Simunek & van Genuchten, 1996). The objective function *Φ* to be minimized during the parameter estimation is given by Eq. 3.31 (Angulo-Jaramillo et al., 2016; Simunek & van Genuchten, 1996), where the sum of squared errors between the measured and the estimated values of the selected variable, *q* is reduced to the minimum by an iterative procedure.

$$\Phi(b,q) = \sum_{j=1}^{M} \left(v_j \sum_{i=1}^{N_j} w_{ij} \left[q_j(t_i) - q_j^*(t_i, b) \right]^2 \right) \tag{3.31}$$

The term on the right-hand side represents deviations between the measured $\left(q_j(t_i)\right)$ and estimated $\left(q_j^*(t_i,b)\right)$ time-dependent variables. These variables can be cumulative flux across a specific boundary at different time intervals, VWC and/or SWP measurements recorded at a particular depth or several depths in the soil, or a suitable combination of these variables. Here, M refers to the number of different sets of measurements, N_j is the number of measurements in a particular measurement, v_j and $w_{i,j}$ represents the weights associated with a particular measurement set j or a measurement i within set j, respectively. b represents the vector of optimized/fitted parameters. The minimization of the objective function (Eq. 3.31) is carried out using Levenberg-Marquardt (L-M) non-linear parameter estimation method (Marquardt, 1963). The L-M method is a weighted least-squares approach based on Marquardt's maximum neighbourhood method. It combines Newton's method (Schiesser, 2012) and the steepest descent method (Cauchy, 1847) and generates confidence intervals for the estimated parameters (Šimunek et al., 2012; Šimůnek & van Genuchten, 1996).

The details of the flow geometry, initial conditions (IC), boundary conditions (BC), and all other relevant information are provided in the respective chapters involving numerical modelling.

Chapter 4

Relationship between imposed tension in MDI and the resulting hydraulic parameters

4.1. Introduction

The infiltration rate from a tension disc infiltrometer into the soil depends on several factors. Among these factors, the suction or negative pressure head (h_0) set in the infiltrometer disc controls or restricts the flow of water into the soil. For a higher h_0, the restriction is more, and hence, the flow rate is less. The traditional version of tension disc infiltrometers (TI) offers a larger range of suction between 0 and 20 cm, while its miniature version, i.e., mini disc infiltrometer (MDI), offers a limited range of negative pressure between 0.5 and 6 cm. The small size of MDI offers several technical advantages over the conventional TI, including easy portability, quick installation, and less water requirement. Because of these advantages, MDI's applicability has increased wide fold in recent years (Li et al., 2004; Lewis et al., 2006; Homolak et al., 2009; Ronayne et al., 2012; Ghosh and Pekkat, 2019) despite its limited range of suction.

It may be noted that the disc infiltrometers were solely developed to provide restriction to water flow so as to allow only soil matrix flow and prevent preferential flow (Minasny and George, 1999; Kohne et al., 2011; Angulo-Jaramillo et al., 2016; Bordoloi et al., 2018; Radinja et al., 2019). Thus, for disc infiltrometer measurements, the role of the h_0 set in the device is deemed crucial. It is essential to assess the influence of h_0 on the infiltration measurements and subsequent determination of hydraulic parameters. This chapter studied the influence of this marginal range of suction in MDI (0.5 to 6cm) on the infiltration rate and the estimated soil hydraulic parameters.

Understanding the role of supplied suction is essential for MDI because of two primary reasons; i) the mathematical formulation used to analyse soil hydraulic parameters is explicitly dependent on h_0 (Zhang's method, Zhang, 1997a, b), and ii) the value of h_0 can be regarded negligible as compared to the inherent suction in the near dry state of the soil where the latter can go up to several meters. Therefore, an attempt was made in this study to exclusively evaluate and understand the influence of h_0 on

a) infiltration measurements from the device and the
b) estimated soil hydraulic parameters, namely soil hydraulic conductivity (K_0) and sorptivity (S_0).

4.2. Experimental Methodology

This objective was accomplished with the help of both in-situ and laboratory MDI measurements. In both cases, four different suction values, 0.5, 2, 4, and 6 cm, were used, and their influence on the infiltration measurements and soil hydraulic parameters were evaluated.

4.2.1. Field experiment

The in-situ experiments with MDI were carried out in an agricultural field located at Dadara, Kamrup (26.21°N 91.63°E), located on the northern bank of the Brahmaputra river and approximately 10 km away from the IIT Guwahati campus. The experiments were conducted for seven different months from September 2018 to March 2019 (Table 4.1) and covered mainly three seasons of the region; post-monsoon, winter, and pre-monsoon. A total of 11 field measurements were made during this entire period. For the field experiments, MDI and the required amount of water in a container were taken to the specific location. The agricultural site chosen in this study is generally utilized all year long for growing seasonal vegetables and plants (e.g., Cucumis sativus, Trichosanthes cucumerina, Trichosanthes dioica, and Spinacia oleracea). However, proper care was taken to select the locations which experienced no tilling practices and least possible intervention due to human activities.

During each field visit, an area of approximately 0.5 m^2 was first cleared for vegetation cover, the top soil was removed up to nearly 10 cm, and plant roots, if any, were removed. The soil surface was then levelled for any undulation. Water was filled inside MDI's upper and lower chambers (section 3.3.1) and placed on the levelled soil surface. To begin the experiment, MDI was first set to a desired h_0 of 0.5 cm by adjusting the suction control tube in its upper chamber. The reading in its reservoir chamber (in ml) was then noted, and MDI was placed on the soil surface. As soon as MDI was placed on the soil, water from its reservoir chamber started flowing out through its porous disc base. The drop in the water volume was recorded at regular intervals, and the time was monitored with the help of a stopwatch. The experiment was conducted for nearly 1 hour or till a near steady-state infiltration rate was attained. Similar experiments were also conducted with the other three suction values (2, 4, and 6 cm), and for each suction, three repetitions were carried out. All the experiments were conducted within the cleared area (0.5 m^2) to avoid any significant variations in the initial condition. For each experiment, a new location was selected, and sufficient distance was maintained between all

the locations to avoid the influence of one measurement on another. Nearly 12 experiments were conducted during a single field visit, and as such, a total of 132 experiments were conducted in the field using MDI.

The experimental setup in the field is shown in Figure 4.1a. The initial and final moisture content values were recorded for all the field experiments. The initial water content w_i was uniform for the whole area where the experiments were conducted. Soil samples were collected from the experiment sites in 4 small containers before starting the experiments to determine w_i using the oven drying method (section 3.2.4). The calculated average values are provided in Table 4.1. To measure the final water content w_f, soil samples were collected from below the MDI disc after the completion of each experiment, and the average values corresponding to each h_0 were calculated separately. Besides soil moisture, the in-situ soil density was also obtained using the core cutter method (IS 2720-part 29). Three soil samples were collected using the core cutters, and the average density was determined.

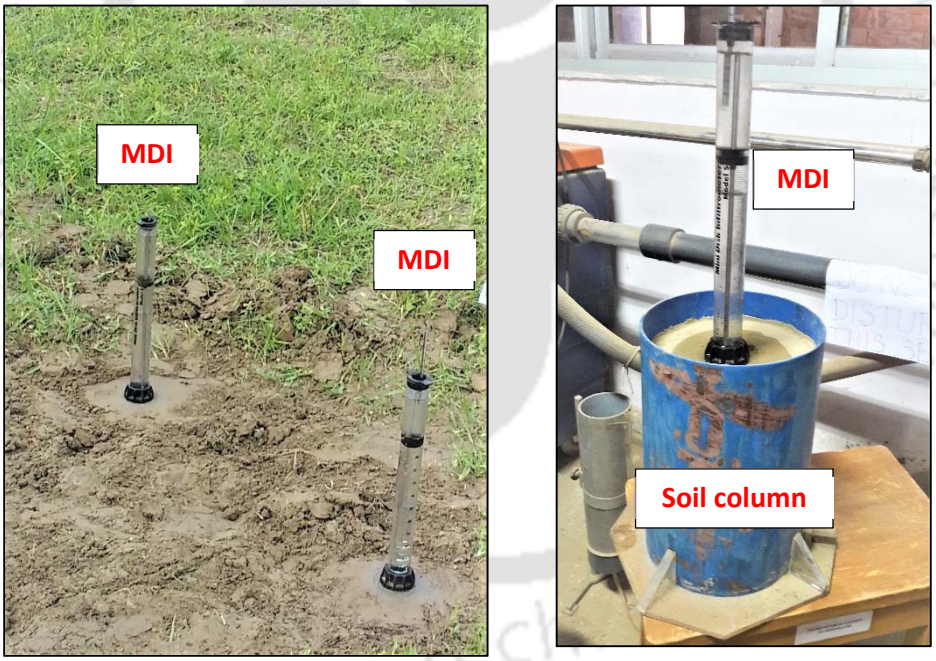

Figure 4.1 a) Field and b) laboratory experiments using Mini disc infiltrometer (MDI)

Table 4.1 Details of field experiments from September 2018 to March 2019

Month	Exp no.	Average γ_d (g/cm^3)	Average w_i (%)	Average w_f (%)			
				0.5	2	4	6
September	1	1.48	26.36	27.97	26.48	27.21	30.09
October	2	1.52	25.76	31.36	31.32	28.44	29.59
October	3	1.43	22.06	32.03	30.49	33.48	29.30
November	4	1.41	22.31	29.17	37.05	31.15	26.41
December	5	1.33	22.31	29.17	37.05	31.15	26.41
December	6	1.52	25.34	29.13	28.76	26.45	29.73
January	7	1.49	23.70	27.06	30.84	27.85	27.01
January	8	1.42	13.60	30.04	26.24	24.20	27.09
February	9	1.42	21.11	31.64	35.07	29.74	27.50
February	10	1.45	17.17	32.78	29.85	29.20	28.17
March	11	1.40	20.24	32.52	32.91	29.89	30.78

γ_d – dry density, w_i – initial gravimetric water content, w_f – final gravimetric water content obtained at the end of the experiment

4.2.2. Laboratory experiment

Aside from h_0, the prevailing compaction state (i.e., the initial soil moisture, w_i, and soil dry density, γ_{di}) can influence the infiltration results during field tests. Additionally, the inherent uncertainties in the field (presence of cracks below the disc and other preferential flow paths) can considerably influence the interpretation of infiltration measurements. As a result, evaluating the influence of only supplied h_0 on infiltration characteristics becomes challenging from the measurements of field experiments. To overcome this limitation, laboratory experiments were carried out using MDI using controlled known initial conditions. Unlike field tests, the initial compaction conditions (w_i and γ_{di}) can be regulated during laboratory experiments, thus allowing evaluation exclusively for the supplied h_0.

The same agricultural soil (AS) was collected from the field site in sufficient quantity to conduct laboratory experiments. The soil was first cleaned for the presence of any debris and plant roots and sieved through a 4.75mm IS sieve to remove unwanted particles and boulders. Following this, its physical properties, including particle size analysis, soil texture classification, moisture content, and specific gravity were determined in the laboratory (ASTM D2487-11; IS 2720) using the methodology described in section 3.2. The details of its properties are provided in Table 4.2. Based on the USDA soil classification system, this soil was identified as silty clay loam (SCL) texture.

Table 4.2. Details of physical properties of the agricultural soil

Soil Name	Particle size fraction (%)				Soil type based on USDA	Specific Gravity
	Gravel (> 2 mm)	Sand (2-0.05 mm)	Silt (0.05-0.002	Clay (< 0.002 mm)		
Agricultural soil (AS)	0	16	57	27	Silty clay loam (SCL)	2.72

The experiments in the laboratory were conducted using PVC moulds of diameter 30 cm and height 20 cm (Figure 4.1b). The size of the mould was decided based on literature (Bordoloi et al., 2018) so that there is no boundary effect on MDI measurements. Three different initial water contents (0%, 5%, and 15%) and dry densities (1.3, 1.4, and 1.6 g/cm^3) were chosen to conduct the laboratory experiments. The AS was manually compacted inside the mould using a rammer of 1.7 kg. The soil was compacted in three layers by giving an equal number of blows per each layer. The number of blows per layer was established by trial and error and depended on the target compaction state of the soil. A higher γ_d represented higher compaction and required more number of blows. For each w_i, the soil was compacted to attain target dry densities of 1.3, 1.4, and 1.6 g/cm^3 separately, and accordingly, the number of blows was adjusted. The w_i of 0% represented the oven-dried state of the soil, while the 5% and 15% represented the medium and near-wet states of the soil, respectively. It may be noted that γ_d of 1.6 g/cm^3 was difficult to attain for a w_i of 15% due to higher initial water content; hence only 1.3 and 1.4 g/cm^3 were used.

Once the soil compaction was over for a given experiment, the weight of the soil-filled column was measured to calculate the bulk density, and its initial water content was recorded by the oven drying method (section 3.2.4). Using these values and Eq. 3.3, the dry density of the sample was determined. This was done to verify whether the achieved compaction state was identical to the targeted values. For each compacted state of the soil, the MDI measurements were performed for the four h_0, 0.5, 2, 4, and 6 cm. Also, the initial condition of the soil sample was kept identical for every h_0. All the experiments were repeated three times to ensure consistency in measurements. A total of 96 laboratory experiments were conducted using MDI for AS.

4.2.3. Transient analysis of soil hydraulic parameters

The near-surface near-saturated soil hydraulic parameters hydraulic conductivity (K_0) and sorptivity (S_0), corresponding to supplied h_0, can be analysed from the transient infiltration response of MDI using various methodologies discussed in section 3.3.1.1. However, in the absence of a code of practice for MDI, neither of the existing methods has been standardised. Several researchers in the past have used Zhang's method (Zhang, 1997a, b) (ZH) to analyse transient measurements from MDI (Li et al., 2004; Lichner et al., 2007; Ronayne et al., 2012; Gadi et al., 2017) while a few have additionally used Haverkamp method (Haverkamp, 1994) (HV) to analyse the same (Dohnal et al., 2010; Ghosh and Pekkat, 2019c, d). Both these methods are based on fitting Philips's two-term infiltration equation (Philips, 1957; 1969) to cumulative infiltration data to determine the coefficients C_1 and C_2, which are later used to calculate K_0 and S_0. In this study, MDI measurements were analysed and interpreted using these two popular transient methods, the HV and ZH (Haverkamp et al. 1994, Zhang, 1997a, b) (section 3.3.1.1), to understand the role of h_0 on estimated parameters. The soil used was of silty clay loam texture with n = 1.23 (<1.35). Thus, the modified ZH expression proposed by Dohnal et al. (2010) (DH method) was additionally used for this soil (section 3.3.1.1).

4.3. Results and discussion

4.3.1. Infiltration measurements

The cumulative infiltration (CI) measurements from MDI corresponding to four different h_0 (0.5, 2, 4, and 6 cm) are shown in Figure 4.2. Figures 4.2 a, b, and c represent the CI vs. time plots for three different field experiments, and e, f, and g represent the CI vs. time plots for three laboratory experiments. The three field experiments correspond to 3 different months, November, January, and March, one each from post-monsoon, winter, and pre-monsoon periods. The three laboratory experiments shown here correspond to three different water contents (0, 5, and 15%) and a fixed γ_d value (≈ 1.4g/cc). The chosen γ_d was closest to the γ_d of field experiments for the three months (Exp 4, 8, and 11 in Table 4.1). A total of 228 experiments (132 field and 96 lab) were conducted using MDI. For the sake of brevity, all the CI versus time response is not presented here.

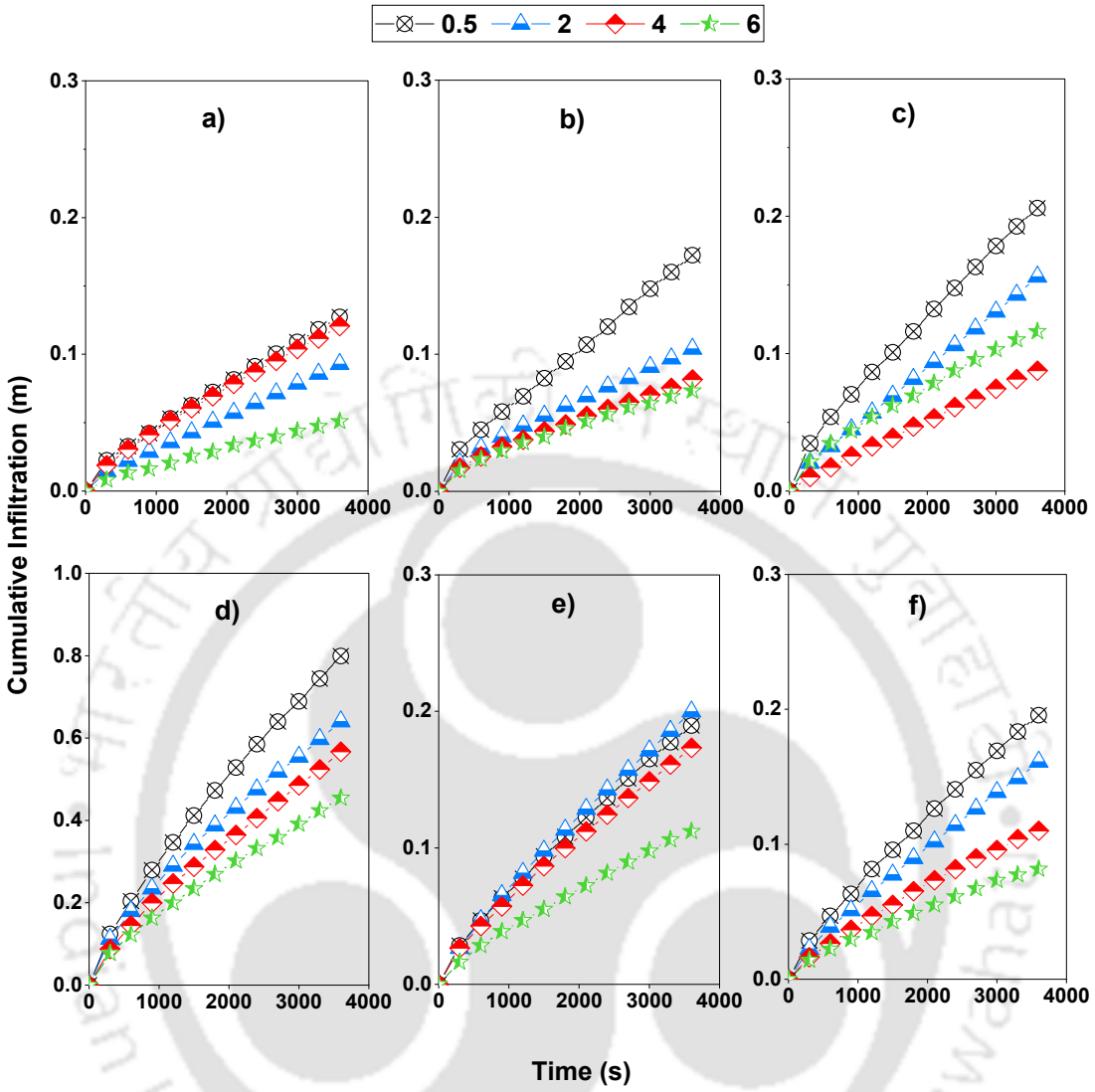

Figure 4.2 Cumulative infiltration versus time response for a) to c) 3 field measurements and d) to f) laboratory measurements

As seen in the figures, the use of four different h_0 has resulted in four different CI curves, indicating a clear influence of suction on CI measurements for both field and lab experiments. This implies that the small h_0 of MDI is able to influence the infiltration measurements. It is also noteworthy that even a small difference in the magnitude of h_0 was able to invoke variations in the infiltration measurements from MDI. A general visible trend was that the CI values decreased with an increase in the h_0. This pattern was clearly noted in a few of the experiments (e.g., Figure 4.2b, d, and f). However, the pattern was not prominent, and deviations were seen for nearly 63% of the field cases and 66% of the laboratory cases. Based on these plots, the relationship between h_0 and CI was not explicit in most cases. For

field cases, such test results were justified since the generated infiltration characteristics were the outcome of the interplay of several existing unknown factors (e.g., preferential pathways, texture inconsistency, local-scale heterogeneity, and flow anisotropy), which are inevitable to control. However, the experiments in the laboratory were carried out under controlled initial conditions by minimising the above unwanted factors and by regulating the water content and dry densities exclusively to assess the influence of h_0 on MDI measurements. Irrespective of the controlled measures, however, the results were not very promising in most cases. While the exact factors contributing to the disparity are unknown, the manual error while recording dropdown volume in MDI and the oscillations in disc water pressure due to air bubble release may be considered two possibilities (Dohnal et al., 2010).

It is essential to understand how the variability in CI (attributed to h_0) versus time influenced the estimated hydraulic parameters, S_0 and K_0. As discussed already, the two methods, HV and ZH, were used to analyse these parameters. Additionally, a third method (DH) was used for K_0 measurements since the criteria of $n < 1.35$ was satisfied for the soil.

4.3.2. Transient analysis of infiltration measurements

4.3.2.1. Field experiments

The mean S_0 and the corresponding standard deviation (SD) (as error bars) for various h_0 calculated using HV and ZH methods for the field experiments are presented in Figures 4.3a and b. Similarly, the estimated mean K_0 and its corresponding SD using HV, ZH, and DH methods are plotted in Figures 4.4 a, b, and c, respectively. The descriptive statistics (mean, SD, standard error, coefficient of variation (CV), minimum, and maximum) for the estimated S_0 and K_0 are listed in Tables 4.3 and 4.4, respectively. By varying the h_0 from 0.5 to 6 cm, the percentage relative difference (RD) in the estimated S_0 and K_0 are also listed in the tables. The RD is calculated by Eq. 4.1, where $P_{0.5}$ and P_s represent the mean estimated parameter value at $h_0 = 0.5$ cm and its corresponding value for any other h_0 (2 or 4, or 6 cm).

$$\text{Relative difference} = \left(\frac{P_{0.5} - P_s}{P_{0.5}} \right) \times 100\% \tag{4.1}$$

From Figure 4.3, it was noted that, unlike CI measurements, the mean S_0 showed a marginal decreasing trend with increasing h_0 for both analysis methods. A similar decreasing trend was also witnessed in the case of mean K_0 estimated using all three evaluation methods (Figure 4.4). For any given method, the overall variations in mean S_0 and K_0 with respect to h_0 were not very prominent and ranged within only one order of magnitude. This can also be

observed from the mean and the RD values in Tables 4.3 and 4.4. For all the evaluation methods, the calculated RD was < 60% when h_0 was varied from 0.5 to 6 cm. Given that there is hardly any variation in the order of magnitude, the RD of 60% is not a significant difference in the case of S_0 and K_0.

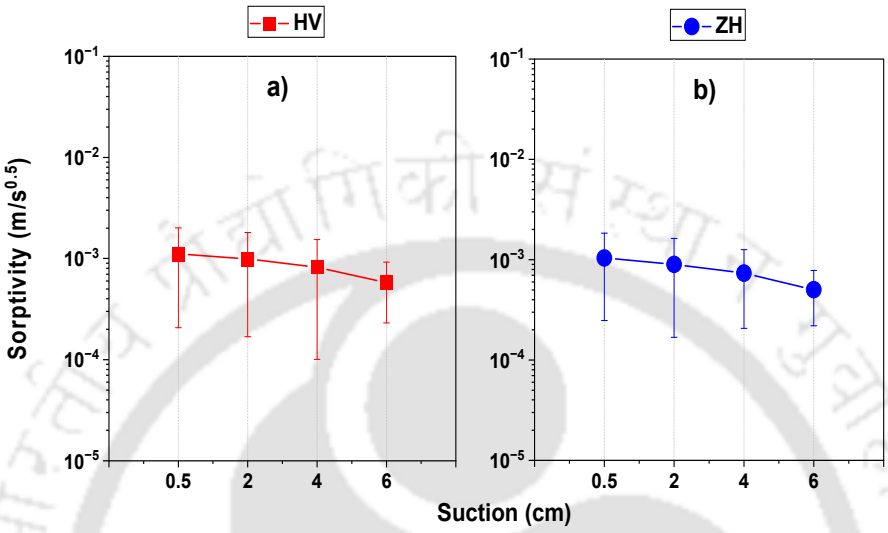

Figure 4.3 Variation of estimated sorptivity (mean) for the four different suctions evaluated using a) Haverkamp (HV) and b) Zhang (ZH) methods for field tests

Figures 4.3 and 4.4 and Tables 4.3 and 4.4 show that the standard deviations in the case of S_0 were relatively higher than that of the K_0. It is to note that S_0 (or capillary force) is prominent when the initial condition of soil is dry (Vandervaere et al., 2000a, b; Angulo-Jaramillo et al., 2016). During the field tests, the initial conditions of the soil were relatively wet (Table 4.1). Therefore, the infiltration process was primarily driven by gravity or the K_0 component of flow compared to the S_0 component (Bagarello and Iovino, 2003; Vandervaere et al., 2000b). Such conditions make the determination of the K_0 parameter more reliable compared to S_0 (Bagarello and Iovino, 2003). Subsequently, the estimation of K_0 was more consistent than S_0, as noted by the relatively lower SD and CV values for the former (Tables 4.3 and 4.4).

It was seen that the mean S_0 from both HV and ZH methods were nearly the same in magnitude (Figure 4.3 and Table 4.3). This is to note that S_0 from the ZH method differs from that of the HV method by a factor of A_1 only (Eq. 3.7 and 3.10). The calculated A_1 (Eq. 3.13) for field experiments were close to unity (i.e., in the range of 0.58 to 1.49); hence, the estimated results were identical. Further, it was observed that the K_0 from the three methods showed identical tend (Figure 4.4). However, they differed in their magnitudes, with K_0 from the HV

method being the highest, followed by the ZH and the DH methods. The discrepancy in the K_0 values was mainly due to the difference in the mathematical formulations (Chapter3, section 3.3.1.1). Unlike the HV method (Eq. 3.8), the ZH and DH methods involve the division of the empirical constant A_2 in their expressions (Eq. 3.11, 3.15, and 3.16). Consequently, the estimated K_0 from these two methods were relatively lower than the HV method. The ZH and DH methods were functionally similar (Eq. 3.11, 3.15, and 3.16); however, the computed A_2 for the two methods were different. Depending on the h_0, the A_2 ranged between 7.9 to 10.4 for the ZH method and 19.3 to 20.8 for the DH method. As a result of higher A_2 for the DH method, its estimated K_0 was relatively lower than the ZH method, as seen in Figure 4.4.

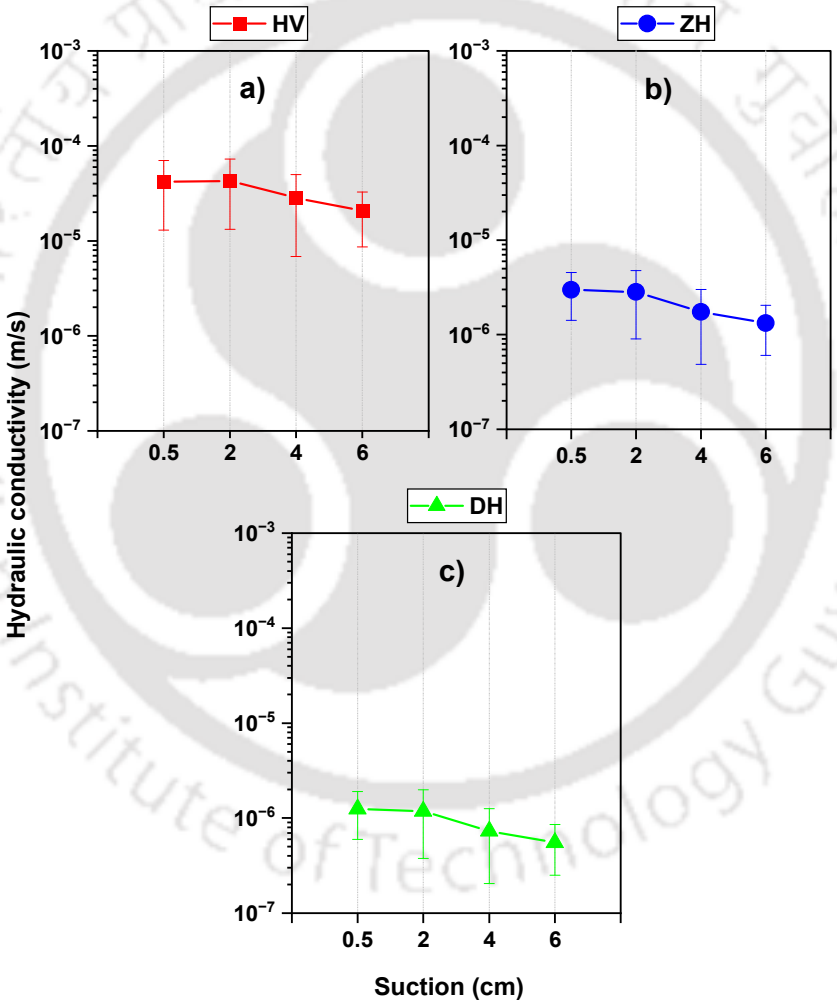

Figure 4.4 Variation of estimated hydraulic conductivity (mean) for the four different suctions evaluated using a) Haverkamp (HV), b) Zhang (ZH), and c) Dohnal (DH) methods for field test

Table 4.3. Descriptive statistics of near-saturated sorptivity (S_0) calculated using Haverkamp (HV) and Zhang (ZH) methods from field measurements

Method	**HV**				**ZH**			
Suction (cm)	**0.5**	**2**	**4**	**6**	**0.5**	**2**	**4**	**6**
*Mean	1.1E-03	9.9E-04	8.2E-04	5.8E-04	1.0E-03	9.0E-04	7.3E-04	5.0E-04
*Standard Deviation	9.0E-04	8.2E-04	7.2E-04	3.5E-04	7.9E-04	7.3E-04	5.3E-04	2.8E-04
*Standard Error	1.9E-04	1.8E-04	1.5E-04	7.4E-05	1.7E-04	1.6E-04	1.1E-04	6.0E-05
Coefficient of variation (%)	81.3	83	87.7	59.9	76.3	81.2	71.8	56.2
*Minimum	2.5E-04	1.9E-04	1.6E-04	1.8E-04	2.8E-04	1.6E-04	1.4E-04	1.8E-04
*Maximum	4.3E-03	3.6E-03	2.8E-03	1.3E-03	3.5E-03	3.1E-03	2.2E-03	1.2E-03
Relative Difference (%)	-	10.7	25.9	48.1	-	13.8	29.5	51.8

* units in $m/s^{0.5}$

Table 4.4. Descriptive statistics of near-saturated hydraulic conductivity (K_0) calculated using Haverkamp, Zhang, and Dohnal methods from field measurements

Method	**HV**				**ZH**				**DH**			
Suction (cm)	**0.5**	**2**	**4**	**6**	**0.5**	**2**	**4**	**6**	**0.5**	**2**	**4**	**6**
[#]Mean	4.2E-05	4.3E-05	2.8E-05	2.1E-05	3.0E-06	2.8E-06	1.7E-06	1.3E-06	1.2E-06	1.2E-06	7.3E-07	5.5E-07
[#]Standard Deviation	2.9E-05	3.0E-05	2.2E-05	1.2E-05	1.6E-06	1.9E-06	1.3E-06	7.2E-07	6.5E-07	8.1E-07	5.2E-07	3.0E-07
[#]Standard Error	6.1E-06	6.3E-06	4.6E-06	2.6E-06	3.3E-07	4.1E-07	2.7E-07	1.5E-07	1.4E-07	1.7E-07	1.1E-07	6.4E-08
Coefficient of variation (%)	68.8	69.1	76	58.2	52.2	68.2	72.1	54.5	52.2	68.2	71.8	54.5
[#]Minimum	1.1E-05	6.4E-06	7.2E-06	2.0E-06	7.9E-07	5.2E-07	2.6E-07	3.7E-07	3.3E-07	2.2E-07	1.1E-07	1.5E-07
[#]Maximum	1.1E-04	1.2E-04	8.4E-05	4.3E-05	6.3E-06	7.2E-06	6.4E-06	2.6E-06	2.6E-06	3.0E-06	2.7E-06	1.1E-06
Relative Difference (%)	-	-3.5	31.5	50.3	-	5.0	41.7	55.7	-	5.0	41.5	55.7

[#] units in m/s

4.3.2.2. Laboratory experiments

The main intention of conducting laboratory experiments was to minimise the contribution of factors influencing the infiltration measurements from MDI. This would aid in evaluating the relationship of estimated parameters (S_0 and K_0) with h_0 only. This was accomplished by regulating the soil's initial conditions (w_i and γ_d) to maintain a homogenous and uniform state during infiltration experiments. Compaction in the laboratory mould also ensured that there were no hidden or unknown preferential flow paths beneath the disc. Similar to field experiments, the laboratory measurements were also analysed using the discussed methods (HV, ZH, and DH) for four different h_0 values. First, the influence of varying γ_d and h_0 on the estimated parameters was studied at a fixed initial w_i. Next, the influence of varying w_i and h_0 was studied for a given initial γ_d. The plots from these two cases are presented in Figures 4.5 to 4.8. For three different w_i, the estimated mean S_0 and K_0 are provided in Figures 4.5 and 4.6, respectively. Similarly, for the three different γ_d, Figures 4.7 and 4.8 present the estimated mean S_0 and K_0 values.

It was observed from Figures 4.5a, b, and c that for a given w_i, there was a marginal decrease in the calculated S_0 for increasing h_0, using the HV (S_{HV}) method. The trends were similar for S_0 calculated using the ZH method (S_{ZH}) as well (Figures 4.5d, e, and f). In all six cases (Figures 4.5a to f), the variations in S_0 due to different h_0 were well within a single order of magnitude. Moreover, for the three different γ_d considered at a fixed w_i and h_0, the calculated S_0 were fairly comparable. Similar to the results of sorptivity, the K_0 calculated at a fixed w_i and varying γ_d (Figure 4.6a to i) also showed a decreasing trend with respect to the increasing h_0. It was also noted that the K_0 calculated using all three methods (K_{HV}, K_{ZH}, and K_{DH}) reported similar patterns in their observations.

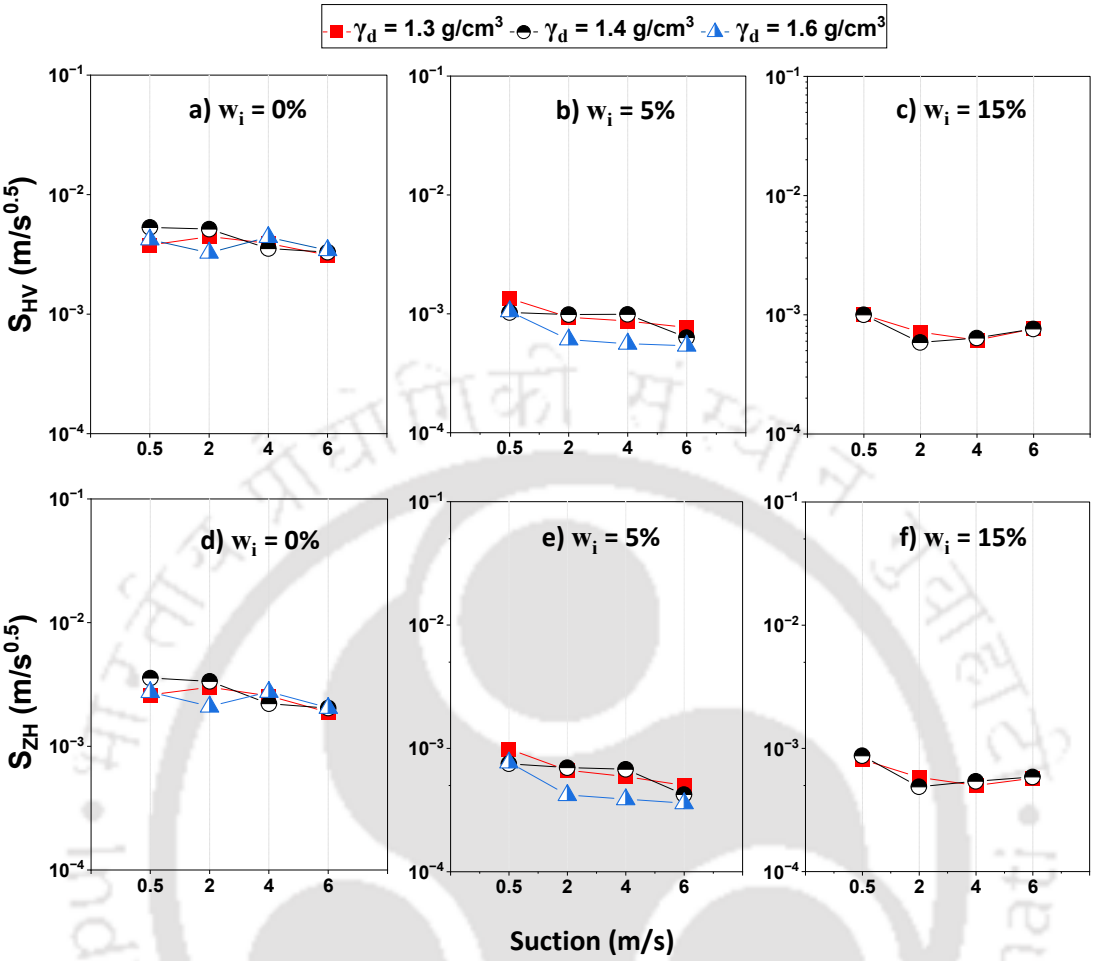

Figure 4.5 Variation of estimated sorptivity (mean) with four different suctions and three different initial water contents (0, 5, and 15%) evaluated using a), b), and c) Haverkamp (HV), and d), e), and f) Zhang (ZH) methods for laboratory test

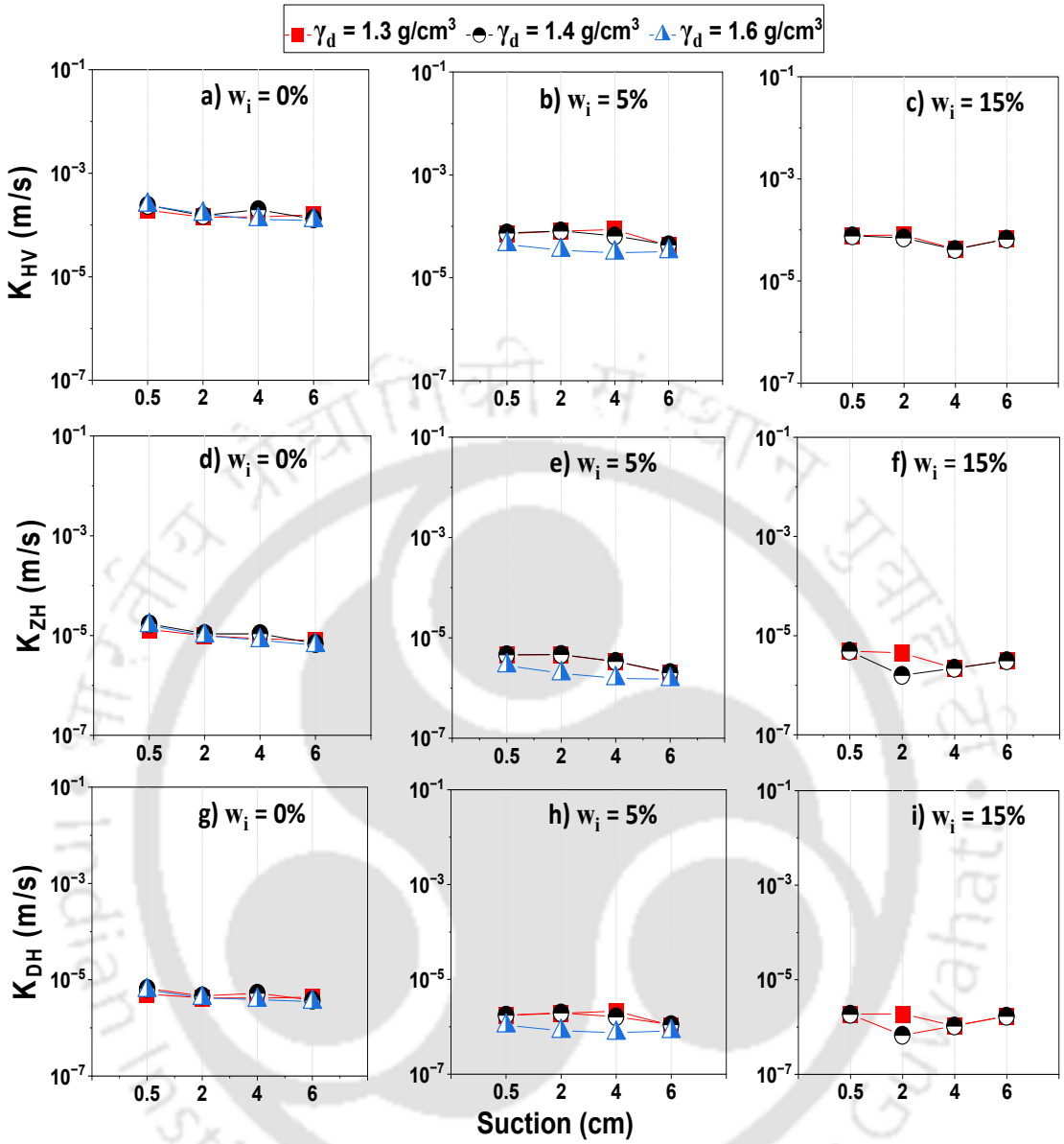

Figure 4.6 Variation of estimated hydraulic conductivity (mean) with four different suctions and three different initial water contents (0, 5, and 15%) evaluated using a), b), and c) Haverkamp (HV), d), e), and f) Zhang (ZH), and g), h), and i) Dohnal (DH) methods for laboratory tests

Figures 4.7 and 4.8 showed that, for a fixed γ_d, an increase in w_i resulted in a decrease of the calculated parameters (S_0 and K_0) at any h_0. The S_0 and K_0 in both the figures were consistently higher for the w_i of 0% than the other two w_i values. For K_0, these differences were marginal (< one order) (Figure 4.8), while for S_0, such differences were noticeable with values ≥ one order (Figure 4.7). Although a clear influence of the lowest w_i was seen on the estimated parameters, no such distinction was visible for the other two higher w_i. As mentioned earlier,

lateral capillary forces predominantly govern the flow when the soil's initial condition is dry. However, such influence is not very prominent in the case of the moist initial state of the soil. Consequently, higher S_0 was reported for w_i = 0% compared to the other two cases with wetter w_i values (5 and 15%). The figures also reported that in a few of the cases, a rise in h_0 resulted in almost no change or a slight increase in the predicted parameters, S_0 and K_0, at a fixed w_i. However, a general pattern showing a decrease in parameter estimates for increasing h_0 was noted in these figures, similar to the observations in Figures 4.5 and 4.6. For a better understanding of the results, quantitative analysis was needed, and therefore, the RD values were calculated (Eq. 4.1).

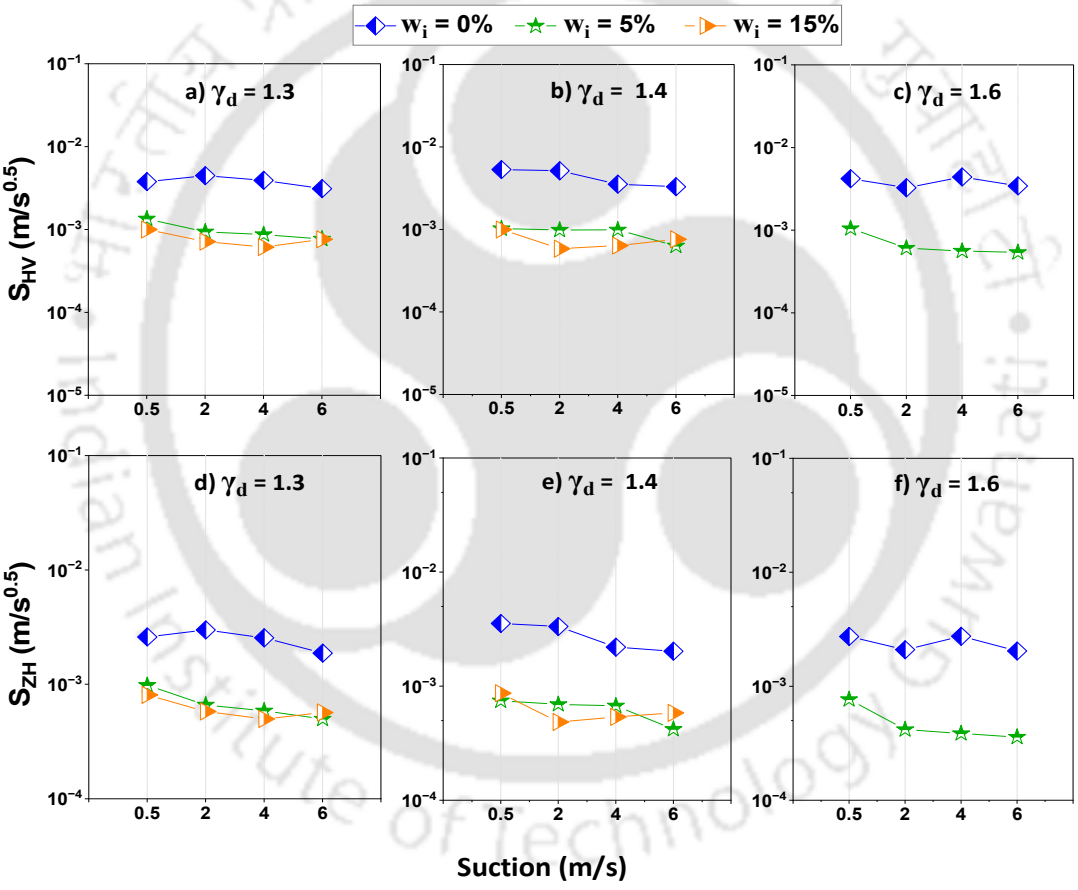

Figure 4.7 Variation of estimated sorptivity (mean) with four different suctions and three different dry densities (1.3, 1.4, and 1.6 g/cc) evaluated using a), b), and c) Haverkamp (HV), and d), e), and f) Zhang (ZH) methods for laboratory tests

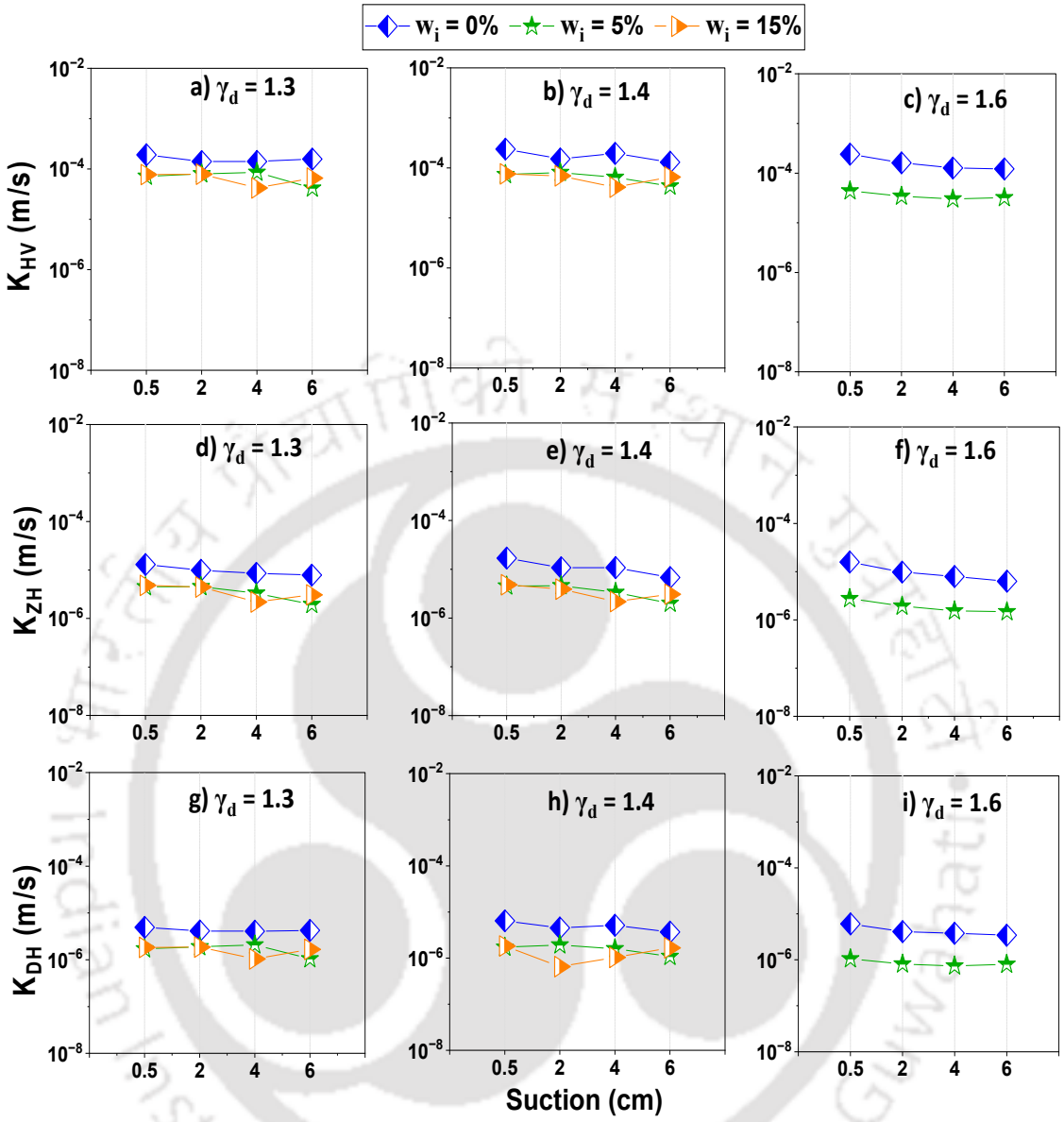

Figure 4.8 Variation of estimated hydraulic conductivity (mean) with four different suctions and three different dry densities (1.3, 1.4, and 1.6 g/cc) evaluated using a), b), and c) Haverkamp (HV), d), e), and f) Zhang (ZH), and g), h), and i) Dohnal (DH) methods for laboratory tests

Table 4.5 lists the RD values (in %) between the estimated parameters for various evaluation methods and initial compaction states when h_0 is varied from 0.5 cm to 2, 4, and 6 cm ($RD_{0.5\text{-}2}$, $RD_{0.5\text{-}4}$, $RD_{0.5\text{-}6}$). For a consistent decreasing pattern in the parameters with respect to increasing h_0, the values should be in the order $RD_{0.5\text{-}2} < RD_{0.5\text{-}4} < RD_{0.5\text{-}6}$. As seen from the table, a consistent increasing RD was reported for nearly 33% of cases, mainly including the parameters K_{ZH}, S_{ZH}, and S_{HV}. Nevertheless, a consistent decreasing pattern in nearly 10% of cases and an irregular pattern in nearly 57% of cases were also seen. For example, at a given

initial compaction condition of 0% w_i and γ_d of 1.3g/cc, the $RD_{0.5\text{-}2}$, $RD_{0.5\text{-}4}$, and $RD_{0.5\text{-}6}$ for K_{HV} were 26.6%, 26.3%, and 17.9% respectively. Decreasing RD, in this case, implies an increase in estimated K_{HV} with the increase in h_0. Similar discrepancies were also noted in a few more instances (10% cases). In some cases, negative RD was also noted, implying a decrease in parameter values for the higher suction compared to 0.5 cm.

Table 4.5. Relative Difference (%) in the estimated soil parameters S_0 and K_0 calculated using the three methods (HV, ZH, and DH) for different initial compaction state (w_i and γ_d) of laboratory experiments with respect to change in suction

Estimated soil parameter	Compared h_0	Relative Difference (%)							
		γ_d (g/cm^3)							
		1.3	1.3	1.3	1.4	1.4	1.4	1.6	1.6
		w_i (%)							
		0	5	15	0	5	15	0	5
K_{HV}	0.5 and 2	26.6	-11.8	-1.7	36.3	-9.8	8.9	33.0	22.2
	0.5 and 4	26.3	-20.2	45.6	17.7	12.1	45.8	47.2	31.4
	0.5 and 6	17.9	41.8	14.9	45.2	41.2	13.9	49.4	27.2
K_{ZH}	0.5 and 2	24.2	-0.3	7.5	36.3	-1.2	18.7	38.2	30.3
	0.5 and 4	34.0	26.5	54.5	36.2	26.1	54.9	49.9	44.3
	0.5 and 6	39.5	57.0	36.1	59.9	55.8	36.1	60.0	46.7
K_{DH}	0.5 and 2	16.5	-10.4	-1.9	29.8	-11.4	64.2	31.9	23.3
	0.5 and 4	17.4	-21.5	43.1	20.1	7.5	43.5	37.3	30.3
	0.5 and 6	13.9	38.9	9.1	42.9	37.1	9.1	43.1	24.1
S_{HV}	0.5 and 2	-18.3	30.1	28.5	3.2	4.2	41.4	22.4	42.1
	0.5 and 4	-4.0	35.1	38.7	33.5	3.9	36.2	-5.0	46.7
	0.5 and 6	17.5	42.7	23.9	38.0	38.7	23.9	18.3	48.7
S_{ZH}	0.5 and 2	-15.4	32.7	28.3	5.9	7.1	44.1	23.4	45.6
	0.5 and 4	1.5	40.2	38.4	38.0	9.8	38.0	-0.4	49.7
	0.5 and 6	27.8	49.2	29.8	42.8	43.8	32.8	25.3	53.3

From both field and laboratory investigations, it is explicit that the role of h_0 on the hydraulic parameters S_0 and K_0 can be considered marginal. A higher RD value close to 50 % need not be considered appreciable since the overall variations were well within one order of magnitude for most cases.

4.4. Summary

In this study, the influence of the MDI's supplied negative pressure head (h_0) on its measured infiltration characteristics and the resulting hydraulic parameters were investigated with the help of both field and laboratory measurements. Multiple repetitions of MDI infiltration experiments were carried out on a silty clay loam soil texture by using four different negative pressure heads, 0.5, 2, 4, and 6cm. The results from the infiltration measurements were evaluated using three different transient methods, Haverkamp, Zhang, and Dohnal, to determine the near-surface near-saturated soil hydraulic conductivity (K_0) and sorptivity (S_0) measurements. From both field and laboratory investigations, it is explicit that the role of h_0 on the hydraulic parameters S_0 and K_0 can be considered marginal. The difference in S_0 and K_0 in all the cases was well within one order of magnitude only.

Further, the results also showed that the three assessment methods used in this study were not identical in magnitude; however, they showed a similar pattern in the estimated K_0 and S_0 measurements. The difference in the magnitudes was mainly due to the difference in their formulations and the use of empirical constants in the mathematical expressions. From laboratory investigation, it was noted that the initial water content (w_i) visibly influenced the estimated parameter compared to γ_d and h_0. However, the influence was prominent only for dry initial conditions and was clearly seen to influence S_0 measurements more than the K_0. This was attributed to the predominance of capillary forces, which primarily drive the flow when the soil is sufficiently dry.

Chapter 5

Experimental evaluation of near-surface wetting hydraulic characteristics and understanding their time-dependence

5.1. Introduction

The appropriateness of the wetting hydraulic characteristics obtained from transient analysis of mini disc infiltrometer (MDI) measurements depends on (a) the adequacy of the model, (b) adequacy of measured data, (c) measurement duration, and (d) measurement footprint. The two transient models, Zhang (ZH) and Haverkamp (HV) (Haverkamp et al., 1994; Zhang, 1997) (section 3.3.1.1, Eq. 3.9 and 3.12) based on the two-term cumulative infiltration equation (Eq. 3.6) are popular for analyzing MDI measurements (Dohnal et al., 2010; Ghosh & Pekkat, 2019b; González-Pelayo et al., 2010; Ronayne et al., 2012). The ZH model considers the soil hydraulic parameters independently related to capillary forces and gravity forces, whereas the HV model considers the influence of S_0 in the determination of K_0. The formulation of both ZH and HV models is for initially dry soil (initial hydraulic conductivity negligible compared to K_0), where S_0 is predominant. However, the HV model is reported to produce irrelevant negative values of K_0 for smaller disc radius (as in MDI) and high S_0 (initially dry soil) conditions (Vandervaere et al., 2000a; Dohnal et al., 2010, also observed in this study). Therefore, previous studies resorted to the initial wet condition of the soil to minimize the influence of S_0 in the determination of K_0 by the HV model (Bagarello and Iovino, 2003). On the other hand, the ZH model, irrespective of the dry or moist initial condition of the soil, has been able to generate reliable K_0 estimates. Despite several criticisms of this method due to the lack of its physical validity, it still stands out as a simple first-hand method to establish infiltration characteristics from MDI measurements (Homolák et al., 2009; Dohnal et al., 2010; Ghosh et al., 2019) and has also been recommended by the manufacturer of MDI (METER Group, USA).

The adequacy of the measured infiltration data for transient analysis can be checked by two linearization methods, namely, cumulative linearization (CL) (Smiles & Knight, 1976) and

differentiated linearization (DL) (Vandervaere et al., 2000a). Any deviation in the initial linearity of the infiltration data is considered as the limit till which the data is adequate for transient analysis. Both CL and DL methods can be employed if no contact layer is used below the MDI disc during infiltration measurements (Angulo-Jaramillo et al., 2016; Bagarello and Iovino, 2004; Vandervaere et al., 2000a). It is reported that the adequacy of data check also helps to minimize the estimation of irrelevant negative values of K_0 while using the HV model for an initially wet sample and higher disc radius tension infiltrometer (TI) (Bagarello & Iovino, 2003; Vandervaere et al., 2000a). The next important aspect is the consideration of measurement duration for transient analysis of disc infiltrometer measurements. The estimation of parameters S_0 and K_0 of the two-term infiltration model can get affected by the duration of the experiments (Angulo-Jaramillo et al., 2016; Bagarello & Iovino, 2003; Bagarello et al., 2004; Clausnitzer et al., 1998; Haverkamp et al., 1994; Vandervaere et al., 2000a).

Table 5.1 lists a summary of the measurement time dependence studies for infiltration measurements. The findings from the literature are mostly confined to sandy loam and clay and initially wet samples. The time-dependent variability was found to be more for sorptivity-related parameter C_1 (Bagarello & Iovino, 2003). The recommended measurement time was one hour for sandy loam and six hours for clay soil based on the simulated infiltration curve for TI in wet soil samples (Bagarello et al., 2004). However, a comparison of the recommended measurement time with the time obtained from the adequacy of the data check was not carried out in the literature. Alagna et al. (2019b) evaluated the applicability of the CL and DL methods for MDI measurements without any recommendation on measurement duration. An appraisal of measurement time dependence based on actual infiltration measurements is still limited in the literature for varying soil textures (relevant surface soils). This topic, although important, has not been considered with due importance specifically for MDI measurements in initially dry samples.

Table 5.1 Summary of literature dealing with time influence on infiltration measurements

Study	Soil texture	Data	Recommendations
Clausnitzer et al. (1998)	Sandy loam, Clay	Simulated infiltration	• Stressed the importance of time invariance of hydraulic parameters. • Extending the measurement period towards the steady-state range increased parameter confidence.
Bagarello and Iovino (2003)	Sandy loam, Clay	Field, initially wet sample	• For gravity dominated flow, estimation of C_1 was difficult than C_2. • More time dependent fluctuations observed for C_1. • Measurement time > 1 hour to avoid time dependence of K_0 (based on DL method).
Bagarello and Iovino (2004)	Sandy loam	Lab, field data from Hussen and Warrick (1993)	• CL method was better than DL method. • C_1 and C_2 obtained using CL and DL methods were not equivalent in all cases.
Bagarello et al., (2004)	Sandy loam, Clay	Simulated infiltration	• DL method to obtain C_1 and C_2. • Initial wet soil provided better estimate of K_0 for lateral capillary dominated flow (for transient single-test). • Choosing an appropriate measurement duration helped to improve accuracy of parameter estimates. • Recommended measurement time was 1 hour for sandy loam and 6 hours in clay. • No experimental evaluation of measurement time.
Alagna et al. (2019b)	Clay loam, Silty clay, Sandy loam	Field	• Linear trend for entire duration observed in 77 % cases using CL and 79% cases using DL. • For remaining cases, 50% of the cumulative infiltration data exhibited linear trend. • Both CL and DL methods were applicable.

The measurement footprint of MDI is significantly different from TI. It is noted from the literature that the measurement footprint has a significant effect on the infiltration measurements (Fodor et al., 2011; Ghosh et al., 2019; Ronayne et al., 2012). Hence, any recommendation in the literature related to the measurement duration for TI can be adopted

for MDI only after careful evaluation. Therefore, it is crucial to assess the appropriate MDI measurement duration that would help in reliable hydraulic parameter estimation. Based on these discussions, the research questions that need to be addressed can be outlined as below.

- How the measurement time (T_m) of MDI influence C_1 and C_2 and hydraulic parameters K_0 and S_0?
- What is the MDI measurement duration to be considered based on the adequacy of data check by CL and DL methods (designated as T_{CL} and T_{DL})?
- What is the duration, T_m recommended for MDI based on (i) and (ii) for different textures?
- Whether the recommendation remains same for initial dry samples (S_0 high) as against the initially wet sample reported in the literature?
- What is the variability of C_1, C_2, K_0 and S_0 for the duration T_m, T_{CL} and T_{DL}?

The current chapter aims to address the above research gaps and determine the ideal MDI measurement duration for six different soil textures. To do this, the time fractionation of measurement duration (T_m) is performed and compared to the time derived from the literature-reported CL and DL methods for assessing the adequacy of measured data. Further, this study investigates the measurement duration for initially dry samples against the wet samples reported in the literature. The variability in infiltration equation parameters (C_1 and C_2) and the hydraulic parameters (K_0 and S_0) corresponding to the duration T_m, T_{CL}, and T_{DL} is also analysed in this study.

5.2. Methodology

Figure 5.1 presents a flow diagram of the methodology used in this chapter. As shown in the figure, the infiltration measurements with MDI were conducted on both laboratory and field soils to carry out this study. For laboratory measurements, homogeneous soil samples with known initial compaction state (soil moisture and density) were used. For this purpose, a cylindrical column of diameter 30 cm and height 30 cm with provision for drainage at the bottom (Figure 5.2) was used to pack the soil. Four different soil textures, namely sand (SN), loam (LM), silt loam (SL), and silty clay loam (SCL), were collected and used for carrying out the experiments. The sampling locations for the laboratory soils were situated within the sub-basin of the Brahmaputra river, Northeast India. The geographic location of the sampling areas lay between 26°11′3.434″N and 26°11′55.122″N latitude and 91°41′14.324″E and

91°42′10.578″E longitude with an elevation varying between 49 m to 97 m above the mean sea level. The sites chosen for soil sampling were free from anthropogenic activities and had bare soil surfaces with no vegetation cover.

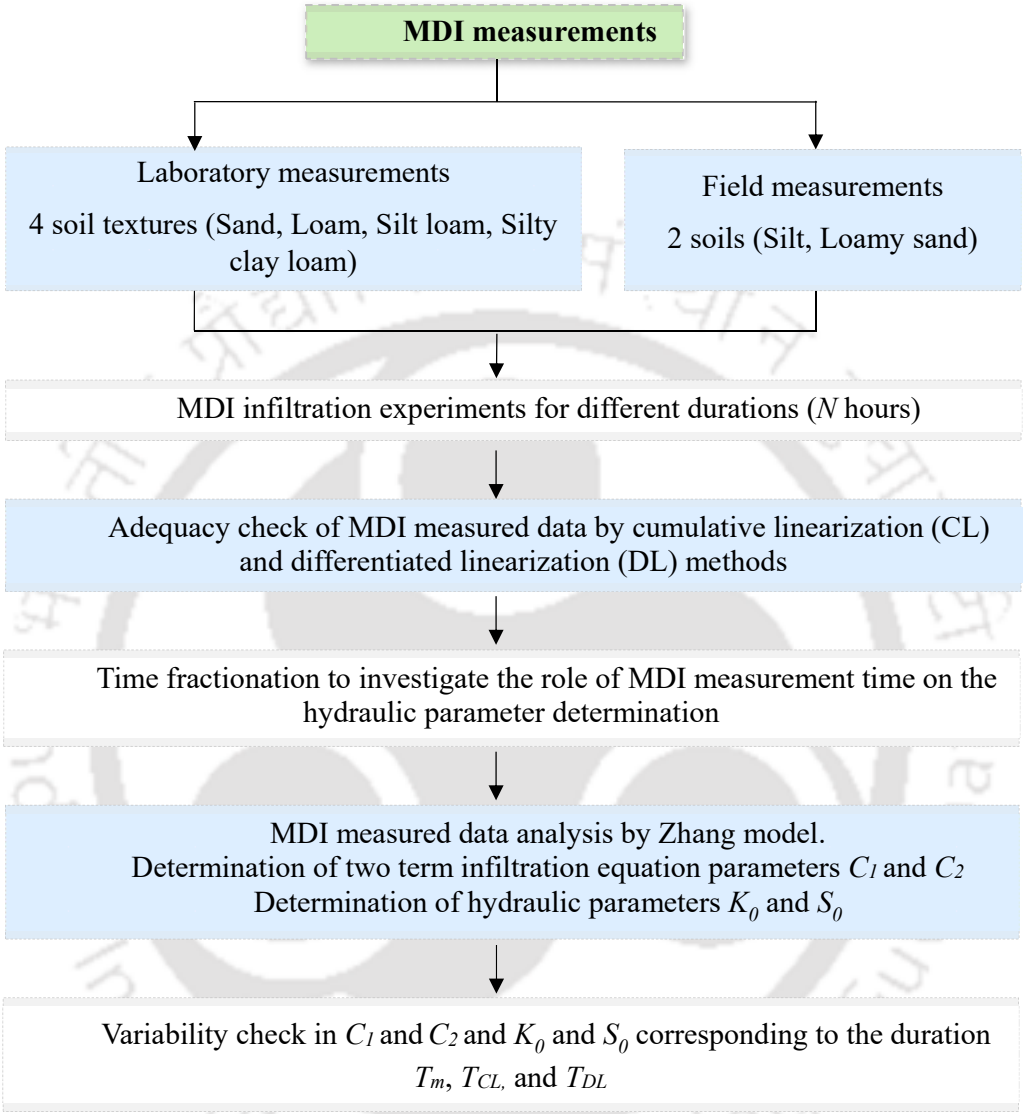

Figure 5.1 Flow diagram illustrating the methodology used in this study

The sampled soils were cleaned for any debris and plant roots and sieved through a 2 mm IS sieve. The soils were characterized for their specific gravity (ASTM D854), particle size distribution (ASTM D2487-11; IS:2720), and soil texture classification (section 3.2), and the results are listed in Table 5.2. The air-dried soil sample was packed inside the cylindrical column in multiple layers by manual compaction to eliminate the presence of macropores. The details of initial water content and dry density are listed in Table 5.2. The MDI was set to a h_0 of 6 cm and placed on the surface for commencing the infiltration measurement. The h_0 was

kept as 6 cm keeping in view the quick infiltration expected in SN soil (METER Group, USA), and for uniformity, the same h_0 was maintained for other soils as well. The volume of water infiltrating into the soil was recorded at an interval of 1 minute for the initial 1 hour, followed by 5 minutes for the remaining experiment duration. Whenever required, refilling was done manually by adding a measured volume of water into the MDI. For each soil, six replicates were performed, resulting in a total of 24 measurements. For the fine soils (LM, SL, and SCL), all the experiments were done for long durations of 8, 9, and 13 hours respectively, and for SN, the duration was 1 to 3 hours, as provided in Table 5.3.

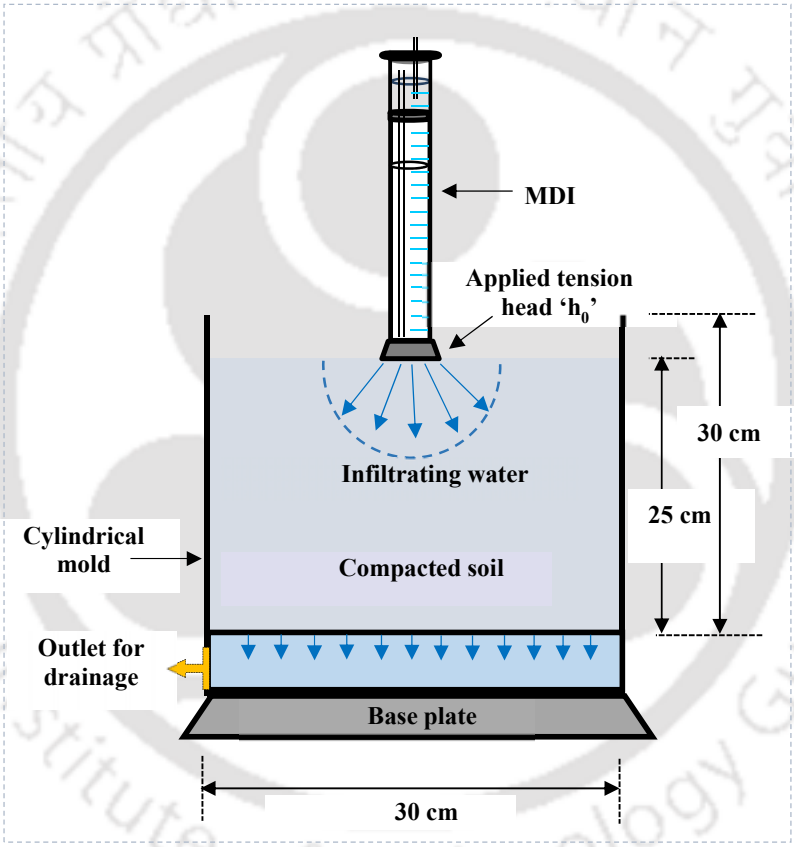

Figure 5.2 Schematic diagram of experimental setup for laboratory experiments

Table 5.2 Details of the six soil textures used for field and laboratory experiments

Parameter		Specific gravity	Particle size fraction (%)			Dry density (g/cm^3)	Initial gravimetric water content (%)
			Sand (2.00-0.05 mm)	Silt (0.05-0.002 mm)	Clay (<0.002 mm)		
Soil Texture	*Silt (ST)	2.54	16	81	3	1.42	1.66
	*Loamy Sand (LS)	2.56	74	22	4	1.88	5.27
	Sand (SN)	2.73	95	5	0	1.54	0.21
	Loam (LM)	2.68	38	44	18	1.39	0.62
	Silt Loam (SL)	2.72	32	62	6	1.42	0.52
	Silty clay loam (SCL)	2.64	16	57	27	1.35	0.77

*Soil texture in the field

The MDI measurements in the field were conducted for two different soil types: loamy sand (LS) and silt (ST). The sites were situated within the same geographical location as the sampling sites of laboratory soils. These locations were also devoid of human intervention and had no plant cover on the surface. All the tests similar to the laboratory soils were also carried out for the field soils to characterize their physical and chemical properties. The details of soil characteristics in the field are listed in Table 5.2. The purpose of conducting the field measurements was to appraise the time dependence of MDI measurements on the undisturbed state of the soils with inherent inhomogeneities if any. For field cases, six repetitions were conducted for each soil texture for a total duration of 90 minutes resulting in twelve measurements. The total duration of the experiment chosen in this study is greater than those specified in the literature (Bagarello & Iovino, 2003; Vandervaere et al., 2000a, b) for TI. For both field and laboratory measurements, no contact layer was used during the infiltration measurements.

Table 5.3 Total experiment duration and the time obtained from adequacy of data check (differentiated linearization (T_{DL}); cumulative linearization (T_{CL}))

Sl. No.	Soil Type	Time (minutes)			Coefficient of Determination R^2	
		Experiment Duration (N)	T_{DL}	T_{CL}	DL	CL
1	*ST1	90	30	35	0.965	0.985
2	*ST2	90	30	40	0.964	0.982
3	*ST3	90	30	35	0.982	0.984
4	*ST4	90	30	35	0.964	0.987
5	*ST5	90	30	40	0.965	0.989
6	*ST6	90	30	35	0.953	0.988
7	*LS1	90	45	45	0.998	0.999
8	*LS2	90	50	60	0.997	0.999
9	*LS3	90	50	40	0.996	0.999
10	*LS4	90	45	45	0.994	0.997
11	*LS5	90	50	60	0.991	0.994
12	*LS6	90	50	40	0.981	0.991
13	SN1	60	30	30	0.97	0.998
14	SN2	60	25	30	0.989	0.997
15	SN3	90	50	60	0.962	0.998
16	SN4	180	55	70	0.981	0.996
17	SN5	180	55	70	0.987	0.997
18	SN6	180	25	65	0.99	0.995
19	LM1	480	55	55	0.909	0.998
20	LM2	480	50	60	0.944	0.993
21	LM3	480	45	50	0.961	0.995
22	LM4	480	45	40	0.909	0.998
23	LM5	480	35	60	0.944	0.993
24	LM6	480	60	65	0.961	0.995
25	SL1	540	100	130	0.962	0.999
26	SL2	540	110	130	0.941	0.999
27	SL3	540	55	110	0.947	0.997
28	SL4	540	90	110	0.982	0.993
29	SL5	540	95	110	0.955	0.999
30	SL6	540	110	110	0.984	0.999
31	SCL1	780	110	140	0.962	0.993
32	SCL2	780	85	135	0.892	0.998
33	SCL3	780	65	85	0.904	0.999
34	SCL4	780	65	85	0.868	0.996
35	SCL5	780	70	110	0.954	0.997
36	SCL6	780	65	110	0.98	0.998

*Field experiments; ST: silt; LS: loamy sand; SN: sand; LM: loam; SL: silt loam; SCL: silty clay loam

5.2.1. Models used for MDI data analysis

The transient infiltration rates corresponding to the three-dimensional infiltration process beneath the MDI can be approximated by the first two terms of Philip's equation (Eq. 3.6) (Philip, 1957), and the same was adopted in ZH and HV models (section 3.3.1.1). The difference between ZH and HV models is in the manner in which S_0 and K_0 are determined from C_1 and C_2. In the ZH model, the coefficients C_1 and C_2 are independently related to S_0 and K_0, as given by Eqs. 3.10 and 3.11. While in the HV model, K_0 is related to both C_1 and C_2 coefficients (Eqs. 3.7 and 3.8). It was noted from this study that the HV method gave physically irrelevant negative K_0 values in the majority of the cases, which was mainly attributed to the high values of S_0 (initially dry soil state) and relatively small radius of MDI (Angulo-Jaramillo et al., 2016). Hence, the HV model was not considered further for analysis in this study.

5.2.2. Adequacy of data check for MDI measurements

Prior to determining the two coefficients C_1 and C_2 from Eq. 3.6, the adequacy of the experimental data need to be assessed. This was done using the two linearization methods; cumulative linearization (CL) and differentiated linearization (DL). The CL method involves linearizing Eq. 3.6 by dividing both sides by $\sqrt{t}$, giving

$$\frac{I}{\sqrt{t}} = C_1 + C_2\sqrt{t} \tag{5.1}$$

Using Eq. 5.1, C_1 and C_2 are obtained, respectively, as the intercept and slope of the regression line between $I/\sqrt{t}$ and $\sqrt{t}$ for the initial set of data that exhibited linearity (Angulo-Jaramillo et al., 2016). The data that departs from the linearity is not considered (inadequacy). The time at which the infiltration data analysed by the CL method deviates from linearity is represented by T_{CL}.

The DL method involves differentiating the cumulative infiltration data with respect to the square root of time given by Eq. 5.2. The $\frac{dI}{d\sqrt{t}}$ can be approximated by Eq. 5.3 (Vandervaere et al., 2000a; Angulo-Jaramillo et al., 2016).

$$\frac{dI}{d\sqrt{t}} = C_1 + 2C_2\sqrt{t} \tag{5.2}$$

$$\frac{\Delta I}{\Delta\sqrt{t}} = \frac{I_{i+1} - I_i}{\sqrt{t_{i+1}} - \sqrt{t_i}} = C_1 + 2C_2\sqrt{t_m} \quad (i = 1, 2, 3, \ldots p\text{-}1) \tag{5.3}$$

$$t_m = \sqrt{t_i \times t_{i+1}} \tag{5.4}$$

Here p represents the number of data points, I_i and I_{i+1} are the cumulative infiltration values respectively at t_i and t_{i+1}, and t_m is the geometric mean time given by Eq. 5.4. If the experimental data is adequately described by Eq. 1, then $\frac{dI}{d\sqrt{t}} vs \sqrt{t}$ $\left(\frac{\Delta I}{\Delta\sqrt{t}} \text{ vs } \sqrt{t_m}\right)$ gives a linear plot, with C_1 equal to the intercept and C_2 equal to half the slope of the regression line. The time at which the DL method data deviates from linearity is represented by T_{DL}, and only the initial infiltration data that exhibit linearity is considered for determining the coefficients.

5.2.3. Evaluation of time dependence of hydraulic parameters by time fractionation

For evaluating the time dependence of K_0 and S_0, cumulative infiltration data was divided into different durations by time fractionation (0 to 15 min; 0 to 20 min; 0 to 30 min; 0 to 35 min; 0 to 40 min; 0 to 45 min; 0 to 1 hour, 0 to 2 hours, and further with one-hour increments till the end of the experiment, N in Table 5.3). Infiltration data for these durations were considered for determining the values of coefficients C_1 and C_2, as stated in the ZH method by METER Group, USA (section 3.3.1.1). The same procedure was repeated for all 36 experiments. Following this, the series of C_1 (C_1^{15}, C_1^{20}, C_1^{30}, …, C_1^{60}, C_1^{120}, …, C_1^{N}) and C_2 (C_2^{15}, C_2^{20}, C_2^{30}, …, C_2^{60}, C_2^{120}, …, C_2^{N}) values obtained for each experiment were used to calculate the corresponding values of K_0 and S_0 with respect to time using the ZH method.

5.3. Results

5.3.1. Adequacy check of measured infiltration data from MDI

For testing the adequacy of data, the CL and DL methods were applied to all 36 MDI measurements (24 from the laboratory and 12 from the field) from 6 soil textures, as shown in Figure 5. 3. It was noted that both the methods exhibited linear trends till certain times, followed by deviation from linearity or a discontinuity. This trend was found to be identical for all the MDI measurements. Thus, both the linearization methods could be used for the adequacy check of measured infiltration data from MDI. The details of data adequacy time (T_{CL} and T_{DL}) and the coefficient of determination (R^2) for the linear fit corresponding to all the experiments

are listed in Table 5.3. The initial straight-line portion data (up to T_{CL} and T_{DL}) was used to determine the infiltration coefficients C_1 and C_2 by the CL and DL methods. The C_1 and C_2 obtained from both the methods, along with T_{DL} and T_{CL}, are compared in Figure 5.4. For quantifying the comparison, slope and Pearson's correlation coefficient were determined for a linear fit for the data passing through the origin. The 1:1 line is also presented in the figure for comparison.

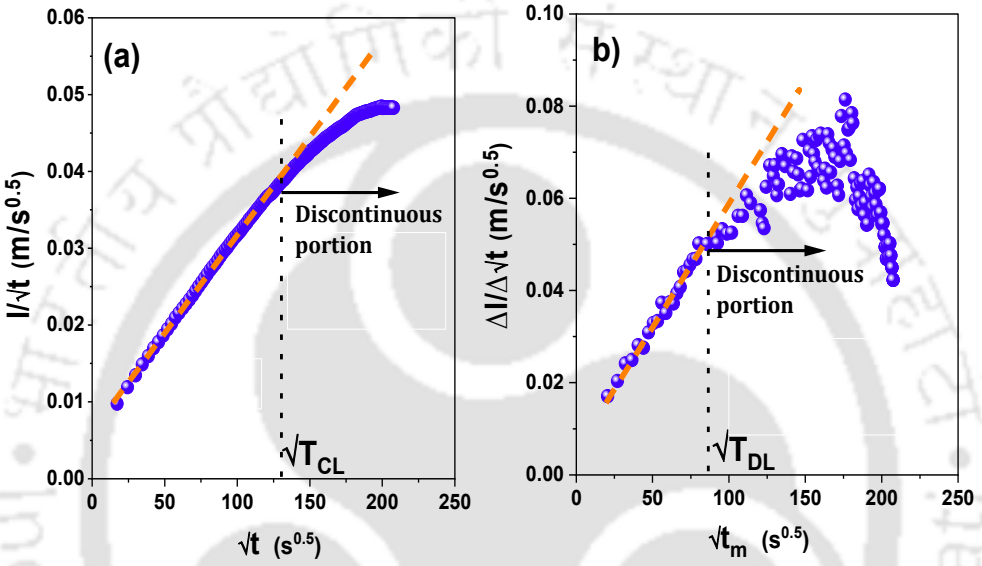

Figure 5.3 A typical representation of MDI measured data for (a) cumulative linearization (CL) (b) differentiated linearization (DL) methods

It can be noted from Figure 5.4 that the linearity time or data adequacy time (T_{DL} and T_{CL}) are strongly correlated (Pearson's r = 0.98) with a slope of 0.8. Figure 5.4a indicates that all the data are below the 1:1 line and the adequacy time is marginally less in the DL method than in the CL method. This T_{DL} is, on average, 0.8 times the T_{CL} by considering six soil textures for MDI measurements in relatively dry soil conditions. The difference in T_{DL} and T_{CL} observed in this study may not be considered significant, given the high variability in soil characteristics. However, it is important to know the impact of this marginal difference in the adequacy time on the estimation of coefficients C_1 and C_2. Generally, it was observed from the literature (Angulo-Jaramillo et al., 2016; Bagarello and Iovino, 2004) that under field conditions, the DL data are more dispersed than the CL, and this would influence the determination of C_1 and C_2.

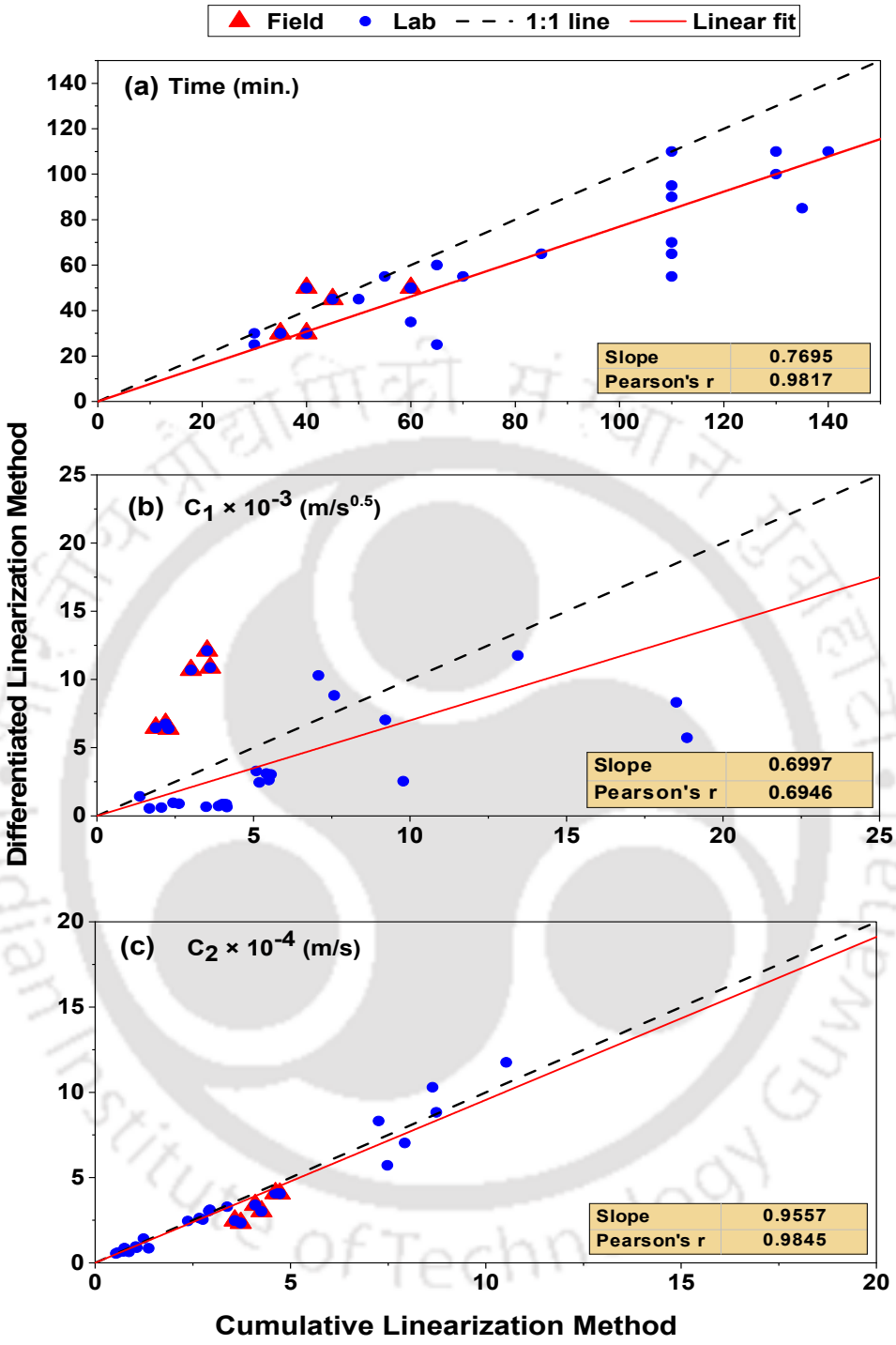

Figure 5.4 Comparison of (a) linearity time T_{DL} and T_{CL}, (b) C_1 and (c) C_2 obtained from cumulative linearization (CL) and differentiated linearization (DL) methods

The coefficients C_1 and C_2 of the infiltration equation were calculated using the respective T_{DL} and T_{CL} for all 36 cases, as shown in the Figures. 5.4(b) and (c), respectively. A strong correlation between T_{DL} and T_{CL} translates to a moderate correlation of C_1 obtained from the DL and CL methods with Pearson r equal to 0.70. However, careful observation reveals that the coefficient C_1 (Figure 5.4b) exhibited high dispersion of data about the 1:1 line, and the correlation is highly biased by a greater number of laboratory data. On an average, the C_1 obtained from the DL method is 0.7 times that of the CL method. However, for all the field measurements, the C_1 estimated by the DL method was higher than the CL method. It is known that the sorptivity of initial dry samples is significantly high. Hence, the coefficient C_1 is highly sensitive to the initial set of data, and therefore it is influenced by choice of the time T_{DL} and T_{CL}. It is to note that, unlike in the laboratory, the surface soil in the field is exposed to the atmosphere and is more prone to disturbance. Moreover, the field soil may also exhibit bigger pores or voids, affecting the initial infiltration measurements into the soil. A combined influence of all these factors may have influenced the observed disparity between the laboratory and field measurements in Figure 5.4b. However, an in-depth analysis of this topic was beyond the scope of this study.

It can be noted from Figure 5.4 (c) that the marginal difference in T_{DL} and T_{CL} does not influence much the variability in C_2 determined from the DL and CL methods. There is a high correlation between the C_2 obtained from the two methods with Pearson r equal to 0.98. For all practical purposes, the C_2 estimated from the DL and CL methods can be considered identical (slope is equal to 0.96). The results, thus, imply an insignificant influence of the adequacy time from the two linearization methods on the determination of the hydraulic conductivity parameter, unlike the sorptivity parameter.

5.3.2. Effect of MDI measurement duration (T_m) on hydraulic characterization: Time fractionation approach

The infiltration coefficients C_1 and C_2 were estimated using the ZH method corresponding to different measurement durations (time fractionation, section 5.2.3) for different soil textures. Figures 5.5 and 5.6 present the box plot variations of S_0 and K_0, respectively, considering measurement variability for every time fractionation. Figure 5.5 shows that there is a visible change in the slope of mean S_0 variation with time after a certain period for all the soil textures, irrespective of laboratory or field data. A tangent line was drawn, encompassing the initial data points to identify the deviation in slope. The point marking the slope change was identified as the optimal MDI measurement time based on S_0 – time variation

and designated as $T_{m,\,S0}$. A similar observation was also made from Figure 5.6 for the variation of K_0 with time fractionation for all the soil textures. However, it is crucial to understand whether the deviation of slope occurs at similar times as that obtained from Figure 5.5. Therefore, the same strategy used in Figure 5.5 was repeated for Figure 5.6, and the time at which there is a change in slope was identified and designated as $T_{m,\,K0}$. The measurement durations determined from Figures 5.5 and 5.6 are plotted as shown in Figure 5.7. As seen in the figure, the adequate MDI measurement times obtained from S_0 and K_0 considerations match well for all the soil textures. Hence, an average value is calculated from $T_{m,\,S0,}$ and $T_{m,\,K0}$, designated as $T_{m,}$ and used for further comparison.

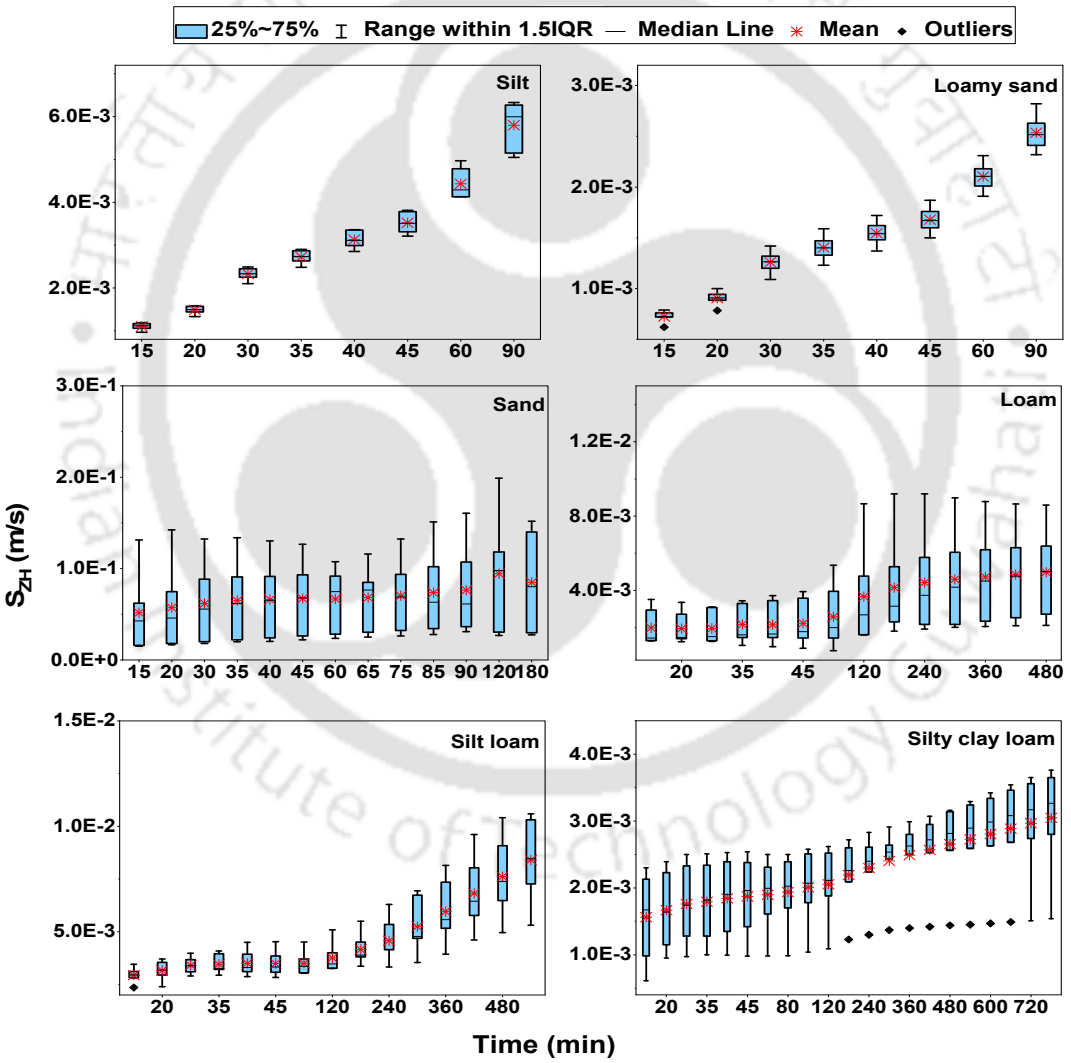

Figure 5.5 Variation of sorptivity S_{ZH} for different soil textures using time fractionation estimated using Zhang method

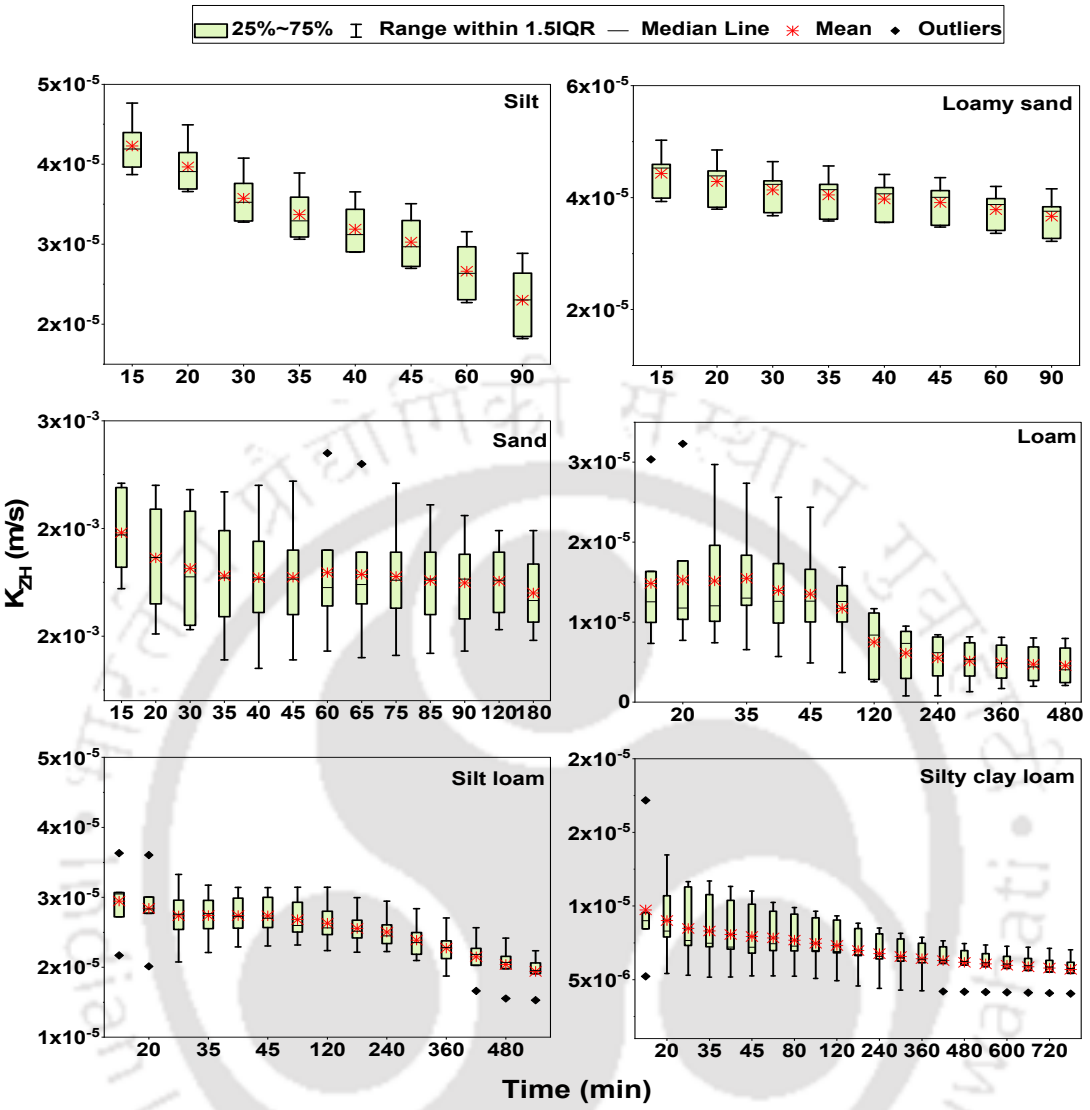

Figure 5.6 Variation of hydraulic conductivity K_{ZH} for different soil textures using time fractionation estimated using Zhang method

The calculated T_m values based on the ZH method, as discussed above, were compared with the T_{CL} and T_{DL}, as shown in Figure 5.8. The recommended optimal MDI measurement durations based on T_m is found to be comparable with the T_{CL} and T_{DL} for all the soil textures considered in this study. In particular, the T_{CL} values were very close to the T_m values for all six textures. The T_{DL} values were also close to T_m; however, they showed a slight difference in the case of SN, SL, and SCL soils.

Following the above observation, it was essential to understand the implications of the marginal difference between T_m, T_{CL}, and T_{DL} on the infiltration equation coefficients C_1 and

C_2. Figure 5.9 compares the C_1 and C_2 obtained based on T_m with the corresponding values obtained from T_{CL} and T_{DL} (linearization methods). It can be noted that there is a strong correlation between the infiltration coefficients with Pearson's $r \geq 0.9$. Except for C_1 obtained from T_m and T_{DL}, the slope of the regression line through zero is close to 1. This shows an excellent match for C_1 and C_2 obtained from time fractionation (optimal measurement duration) and linearization methods. This implies the marginal variations in T_m, T_{CL}, and T_{DL} do not result in significant variations in C_1 and C_2.

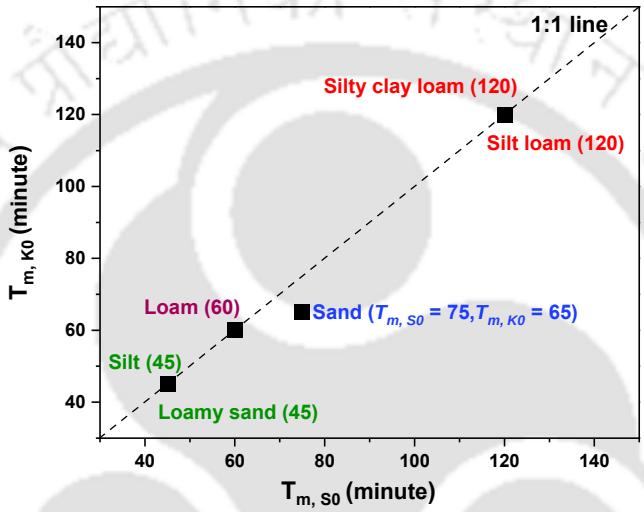

Figure 5.7 Comparison of measurement duration obtained from time fractionation by considering S_0 and K_0

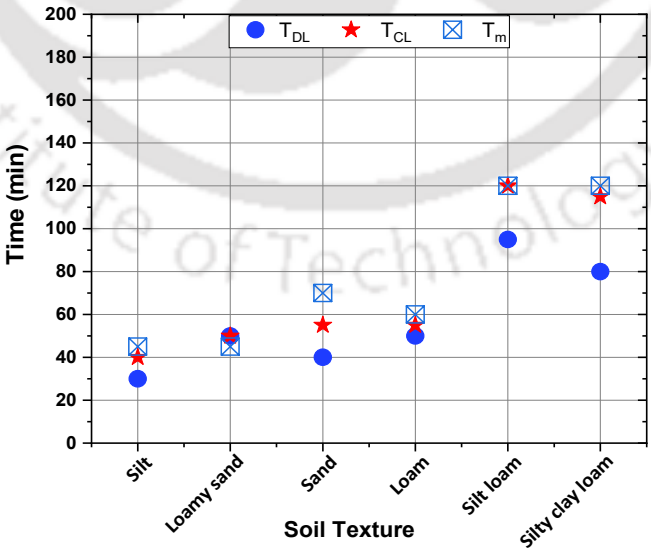

Figure 5.8 Comparison of T_m obtained from time fractionation with T_{CL} and T_{DL}

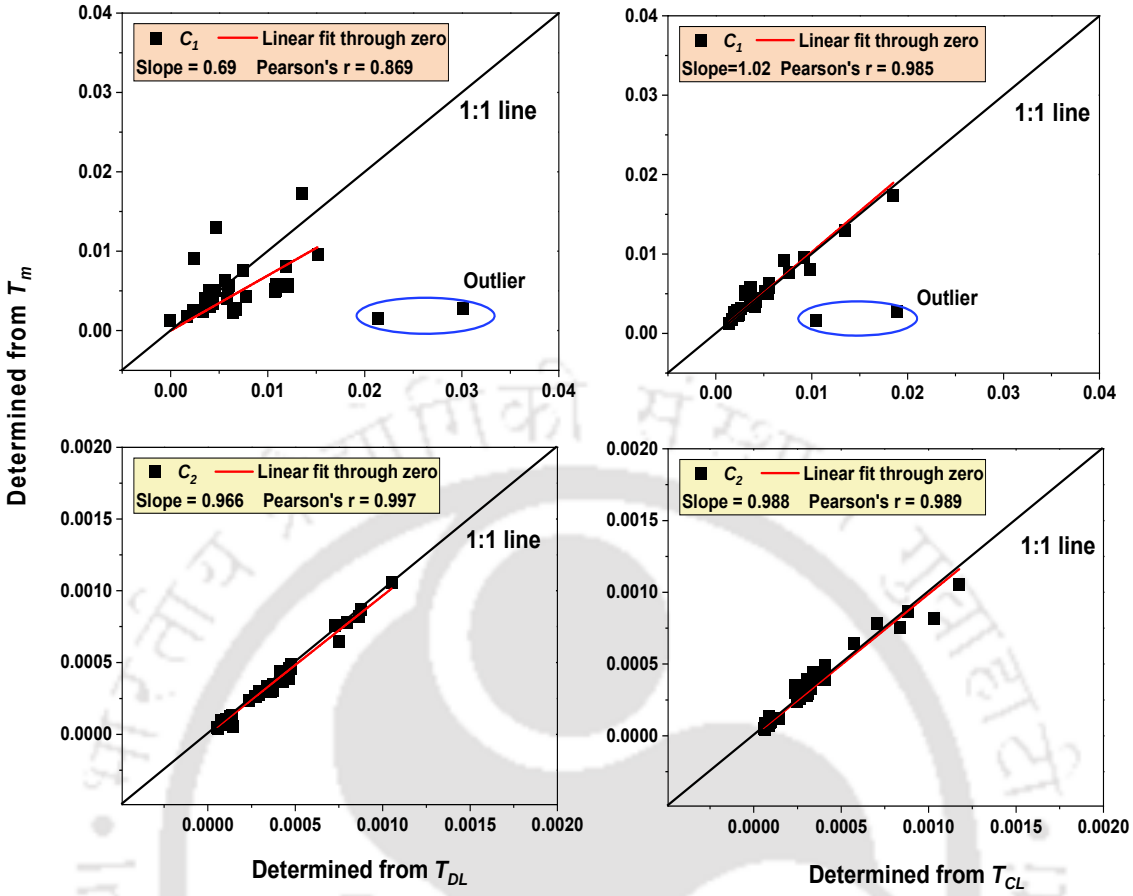

Figure 5.9 Comparison of infiltration equation coefficients C_1 and C_2 obtained based on T_m with those obtained from T_{CL} and T_{DL}

5.4. Discussion

As seen in Figure 5.4a, the T_{DL} values were consistently lower than the T_{CL} values for all the soil textures. Past literature has compared and reported such differences in T_{DL} and T_{CL} for TI measurements in the case of laboratory-repacked sandy loam soil (Bagarello and Iovino, 2004). As stated in Table 5.1, Alagna et al. (2019b) have investigated the adequacy of data for MDI measurements in three soil textures using both CL and DL methods. However, no relationship between T_{DL} and T_{CL} was explored for different soil textures in their study. Based on the current study, the difference in adequacy time calculated by the two linearization methods was marginally different, differing on an average by a factor of 0.8. In real cases, the soils exhibit higher variability in their characteristics, and consequently, the small difference in T_{DL} and T_{CL} (as seen in this study) may not have much influence on the soil hydraulic characterizations. Keeping this point in view, the two linearization methods used to analyze the adequacy of MDI measurements were considered suitable for the six textures in this study.

Regardless of the marginal difference between T_{DL} and T_{CL}, its influence on coefficients C_1 and C_2 was analysed (Figures 5.4b and c). The results from Figures 5.4b and c indicate that the choice of T_{DL} and T_{CL} is more influential on the determination of the sorptivity parameter (associated with C_1) and has a negligible effect on the hydraulic conductivity estimation (associated with C_2) for all the soil samples. In the study by Bagarello & Iovino (2004), a similar difference in the infiltration coefficients from the DL and CL methods was reported for TI measurements of sandy loam soil. This is to note that in the current study for MDI, both field and lab soil samples had dry initial conditions, and consequently, the sorptivity parameter dominated the flow condition at the beginning. Since the T_{DL} and T_{CL} are explicitly determined from initial infiltration measurements, a small variation in the T_{DL} and T_{CL} affected the C_1 parameter more prominently than the C_2. In Figure 5.4b, the C_1 values for field soils were reported to be higher than those of the laboratory soils. However, based on this study, it is not possible to infer whether the inherent inhomogeneity in the field and/or the soil texture have influenced the exhibited trend. For the present study, nevertheless, it is considered as a combined influence affecting the observed discrepancy.

The findings from this study indicate that both the linearization methods can be used for analyzing MDI measured data for determining infiltration coefficients C_1 and C_2. These coefficients can then be used for determining S_0 and K_0 by Zhang's method because the magnitude of S_0 does not partake in the determination of K_0. The original formulation of Zhang's method adopts a polynomial fitting procedure for determining C_1 and C_2. Hence, we limited further discussion on the MDI measurement time effect on C_1 and C_2 only to Zhang's analysis method based on the original polynomial fitting concept.

Based on the time fractionation concept applied to the ZH method for MDI measurements, the T_m values calculated (section 5.3.2) were found to be texture dependent. Similar texture-dependent variation was also witnessed in a previous study for TI (Bagarello et al., 2004). For the two textures used in their study (sandy loam and clay), the reported measurement durations were not the same (Table 5.1). In this study, the values of T_m (average of $T_{m,K0}$ and $T_{m,S0}$) varied from 45 minutes for ST and LS textures to 120 minutes for SL and SCL textures (refer Figure 5.8). For LM and SN soils, the T_m values were 60 and 70 minutes, respectively.

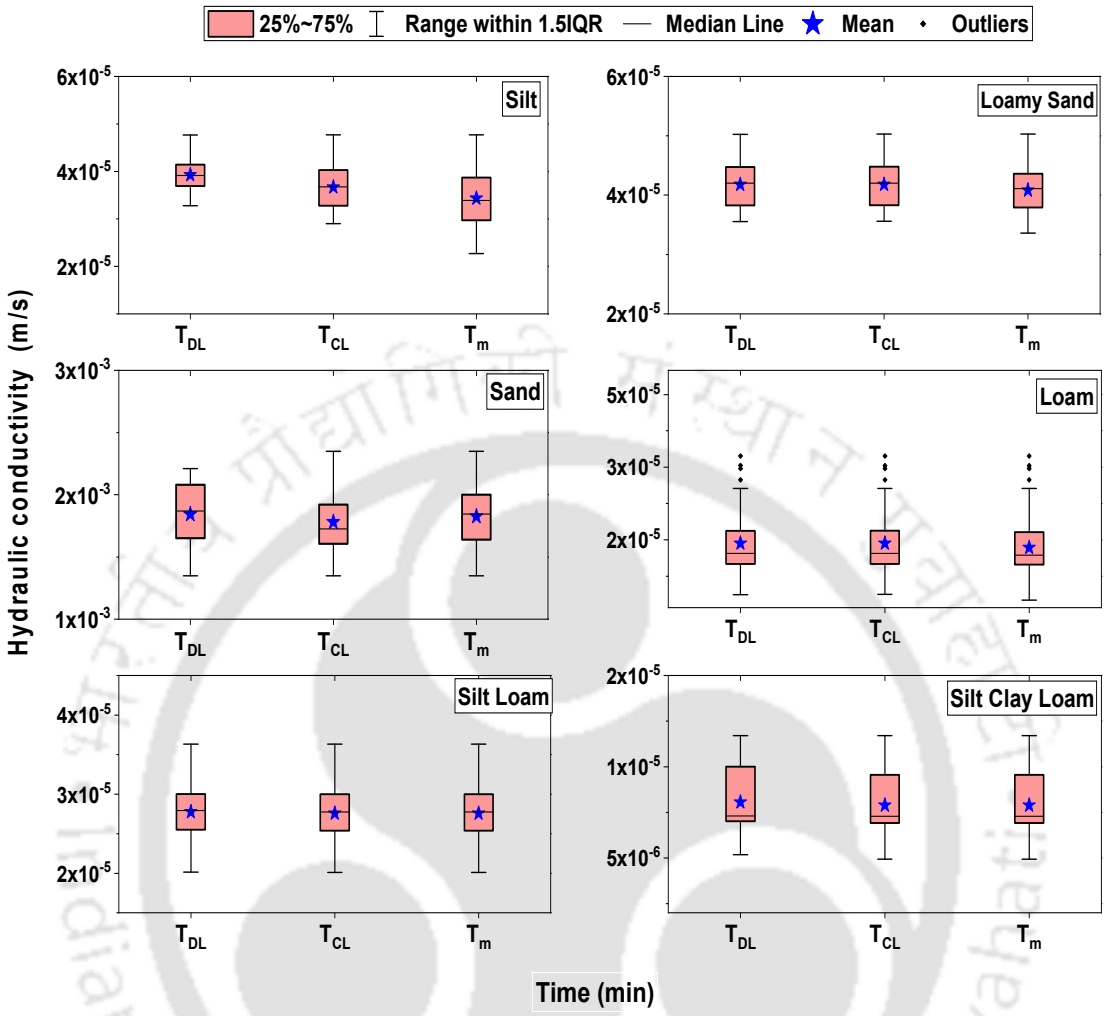

Figure 5.10 Comparison of hydraulic conductivity calculated by Zhang's method considering T_{DL}, T_{CL}, and T_m

The T_m values were overall in close agreement with the T_{CL} and T_{DL} was calculated from the linearization methods for all the textures (Figure 5.8). This was also evident from the matching results seen for C_1 and C_2 in Figure 5.9 calculated from the corresponding T_m, T_{CL}, and T_{DL}. Finally, Figure 5.10 compares the K_0 determined by the ZH method by considering T_m, T_{CL}, and T_{DL} to understand the influence of the latter on the former. It is explicit from Figure 5.10 that the mean values of K_0 from all the time considerations are practically the same. The variability denoted by 25%-75% is also fairly comparable for all the cases. The observations from Figures 5.9 and 5.10 state that the difference in C_1, C_2, and K_0 based on the recommended time from the two linearization methods (CL and DL) and the time fractionation approach to the ZH model were insignificant. It is also important to note that the CL method is intrinsically

similar to the time fractionation approach by considering the ZH model (Eqs. 3.6 and 5.1) and hence would result in comparable results. Consequently, for the six textures in this study, any of the values among T_m, T_{CL}, and T_{DL} can be considered for conducting the MDI measurements.

For simplicity, we recommend considering the maximum value among T_m, T_{CL}, and T_{DL} as the MDI measurement duration for the soils in this study, and the same values are listed in Table 5.4. To date, there are no recommendations in the literature for adequate MDI measurement duration for these soil textures considering T_m, T_{CL}, and T_{DL}. For sandy loam, the adequate measurement duration was recommended as 60 minutes by Bagarello et al. (2004). This value is close to the recommendation for sand (70 minutes) suggested in this study.

Table 5.4 Recommended MDI measurement duration for different soil textures.

Soil texture	Measurement duration (minute)
ST	45
LS	50
SN	70
LM	60
SL	120
SCL	120

5.5. Summary

This study investigated the adequacy of data (using the linearization methods, cumulative linearization (CL), and differentiated linearization (DL)) and the influence of measurement time on the hydraulic parameters determined from the transient analysis of MDI measurements for six soil textures. The main objective of the study was to identify the adequate MDI measurement duration for different soil textures for initially dry soil samples considering both the adequacy of the data approach and the time fractionation approach (measurement time influence). Based on the analysis of the results, the following major conclusions were derived from this chapter.

- Both the linearization methods can be used for the adequacy check of measured infiltration data from MDI. The linearity time or data adequacy time obtained from the linearization methods, T_{DL} and T_{CL}, are strongly correlated. The time obtained from the differentiated linearization is nearly 0.8 times the value obtained from cumulative linearization by considering six soil textures having an air-dried initial state. Given the

high variability and uncertainties associated with other soil-related factors, the difference in T_{DL} and T_{CL} observed in this study may be considered marginal.

- The marginal difference in T_{DL} and T_{CL} has a significant influence on C_1 and a negligible influence on the determination of C_2.
- The time fractionation method (based on Zhang's method (ZH)) adopted for the initially dry soil samples to identify the adequate MDI measurement duration (T_m) showed that the T_m identified based on both S_0 and K_0 variations were similar.
- The obtained final T_m was comparable with the time obtained from the adequacy of data approach (T_{DL} and T_{CL}) for all the soil textures considered in this study.
- An investigation of the impact of marginal differences among T_m, $T_{DL,}$ and T_{CL} on the determination of C_1, $C_{2,}$ and K_0 revealed an excellent match for C_2 obtained from time fractionation and linearization methods. The C_1 obtained from T_m and T_{DL} exhibited some deviations from the 1:1 line. The mean values of K_0 from all the time considerations were found to be practically the same. There was a strong positive correlation of T_m with T_{DL} and $T_{CL,}$ with Pearson's correlation close to 1.
- It is recommended to consider the maximum value among T_m, $T_{DL,}$ and T_{CL} as the MDI measurement duration for the soil texture considered in this study. The recommended MDI measurement duration depended on the soil texture and varied from 45 minutes for silt to 120 minutes for silt loam and silty clay loam. For loamy sand, it was 50 minutes; for sand, it was 70 minutes, followed by 60 minutes for loam.

It was noted that there are no recommendations available in the literature on the adequacy of MDI measurement time by considering T_m, $T_{DL,}$ and T_{CL} together. The recommended adequate measurement duration reported in the literature for sandy loam was 60 minutes, which is close to the time for sand (70 minutes) suggested in this study. Further studies are needed to generalize the findings for other surface soil textures to adopt adequate MDI measurement time based on both time fractionation and adequacy of the data approach.

Chapter 6

Evaluating and analysing the saturated hydraulic conductivity from MDI measurements by comparing with other head-based and flux-based methods

6.1. Introduction

One of the most important soil parameters influencing water infiltration and redistribution is near-surface saturated soil hydraulic conductivity (K_s) (Ghosh et al., 2019; Kruk et al., 2017; Radinja et al., 2019). Being an important input parameter for various hydrological and geo-environmental studies, its unambiguous and precise determination is crucial (Köhne et al., 2011; Radinja et al., 2019). It is also an essential parameter for seepage and contaminant transport modelling studies (Gupta et al., 1993; Köhne et al., 2011). The true value of K_s is mostly unknown. Hence, evaluating the accuracy of K_s determination demands repeatability and extensive comparisons among different measurement methodologies.

There are different flux-based and head-based methods for measuring infiltration and determining K_s (Ghosh et al., 2019; Gupta et al., 1993; Nestingen et al., 2018; Radinja et al., 2019; Verbist et al., 2013). The rainfall simulator (RS) is a prominent flux-based method for characterizing K_s, while the head-based methods include single ring infiltrometer (SRI), double ring infiltrometer (DRI), tension infiltrometer (TI), and the recent dual head infiltrometer (SATURO). All these methods determine K_s based on cumulative infiltration (CI) versus time measurement by employing specific mathematical formulations. The mini disc infiltrometer (MDI), like other head-based devices, can be used to estimate K_s based on its CI versus time recordings.

Literature shows several studies where MDI's K_s has been analysed and compared with other devices like DRI, TI, Guelph Permeameter (GP), and SATURO (Fodor et al., 2011; Ronayne et al., 2012; Nestingen et al., 2018; Ghosh et al., 2019; Radinja et al., 2019). The comparison of MDI with SATURO showed higher estimates in the case of SATURO (by 3.2 times) than MDI (Radinja et al., 2019), while the comparison of MDI with TI showed comparable results (Alagna et al., 2016; Ghosh et al., 2019). On the other hand, results from

comparisons of MDI with DRI and GP have reported contradicting observations, with MDI K_s overestimated in some studies (Radinja et al., 2019; Ghosh et al., 2019) and underestimated or nearly comparable in others (Ronayne et al., 2012; Nestingen et al., 2012). Based on the comparative assessments of MDI with other devices, the observations are inconclusive and require further evaluation.

It should be noted that the methodology employed for estimating K_s from MDI measurements may be biased by the associated inherent assumptions. For example, Ghosh and Pekkat (2019b) have considered a linear relationship between K_0 and h_0 for MDI measurements and have obtained K_s by extrapolating the relationship to $h_0 = 0$ cm. Ronayne et al. (2012), Nestingen et al. (2018), and Ghosh et al. (2019) have considered the K_0 calculated using Zhang's relationship (section 3.1.1.1., Eq. 3.9) as the K_s by ignoring the effect of the small supplied tensions used in their studies (0.5 to 6cm). Further, Fodor et al. (2011) have analysed K_s using specific soil hydraulic conductivity functions (SHCFs) and measured water retention data, while Radinja et al. (2019) have used an empirical relationship (Kutilek and Nielson, 1994) to measure K_s from MDI. It should be noted that Zhang's method has been recommended by the MDI's manufacturer for characterising unsaturated or near-saturated hydraulic conductivity from its measurements (section 3.1.1.1). However, no such method has been recommended for analysing K_s from its measurements. Consequently, researchers have adopted different methods based on their judgement and convenience.

The literature also reports the comparison of K_s among various other devices. Gupta et al. (1993) compared K_s results of RS with DRI, GP, and Guelph infiltrometer (GI) by conducting field studies. They noted that the mean K_s from RS was 2.5 to 3 times higher than that of DRI and GP but compared well with GI. Morbidelli et al. (2017) used deep flow measurements from rainfall-runoff experiments of RS as the reference for comparing three different instruments (DRI, Guelph version of the constant-head well permeameter, and CSIRO version of the tension permeameter) and reported discrepancies in the measurements. SATURO K_s was compared with modified Philip-Dunne infiltrometer (MPD) measurements by Ebrahimian et al. (2020) and were reported to show promising results. Further, SATURO has been successfully employed in several other studies to determine K_s from field measurements (Ravi et al., 2017; Thomas et al., 2018; Jahanzad et al., 2020; Norris et al., 2020; Fae et al., 2020). It should be noted that the flux-based RS is applicable for large-scale field measurements, while the head-based methods like MDI and SATURO are essentially point measurements due to their small sizes. Compared to RS, the latter methods are handy, require

less water, follow easy measurement procedures, and hence can be conveniently used for establishing spatio-temporal variability of hydraulic conductivity with adequate repetitions (Ebrahimian et al., 2020; Ghosh & Pekkat, 2019a; Nestingen et al., 2018; Radinja et al., 2019).

Previous studies have appraised the instrument related bias on near-surface K_s characterization based on infiltration measurements (Alagna et al., 2016; Ghosh et al., 2019; Gupta et al., 1993; Köhne et al., 2011; Morbidelli et al., 2017; Nestingen et al., 2018; Radinja et al., 2019; Zhang et al., 2019). Keeping in view the abundance of available measurement methods, it is essential to understand the measurement methodology-related variability in K_s and the underlying causes. The inherent variability in K_s determined from infiltration measurements may be associated with several factors. These include differences in measurement footprints (area of measurement), measurement signature (cumulative infiltration versus time response), mathematical equations adopted for data analysis, the assumptions associated with the mathematical equations, the working methodology, flow dimensionality, and other unforeseen factors under field conditions (e.g., presence of macro/micro cracks, vegetation roots, other preferential pathways, and low permeable zones). There are only a few studies that compared the K_s measurements based on flux-based and head-based methods (Ghosh et al., 2019; Gupta et al., 1993; Morbidelli et al., 2017; Verbist et al., 2013). The majority of the past studies were conducted only for head-based measurements (Fodor et al., 2011; Köhne et al., 2011; Nestingen et al., 2018; Radinja et al., 2019; Zhang et al., 2019). Furthermore, most of the existing comparative studies were conducted in the field where the results are highly influenced by inherent factors like preferential pathways, which are mostly unknown. Hence, it is difficult to conclude whether the variabilities in K_s are associated with measurement methodology or unknown factors existing in the field.

Based on these understandings, the following research questions were formulated for this chapter.

* Which factor(s) (measurement footprints, measurement signatures, and the mathematical equations/ evaluation methodologies) influence the variability in K_s obtained from flux-based and head-based methods?
* How precise and consistent is the tension MDI for determining near-surface K_s in comparison with other established head-based and flux-based methods?
* Whether numerical inversion technique can aid in improving the K_s predictions from MDI?

To address the above questions, a comparative study was performed under controlled laboratory conditions with an objective to elucidate the differences in K_s determination from flux-based (RS) and head-based (MDI, SATURO, and falling-head laboratory permeameter (PM)) methods. An empirical procedure and inverse estimation were adopted for determining K_s from MDI measurements. The infiltration measurements for all instruments correspond to the identical compaction state of the soil. A carefully packed/ compacted soil in the laboratory RS container minimized the possibilities of preferential pathways and other unforeseen factors, which are common under field measurements. In this manner, the observed K_s variability can be exclusively attributed to the instrument measurement methodology. The observations were used to investigate the statistical significance of differences in the K_s for two different soil textures. Based on this investigation, the preciseness and consistency of the tension MDI for determining near-surface K_s was appraised in this chapter.

6.2. Methodology

For an unambiguous comparison of flux-based and head-based methods for near-surface K_s determination, it is crucial to alleviate inherent uncertainties (soil heterogeneity, macropores, layer anisotropy) encountered in the field. Hence, the infiltration measurements in this study were performed in controlled laboratory-packed samples. In addition, the initial conditions were kept identical for all the instruments to maintain parity.

6.2.1. Soil texture classification

Two different soils, one fine-grained and one coarse-grained were used to conduct this study. These two surface soils were collected locally, cleaned, and sieved for any unwanted debris. The soils were then characterized for their index properties (particle size distribution and specific gravity) (ASTM D2487-11; IS:2720, ASTM D854) (section 3.2), and the results are listed in Table 6.1. The soils are classified as loam (LM) and sand (SN) textures based on USDA soil textural classification.

Table 6.1 Details of the physical characteristics and initial conditions of soils

Soil type	Loam (LM)	Sand (SN)
Specific gravity	2.68	2.66
Particle size distribution Gravel (> 2 mm) Sand (2 – 0.05 mm) Silt (0.05 – 0.002 mm) Clay (< 0.002 mm)	 0 44 38 18	 0 98 2 0
Initial air-dried gravimetric water content (%)	6.65	2.14
Initial packing dry density (g/cc)	1.63	1.41

6.2.2. Instruments used

6.2.2.1. Infiltration measurement

Three measurement methodologies, (a) flux-based RS, (b) head-based MDI, and (c) SATURO infiltrometer, were used for determining the K_s of the two soil textures (coarse-grained sand and fine-grained loam). The results from these instruments were analysed using specific methodologies to determine K_s. The RS data was analysed using Green-Ampt (GA) (Green and Ampt, 1911) and Philips (PH) (Philip, 1957, 1969) methods (Chow et al., 1988), SATURO data was analysed using the modified expression of Reynolds and Elrick (1990) given by Nimmo et al. (2009), and MDI data was analysed using the expression of Kutilek and Nielsen (1994) as adopted in the literature Radinja et al. (2019). In addition, the K_s measured under identical conditions in PM were used as the reference value for comparison. The PM measurements for both the soil textures were carried out using the standard procedures (ASTM D5084). The details of all the instruments and their analysis methods are provided in Chapter 3 (section 3.3).

6.2.2.2. Volumetric water content and soil water potential measurement

During the infiltration experiments, the wetting front moves downward and gradually saturates the soil. This increases the volumetric water content (VWC) and decreases the soil water potential (SWP) with time and depth. For RS and MDI experiments, the temporal evolution of VWC (θ vs. t) were recorded in this study by using 5TM sensors (METER Group Inc., USA). Additionally, for RS experiments, the SWP (ψ vs. t) values were recorded during the wetting process as it was needed for obtaining the wetting front ψ in the Green-Ampt calculation of K_s (Eq. 3.23). Depending on the soil type, TEROS-21 and T5 Tensiometer

(METER Group Inc., USA) were used to record the ψ values. For the fine-textured loam soil, TEROS-21 was used, while for the coarse-textured sand, T5 tensiometers were used. The usefulness of these three sensors has already been demonstrated by several researchers (Haghverdi et al., 2021; B. Li et al., 2020; Saha et al., 2020; Shaikh et al., 2019; Wang et al., 2020). The recorded ψ and θ from the sensors were continuously monitored using Em50 and DL6-te tensiometer logger (Meter Group, USA). The measured raw counts from VWC sensors were converted to θ using soil specific calibration equations, discussed in Chapter 3. The details about these sensors and the calibration equations are given in section 3.3.5. In addition to experimental evaluation, the K_s from MDI measurement were also evaluated using the numerical inversion technique performed in HYDRUS 3D-3.01 (Simunek et al., 2018), discussed in section 6.2.4.

6.2.3. Laboratory investigation

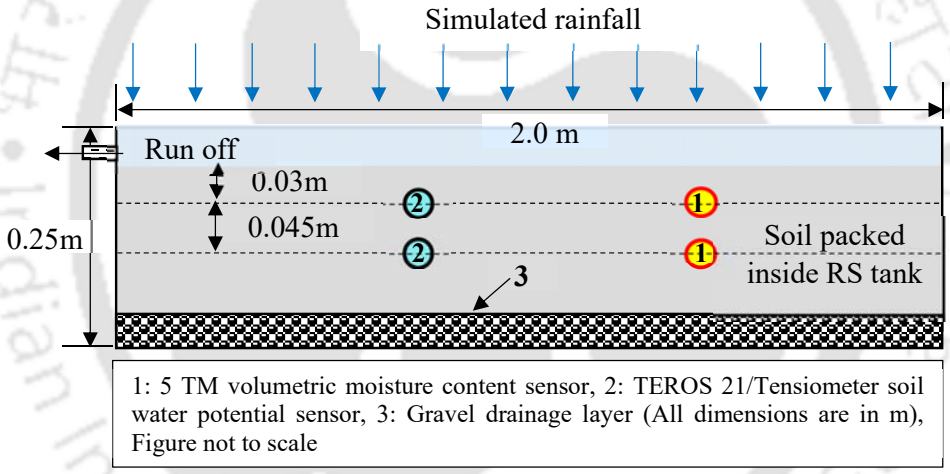

Figure 6.1 Sectional view of the laboratory rainfall simulator (RS) with depth wise placement of sensors

Before conducting RS measurements, the soil was first packed inside the RS tank in different layers and two 5TM and TEROS21/Tensiometers were placed at depths 3cm and 7cm below the soil surface as shown in Figure 6.1. For simulating rainfall, varying rainfall intensities (R_i) were considered based on the suggestion of Holden and Burt (2002) to check their influence (if any) on K_s determination. For each soil, four repetitions were carried out. For LM soil, the experiment duration was fixed at 60 minutes, while for SN soil, it was varied based on R_i, as listed in Table 6.2. The rainfall intensity considered in this study corresponds

to very high rainfall (Subramanya, 2013) for simulating the worst conditions where both runoff and infiltration will be prominent.

Table 6.2 Details for rainfall simulator and mini disc infiltrometer measurements

Soil	Repetition for RS	Rainfall intensity used in RS (mm/h)	Measurement duration (minutes)		*Suction set in MDI (cm)
			RS	MDI	
Loam (LM)	1	99	60	130	2
	2	99			2
	3	73			5
	4	73			5
Sand (SN)	1	99	35	100	5
	2	132	26		5
	3	264	16		5
	4	148	24		5

*Same suction value was used at all the six locations for a given set of experiment

The MDI experiments were also carried out on the soil bed prepared inside the RS. Similar to the RS experiments, the initial conditions (w_i and γ_d) were kept constant, and the soil bed was freshly prepared for the MDI experiments each time. Four sets of MDI experiments were conducted for each soil, corresponding to four repetitions of RS experiments. Each set of MDI measurements consisted of six experiments at different locations inside the RS setup, as shown in Figure 6.2. A 5TM sensor was also placed at each of the six locations at a depth of 3 cm below the soil surface for simultaneous recording of VWC variation over time during MDI measurements. The spacing between six MDI locations was sufficient to avoid any boundary effect on the wetting front from the 3-D flow of MDI (Bordoloi et al., 2018). For a set of MDI measurements, the duration and negative pressure head (h_0) values were kept the same at all six locations. A total of 8 experiments with RS (four repetitions each for LM and SN) and 48 MDI measurements (four sets each for LM and SN in which each set had six measurements) were conducted. A nominal h_0 of 2 cm was applied for the first two sets (12 experiments) of MDI measurements of LM, and for the remaining 12 experiments, h_0 of 5 cm was selected. For SN soil, all four sets of MDI experiments were conducted at h_0 of 5cm. The details are listed in Table 6.2. Similarly, for conducting experiments with SATURO, the infiltrometer was placed at the centre over the freshly prepared soil bed in the RS container (Figure 6.2). Four repetitions for each soil were also carried out for the SATURO infiltrometer. The details of test configurations are given in Table 6.3. The duration of soak time and hold time (User manual,

SATURO, METER Group) were kept varying for the repetitions to check if there was any influence of those factors on the estimated K_s values.

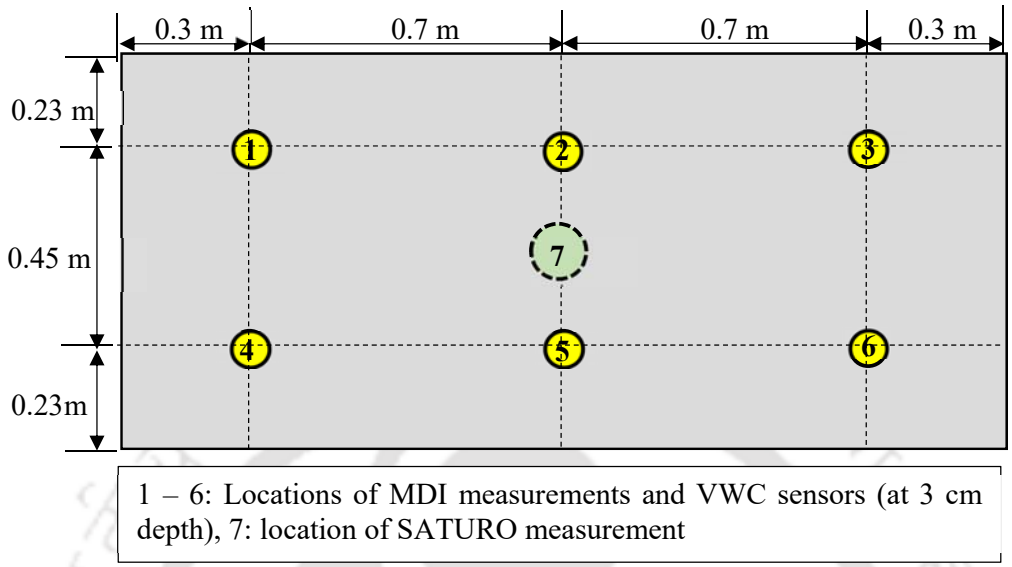

Figure 6.2 Plan view of MDI, VWC sensors, and SATURO locations inside laboratory rainfall simulator

Table 6.3 Test conditions adopted in SATURO infiltrometer

Soil Type	Repetitions	Soak Time (min)	Low Pressure head (cm)	High pressure head (cm)	Hold time (min)	No of Pressure cycle	Total run time (min)
Loam	1	25	5	10	15	3	115
	2	25			15	4	145
	3	30			20	3	150
	4	15			20	2	95
Sand	1	10	5	10	10	3	70
	2	15			10	3	75
	3	25			15	3	115
	4	15			15	2	75

In addition to three instruments (RS, MDI, and SATURO), PM tests were conducted for both the soils corresponding to the same initial compaction conditions listed in Table 6.1. A total of 8 repetitions of PM measurements were conducted for both the soils, and average K_s was computed. The average value was used as the reference K_s for comparing the estimates from the other three instruments.

It was reported in the literature that the initial conditions would influence near-saturated hydraulic conductivity (Ghosh & Pekkat, 2019c). It is crucial to alleviate the effect of initial conditions on the comparison of the methods considered in this study. Therefore, the soil was packed at the same w_i and γ_d (Table 6.1) for RS, MDI, SATURO, and PM measurements in order to maintain identical initial conditions as stated above. Care was taken to pack fresh air-dried soil samples for every measurement. The controlled laboratory measurements adopted in this study alleviate the influence of soil heterogeneity and unknown preferential flow paths expected in the field. The uncertainties associated with such influences in the field may complicate the comparisons of different infiltration measurement methods and mislead the interpretations.

6.2.4. Inverse estimation of K_s from MDI measurements

Besides all the experimental evaluations, the K_s from MDI measurements were also evaluated using the numerical inversion technique performed in HYDRUS 3D-3.01 (Simunek et al., 2018). The flow measurements from MDI were numerically simulated in HYDRUS-3.01 with the help of a 2-D axisymmetric geometry by keeping the initial and boundary conditions the same as in the laboratory experiments. The depth (z) and radius (r) of the flow domain were kept as 0.23 m and 0.2 m, respectively. A schematic diagram illustrating the domain geometry along with its dimensions and boundary conditions (BC), is presented in Figure 6.3. The BC-1, BC-2, and BC-3 in the figure represent the constant head, no flux, and free drainage boundary conditions, respectively. The value of BC-1 was equal to the h_0 set in the MDI (Table 6.2). Node 1 represents the location (observation node) where VWC was recorded using the 5 TM sensor.

The modified form of the Richards flow equation (Warrick, 1992) along with van Genuchten-Mualem (VGM) soil hydraulic function (Mualem, 1976; van Genuchten, 1980) were used for the inverse estimation of K_s from the measured MDI data. HYDRUS employs the Levenberg Marquardt algorithm (Marquardt, 1963) for optimization. The optimization technique is based on minimising the objective function, which represents the sum of squared deviations between the simulated and measured values (Rashid et al., 2015). The details related to the flow equation, soil hydraulic models, objective function, and the optimization technique are discussed in detail in Chapter 3 (section 3.4) and also in the literature (Šimůnek et al., 1998; Šimůnek and van Genuchten, 1996; Šimůnek et al., 2012). For carrying out the inverse simulation in HYDRUS, the MDI measured CI versus time response, VWC versus time (t) (measured with 5 TM sensor), and final VWC (θ_f) recorded at the end of each MDI experiment

were used as input parameters. The θ_f was estimated $\left(\theta_f = w_f.\frac{\gamma_d}{\gamma_w}\right)$ from the final gravimetric water content (w_f) determined immediately after the termination of the test. For all the MDI measurements, the estimated θ_f values matched well with the recorded θ_f from 5 TM measurements.

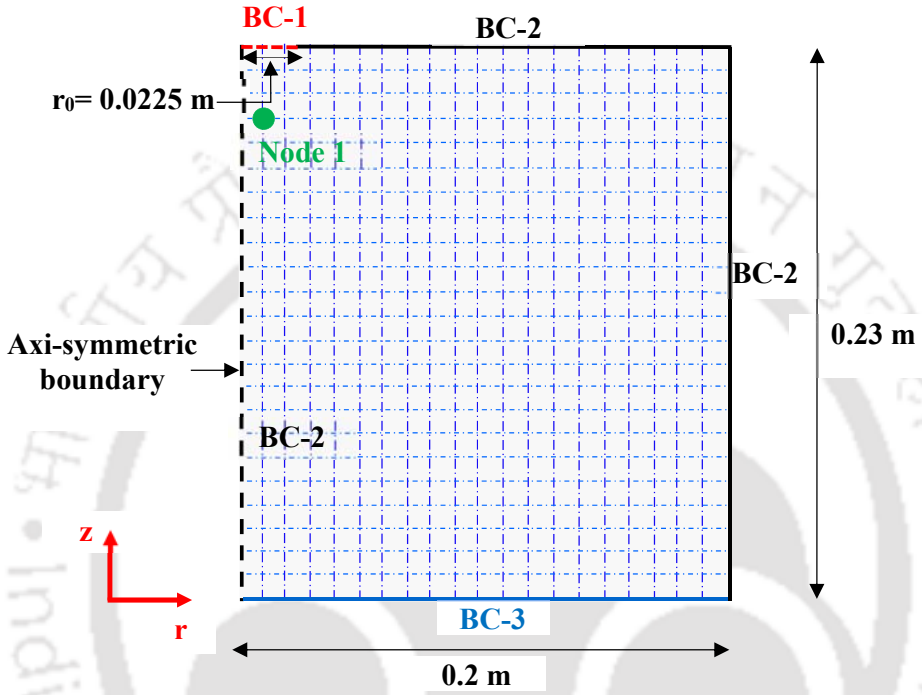

Figure 6.3 Schematic diagram showing flow domain and the boundary conditions (BC) used in numerical simulations of MDI experiments (BC-1-constant head; BC-2-No flux; BC-3- free drainage; Node 1- The observation node where soil moisture is recorded, Figure not to scale)

The initial condition was defined in terms of moisture content (θ_i) and was obtained from the sensor measurements for each experiment (at t=0). The θ_i was identical for all repetitions, with values ranging between 0.05 to 0.09 m^3/m^3 for LM and 0.02 to 0.03 m^3/m^3 for SN soil. The VGM hydraulic model has six parameters; θ_r, θ_s, α, n, l, and K_s. (section 3.4). For all the experiments, the value of θ_r (residual water content) was considered as 0.001 m^3/m^3, which is less than θ_i for all cases (Šimůnek and van Genuchten, 1996). The θ_s were calculated from the measured initial compaction state (Table 6.1), and l was taken as 0.5 (Mualem 1976). For a given MDI experiment, the parameters α, n, and K_s were optimized in three different combinations {(α, n, K_s), (n, K_s), and (α, K_s)} by using texture-based initial guess values reported in the literature (Carsel & Parrish, 1988; Naik et al., 2019). To address the issue of parameter uniqueness, different initial values were used to check whether the inverse

estimation gave similar final estimates, as suggested by Šimůnek et al. (2012). Six simulations were run for a single MDI experiment (the average was denoted as MDI-inv), resulting in 36 simulations for a set of MDI measurements. Previous studies have reported that using additional information (in terms of VWC/SWP or θ_f along with CI improved the parameter uniqueness during the inverse estimation (Schwartz and Evett 2003; Šimůnek et al. 1998; Šimůnek and van Genuchten 1996). Hence, the same optimization strategy was adopted in this study. For a given soil, nearly 144 simulations were carried out, resulting in a total of 288 simulations. The optimized K_s from MDI-inv were compared with the results from other instruments.

6.2.5. Statistical analysis of saturated hydraulic conductivity

The K_s values estimated by different methods were analysed using statistical tests with the help of SPSS software version 25. A one-way ANOVA test was conducted to find the significance of the differences in the mean values of K_s. This was followed by post hoc Tukey HSD (Honest Significant Difference) multiple comparison tests to identify the statistically homogeneous subsets (at a significance level, $\alpha = 0.05$). In addition to this, the Bland-Altman plots (BAp) (Bland and Altman, 1986) were used to compare the K_s estimated from different instruments. The BAp is a statistical method which graphically displays the relationship between two paired variables using the same scale (Ghosh et al., 2019). It is a simple method for assessing any existing bias between the mean differences and estimating an agreement interval within which 95% of the differences between the two methodologies would fall (Giavarina, 2015). In these plots, the mean of the two methods is plotted along the x-axis, and the difference between the two methods is plotted along the y-axis. The plots additionally contain the bias and the 95 % upper and lower limits of agreements (LoA). The bias is calculated by averaging all the difference values. The upper and lower LoA is equal to ±1.96 times the standard deviation of the bias. The existence of any systematic difference between the two methods can be easily evaluated with the BAp. Whether the difference is uniform for the whole measurement range or is limited to any specific range can be graphically assessed with BAp (Ghosh et al., 2019).

6.3. Results

6.3.1. Infiltration measurements

The temporal evolution of rainfall, runoff, infiltration rate, and VWC during RS experiments is presented in Figure 6.4. For four repetitions of each soil, the observed trends

were similar. Hence, the results are presented only for two repetitions, each for LM (Figure 6.4a and b) and SN (Figure 6.4c and d). For a given rainfall intensity, the runoff was initiated when the soil mass was progressively saturated. This is visible from the variation of VWC with time. Beyond a certain duration of time, the VWC attained its maximum value at saturation, which can be considered as a steady-state condition. Similarly, the runoff and infiltration rate approached constant rates. The observation justifies the assumption of a steady-state, which is essential for the determination of K_s. The cumulative infiltration versus time response from the flux-based RS was compared with the head-based SATURO and MDI for LM soil, as shown in Figure 6.5. The results for SN soil have not been provided here for brevity.

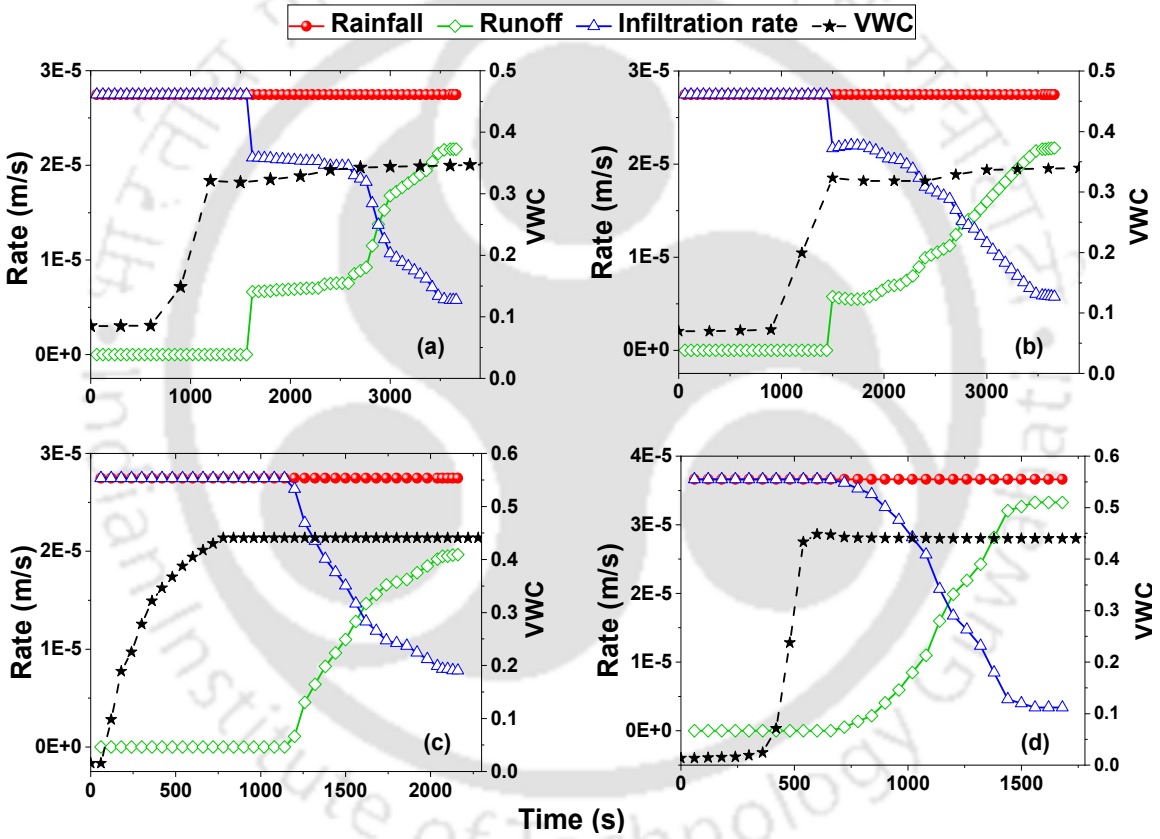

Figure 6.4 Temporal evolution of rainfall, runoff, infiltration rate and volumetric moisture content (VWC) during RS experiments for two repetitions of loam (a and b) and sand (c and d)

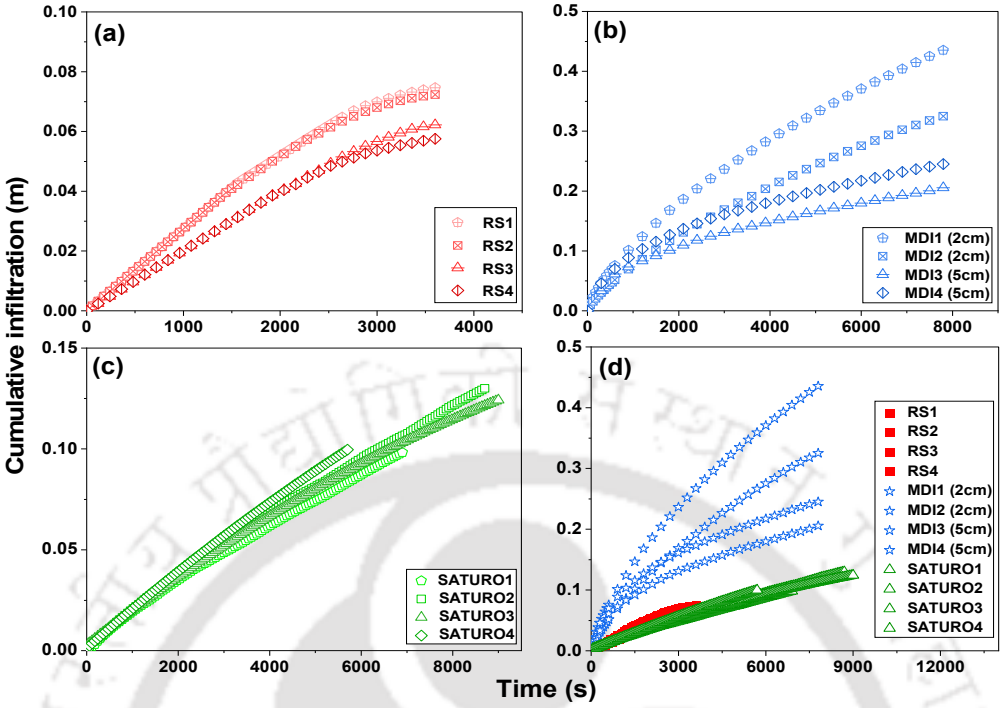

Figure 6.5 Comparison of cumulative infiltration versus time for loam among various repetitions corresponding to a) RS, b) MDI, and c) SATURO and d) comparison between measurements from three devices

Figure 6.5 indicates that all the measured methods gave fairly repeatable CI versus time results. In the case of MDI, the mean CI values from 6 locations (or one set of the experiment) were used for comparison (Figure 6.5b and d). The MDI measurements were performed at two different negative pressure heads (2cm and 5 cm) for LM soil (Table 6.2). As expected, the CI values obtained for the lower pressure head (2 cm) were marginally higher than 5 cm suction. In the case of RS measurements (Figure 6.5a), the use of varying intensities for the repetitions (Table 6.2) has resulted in a minor variation in the slopes of the CI curves. Further, Figure 6.5d indicates that the magnitude of cumulative infiltration response differs for all three measurement methods for the same soil, with RS exhibiting the lowest CI and MDI the highest.

The VWC measurements recorded during RS (at 3 cm and 7 cm depths below the surface) and MDI measurements (3 cm depth below the surface for six locations of a single set) were compared, as shown in Figure 6.6 for soils LM and SN. Figures 6.6 a and b correspond to two repetitions of RS measurements for LM. Similarly, Figures 6.6c and d correspond to two repetitions of RS measurements for SN. The six MDI measurements from a set were used to obtain mean VWC with the corresponding standard deviation curve, as shown in the figure.

The standard deviation curve for MDI measurements shows the influence of soil conditions at specific locations on measurement variability. This endorses that the small measurement footprint of MDI is highly sensitive to the initial soil conditions and hence can capture the spatial heterogeneity with precision. The variability in the measured VWC was more for SN as compared to LM. This may be due to the non-cohesive nature of sand, resulting in spatially non-uniform compaction near to soil surface.

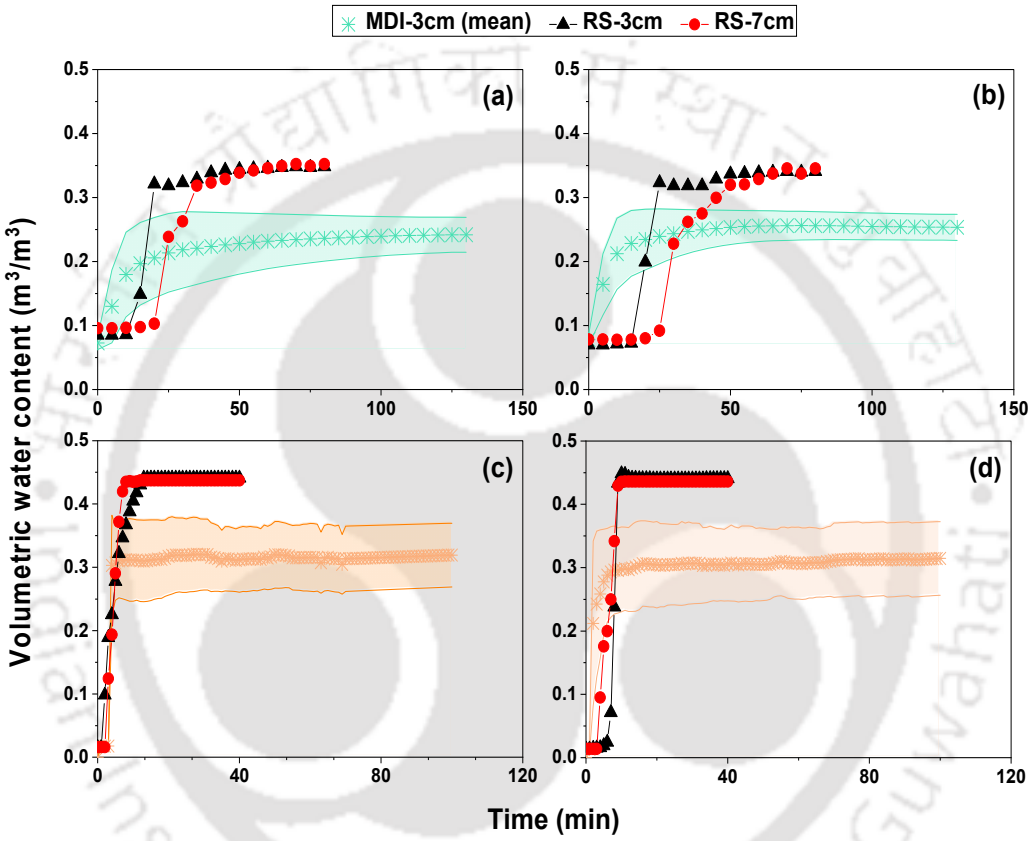

Figure 6.6 Comparison of VWC measured during RS and MDI experiments for two repetitions each of loam (a, b) and sand (c, d) (For MDI, all six measurements from a set were used to obtain mean curve along with its standard deviation)

The initial VWC recorded by the sensors was the same for both RS and MDI, which indicates a nearly uniform initial soil moisture condition within the packed soil. However, the final VWC (θ_f) did not match for RS and MDI measurements. The measured θ_f for LM varied in the range 0.329 to 0.346 m^3/m^3 for RS, while it was 0.205 to 0.275 m^3/m^3 for MDI (Max_{mean} = 0.253 and Min_{mean} = 0.242). Similarly, for SN, the θ_f from RS varied from 0.422 to 0.443 while for MDI it was 0.260 to 0.404 (with Max_{mean} = 0.319 and Min_{mean} = 0.314). It was observed that the RS measured θ_f was always higher than that of MDI, irrespective of the soil

texture. Since all the MDI measurements were conducted under a negative pressure head (Table 6.2), the soil below the MDI did not attain full saturation and hence the low value. The 5TM measures the VWC during the redistribution of infiltrated water in the subsurface. In the case of RS, the VWC redistribution is uniform and one-dimensional due to continuous water infiltration over the whole area. It results in a ponding condition, and hence the VWC measured corresponds to θ_s (or saturated VWC). In MDI, there is a three-dimensional redistribution of water from a point source under a negative pressure head that does not result in full saturation (Bordoloi et al., 2018), and hence the θ_f values are lower than θ_s. A time lag was noticed between measured VWC at 3cm (top) and 7 cm (bottom) depths of RS, implying the progressive saturation as the wetting front advances downwards. The time lag was more prominent for LM (Figures 6.6 a and b) than SN (Figures 6.6 c and d), which was mainly due to higher flow characteristics of the latter resulting in quick saturation. An approximate time to saturation for RS (at 3cm depth) in comparison to MDI was nearly 0.15 times for LM soil and 0.67 times for SN.

6.3.2. Comparison of saturated hydraulic conductivity measurements

The logarithm of saturated hydraulic conductivity (K_s) estimated from RS (using PH and GA methods designated as RS-PH and RS-GA, respectively), SATURO, MDI (using Eq. 3.18, section 3.1.1.1 and inverse analysis designated as MDI-emp and MDI-inv, respectively), and PM are compared as shown in Figures 6.7a and b. The four repetitions of RS and SATURO and four sets of repetitions from MDI (6 MDI measurements for each set = 24 measurements) for the two soils are shown separately. For each soil, PM measurements were repeated eight times, considering its importance as the reference value for comparison. The average K_s from PM and their corresponding standard deviations (in brackets) were 5.8×10^{-7} m/s ($\pm$ 7.4×10^{-9} m/s) and 2.4×10^{-5} m/s ($\pm$ 1.1×10^{-6} m/s) for LM and SN, respectively. Considering minimal variation, the average K_s measured using PM were presented as the reference line in Figure 6.7. It can be noted from the figure that the K_s were repeatable (among four repetitions) for all three devices (RS, SATURO, and MDI), with variations lying within the same order of magnitude for the majority of the cases. The K_s estimated from RS measurements were influenced by the equation chosen. The K_s from RS-PH were consistently one order of magnitude higher for LM and marginally higher for SN (within an order) as compared to RS-GA. The K_s obtained from the RS-GA method matched well with MDI-inv, SATURO, and PM results for both soils. The results of RS and SATURO were consistently marginally higher than PM results for LM soil. This may be due to the effect of better packing in the case of laboratory PM (confined rigid

wall permeameter), resulting in lower K_s for LM. The statistical significance of the observed differences is discussed in section 6.3.3.

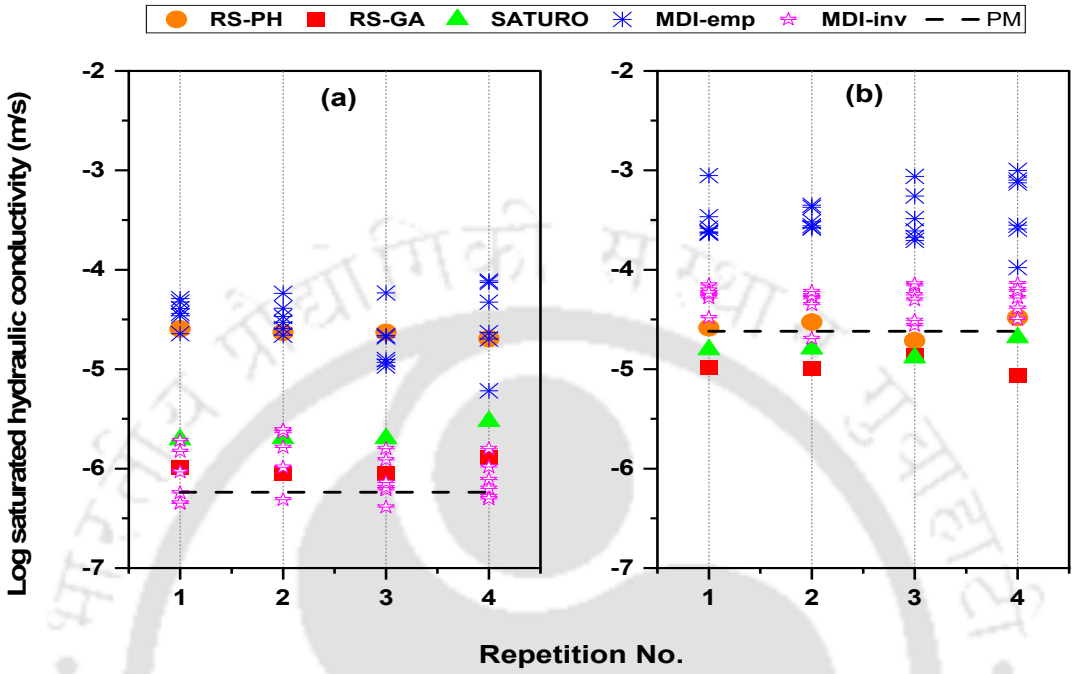

Figure 6.7 Comparison of log saturated hydraulic conductivity estimated using various methods for a) Loam, and b) Sand soils

The K_s determined from MDI-emp were nearly one order higher than the results obtained from other methods for both soils. The MDI-emp results were overestimated from the reference PM values by a factor of 60 for LM and 17 for SN soil. Compared to RS-PH, RS-GA, and SATURO, the K_s from MDI-emp were 1.5, 29, and 13 times for LM, and 15, 38, and 25 times for SN, respectively. The MDI-emp results also exhibited relatively low repeatability for both the soil textures. The coefficient of variation (CV) for the four sets of measurements was in the range of 26-80% for LM and 25-70% for SN. In contrast, the results from MDI-inv were repeatable, and the K_s estimates were fairly close to other devices, including the reference PM for both the soils (Figure 6.7a and b). The K_s from MDI-inv from all the repetitions of LM soil were in the order of 10^{-6} to 10^{-7} m/s and 10^{-5} m/s for SN soil. Considering the measurements from the other methods, the K_s estimates from MDI-inv varied only marginally by factors lying within the range of 0.03 to 4.8, which can be considered negligible for a highly variable parameter like K_s. It is explicit from this study that compared to the empirical method, inverse estimation is a reliable method for K_s estimation while using MDI measurements.

6.3.3. Descriptive statistics of the Ks determined by different methods

Before understanding the factors influencing the K_s determined by three methods, it is essential to quantify the statistical significance of the difference among these methods. As stated before, the PM was considered as the reference method for statistical analysis. The details of descriptive statistics of K_s determined by the three methods are presented in Tables 6.4 and 6.5 for LM and SN, respectively. The statistical values include the mean, standard deviation (SD), standard error (SE), 95% confidence interval, minimum value, and maximum value. For LM, the methods MDI-emp and RS-PH exhibited a maximum difference of two orders of mean K_s compared to PM. The difference in mean K_s values among different methods was relatively negligible for SN except for a one-order difference for MDI-emp. The SD and SE were maximum for MDI-emp for both the soils, which may be attributed to the inappropriate empirical method used to determine K_s.

Table 6.4 Descriptive statistics of saturated hydraulic conductivity determined for loam

Method	Count	Mean	Standard Deviation	Standard Error	95 % confidence interval		Min.	Max.
					Lower bound	Upper bound		
RS-PH	4	2.3E-05	2.2E-06	1.1E-06	2.0E-05	2.7E-05	2.0E-05	2.5E-05
RS-GA	4	1.2E-06	3.2E-07	1.6E-07	7.0E-07	1.7E-06	9.0E-07	1.6E-06
SATURO	4	2.6E-06	6.8E-07	3.4E-07	1.5E-06	3.6E-06	2.0E-06	3.3E-06
MDI-emp	24	3.4E-05	1.9E-05	4.0E-06	2.6E-05	4.3E-05	6.1E-06	7.7E-05
MDI-inv	24	1.1E-06	6.7E-07	1.4E-07	8.2E-07	1.4E-06	4.1E-07	2.4E-06
PM	8	5.8E-07	7.6E-09	2.7E-09	5.7E-07	5.9E-07	5.7E-07	5.9E-07
Total	68	1.4E-05	2.0E-05	2.4E-06	9.5E-06	1.9E-05	4.1E-07	7.7E-05

RS-Rainfall simulator, PH-Philips, GA- Green-Ampt, MDI- mini disc infiltrometer (emp-empirical method, inv-inverse simulation), PM- permeameter

A one-way ANOVA test was carried out to understand the statistical significance of the differences in K_s estimated by different methods. For conducting the ANOVA tests, all the methods (RS-PH, RS-GA, SATURO, MDI-emp, MDI-inv, and PM) were considered as groups, and the significance level (α) was considered equal to 0.05. Table 6.6 provides the ANOVA results for both soils. It can be noted that the calculated F value > $F_{critical}$ and significance value $p < 0.05$. The results indicate a significant difference between the means of the compared methods. To identify precisely which group differs from each other, the Tukey's HSD pairwise multiple comparison test was carried out as the posthoc test following the ANOVA test.

Table 6.5 Descriptive statistics of saturated hydraulic conductivity determined for sand

Method	Count	Mean	Standard Deviation	Standard Error	95 % confidence interval		Min.	Max.
					Lower bound	Upper bound		
RS-PH	4	2.7E-05	5.9E-06	2.9E-06	1.8E-05	3.6E-05	1.9E-05	3.3E-05
RS-GA	4	1.1E-05	2.2E-06	1.1E-06	7.3E-06	1.4E-05	8.7E-06	1.4E-05
SATURO	4	1.6E-05	3.2E-06	1.6E-06	1.1E-05	2.1E-05	1.3E-05	2.1E-05
MDI-emp	24	4.1E-04	2.6E-04	5.2E-05	3.0E-04	5.1E-04	1.1E-04	1.0E-03
MDI-inv	24	5.2E-05	1.5E-05	3.0E-06	4.5E-05	5.8E-05	2.0E-05	7.2E-05
PM	8	2.4E-05	1.1E-06	3.8E-07	2.3E-05	2.5E-05	2.3E-05	2.5E-05
Total	68	1.7E-04	2.3E-04	2.8E-05	1.1E-04	2.2E-04	8.7E-06	1.0E-03

RS-Rainfall simulator, PH-Philips, GA- Green-Ampt, MDI- mini disc infiltrometer (emp-empirical method, inv-inverse simulation), PM- permeameter

Table 6.6 Results from One-way ANOVA test for two soil textures

	Sum of Squares	Degree of freedom (df)	Mean Square	F value	p-value	$F_{critical}$
Loam						
Between Groups	1.70E-08	5	3.40E-09	24.248	1.95E-13	2.363
Within Groups	8.71E-09	62	1.40E-10			
Total	2.57E-08	67				
Sand						
Between Groups	2.13E-06	5	4.25E-07	17.451	9.46E-11	2.363
Within Groups	1.51E-06	62	2.44E-08			
Total	3.64E-06	67				

The results from the Tukey HSD test are summarized in Tables 6.7 and 6.8 for LM and SN soils, respectively. In this pairwise comparison between two groups (G_1 and G_2), if the significance value is < 0.05, the difference is significant (no similarity). The results summarized in Tables 6.7 and 6.8 indicate that all the methods considered in this study are not significantly different except for MDI-emp. Among others, only RS-PH of LM was comparable with MDI-emp measurement. Based on the above observations, it can be concluded that RS-PH, RS-GA, SATURO, MDI-inv, and PM methods gave statistically comparable results for both the soils, and MDI-emp results were consistently different from all other methods.

Table 6.7 Statistics of multiple comparison using Tukey HSD test for loam soil

Method		Mean difference (G_1- G_2)	Standard Error	p-value	95% confidence interval	
(G_1)	(G_2)				Lower Bound	Upper Bound
RS-PH	RS-GA	2.21E-05	8.38E-06	0.104	-2.57E-06	4.67E-05
	SATURO	2.07E-05	8.38E-06	0.149	-3.94E-06	4.53E-05
	MDI-emp	-1.12E-05	6.40E-06	0.504	-3.00E-05	7.61E-06
	MDI-inv	*2.22E-05	6.40E-06	0.012	3.36E-06	4.10E-05
	PM	*2.27E-05	7.26E-06	0.031	1.36E-06	4.40E-05
RS-GA	SATURO	-1.38E-06	8.38E-06	1.000	-2.60E-05	2.33E-05
	MDI-emp	*-3.33E-05	6.40E-06	3.4E-05	-5.21E-05	-1.45E-05
	MDI-inv	1.03E-07	6.40E-06	1.000	-1.87E-05	1.89E-05
	PM	6.21E-07	7.26E-06	1.000	-2.07E-05	2.20E-05
SATURO	MDI-emp	*-3.19E-05	6.40E-06	7.49E-05	-5.07E-05	-1.31E-05
	MDI-inv	1.48E-06	6.40E-06	1.000	-1.73E-05	2.03E-05
	PM	2.00E-06	7.26E-06	1.000	-1.93E-05	2.33E-05
MDI-emp	MDI-inv	*3.34E-05	3.42E-06	1.17E-12	2.33E-05	4.34E-05
	PM	*3.39E-05	4.84E-06	3.09E-08	1.97E-05	4.81E-05
MDI-inv	PM	5.18E-07	4.84E-06	1.000	-1.37E-05	1.47E-05

* The mean difference is significant at α = 0.05

Table 6.8 Statistics of multiple comparison using Tukey HSD test for sand soil

Method		Mean difference (G_1- G_2)	Standard Error	p-value	95% confidence interval	
(G_1)	(G_2)				Lower Bound	Upper Bound
RS-PH	RS-GA	1.62E-05	1.10E-04	1.000	-3.08E-04	3.41E-04
	SATURO	1.07E-05	1.10E-04	1.000	-3.14E-04	3.35E-04
	MDI-emp	*-3.79E-04	8.43E-05	4.21E-04	-6.27E-04	-1.32E-04
	MDI-inv	-2.46E-05	8.43E-05	1.000	-2.73E-04	2.23E-04
	PM	2.91E-06	9.56E-05	1.000	-2.78E-04	2.84E-04
RS-GA	SATURO	-5.54E-06	1.10E-04	1.000	-3.30E-04	3.19E-04
	MDI-emp	*-3.96E-04	8.43E-05	2.14E-04	-6.44E-04	-1.48E-04
	MDI-inv	-4.08E-05	8.43E-05	0.997	-2.89E-04	2.07E-04
	PM	-1.33E-05	9.56E-05	1.000	-2.94E-04	2.68E-04
SATURO	MDI-emp	*-3.90E-04	8.43E-05	2.70E-04	-6.38E-04	-1.42E-04
	MDI-inv	-3.53E-05	8.43E-05	0.998	-2.83E-04	2.13E-04
	PM	-7.76E-06	9.56E-05	1.000	-2.89E-04	2.73E-04
MDI-emp	MDI-inv	*3.55E-04	4.51E-05	9.72E-10	2.22E-04	4.87E-04
	PM	*3.82E-04	6.37E-05	1.63E-06	1.95E-04	5.70E-04
MDI-inv	PM	2.75E-05	6.37E-05	0.998	-1.60E-04	2.15E-04

* The mean difference is significant at α = 0.05

Following ANOVA and posthoc test, the Bland-Altman plots (Bland and Altman, 1986) were used for the visual illustration of the bias, agreement, and for understanding any systematic difference exhibited by the compared methods. The Bland-Altman plots for LM and SN soils are shown in Figures 6.8 and 6.9, respectively. It is noteworthy that the trends observed in a majority of the cases are similar for both the soil textures. The figures show that in all the cases, the data points fall well within the LoA. The RS-PH results have a positive bias with respect to RS-GA results, and the bias is not close to zero stating the existence of method dependency on the estimates. Compared with SATURO, the RS-PH and RS-GA values exhibit positive and negative bias, respectively. Compared with MDI-emp, all the other methods were negatively biased for both soils. In the case of LM soil, SATURO, RS-PH, and MDI-emp were positively biased compared to MDI-inv, while RS-GA had a bias close to zero. For SN soil, all the methods were negatively biased compared with MDI-inv except MDI-emp.

Closer inspection of the plots reveals the presence of systematic differences in the majority of the cases for both soils. There is either a consistently increasing trend (RS-PH vs. RS-GA, RS-PH vs. SATURO, RS-PH vs. MDI-inv, and MDI-emp vs. MDI-inv) or a decreasing trend (RS-PH vs. MDI-emp, RS-GA vs. MDI-emp, SATURO vs. MDI-emp) observed in the results. For RS-GA vs. SATURO, RS-GA vs. MDI-inv, and SATURO vs. MDI-inv, the data points were scattered around the bias stating that there was no systematic difference. Also, in LM soil, the bias was close to zero for the above three comparisons implying that the three methods were highly comparable. On a similar basis, the methods RS-GA and SATURO are found to be highly comparable for SN soil. Based on the BAp results, the sequence of K_s estimation followed the order; RS-GA ≈ SATURO ≈ MDI-inv ≤ RS-PH < MDI-emp. Three important aspects are relevant from these observations, (i) SATURO, RS-GA, MDI-inv are consistent for determining K_s, (ii) RS is sensitive to the mathematical formulation adopted for determining K_s, and (iii) K_s from MDI-emp is inconsistent for both the soil textures.

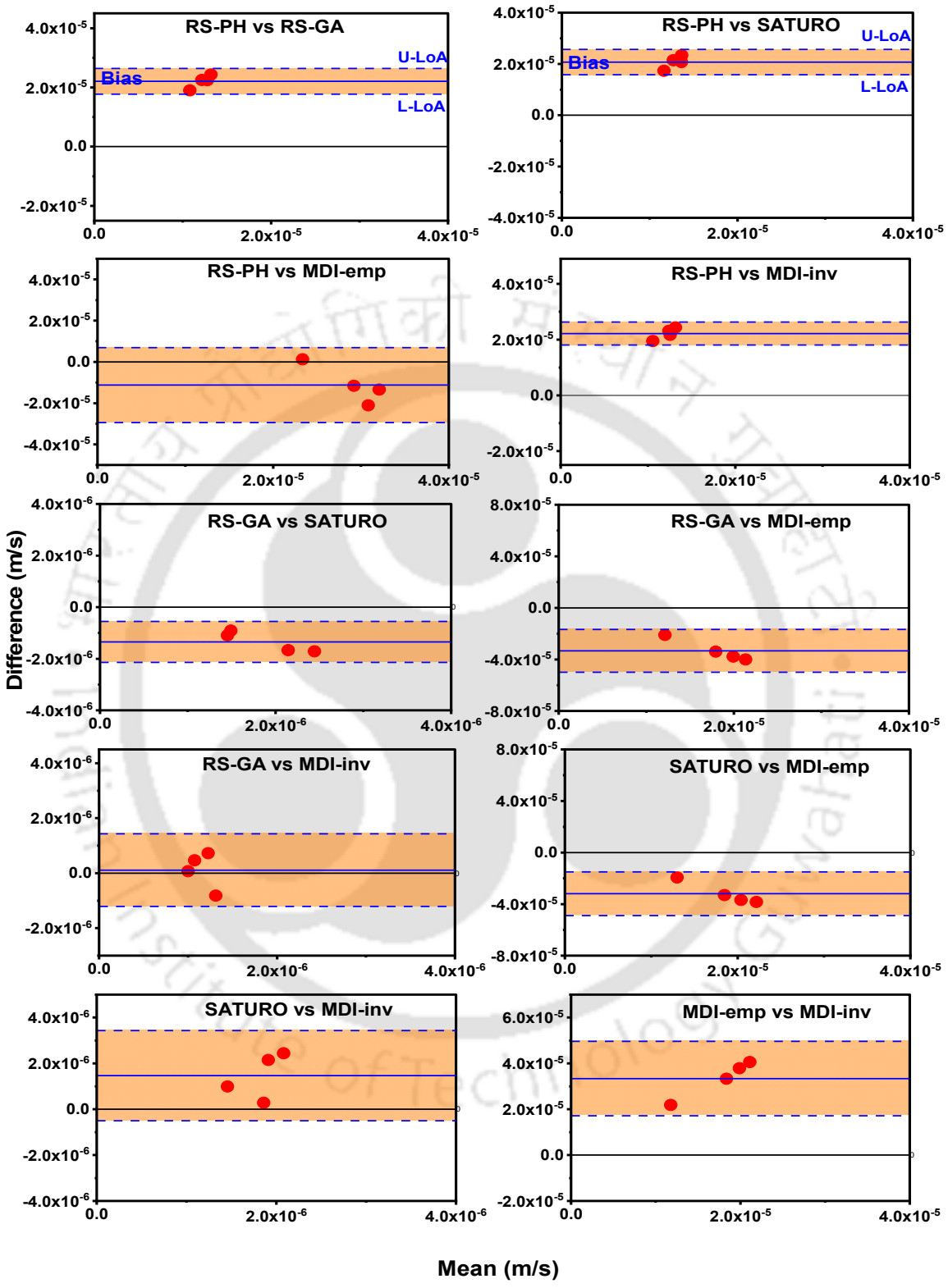

Figure 6.8 Bland-Altman plot showing comparison between various methods for loam soil (U-LoA- Upper Limit of Agreement, L-LoA- Lower Limit of Agreement)

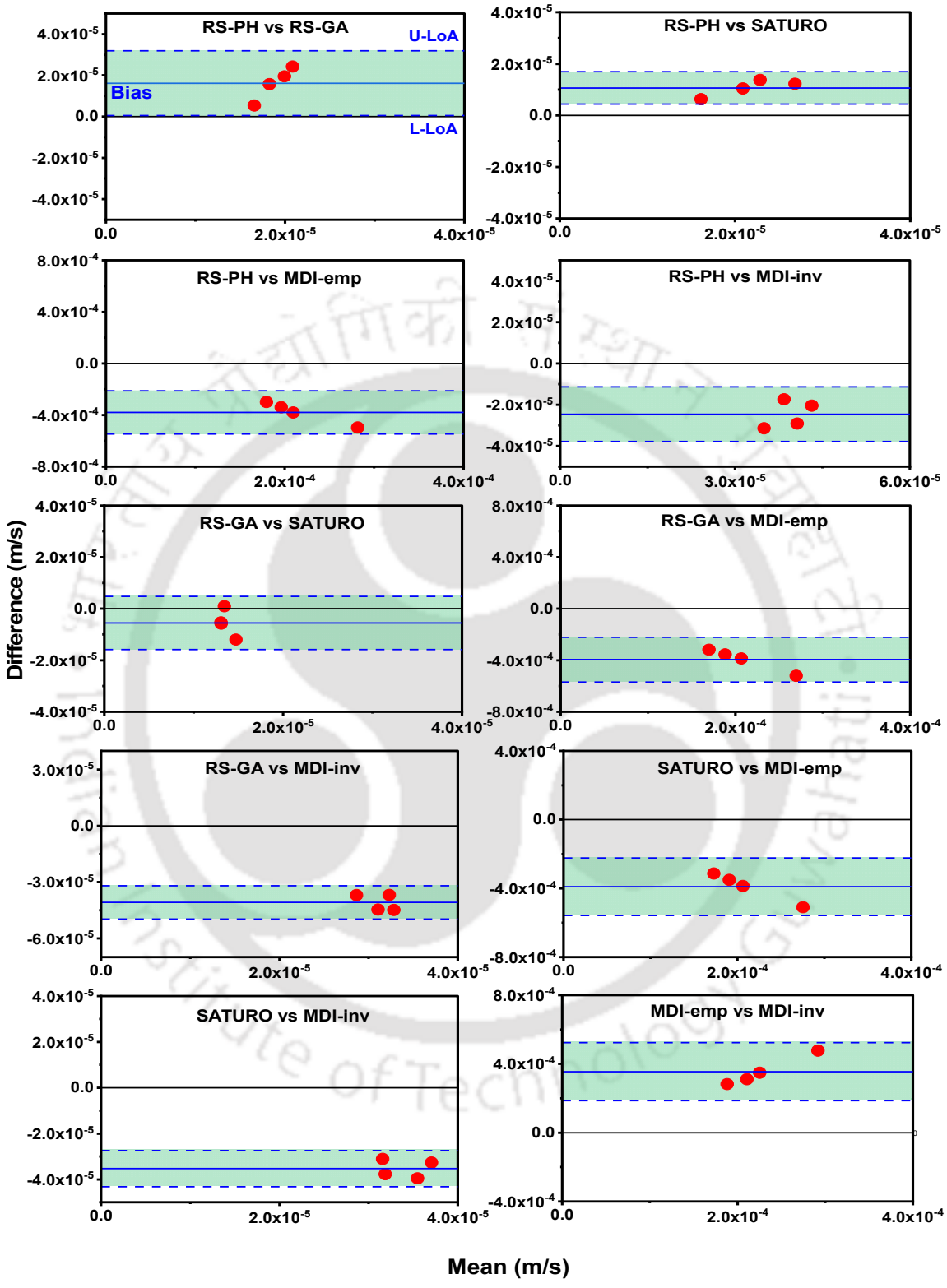

Figure 6.9 Bland-Altman plot showing comparison between various methods for sand soil (U-LoA- Upper Limit of Agreement, L-LoA- Lower Limit of Agreement)

6.3.4. Influence of measurement signature and mathematical formulations on K_s determination

For the same soil texture and initial conditions, it is apparent from the earlier results that (i) measurement footprint (MF) and (ii) mathematical formulations (M-EQ) are the two important factors that result in the variation in K_s determined by flux-based and head-based methods. For quantifying the influence of these two factors, a mean CI versus time curve, as shown in Figure 6.10, was considered for each instrument, and GA, PH, and ZH (Eq. 3.11) were selected as the mathematical formulations. For quantifying the influence of MF, the mean CI curves from all three devices were analysed using the same mathematical formulation, and the K_s values were obtained. Similarly, the three mathematical formulations were applied separately to the mean CI curve of each device for quantifying the influence of M-EQs. A graphical representation of K_s variability for each soil is presented as a box and whisker plot (25-75%), as shown in Figure 6.11. The variations in K_s for different MFs using specific M-EQs are presented along the x-axis as GA, PH, and ZH. Similarly, the variations by using different M-EQs for each MF are presented along the x-axis as RS, SATURO, and MDI. Considering all the values together, the variations are shown as ALL along the 1st column on the x-axis. The standard deviation and CV (in parenthesis) in the estimated K_s for each case were also determined and listed in Table 6.9.

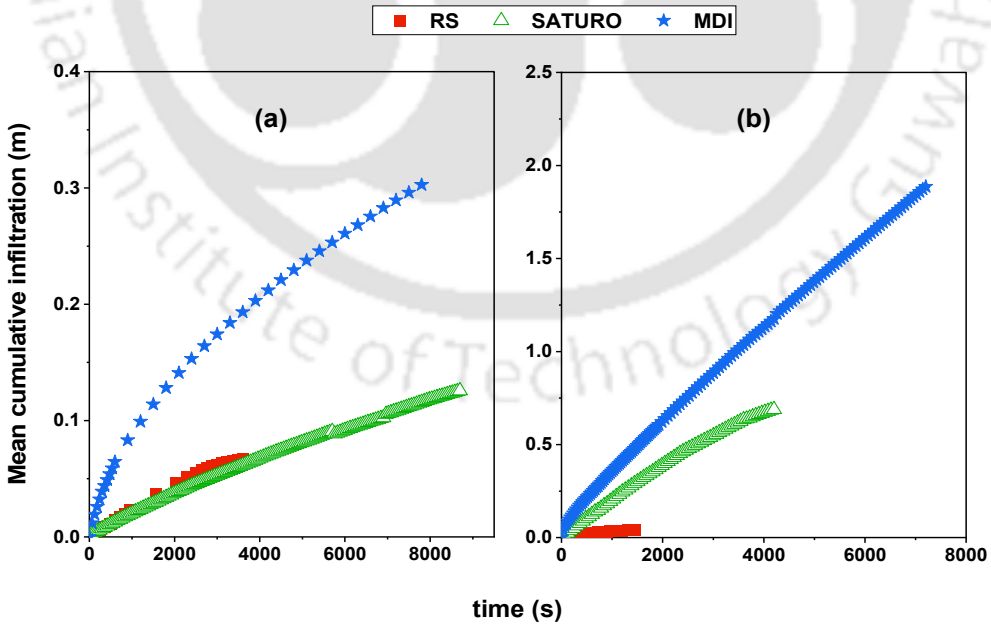

Figure 6.10 Mean cumulative infiltration versus time curve for different instruments considered in this study for (a) loam and (b) sand

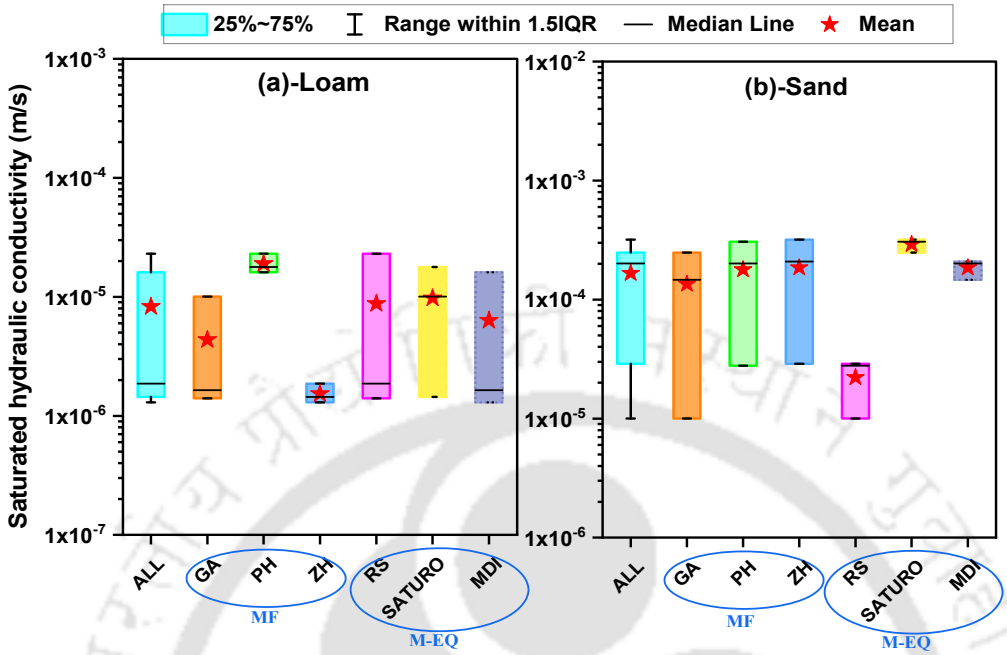

Figure 6.11 Box plots showing K_s variability for (a) loam and (b) sand for understanding the influence of measurement footprint (MF) and mathematical formulations (M-EQ)

Table 6.9 Calculated standard deviation (x 10^{-6} m/s) and coefficient of variation (%) values of K_s for elucidating the influence of measurement footprint (MF) and mathematical formulation (M-EQ)

Soil	Same M-EQ applied to mean curves of 3 different MFs			Different M-EQs applied to mean curve of each MF		
	GA	PH	ZH	RS	SATURO	MDI
LM	4.93 (113)	3.64 (19)	0.29 (19)	12.38 (141)	8.44 (133)	8.19 (84)
SN	119.6 (89)	140.7 (79)	146.2 (79)	10.57 (48)	34.06 (18)	37.52 (13)

GA- Green-Ampt, PH-Philips, ZH-Zhang. The values in parenthesis are coefficient of variation values in %.

From Table 6.9 and Figure 6.11, it can be noted that the results are texture-dependent. For LM soil, the use of different M-EQs has resulted in higher variability than the MF. For SN, different MFs exhibited high variability compared to M-EQs (Figure 6.11b). The observations are also fairly supported by the CV values listed in Table 6.9. It is seen that the standard

deviation and CV values are relatively higher for M-EQs in LM and MFs in SN. It was also noted from Table 6.9 that the GA formulation was relatively more sensitive to variations in CI response in both the soils (high CV). This behaviour is expected as the GA method is highly dependent on CI response (Eq. 3.23), and the other two formulations (PH and ZH), being mathematically similar, have resulted in nearly the same CV for both the soils.

6.4. Discussion

It was reported from Figures 6.5 and 6.10 that an increase in measurement footprint resulted in low CI. Such variations in CI versus time response were also reported by Ghosh and Pekkat (2019a). Furthermore, the RS strictly follows a one-dimensional flow condition and has a no-flux boundary on all four sides (Figure 6.1). On the other hand, SATURO has a circular geometry with a partially restricted flow zone (5cm depth like ring infiltrometer) and three-dimensional flow, whereas the MDI has a three-dimensional flow regime with no restrictions. For the LM soil (Figure 6.5d), the SATURO measurements were comparable with RS and lower than the MDI. For the SN soil, the SATURO measurements were higher than the RS and lower than the MDI (Figure not shown). The initial soaking period mandated in SATURO (as a part of its procedure) would also result in lower infiltration than MDI (for MDI measurements, initial conditions were relatively dry).

A comparison of K_s between various methods (Figure 6.7) showed that the MDI-emp results were highly variable. Such variability in MDI-emp results is expected due to the smaller measurement footprint of MDI, making it more sensitive to initial soil conditions (Ghosh and Pekkat, 2019d; Lai and Ren, 2007; Zhang et al., 2019). Hence, any small variations in the initial condition influenced the MDI-emp estimates. Despite all this, the variability in MDI-emp was still within one order of magnitude for most of the measurements. It is noteworthy that the moderate variations in the observed CI responses resulted in negligible variations in the K_s estimated from MDI-inv for both the soil textures. It is reported that the parameter optimization technique results in unique and stable final estimates when the inverse problem is well-posed (Nakhaei and Šimůnek, 2014). By providing sufficient input and optimizing fewer parameters, well-posedness can be ensured during inverse estimation (Ritter et al., 2003). In this study, the number of optimized parameters was kept less (maximum three simultaneously), and sufficient input in terms of CI and VWC resulted in consistent estimates of K_s. Moreover, the empirical method adopted for analysis has a high chance of getting biased by the choice of the retention parameters (α, n) and the factor m (Fodor et al., 2011; Ronayne et al., 2012). On the other hand, the inverse estimation enables optimizing these parameters based on the realistic

measured signature (CI versus time), which is a function of actual subsurface condition and thus, results in the reliable prediction of K_s.

Based on these discussions, it is understood that there are two major factors affecting K_s determination for given identical soil conditions vis (a) measurement signature (CI versus time response) and (b) the mathematical formulations inclusive of its assumptions. For unraveling this better, an effort was made to study the influence of both these factors on the determination of K_s (section 6.3.4). Based on the overall results, it can be summarized that M-EQ has more influence on K_s determination than MF for fine-textured soil. For coarse-textured SN, the MF has more influence than M-EQ. However, this conclusion needs to be further validated by considering different soil textures and other mathematical formulations.

6.4.1. Relevant K_s comparisons reported in the literature

The observations from this study indicate that the K_s determined from the infiltration measurements of RS and SATURO compared well with each other and also with laboratory 1-D permeameter. The RS measures K_s corresponding to 1-D flow and for SATURO while the flow is 3-D, the correction factor takes care of the lateral divergence component to provide 1-D K_s measurements (section 3.3.2). Hence, the three devices resulted in comparable K_s estimates. However, K_s obtained from 3-D MDI measurements were overestimated for both the soil textures when empirical equation was used. Such an overestimation can be alleviated by employing inverse estimation of K_s based on MDI measurements. An attempt was made to cross-verify the K_s comparisons from this study with the details reported in the literature, as summarized in Table 6.10. The table lists different field and laboratory comparisons with inherent theoretical constraints and mathematical equations used for estimating K_s. It is worth noting that out of 22 studies, only 4 focused exclusively on comparing flux-based and head-based methods for K_s determination. The majority of the studies were conducted in the field, and hence there is a possibility of inherent unknown, unintentional factors influencing the results, and hence comparison of K_s becomes difficult. In addition, it was noted that flow dimensionality and the scale effect do influence the K_s determination.

The role of macro/micro-cracks and the heterogeneities are more prominent when the comparisons are made in the field (natural state of soil). Depending on the MF and location of measurements, a given instrument is likely to be influenced by the presence or absence of cracks. This aspect was highly relevant for MDI due to its small MF. The MDI measurements gave lower or higher K_s depending on whether the soil below the disc was low permeable fine-grained soil or had cracks (preferential flow), respectively. The results of MDI are also biased

by the choice of water retention parameters (Fodor et al., 2011; Ronayne et al., 2012) and empirical factor (m) used in the data analysis. This study and others in the literature (Mohanty et al., 1994; Radinja et al., 2019) gave higher K_s based on MDI, whereas others indicated lower K_s (Ronayne et al., 2012) when empirical procedure is considered. Most field studies gave lower K_s from MDI, whereas laboratory studies gave comparable or higher K_s. Since the MDI measurements in this study were performed on laboratory-packed samples, the influence of preferential flow paths was negligible. Hence, the difference in results reported in this study is exclusively dependent on the MF, M-EQ, and inherent assumptions (already well-established in the literature). It is worth noting that there are no studies in the literature that compare the K_s determination from MDI by considering empirical formulation and inverse estimation with other K_s measuring methods like RS, SATURO and PM.

The determination of K_s by the RS method is influenced by the mathematical procedure adopted. Although the RS has been recognised as a promising device for K_s estimation, its major handicap is that it can only be used in large field applications, necessitating extensive instrumentation and monitoring, which is not always practical. There are several literatures that have demonstrated the utility of SATURO for determining K_s in the field. In the case of SATURO (or any ring infiltrometer), if the soil conditions are such that the ring installation (driving) causes closure of preferential paths, it can lower K_s. However, if the ring installation results in dilation of soil or cracks formation, it can increase K_s. Being a new instrument, it was opined that more comparative assessments are needed to gain more confidence in using SATURO. The controlled laboratory measurements conducted in this study clearly endorse the accuracy of the head-based SATURO based on its closeness with flux-based RS and head-based PM methods. A comparison with the other discussed reliable instruments showed that the handy MDI can also be used reliably for K_s, provided an inverse estimation procedure is followed, and additional information is available (VWC measurements).

Table 6.10 Comparison of K_s obtained from infiltration measurements reported in the literature

Literature	Comparison	Major findings
Gupta et al., (1993, 1994)	Flux based RS Head based DRI, GP, GI	•RS analysed by PH method was 2.5 to 3 times higher than DRI and GP •Insignificant statistical difference of RS with GI •Differences due to (a) measurement methodologies, (b) theoretical constraints/ mathematical models, (c) different depths of measurement (d) large surface area sampled by the RS
Paige and Hillel (1993)	GP, IPM, Soil cores	• GP gave one to three orders lower value than soil cores and IPM
Mohanty et al. (1994)	GP, VP, DP, DTM, LP	• GP gave lowest values • VP gave intermediate values • DTM and DP gave highest values • VP and LP were comparable
Vanderlinden et al. (1998)	DRI, TI, FP, LP	•DRI geometric means were one order higher than TI •LP and DRI were comparable • FP and TI were comparable
Reynolds et al. (2000)	TI, SRI, soil cores	•For high permeability condition TI method yielded lower values • For low permeability conditions the methods were comparable
Fodor et al. (2011)	Head based DRI, MDI, TI, SCI in the field LP (reference method)	• Quantified the variations due to different evaluation methods for individual devices • Variations in MDI was associated with different WRCCs • No comparison made for K_s
Kohne et al. (2011)	DRI, TI in the field	• K_s from DRI was 7 to 33 times higher than TI
Ronayne et al. (2012)	DRI, MDI and GP in the field	•For MDI, $K(h) \approx K_s$ (due to low negative pressure head of 0.5 cm to 2.0 cm) •MDI $K_s <$ DRI and GP K_s

		•MDI K_s sensitive to WWRC, flow dimensionality, macropores, scale effect, small size of MDI •MDI preferentially sample low permeable fine-grained fraction of the till giving low K_s
Verbist et al. (2013)	Flux-based RS Head based SRI, DRI, LP, IA, TI	• SRI and DRI gave higher values • IA and LP gave similar results •TI gave the lowest values
Bagarello et al. (2014a)	SRI, FH	•FH gave higher values than SRI by a factor ranging from 3 to 190
Alagna et al. (2016)	BEST, SRI, TI, MDI, FH, BB	• All methods yielded statistically similar estimates • Highest for TI and MDI • Intermediate for FH •Lowest for BB, BEST and SRI
Morbidelli et al. (2017)	Flux-based RS (reference method) Head based DRI, GP, TP	• DRI overestimated • GP overestimated at lab scale and underestimated at plot scale • TP overestimated • Observations influenced by spatial heterogeneity, sensitivity to standard procedures, unstable equations •Causes of the observed discrepancies need further research
Nestingen et al. (2018)	MPD, DRI, and MDI in the lab LP (reference method)	•MPD had the lowest relative error •DRI was precise •MDI had high relative error for coarse texture •Three instruments assumed different flow regime and mathematical procedures
Ghosh et al. (2019)	DRI, MDI, TI, GP in the field LP	•DRI result was between lab permeameter and disc infiltrometer •MDI and TI exhibited negative bias with DRI, GP •MDI versus TI exhibited bias close to zero

		•GP versus DRI exhibited bias close to zero
Radinja et al. (2019)	DRI, MDI, and SATURO in the field	•SATURO > MDI > DRI •SATURO gave 6.8 times higher values than DRI •Installation disturbance closed preferential pathways resulting in low K_s from DRI
Zhang et al. (2019)	DRI and SATURO in the field	•9 out of 14 cases gave similar results •5 cases gave higher SATURO values •Larger footprint for SATURO than DRI •Different operational procedures, infiltration time, and soil spatiotemporal variability •Smaller infiltration area of DRI possibly missed soil macropores
Ebrahimian et al. (2020)	DRI, SRI, MPD, and SATURO in the field	•MPD and SATURO showed promising results for K_s determination •SATURO being a new test method needs more comparisons with the existing methods
Ravi et al. (2017) Thomas et al. (2018), Jahanzad et al. (2020), Norris et al. (2020), Fae et al. (2020)	SATURO	•These studies established the successful use of SATURO for K_s determination •No comparisons were made with other instruments

RS: rainfall simulator; DRI: double ring infiltrometer; SRI: single ring infiltrometer; GP: Guelph permeameter; GI: Guelph infiltrometer; TP: tension permeameter; TI: tension infiltrometer; MDI: mini disc infiltrometer; SCI: suction crust infiltrometer; MPD: modified Philip-Dunne infiltrometer; IPM: instantaneous profile method; VP: velocity permeameter; DP: disc permeameter; DTM: double tube method; FP: falling head borehole permeameter; IA: inverse auger hole method; BB: bottomless bucket method; BEST: Beerkan estimation of soil transfer parameters; FH: falling head permeameter; LP: laboratory permeameter; PH: Philip's method; WRCC: water retention characteristics curve

6.5. Summary

This study compared the saturated soil hydraulic conductivity (K_s) determined using a flux-based measurement (rainfall simulator, RS), two head-based infiltration measurements (SATURO and mini disc infiltrometer, MDI), and laboratory falling head permeameter (PM). Two soil textures, loam (LM) and sand (SN) were packed in the RS tank, instrumented with volumetric moisture content (VWC) and soil water potential sensors for continuous real-time monitoring. All the measurement methods exhibited fair repeatability, and the variability of results was within one order of magnitude. The VWC measured during the RS experiments justifies the assumption of steady-state, which is vital for the determination of K_s. The measurement signature in terms of cumulative infiltration (CI) versus time was influenced by measurement footprint area, with RS exhibiting the lowest CI and MDI the highest. The K_s estimated from RS measurements were sensitive to the mathematical equations, wherein RS analysis based on Philip's equation (RS-PH) gave higher values as compared to the Green Ampt equation (RS-GA). The K_s obtained from the RS-GA method matched well with head-based SATURO and PM results for both the soils. The K_s from MDI measurements were obtained using a combined empirical formulation based on Zhang (ZH) and Kutilek and Nielson method (designated as MDI-emp). In addition, K_s were determined by inverse estimation from the CI versus time measurement signature of MDI (designated as MDI-inv). The following conclusions were derived based on the above study.

- The K_s determined from MDI-emp were one order higher than the results obtained from other methods for both the soils. The small measurement footprint of MDI is highly sensitive to the initial soil conditions, thereby resulting in high measurement variability when analysed using empirical method.
- The K_s obtained from MDI-inv were consistent and more repeatable as compared to MDI-emp, and also matched well with the other flux-based and head-based methods for both the soil textures.
- Statistical significance tests indicated that RS-GA, RS-PH, SATURO, MDI-inv, and PM results were not significantly different, whereas K_s from MDI-emp were statistically different from all other methods. Based on the graphical statistical assessment using Bland Altman plot (BAp), the sequence of K_s estimation followed the order RS-GA ≈ SATURO ≈ MDI-inv ≤ RS-PH < MDI-emp. Three important conclusions derived from these observations are
    i. SATURO, RS, and MDI-inv are reliable methods for determining K_s,

ii. RS is influenced by the mathematical formulation adopted for determining K_s, and
iii. MDI-emp resulted in the overestimation of K_s.

- The difference in results reported in this study among various instruments is exclusively dependent on the (a) measurement footprint, (b) measurement signature, (c) flow dimensionality, and (d) mathematical procedure with its underlying assumptions. Among these, the measurement footprints have more influence on K_s determination as compared to the mathematical formulation for the coarse-textured SN soil and vice versa for the fine-textured LM soil.

The observations from this study were compared with 22 studies from the literature. The advantage of the current study is that due to the controlled laboratory measurements, the results are not biased by unknown or hidden factors (like the presence of cracks) that may exist in the field. The results clearly endorse the accuracy of head-based SATURO and MDI-inv for determining K_s based on their closeness with the flux-based RS method and laboratory PM. The advantage of MDI-inv is that there is no need for the prior input of water retention parameters (rather, it is estimated), which is otherwise required in MDI-emp. Furthermore, MDI-inv was dependent on the well-posedness of the problem, which was taken care of by providing sufficient information and limiting the number of optimized parameters in this study. Hence, for all practical purposes, SATURO and MDI-inv can be considered as reliable and handy methods for K_s determination in the field and laboratory.

Chapter 7

Investigation of the utility of MDI to obtain soil hydraulic conductivity function (SHCF) using laboratory soil column study

7.1. Introduction

The flow through unsaturated soils is characterized by soil hydraulic conductivity function (SHCF), which is the relationship between hydraulic conductivity and matric suction (ψ). The knowledge of SHCF is essential for modelling the migration of water and solute through the vadose zone, seepage analysis in the saturated-unsaturated soil system, and rainfall-induced slope failure (Li et al., 2009; Watson, 1966; Askerinejad et al., 2012). In the laboratory, the SHCFs can be determined both directly and indirectly using several existing methods. Some of the direct evaluation techniques include the use of steady-state methods (Klute, 1965) and unsteady/transient-state methods (Watson, 1966; Cui et al., 2008; Li et al., 2009). Among the indirect evaluation techniques, empirical models, statistical models, artificial neural network techniques, and the parameter estimation technique using inverse simulation are the most commonly used methods (Simunek et al., 1998; Rahimi et al., 2015; Sihag, 2018; Liu et al., 2020).

Among the direct evaluation techniques, the transient-state methods are preferred over the steady-state methods. The steady-state methods are relatively time-consuming and tedious due to the time taken for suction equilibrium and steady-state flow. The transient methods are relatively faster and follow simple procedures (Li et al., 2009; Zhang and Li, 2011; Hu et al., 2021). The instantaneous profile method (IPM) (Watson, 1966, Leung et al., 2016) and wetting front advancing method (WFAM) (Li et al., 2009; Li et al., 2021) are the two established transient-state methods to determine SHCF directly in the laboratory. Both the methods are based on the measurement of wetting processes under infiltration or capillary rise in soil columns (Li et al., 2021). Among the indirect methods, the parameter estimation techniques are preferred since they offer more flexibility in the design of the experiments in terms of initial and boundary conditions. It also eliminates the need for tedious laboratory/in-situ experiments, thus, saving a significant amount of time (Li et al., 2009). However, the major drawback of this method is that it needs prior information of the SHCF model as input (Li et al., 2009).

The past studies show that over several decades, the IPM has been widely used by researchers to establish SHCF using both laboratory and field measurements (Baker et al., 1974; Nagpal and Vries., 1976; Cui et al., 2008; Song et al., 2017; Hussain and Ravi, 2021). On the other hand, the WFAM (Li et al., 2009) is a recently developed technique and has not been widely reported in the literature, primarily due to its requirement for visually tracking the wetting front's location (Liu et al., 2020; Li et al., 2021). To overcome this limitation, a new interpretation method called the digital WFAM method was proposed by Li et al. (2021). In the new method, the monitored water content data at a particular section was utilised to identify the wetting front instead of locating it subjectively by visual observation. The new method, however, was carried out using numerical experiments and therefore requires more evaluation using real soil measurements in the laboratory for endorsing its accuracy and reliability. Similar to WFAM, the traditional IPM was also modified by Leung et al. (2016) using numerical experiments to overcome the constraint of measuring or assuming the boundary flux. Although it seemed promising, this new interpretation method of IPM has not been widely adopted in the literature after its proposal and therefore requires more evaluation using real soils.

The mini disc infiltrometer (MDI), due to its small size, can be conveniently used for infiltration measurements in laboratory soil columns. Earlier studies have effectively utilised MDI infiltration measurements for quantifying near-surface near-saturated soil hydraulic conductivity (K_0) using empirical and physical models (section 3.3.1.1). However, these methods are indirect, and the calculated K_0 corresponds to a specific tension or negative pressure head (h_0) applied on the soil surface. Studies evaluating and appraising SHCFs utilising infiltration measurements of MDI in soil columns are still lacking in the literature. Such investigations are necessary since MDI can offer a transient wetting process and substantially reduce the overall experiment duration compared to other traditional or steady-state wetting techniques (Zhang et a., 2011; Liu et a., 2020). Additionally, the SHCF measurements using soil columns require that the flow should occur in a controlled manner (that is neither too slow nor too fast). With the help of the suction adjustment provision in MDI (section 3.3.1), the flow adjustment requirement can be accomplished for different soils.

Based on the above understanding, the research questions addressed in this chapter are as below

* Whether controlled MDI measurement in a soil column can be used to generate SHCF relationships?
* If regulated flow using MDI is able to produce appropriate soil moisture and suction profiles suitable for applying IPM and WFAM methods?
* Whether IPM and WFAM methods produce comparable SHCFs from the same measured data?

Both soil moisture and matric suction measurement sensors were used in the soil column to obtain the variation of volumetric water content and soil suction during the MDI experiment along with direct evaluation methods, IPM and WFAM. The success of this methodology will offer an easy procedure to directly measure SHCF in the laboratory using a portable MDI for various soil textures. Most importantly, it will reduce the time needed for measurements of SHCF (several days as in the traditional laboratory measurements). Furthermore, the findings from this investigation will help in understanding the interaction between infiltration and flow re-distribution beneath MDI.

7.2. Methodology

The flow diagram of the methodology followed in this chapter is provided in Figure 7.1. It involved conducting laboratory infiltration experiments for three soil textures in cylindrical soil columns using MDI and simultaneously recording the spatio-temporal variation of soil moisture and soil suction at three depths during the wetting process with the help of relevant sensors. The sensor data for each soil was then analysed using both IPM and WFAM to determine SHCF or $K(\psi)$ relationship. Additionally, the infiltration measurements from MDI were inversely analysed using numerical modelling technique to determine the indirectly measured $K(\psi)$ for each soil. Finally, the $K(\psi)$ from the direct methods (IPM and WFAM) were compared with each other and also with the indirectly determined $K(\psi)$ (numerically simulated from MDI measurements).

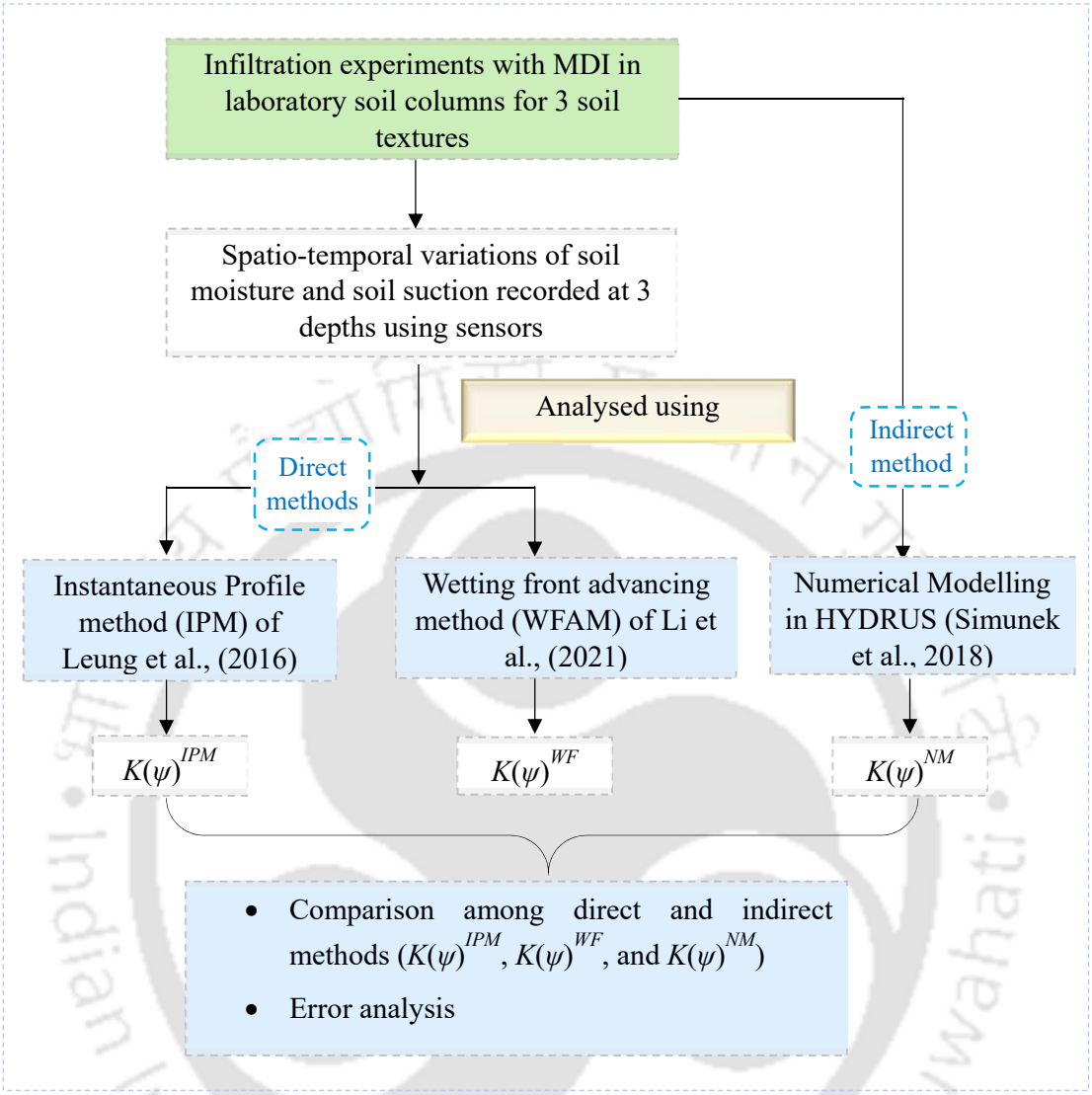

Figure 7.1 Flow chart presenting the methodology used in this study

7.2.1. Soil texture classification and physical properties

Three different fine-grained soils were used to conduct this study. The grain size analysis and physical properties of these soils were determined using the standard procedures (ASTM D2487-11; IS:2720, ASTM D854) (section 3.2), and the results are listed in Table 7.1. The textures of these soils were identified as loam (LM), silt loam (SL), and silty clay loam (SCL) based on USDA soil classification.

Table 7.1 Details of textures and physical properties of the soils used for laboratory experiments

Parameter		Particle size fraction (%)			Specific gravity (G)
		Sand (2.00-0.05 mm)	Silt (0.05-0.002 mm)	Clay (<0.002 mm)	
Soil texture	Loam (LM)	38	44	18	2.68
	Silt Loam (SL)	32	62	6	2.72
	Silty clay loam (SCL)	16	57	27	2.64

7.2.2. Experimental setup in the laboratory

The SHCF measurements were carried out in a cylindrical column setup in the laboratory. The cylindrical column was of 30 cm height and 30 cm diameter, with provision for sensor placement at different heights and drainage at the bottom. Figure 7.2 shows the laboratory setup with 5TM and TEROS21 sensors placed at various depths for measuring soil volumetric water content (VWC) and soil water potential (SWP), respectively. The soil was compacted inside the column in three layers, and simultaneously sensors were installed horizontally at three different depths, as shown in the figure. In each layer, one 5TM and one TEROS 21 were placed diagonally opposite to each other. All the sensors were connected to data loggers for continuous data recording throughout the experiment. Calibrated VWC from 5TM sensors were calculated using the soil specific calibration equations discussed in Chapter 3 (section 3.3.5.4).

The SHCFs recorded in this study correspond to the wetting process in the soil. To simulate the wetting process, infiltration experiments with MDI were conducted. MDI was filled with water and placed on the soil surface for starting the experiment (Figure 7.2), and infiltration measurements were recorded (section 3.3.1). Each MDI experiment was continued for nearly 12-16 hours till the soil was nearly saturated (monitored from the sensor recordings). For each soil texture, six repetitions were carried out. As such, total 18 infiltration experiments with MDI were carried out. To ensure parity, the initial compaction condition (w_i and γ_d) was kept identical (listed in Table 7.2) for all the repetitions of a given soil, and a fixed negative pressure head (h_0) of 6 cm was applied at the surface. In order to maintain uniform initial

moisture conditions for the repetitions, the required quantity of soil before each experiment was first oven dried for 24 hours and then kept open to the atmosphere for two days to attain hygroscopic water content (w_i). The soil was then compacted inside the cylindrical column using identical number of blows per layer (pre-determined) to maintain uniform γ_d.

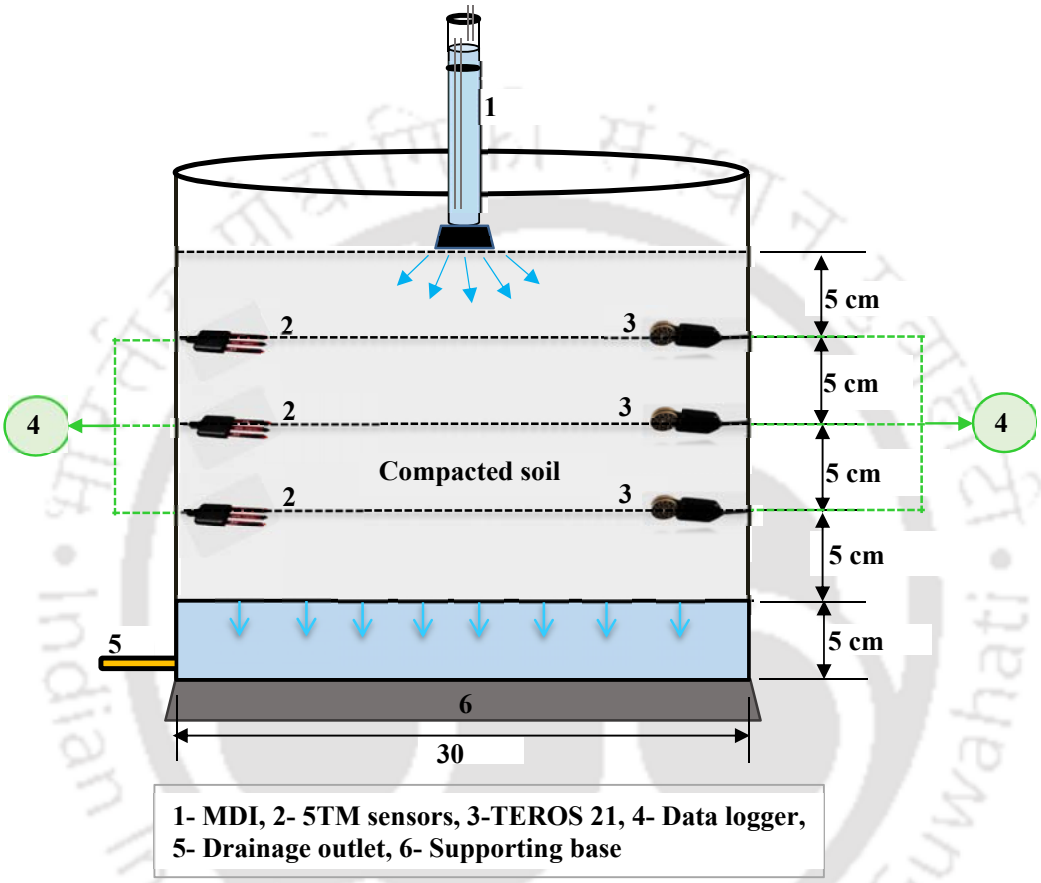

Figure 7.2 Schematic diagram of experimental setup for laboratory experiments

Table 7.2 The initial conditions used for various repetitions of MDI measurements during laboratory soil column tests and numerical experiments

Soil texture	Repetitions	Dry density (γ_d) (g/cm^3)	Initial volumetric water content (θ_i) (m^3/m^3)	Final volumetric water content (θ_f) (m^3/m^3)
Loam	1	1.38	0.031	0.371
	2	1.40	0.031	0.387
	3	1.39	0.035	0.374
	4	1.38	0.048	0.360
	5	1.38	0.051	0.374
	6	1.38	0.050	0.380
	Average	1.39	0.041	0.374
Silt Loam	1	1.42	0.008	0.412
	2	1.41	0.009	0.412
	3	1.42	0.009	0.423
	4	1.40	0.010	0.435
	5	1.42	0.006	0.444
	6	1.41	0.004	0.413
	Average	1.42	0.012	0.423
Silty clay Loam	1	1.35	0.008	0.437
	2	1.35	0.009	0.410
	3	1.35	0.009	0.417
	4	1.35	0.010	0.426
	5	1.34	0.010	0.418
	6	1.36	0.005	0.424
	Average	1.35	0.010	0.422

7.2.3. Evaluation methods for SHCF

The SHCFs were determined using IPM, WFAM, and the inverse modelling technique. The two direct methods, IPM and WFAM, require at least three temporal measurements of VWC and SWP to determine the SHCF. The three monitored sections chosen in this study were 5 cm, 10 cm, and 15 cm below the soil surface, as shown in Figure 7.2. It may be noted that the soil moisture sensors have a radial influence zone of 2.5 cm (Hussain and Ravi, 2021). Hence, a gap of 5 cm was maintained between the sensors to avoid the influence of one sensor on the measurements of another. During the infiltration experiment, the water from the MDI infiltrates into the soil, gradually increasing the soil moisture and decreasing the soil suction. Both IPM and WFAM are based on the one-dimensional continuity equation and Darcy's law

of analysis (Darcy, 1856). The basic principles of the two methods and the methodologies followed in this chapter are discussed below.

7.2.3.1. Instantaneous Profile Method (IPM)

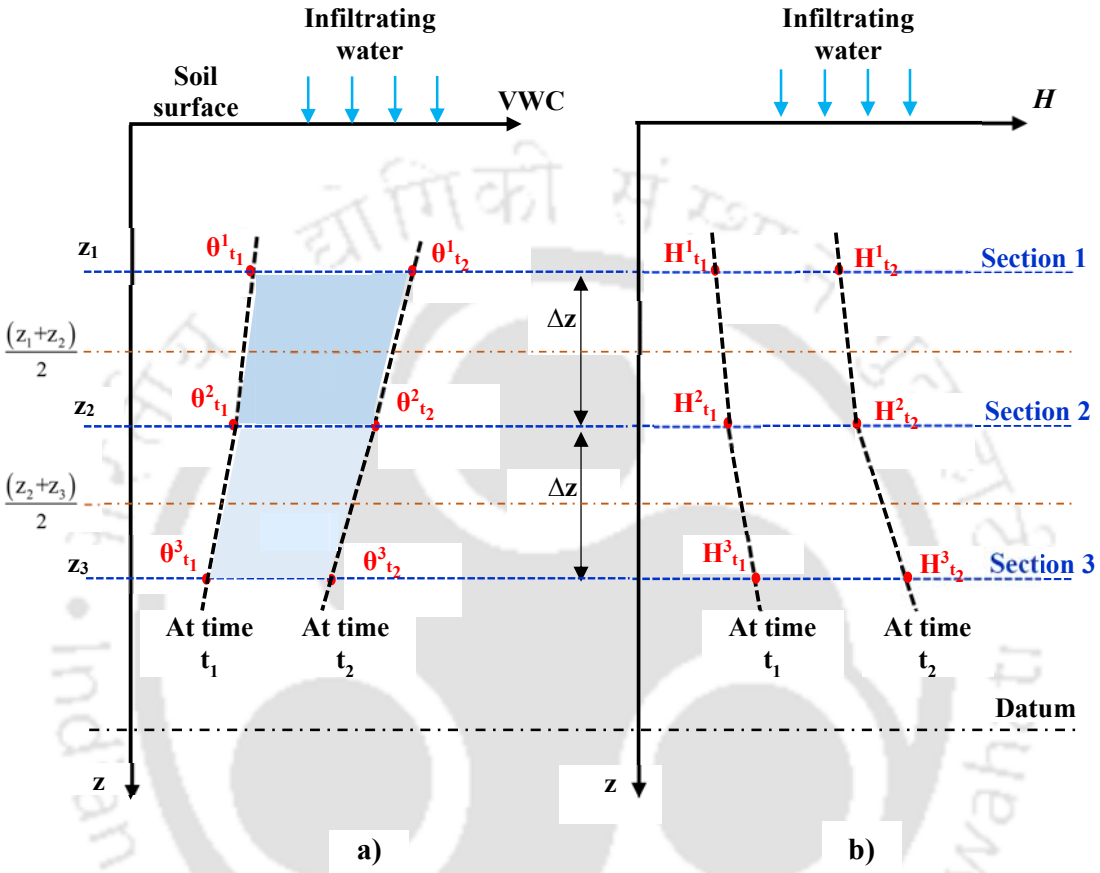

Figure 7.3 Instantaneous profiles of a) Volumetric water content (θ) and b) hydraulic head (H) at two different elapsed times, t_1 and t_2, during the downward wetting process

The SHCF using the IPM ($K(\psi)^{IPM}$) for the three soil textures was calculated using the procedure described in the literature (Leung et al., 2016; Hussain and Ravi, 2021). Unlike the original interpretation of IPM by Watson (1966), the new interpretation proposed by Leung et al. (2016) eliminates the requirement to measure, control, or assume any boundary flux during the testing process. This method is based on setting up a transient flow in a cylindrical soil column and then monitoring the VWC and SWP profile changes at different time intervals. For reference, Figure 7.3 presents the instantaneous profiles of VWC (θ) and hydraulic heads (H) at three monitored sections (sections 1 to 3) at two elapsed times, t_1 and t_2, during the wetting

process. The average hydraulic conductivity is calculated from Darcy's law by dividing the average flux between any two monitored sections by the average hydraulic gradient. The series of expressions (Eq. 7.1 to 7.3) (Leung et al., 2016) were used to determine the $K(\psi)^{IPM}$ using the new method. Here, $K(\psi)^{IPM}_{z_{\text{mean}},t_{mean}}$ (m/s) is the unsaturated hydraulic conductivity at depth z_{mean} (i.e., between any two rows of sensors) and at time t_{mean} (given by $(t_1+t_2)/2$), $\xi_{z_{mean}t_{mean}}$ is the hydraulic gradient at z_{mean}, and V is the water volume change between two sensors in time interval Δt (where, $\Delta t = t_2 - t_1$). The hydraulic head (H) is the sum of the datum head, z (m), and matric suction head, ψ (m) given by $z + \frac{\psi}{\gamma_w}$.

$$K(\psi)^{IPM}_{z_{\text{mean}},t_{mean}} = \frac{V/\Delta t}{\xi_{z_{1mean}t_{mean}} - \xi_{z_{2mean}t_{mean}}} \tag{7.1}$$

$$\xi_{z_{mean},t_{mean}} = \frac{1}{2}\left[\left(\frac{H_{1,t_1} - H_{2,t_1}}{z_{1,t_1} - z_{2,t_1}}\right) + \left(\frac{H_{1,t_2} - H_{2,t_2}}{z_{1,t_2} - z_{2,t_2}}\right)\right] \tag{7.2}$$

The value of V (i.e., V_1 or V_2) was calculated using the formula for the area of a trapezoid (the shaded portion in Figure 7.2) given by Eq. 7.3. Similarly, V_2 was also calculated using Eq.7.4. Using the measured VWC and SWP profiles from sensors, the $K(\psi)^{IPM}$ was calculated.

$$V_1 = \left\{\frac{\left(\theta_{1,t_2} - \theta_{1,t_1}\right) + \left(\theta_{2,t_2} - \theta_{2,t_1}\right)}{2\Delta z}\right\} \tag{7.3}$$

$$V_2 = \left\{\frac{\left(\theta_{2,t_2} - \theta_{2,t_1}\right) + \left(\theta_{3,t_2} - \theta_{3,t_1}\right)}{2\Delta z}\right\} \tag{7.4}$$

7.2.3.2. Wetting front advancing method (WFAM)

The digital WFAM proposed by Li et al. (2021) was used to calculate the unsaturated hydraulic conductivity function ($K(\psi)^{WF}$) for all the three soil textures. The original WFAM developed by Li et al. (2009) required wetting experiments to be carried out in a transparent soil column in order to allow for visual tracking of the migration of the wetting front (i.e., the boundary between the wetted area and dry area) over time. The digital WFAM, however, was

able to overcome this limitation (Li et al., 2021). The methodology of the digital WFAM (henceforth called as WFAM) is described below.

In this method, the wetting front movement during the wetting/infiltration process in the soil column at three sections (5, 10, and 15cm depths, refer Figure 7.2) was monitored by measuring VWC using the 5TM sensors. Simultaneously, the SWP was recorded at the three sections using the TEROS 21 sensors. Figure 7.4 presents the schematic diagram showing the monitored sections and the wetting front boundary separating wet and dry soil portions during the infiltration test in the soil column.

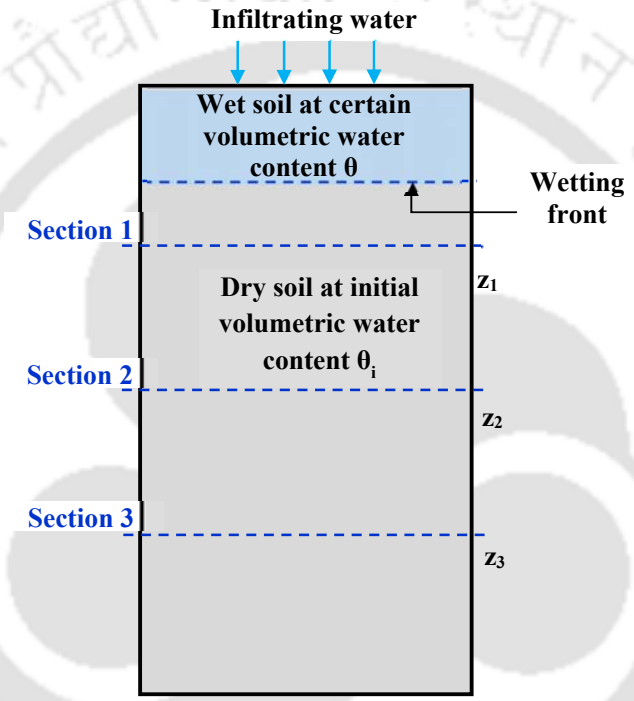

Figure 7.4 Wetting front advancing during the infiltration test in the soil column

The main assumption involved in WFAM is that the water content contour in the wetted zone advances smoothly during the wetting process (Li et al., 2009; Li et al., 2021). Based on this assumption, the infiltration profile follows Eq. 7.5.

$$\chi(z_{WF} + \Delta z_{WF}, t + \Delta t) = \chi(z_{WF}, t) + \varepsilon(\Delta z_{WF}, \Delta t) \tag{7.5}$$

Where χ represents the variables of the wetting process (θ or ψ, or K), ε represents a small negligible quantity, z_{WF} is the depth of the wetting front location, and Δz_{WF} is the advancing distance of the wetting front in time increment Δt. The water flux (q_{WF}) in the wetting front advance zone can be determined using Eq. 7.6.

$$q_{WF} = \Delta\theta_{WF} \times A \times d_{WF} = \frac{(\theta_2 + \theta_1) - 2\theta_i}{2} A v \Delta t \tag{7.6}$$

Where, $\Delta\theta$ represents the increment in VWC during the wetting front advancing process in time Δt, θ_i is the initial VWC, θ_1 and θ_2 are the monitored VWC at times t_1 and t_2 at a particular monitoring section, d_{WF} is the wetting front advancing distance over Δt, and A is the cross-sectional area of the soil column. The wetting front advancing velocity (v_{WF}) and the hydraulic gradient (ξ_{WF}) are then calculated using Eq. 7.7 and 7.8, respectively.

$$v_{WF} = \frac{\partial z}{\partial t} \tag{7.7}$$

$$\xi_{WF} = \frac{\psi_1 - \psi_2}{\gamma_w d_{WF}} + a = \frac{\psi_1 - \psi_2}{\gamma_w v_{WF} \Delta t} + a \tag{7.8}$$

ψ_1 and ψ_2 represent the soil matric suctions at times t_1 and t_2 at the same monitoring section as of θ_1 and θ_2, a is the hydraulic gradient induced by gravity (measured as the cosine of the angle between the gravity direction and the wetting front advancing direction, (for downward infiltration process a =1). The $K(\psi)$ relationship from WFAM is then obtained using Eq. 7.9.

$$K(\psi)^{WF} = \frac{q_{WF}}{\xi_{WF} \times A \times \Delta t} = \frac{(\theta_2 + \theta_1) - 2\theta_i}{2(\psi_1 - \psi_2 + a\gamma_w v_{WF} \Delta t)} \gamma_w {v_{WF}}^2 \Delta t \tag{7.9}$$

The determination of v_{WF} was carried out with the help of VWC measurements at various sections using the steps given by Li et al. (2021) as follows.

Based on the VWC profiles obtained at the monitoring sections, a digital indicator of VWC (θ_m) was first chosen. Figure 7.5 presents a sample plot showing VWC curves obtained at three sections of a soil column during the infiltration test. As seen from the figure, each VWC curve has an initial phase (with VWC = θ_i), a rising phase (marked by a sharp increase in VWC, θ_i < VWC < θ_{rs}), and a steady phase (with VWC ≈ θ_f). The θ_m was chosen such that it was within the rising phase of all the three curves ($\theta_i < \theta_m < \theta_{rs}$). In the next step, the time taken by the wetting front to attain VWC equal to θ_m at section 1 (t_{s1}) was determined. Similarly, the time taken for the other two curves (t_{s2} and t_{s3}) was also obtained. Based on the locations of the three sections (z_1, z_2, and z_3) and their corresponding time to attain θ_m (t_{s1}, t_{s2}, and t_{s3}), three sets of data points were obtained (z_1, t_{s1}), (z_2, t_{s2}), and (z_3, t_{s3}). The three points were plotted (with t on the x-axis and z on the y-axis) and fitted with an exponential curve. The

fitted exponential equation was then used to determine v_{WF} from Eq. 7.7 and used for $K(\psi)^{WF}$ calculation.

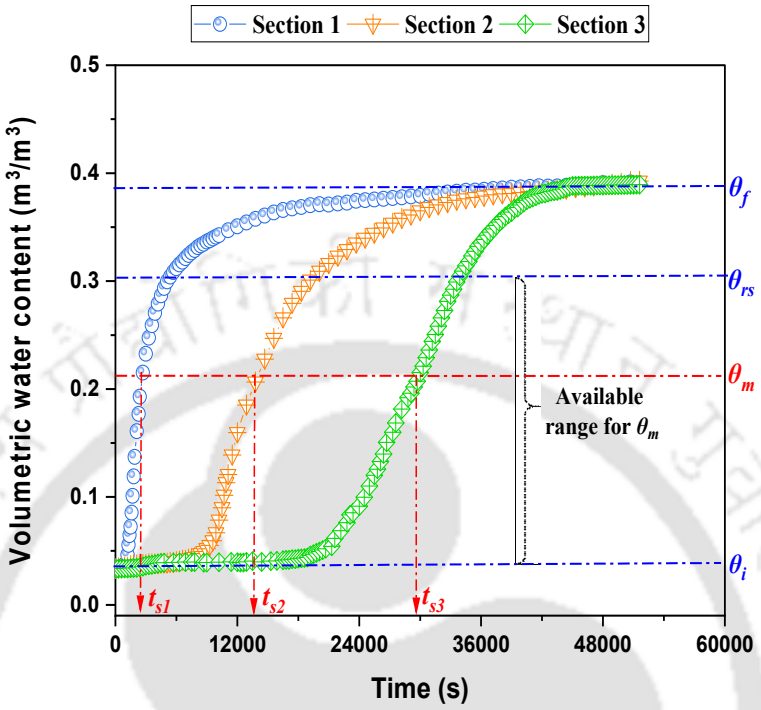

Figure 7.5 Sample plot showing VWC profiles at three monitoring sections and an arbitrary θ_m value

7.2.3.3. SHCF from Numerical modelling

Indirect determination of SHCF from MDI infiltration measurements was carried out using HYDRUS 3D-3.01 (Simunek et al., 2018) using the methodology described in section 3.4. The cumulative infiltration (CI) measurements of MDI, with and without final VWC (θ_f), were used as input for the inverse simulation (IS). For each repetition, two separate inverse simulations were performed, one using CI data only (denoted as IS-CI) and another using (CI + θ_f) data (denoted as IS-CI+θ_f) as input. The θ_f was determined using the oven-dried method (section 3.2.3 and Eq. 3.5) by collecting soil samples after the termination of each MDI experiment. The same value was also obtained from the final VWC (refer Figure 7.5) measured using the 5TM sensors during each experiment. A 2-D axisymmetric domain, as discussed in Chapter 6 (Figure 6.3, section 6.2.4), was considered with depth (z) as 0.20 m and radius (r) as 0.15 m, depending on the dimension of the soil column (Figure 7.2). The boundary conditions BC1, BC2, and BC3 (refer Figure 6.3) were kept as constant head (= -0.06 m), no flux, and free drainage conditions, respectively. The initial condition was given in terms of θ_i (Table

7.2). The initial guess values of parameters α, n, and K_s of the VGM model (Eq. 3.27 to 3.30) were taken from the literature (Carsel and Parrish 1988 denoted as CP) based on the soil texture (also readily available in HYDRUS and MDI user manuals). Among other parameters, θ_r and l were used as 0.001 m^3/m^3 and 0.5, respectively, for all the cases following the recommendations of past literature (van Genuchten, 1980; Simunek et al., 1996), and θ_s was kept the same as θ_f (Table 7.2). For each soil, total 12 numerical experiments were carried out with CI and (CI+ θ_f) as separate inputs, and in all the cases, the parameters α, n, and K_s were optimized to determine the simulated $K(\psi)^{NM}$.

7.2.4. Comparison between various SHCFs and the optimized model parameters

To determine the accuracy of SHCFs, the normalized root mean square error (NRMSE) was used (Leung et al., 2016). It is a statistical method for measuring the difference in values estimated by two different methodologies. A lower NRMSE implies a better agreement between the two methods, with zero value indicating a perfect ideal agreement. The NRMSE between the SHCFs from various methods was determined using the below expression (Eq. 7.10). Here N is the total number of observations, $K(\psi)^M$ is the calculated SHCF for a given method M, and the superscripts M_1 and M_2 stand for any two methods used for comparison.

$$NRMSE^{M_1,M_2} = \frac{\left[\frac{1}{N}\sum_{\psi=\psi_{\min}}^{\psi_{\max}}\left\{\log K(\psi)^{M_1} - \log K(\psi)^{M_2}\right\}\right]^{0.5}}{\log\left[Max\left\{K(\psi)^{M_1}, K(\psi)^{M_2}\right\}\right] - \log\left[Min\left\{K(\psi)^{M_1}, K(\psi)^{M_2}\right\}\right]} \times 100\% \quad (7.10)$$

For the SHCFs determined using various methods in this study, the VGM model parameters α, n, and K_s were obtained by fitting the VGM model (Eq. 3.27 to 3.30, Chapter 3) to the calculated SHCFs. The non-linear fitting of each SHCF was carried out in excel solver by minimizing the sum of squared error (SSE) between the measured and computed K-ψ relationship (Sreedeep & Singh, 2006). To determine the accuracy of the optimized K_s, the maximum error as in the literature (Li et al., 2021) was calculated using Eq. 7.11, where $(K_s)^r$ represents the reference method and $(K_s)^c$ represents the calculated method whose accuracy has to be determined.

$$E_{\max} = \left|\log\frac{(K_s)^r}{(K_s)^c}\right| \quad (7.11)$$

$$\text{RE} = \left(\frac{VG_r - VG_c}{VG_r} \right) \times 100\% \quad (7.12)$$

For the optimized parameters α and n, relative error (RE) (Eq 7.12) was used as a measure to quantify their accuracy. The VG_r and VG_c in the expression represent the parameter values from reference and calculated methods, respectively. In the absence of true SHCFs, the IPM parameters were considered as references (in Eq. 7.11 and 7.12) for determining the accuracy of the fitted parameters. Moreover, the IPM was extensively reported in the literature over more than a decade (Cui et al., 2008; Wang et al., 2013, Song et al., 2017; Hussain and Ravi, 2021; Zeng et al., 2022); thus, making it more appropriate as the reference method.

7.3. Results

7.3.1. The VWC and SWP profiles

The temporal variation of VWC and SWP recorded at three different depths (5, 10, and 15cm) below the soil surface are presented in Figure 7.6 and Figure 7.7, respectively. Similar profiles of VWC and SWP are also reported for all the other repetitions of the soils and are not presented here for the sake of brevity. As seen in Figure 7.6, the θ_i recorded by the 5TM sensors placed at all the three depths for a given soil are nearly the same implying a uniform initial condition inside the soil column during the experiment. Consequently, the ψ_i recorded by TEROS 21 sensors placed at the three depths are also the same for a given soil (Figure 7.7).

The water from the MDI disc reaches the sensors placed at 5cm depth (top layer) first, followed by the sensors placed at 10cm (middle layer) and 15 cm (bottom layer) (Figure 7.2). The top layer sensor attains θ_f first, followed by the middle and bottom layer sensors. This explains the time lags observed in the case of the lower layer profiles (Figure 7.6). Depending on the soil texture, the range of VWC obtained was different. The maximum θ_f obtained among various repetitions were 0.37, 0.40, and 0.42 for loam, silt loam, and silty clay loam, respectively. An average rise of 24% was seen in the soil moisture for loam soil, while the same for silt loam and silty clay loam was 29% and 30%, respectively. The corresponding fall in SWP recorded was within approximately 200 m to 1m in the case of all three soil textures. With a gradual increase of θ during the wetting process, the ψ in the soil decreases, which is recorded by the SWP sensors placed at different depths, as seen in Figure 7.7.

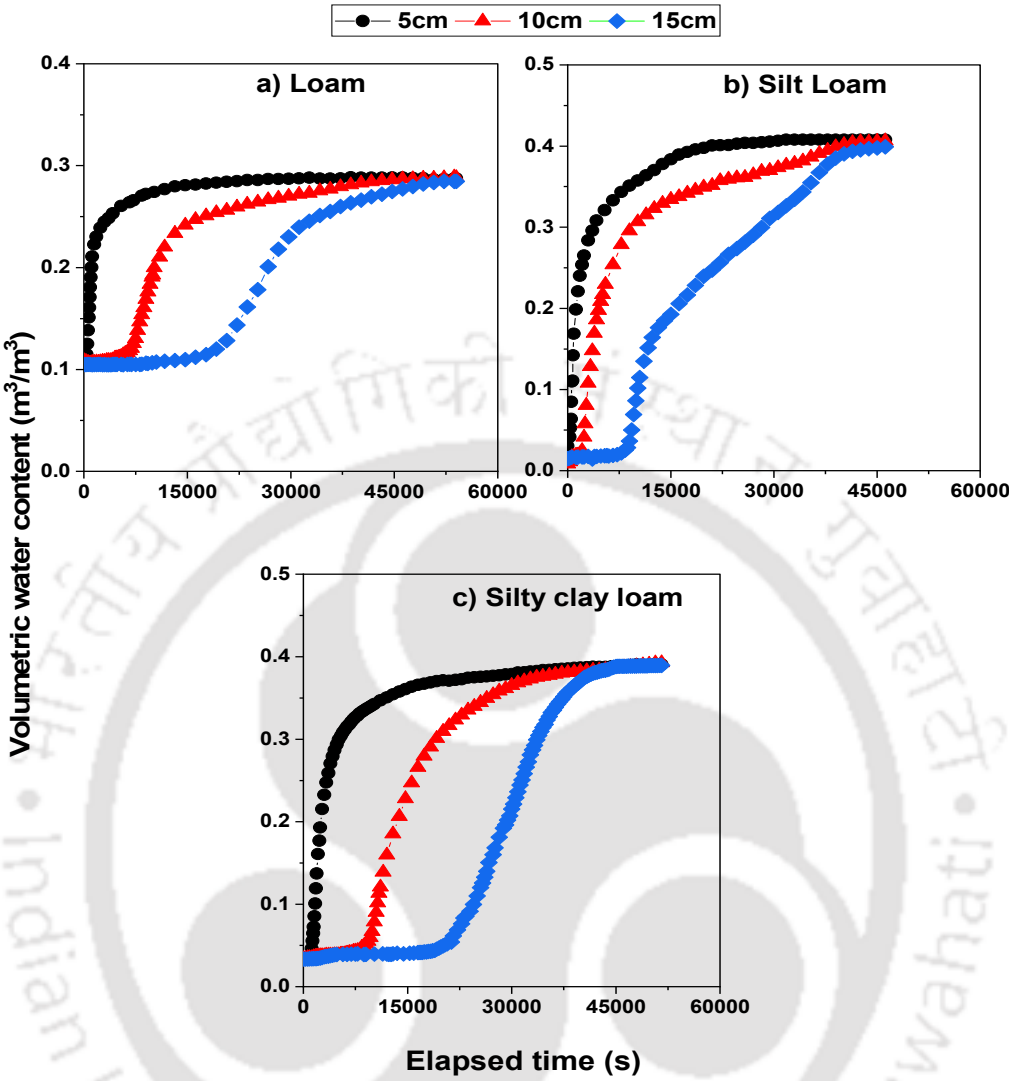

Figure 7.6 The volumetric water content (VWC) recorded at three monitoring sections (5, 10, and 15cm) below the soil surface for a) loam, b) silt loam, and c) silty clay loam soils

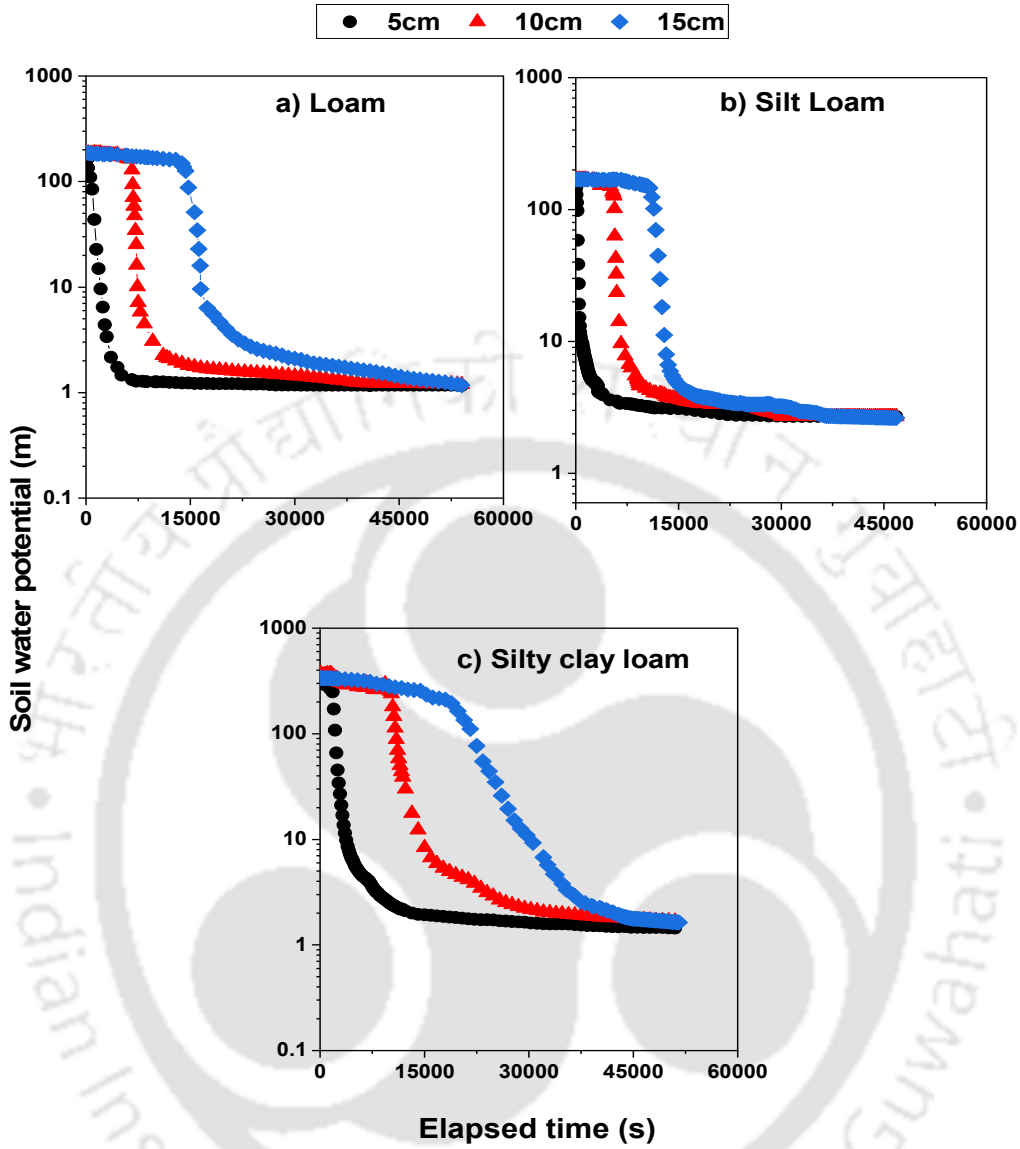

Figure 7.7 The soil water potential (SWP) recorded at three monitoring sections (5, 10, and 15cm) below the soil surface for a) loam, b) silt loam and c) silty clay loam soils

Figure 7.8a and b present the VWC and SWP profiles at various infiltration times (t_0 to t_N) obtained along the direction of flow for a given experiment. It may be noted that the 0 cm depth in the figures represents the soil surface where MDI was placed (Figure 7.2), and no sensor recordings were made at the surface level. The isochrones (the lines joining the measurements at equal times) obtained for VWC (Figure 7.8a) show a gradual increase of the moisture value at the three monitoring depths over t_0 to t_N, in accordance with that of the patterns seen in Figure 7.6. Similarly, the isochrones for SWP at the three depths mark a gradual decrease of soil suction over t_0 to t_N, similar to that of the patterns observed in Figure 7.7. As

can be seen from the figures, both VWC and SWP profiles have reported gradual changes over time. Hence, the results are suitable for further investigation using both IPM and WFAM methods. Similar profiles were obtained in the case of all the three soil textures (LM, SL, and SCL) used in this study. The results from the above figures imply that MDI infiltration experiments with appropriate supplied negative pressure can be recommended as suitable for simulating the wetting process in soil columns to measure SHCFs for fine-textured soils.

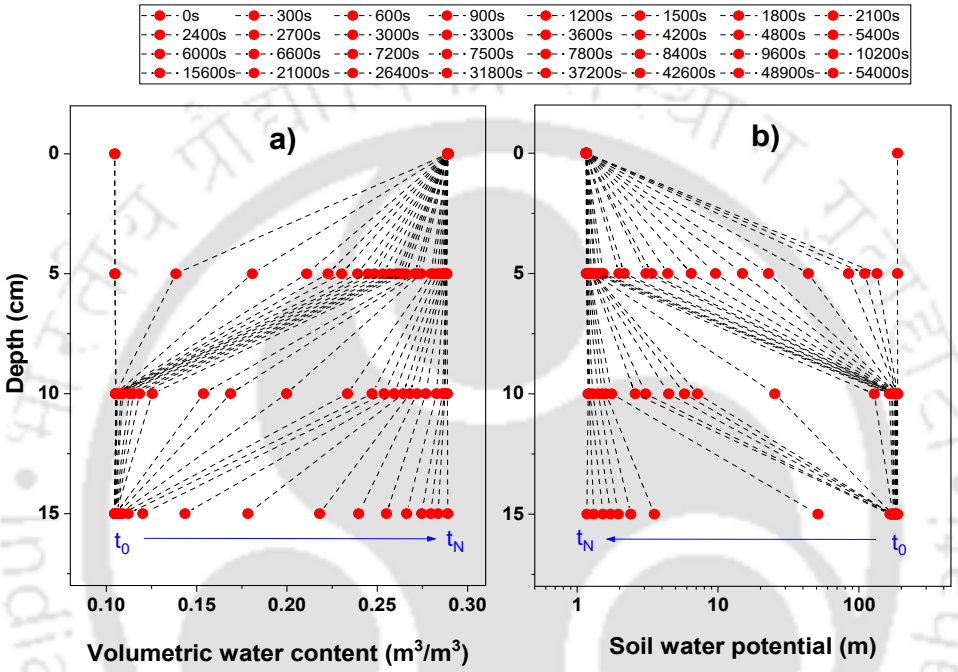

Figure 7.8 (a) The volumetric water content (VWC) and (b) the soil water potential (SWP) profiles recorded at various times during infiltration experiment

7.3.2. Determination of SHCF

The $\theta(t)$ and $\psi(t)$ data obtained from the VWC and SWP profiles for each repetition were utilised to calculate the SHCFs using IPM and WFAM (Eqs. 7.1 and 7.9). The SHCFs calculated from IPM and WFAM for all the three soil textures are provided in figures 7.9a to c. The figures show that for each soil, nearly consistent $K(\psi)$ curves are obtained from all the repetitions. An increasing trend in hydraulic conductivity values with decreasing ψ was reported in all the cases, similar to the results of past literature (Fredlund et al., 1994; Leong and Rahardjo, 1997; Ng and Leung, 2011; Wang et al., 2013; Cai et al., 2014). It is to note that the gradual wetting of the soil results in better capturing of spatio-temporal variation of both VWC and SWP. This facilitates an appropriate data measurement for determining SHCF.

It is also worth reporting from the figures that both IPM and WFAM have produced comparable SHCFs in two soils out of three. While for SCL soil, the $K(\psi)^{WF}$ results were nearly one order higher than the $K(\psi)^{IPM}$, whereas, for LM and SL soils, both the results are highly comparable. For ψ in the range of 3 to 100 m, both $K(\psi)^{IPM}$ and $K(\psi)^{WF}$ are in the order of 10^{-8} to 10^{-11} m/s in LM soil and 10^{-7} to 10^{-11} m/s in case of SL soil. In SCL soil, for a ψ range of 2 to 100m, the $K(\psi)^{IPM}$ and $K(\psi)^{WF}$ are in the order of 10^{-8} to 10^{-10} m/s and 10^{-7} to 10^{-11} m/s, respectively.

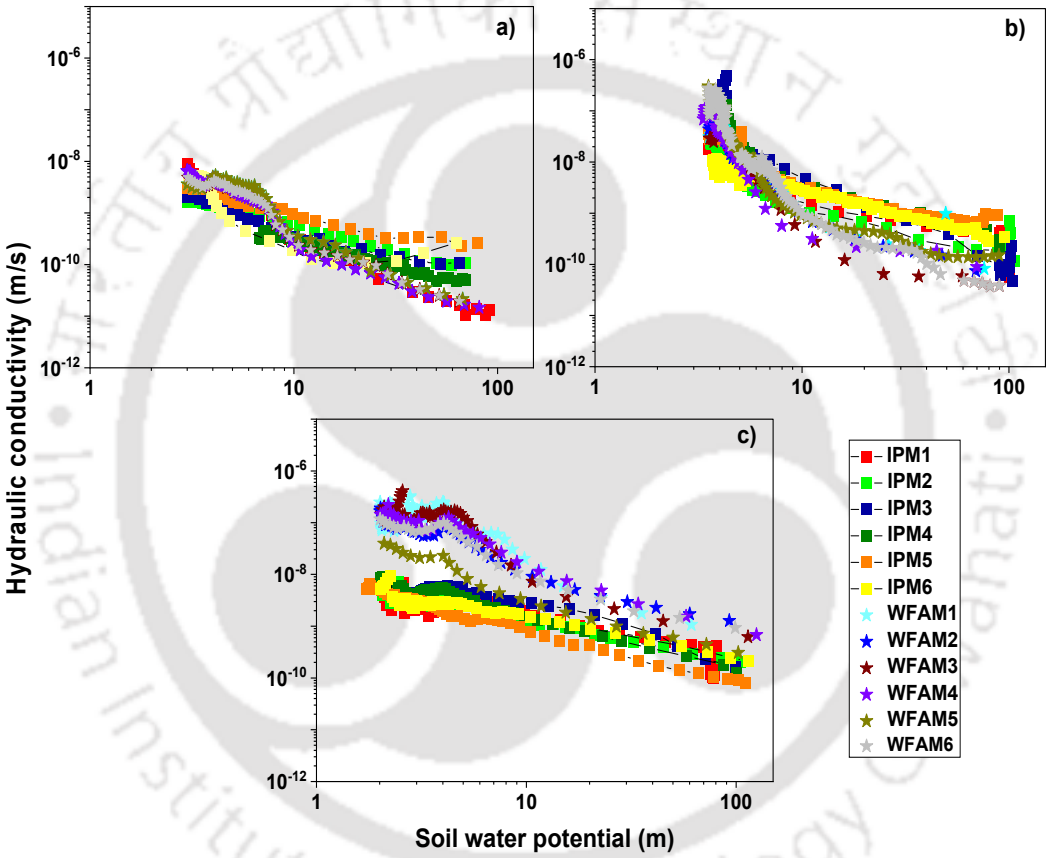

Figure 7.9 The soil hydraulic conductivity functions calculated using instantaneous profile method (IPM) and wetting front advancing method (WFAM) using measured data from all the repetitions in (a) loam, b) silt loam, and c) silty clay loam soils

The methods, IPM and WFAM, were applied to the data measured using sensors during the redistribution of water. Thus, the $K(\psi)^{IPM}$ and $K(\psi)^{WF}$ are obtained from the flow data measured underneath the disc of MDI. Simultaneously, the measured water entry at the soil

surface (infiltration measurements from MDI) are also analysed using the numerical inversion technique to produce $K(\psi)^{NM}$. The results from the two separate inverse simulations ((IS-CI) and (IS-CI+θ_f)) conducted for each repetition are provided in Figure 7.10a to c for LM, SL, and SCL soils, respectively. It is observed from the figure that the simulated curves from the six repetitions of a given soil are identical. It is also noted that the curves from the two separate runs, (IS-CI) and (IS-CI+θ_f), are also comparable in the case of all three soils.

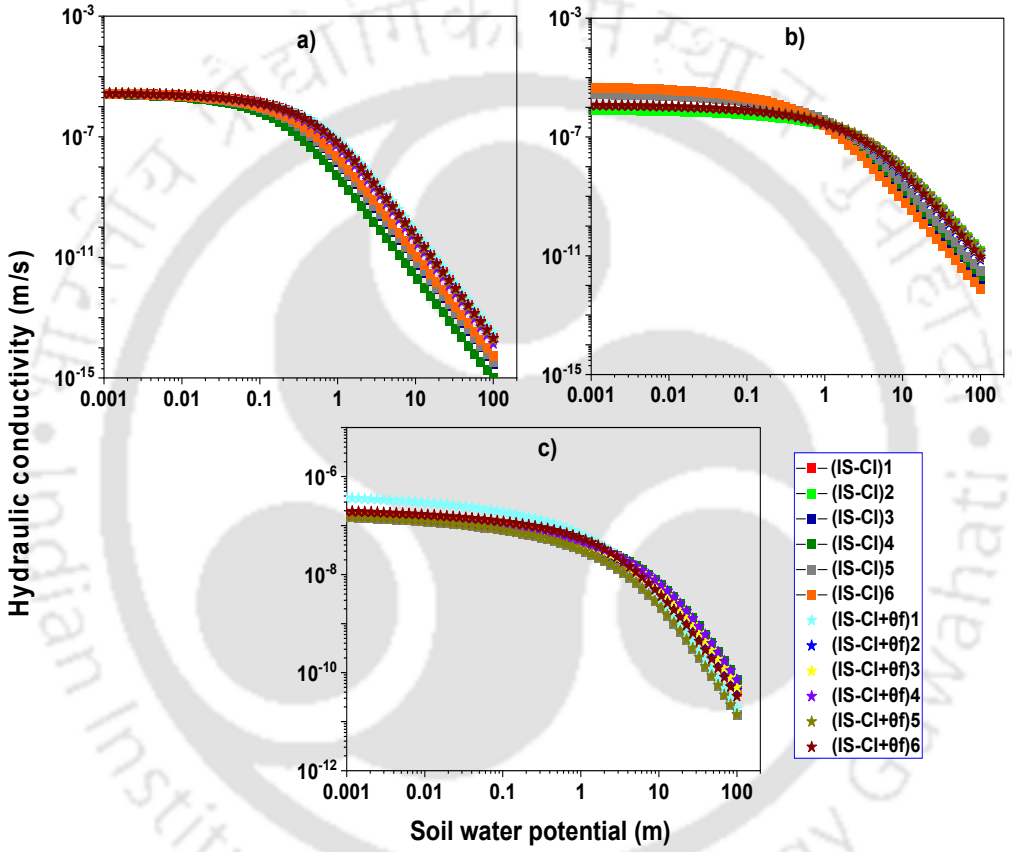

Figure 7.10 The soil hydraulic conductivity functions inversely simulated from MDI measurements from all the repetitions in (a) loam, b) silt loam, and c) silty clay loam soils

7.3.3. Error analysis

For a given soil, mean $K(\psi)^{NM}$ was calculated using the simulated curves from six repetitions for further analysis. The results from (IS-CI) and (IS-CI+θ_f) were averaged separately. The $K(\psi)^{IPM}$ and $K(\psi)^{WF}$ curves from six repetitions of each soil are also averaged and used for comparison. Figure 7.11 shows the mean curves from all the methods obtained for the three soil textures. The $K(\psi)$ curves for the three soils are also calculated from the VGM

model (Eq. 3.28, Chapter 3) by directly using the CP parameters (α, n, and K_s) and are plotted for comparison in each case. To quantify the discrepancy between the methods, NRMSE (%) is calculated and listed in Table 7.3.

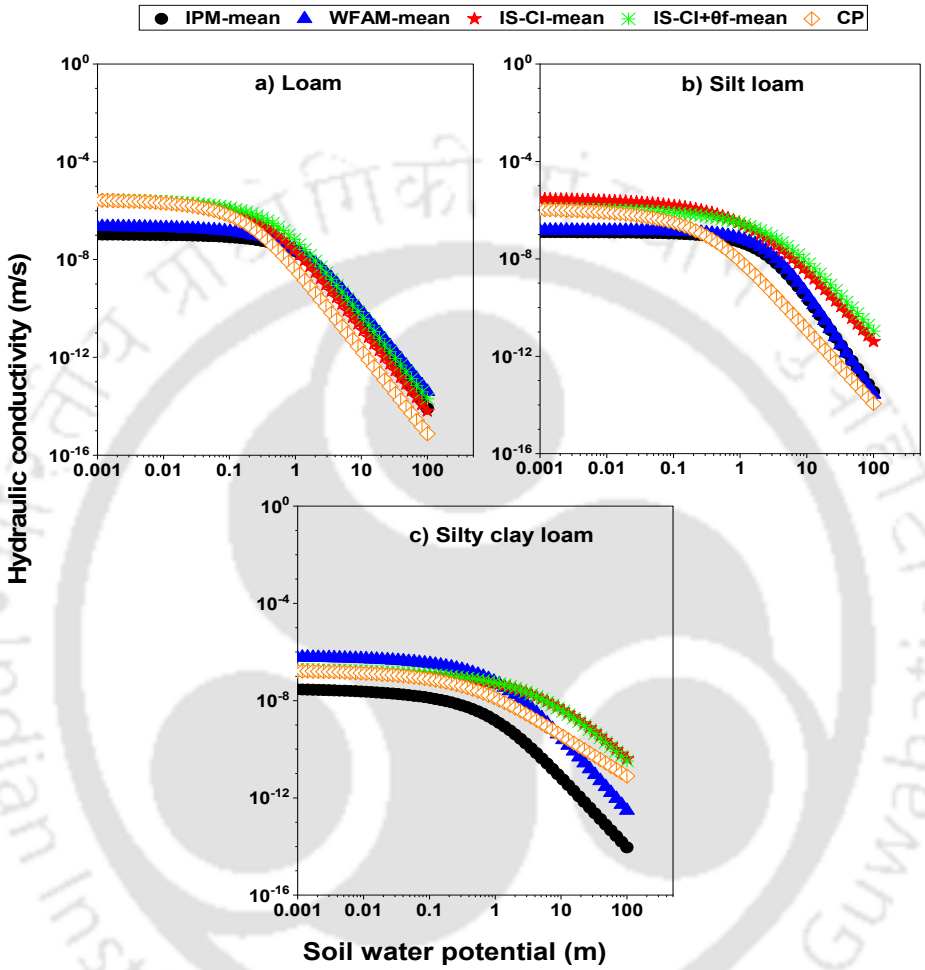

Figure 7.11 The mean soil hydraulic conductivity functions calculated using various methods for a) loam, b) silt loam, and c) silty clay loam (IPM: Instantaneous profile method, WFAM: Wetting front advancing method, CP: Carsel and Parrish, IS: Inverse simulation, CI: Cumulative infiltration, θ_f: final volumetric water content)

It is observed from Figure 7.11a that for LM soil, the mean $K(\psi)$ results for most of the methods are comparable. The calculated NRMSE in almost all cases was considerably low (i.e., <10%) (Table 7.3). However, the mean $K(\psi)$ for IPM was slightly different from that of the (IS-CI+θ_f) method with an NRMSE of 10.6%. For SL soil (Figure 7.11b), the mean results from IPM are highly comparable with WFAM and CP with NRMSE of 3.6% and 6.3%, respectively. The two inverse methods, (IS-CI) and (IS-CI+θ_f) are also comparable with

NRMSE of 5%, and WFAM and CP are comparable with NRMSE of 5.2%. For the other cases of SL soil, NRMSE is > 10%. For SCL soil (Figure 7.11c), the WFAM has given comparable results with all the indirect methods (NRMSE < 10%) as listed in Table 7.3. The (IS-CI) and (IS-CI+θ_f) methods are also comparable with NRMSE of 2.9%. However, the IPM is slightly different compared to all other methods with NRMSE>10%.

Table 7.3 The normalised root mean square errors calculated for comparison of various methods

Compared methods	NRMSE (%)		
	Loam	Silt loam	Silty clay loam
IPM and WFAM	5.6	3.6	15.2
IPM and (IS-CI)	9.7	13.4	14.6
IPM and (IS-CI+θf)	10.6	12.4	14.9
IPM and CP	7.8	6.3	13.0
WFAM and (IS-CI)	7.9	12.9	4.1
WFAM and (IS-CI+θf)	9.0	11.9	3.0
WFAM and CP	5.4	5.2	7.9
(IS-CI) and CP	5.7	11.8	6.7
(IS-CI+θf) and CP	7.1	10.7	7.3
(IS-CI) and (IS-CI+θf)	4.3	5.0	2.9

IPM: Instantaneous profile method, WFAM: Wetting front advancing method, CP: Carsel and Parrish, CI: Cumulative infiltration, IS: Inverse simulation, θ_f: final volumetric water content

7.4. Discussion

The $K(\psi)$ relationship in the VGM model is dynamic in nature and should, therefore, be determined under transient conditions and not steady-state conditions (Watson, 1966). Hence, the analysis of SHCFs in this study is carried out using transient infiltration measurements from MDI in soil column setups. The main reason for choosing MDI is due to its small size (height and disc diameter), which enables to use the device for laboratory scale measurements. Moreover, being a tension infiltrometer, MDI is equipped to regulate the flow into the soil of different textures by offering a tension head h_0 variable in the range of 0.5 to 6cm. It is required that for the transient analysis methods, IPM and WFAM, the infiltration process should be well controlled. It is expected that the infiltration rate is neither too small, nor too fast; it is smaller than the K_s and can prevent ponding on the surface (Li et al., 2021). Hence, the h_0 provision in MDI is ideal for simulating the wetting process for determining SHCF using IPM and WFAM.

Figures 7.6 to 7.8 showed that for all the three soil textures, the evolution of VWC and SWP over time at the three monitoring sections in the soil columns are gradual and smooth. Such VWC and SWP profiles are promising for the application of methods IPM and WFAM. Consequently, encouraging results of SHCFs were obtained for both IPM and WFAM, as shown in Figure 7.9. Moreover, the simulated results using inverse modelling were also able to produce comparable SHCFs from all the repetitions of MDI measurements (Figure 7.10). Hence, for the three soil textures used in this study, the supply flux needed for SHCF measurements can be provided through MDI infiltration. The results clearly endorse the efficacy of MDI in simulating the wetting process needed for SHCF measurements using both direct and indirect measurement methods.

A comparison between the mean $K(\psi)$ curves from the direct methods IPM and WFAM with the mean $K(\psi)$ curves from indirect methods (using MDI infiltration measurements and CP parameters) is shown in Figure 7.11. The difference between these methods was quantified by determining NRMSE (Table 7.3). The direct methods have produced comparable results for two soil textures, LM and SL. However, the results of the inverse simulation, (IS-CI) and (IS-CI+θ_f), have produced comparable results for all three soil textures; LM, SL, and SCL. The IS results for LM soil were comparable with both IPM and WFAM, while for SCL soil, they were more comparable with WFAM than IPM. For SL soil, the IS-CI results differed from both IPM and WFAM. However, its results were marginally improved by using θ_f information during the IS. The results from texture-based CP were also not consistent. For LM and SL, it was comparable with both IPM and WFAM, while for SCL, it was more comparable with WFAM.

Based on the error calculation (Table 7.3), it is noted that the overall NRMSE by considering the three soils and all the cases in this study is < 16% (maximum 11% for LM, 14% for SL, and 15.2% for SCL). In the literature (Leung et al., 2016), an NRMSE up to 17% in SHCF was considered acceptable for real soils. Hence, the SHCFs from all the five methods (IPM, WFAM, (IS-CI), (IS-CI+θ_f), and CP in this study can be considered comparable. The results from this analysis endorse that for the three fine-textured soils considered in this study, all the five methods can be recommended to produce SHCFs in the laboratory.

To further analyse the results, the optimized α, n, and K_s are obtained by fitting the VGM model (Eq. 3.28, Chapter 3) to the mean $K(\psi)$ curves from the four methods, IPM, WFAM, (IS-CI), and (IS-CI+θ_f). The optimized K_s from the four methods and the CP-Ks are evaluated for E_{max} using Eq. 7.11. Similarly, the optimized α and n, and CP-α and n are evaluated for RE using Eq. 7.12. The optimized parameters and the calculated error values for each case (with respect to the reference IPM) are listed in Table 7.4.

Table 7.4 The list of the optimized parameters (α, n, and K_s) of the van Genuchten Mualem model (1980) for soil hydraulic conductivity functions and the error calculated for various methods for three soil textures in this study.

Soil texture	Method	Optimized parameters			RE (%)		E_{max}
		α	n	K_s	α	n	K_s
Loam	IPM*	0.48	1.71	1.1E-07	-	-	-
	WFAM	0.57	1.53	2.3E-07	-17.9	10.5	0.34
	IS-CI	0.39	1.48	2.6E-06	19.1	13.5	1.39
	IS-CI+θ_f	0.35	1.35	2.8E-06	27.4	21.1	1.43
	#CP	3.60	1.56	2.9E-06	-646.3	8.8	1.44
Silt loam	IPM*	0.30	1.78	1.2E-07	-	-	-
	WFAM	0.28	1.88	1.5E-07	6.7	-5.6	0.08
	IS-CI	0.41	1.74	3.4E-06	-38.0	2.1	1.44
	IS-CI+θ_f	0.39	1.65	1.3E-07	-30.0	7.3	0.02
	#CP	2.00	1.41	1.3E-06	-566.7	20.8	1.00
Silty clay loam	IPM*	0.74	1.37	3.3E-08	-	-	-
	WFAM	0.54	1.42	6.6E-07	27.0	-3.6	1.30
	IS-CI	0.96	1.38	1.8E-07	-29.7	-0.7	0.74
	IS-CI+θ_f	0.99	1.41	1.9E-07	-33.1	-2.9	0.77
	#CP	1.00	1.23	1.9E-07	-35.1	10.2	0.77

*Reference method for comparison, #Mean values from literature Carsel and Parrish, (1988), (IPM: Instantaneous profile method, WFAM: Wetting front advancing method, CP: Carsel and Parrish, CI: Cumulative infiltration, IS: Inverse simulation, θ_f: final volumetric water content, RE: relative error, E_{max}: maximum error Li et al., 2021)

As seen from the table, for any given soil, the optimized α and n from the mean curves of different methods exhibit only marginal differences. As a result, the calculated RE values in most of the cases are < 50%. It is also noted from the table that for LM and SL soils, the texture-based CP-α are relatively different from the optimized IPM-α with RE equal to 646% and 567%, respectively. However, irrespective of such higher RE, the calculated NRMSE between their corresponding $K(\psi)$ was <10%, as seen in Table 7.3. The overall optimized K_s from various methods in Table 7.4 is nearly of the same order or, at most, exhibit a single-order difference from the reference IPM. Consequently, the calculated E_{max} in all the cases is relatively low (i.e., < 2). The results from Table 7.4 show that the direct and indirect methods employed for analysing MDI measurements in this study have reported identical optimized parameters for each of the soil textures. Consequently, the mean curves from all these methods in Figure 7.11 were identical with very low NRMSE (Table 7.3). The marginal difference in

the mean curves can be associated to the interplay of variations among all the three parameters (α, n, and K_s) as observed in this study.

It should be noted that the main constraint of the direct methods is the requirement of conducting the experiments for long durations. While the time required for traditional IPM is nearly a few months, the same can be considerably reduced to a few days by using WFAM (Li et al., 2021). With the help of MDI infiltration, it was observed that the duration of the experiment can further be reduced to a few hours (12-16 hours), as seen in this study. However, the major disadvantage is the limited range of ψ (≈ 2 to 100 m) (Figure 7.9), for which the $K(\psi)$ relationship could be measured during the flow process in this study. Determining the $K(\psi)$ relationship beyond this range can also be made from MDI flow; however, more sophisticated sensors offering higher ψ range will be needed for the same. Considering the ψ range offered by the TEROS 21 sensors (-0.9 to -1000 m) used in this study, the results from both IPM and WFAM were highly comparable and reliable.

7.5. Summary

This study has analysed and evaluated the potential of infiltration measurements from mini disc infiltrometer (MDI) to produce soil hydraulic conductivity functions (SHCFs) by using laboratory soil column experiments. The data measured during the experiments included a) the infiltration measurements from MDI (at surface level) and b) the temporal variation of volumetric water content (VWC) and soil water potential (SWP) at various monitoring sections (underneath the surface) using appropriate sensors. The sensor measurements were further analysed using direct methods, instantaneous profile method (IPM), and wetting front advancing method (WFAM), while the infiltration measurements from MDI were analysed using indirect method (inverse simulation, IS-CI, and IS-CI+θ_f) to produce SHCFs. The results from these four direct and indirect methods were compared, and error analysis was performed. Additionally, SHCFs were determined using texture-based parameters from the literature Carsel and Parrish (CP, Carsel and Parrish, 1988) and used for comparison. The following conclusions were derived based on the above study.

- The methods, IPM and WFAM, could be successfully applied to obtain SHCFs or $K(\psi)$ relationships using flow measurements from MDI.
- The flow measurements analysed using IPM and WFAM were able to produce consistent $K(\psi)$ relationships from various repetitions of soil. Moreover, the results of $K(\psi)^{IPM}$ and $K(\psi)^{WF}$ were also comparable for the soil textures considered in this study.

- The calculated NRMSE between all the considered methods (IPM, WFAM, (IS-CI), (IS-CI+θ_f), and CP) was <16%, which is considered appropriate for real soils. The results imply that all the five methods can be recommended to produce SHCFs from laboratory soil column study simulated with MDI infiltration wetting. This also indicates that in the absence of sensor measurements, the infiltration measurements from MDI can be utilised to produce SHCFs using inverse simulation technique.
- The results endorse the utility of MDI as a convenient handy device to generate unsaturated SHCFs in the laboratory using soil column studies
- The use of MDI for the infiltration process could considerably reduce the total time taken for the wetting process (< 24 h). However, the results were produced only for a limited range of suction (2-100m).

While WFAM and IPM offer several advantages to directly measure the $K(\psi)$ curve or SHCF for a soil, the major disadvantage is the time taken to conduct these tests for capturing the VWC and SWP measurements. This study has attempted to evaluate a quick flow method using a miniature infiltrometer and demonstrated the utility of the method with the help of both direct (IPM and WFAM) and indirect (inverse simulation) methods.

Chapter 8

Investigation of the utility of MDI to generate wetting water retention characteristics curve (WWRCC) using laboratory measurements and numerical modeling

8.1. Introduction

The soil moisture and water potential significantly affect the infiltration process (Bordoloi et al., 2021; Kumar et al., 2010). It is known that there is an inherent relationship between water retention characteristics (relationship between soil moisture and soil water potential) and infiltration characteristics of the soil (Šimůnek & van Genuchten, 1996). For analyzing seepage loss, soil deformation, slope stability, and modelling of the hydro-mechanical behaviour in unsaturated soils, the water retention characteristic curve (WRCC) plays a crucial role (Cai et al., 2022; Milatz et al., 2018).

The determination of WRCC can be done by both drying and wetting processes. The WRCC estimated directly from infiltration corresponds to the wetting process and is more realistic in describing the flow and transport through the vadose zone (Šimůnek et al., 1999). In this context, researchers have tried to generate and evaluate the WRCC directly from infiltration measurements in the field (Ramos et al., 2006; Rashid et al., 2015; Schwartz & Evett, 2003; Šimůnek et al., 1998; Wang et al., 1998), laboratory (Šimůnek et al., 1999), and synthetic measurements of disc infiltrometers (Šimůnek et al., 1999; Šimůnek & van Genuchten, 1996; Šimůnek & Van Genuchten, 1997). In addition, upward infiltration (Latorre & Moret-Fernández, 2019; Moret-Fernández et al., 2016; Young et al., 2002), horizontal infiltration (Shao & Horton, 1998), and drip infiltration in soil columns (Bruckler et al., 2002) have also been used. Based on these studies, three major conclusions are derived, (i) WRCC can be adequately determined from infiltration measurements (Bruckler et al., 2002; Ramos et al., 2006; Shao & Horton, 1998), (ii) numerical inversion is useful for estimating WRCC

and hydraulic conductivity parameters (Ramos et al., 2006; Šimůnek et al., 1998; Ventrella et al., 2005), and (iii) the combination of soil hydraulic parameters along with the selection of initial guess values chosen for optimization will affect the numerical inversion results (Latorre & Moret-Fernández, 2019; Moret-Fernández et al., 2016; Ramos et al., 2006; Schwartz & Evett, 2003; Šimůnek et al., 1999; Šimůnek & van Genuchten, 1996).

The previous studies employing mini disc infiltrometer (MDI) were mainly to determine infiltration rates and soil hydraulic properties, hydraulic conductivity (K_0), and sorptivity (S_0) (Gordillo-Rivero et al., 2014; Huang et al., 2015; Lewis et al., 2006; Gadi et al., 2017; Ghosh et al., 2019; Ghosh & Pekkat, 2019; Homolák et al., 2009; Lichner et al., 2007). The K_0 and S_0 from MDI measurements in these studies were determined using Zhang's method (Zhang, 1997a, b) (section 3.3.1.1, Chapter 3) recommended by the manufacturer (METER Group., USA). It should be noted that Zhang's method requires the use of van Genuchten (vG) WRCC parameters, α and n (van Genuchten, 1980), for various soil textures. In the majority of the studies (Gadi et al., 2017; Ghosh et al., 2019; Ghosh & Pekkat, 2019a; Homolák et al., 2009; Lichner et al., 2007; Ronayne et al., 2012), these parameters were obtained from texture based databases reported in the literature (Carsel & Parrish, 1988, CP). The accuracy of α and n obtained based on only soil texture may not be truly representative of the field situations. Contradictory results were obtained when CP and measured WRCC parameters were used for MDI data analysis (Bordoloi et al., 2018; Fodor et al., 2011). Bordoloi et al. (2018) used drying WRCC parameters, while there was no mention of the nature of WRCC in Fodor et al. (2011). Similarly, most of the databases, including CP, do not mention whether wetting or drying WRCC was considered for determining α and n. Since infiltration is essentially a wetting process, α and n established from wetting WRCC may be ideal for quantifying soil hydraulic properties from MDI measurements.

The use of MDI for determining wetting WRCC (designated as WWRCC) parameters has not been critically analysed and demonstrated in the past literature. Such a determination would minimize the uncertainty in wetting α and n parameters used for MDI analysis. Another advantage is that α and n parameters can be determined in a non-destructive and non-invasive manner when MDI is used. Further, it is determined for the same state of the soil existing in the field/lab on which the hydraulic properties are measured. Based on this understanding, the following research questions are identified for addressing in this chapter.

- Whether MDI infiltration data in a soil column under controlled condition can be used to generate WWRCC?
- Whether the water retention parameters estimated from MDI measurements are similar to those obtained from other independent WWRCC measurements?
- What is the comparison of WWRCC parameters (α and n) obtained from MDI measurements with the texture-based retention parameters?
- Which combinations of input data and optimized parameters are most reliable for accurately quantifying WWRCC from MDI using inverse analysis?

This study evaluated and demonstrated the utility of MDI for estimating WWRCC for two soil textures with the help of both experimental and numerical analysis. Additionally, the results from MDI were validated with the help of independently measured WWRCC for the same soils using capillary rise experiments.

8.2. Methodology

Figure 8.1 presents a flow diagram outlining the methodology used in this study. Infiltration experiments were conducted using MDI in laboratory soil columns instrumented with volumetric water content (VWC) and soil water potential (SWP) sensors at two different depths. The VWC and SWP recorded using the sensors during the wetting process provide the directly measured WWRCC from MDI flow. Simultaneously, the infiltration measurements from MDI were analysed using inverse modelling to obtain the simulated or indirectly determined WWRCC parameters. In addition to the infiltration experiments, capillary rise experiments were conducted in separate soil columns instrumented with VWC and SWP sensors to obtain independently measured WWRCC for the same soil textures. By comparing the modelled and measured results, the usefulness of MDI to determine WWRCC was ascertained.

8.2.1. Infiltration measurements using MDI (direct evaluation of WWRCC)

The MDI infiltration experiments on remolded soil samples were performed under controlled conditions in the laboratory soil column. The same soil column described in Chapter 7, with height and diameter of 30 cm, was used for the experiments. The instrument setup and the placement of the sensors were the same as the steps stated in section 7.2.2. Two sets of sensors (one 5TM and one TEROS 21) were deployed at a depth of 5 cm and 10 cm below the soil surface (refer Figure 7.2). The two sensors placed at a given depth

simultaneously monitor the variation in VWC and SWP due to the infiltrating water and, thus, provide the WWRCC. The two soils used for this study were loam (LM) and silt loam (SL) textures. The details of the physical properties and grain size analysis of the two soils are listed in Table 7.1.

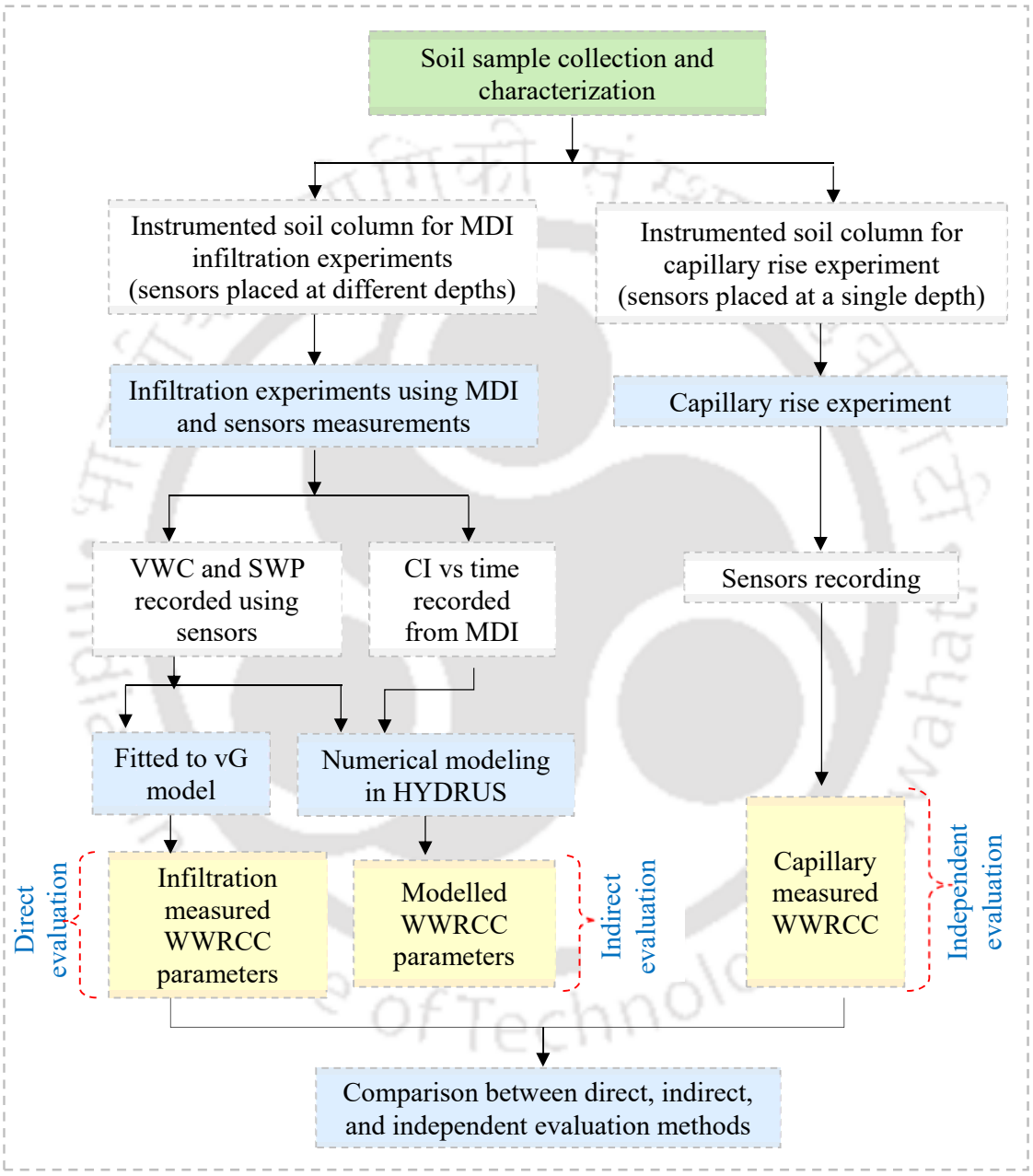

Figure 8.1 Flow chart describing methodology of the study
(CI- Cumulative infiltration, MDI- Mini disc infiltrometer, VWC- Volumetric water content, SWP- soil water potential, vG model- van Genuchten model (van Genuchten, 1980), WWRCC- Wetting water retention characteristics curve)

For each soil, six repetitions of infiltration experiments were carried by setting MDI to a tension head h_0 of 6 cm. All the experiments were conducted for 7 hours to achieve sufficient water percolation up to the depth of sensor placement. It was noted that Kool et al. (1985) had obtained satisfactory results by considering cumulative outflow for 6 and 12 hours. While preparing the soil columns, average γ_d of 1.39g/cm^3 and 1.42g/cm^3 was maintained for all the repetitions of LM and SL soils, respectively. The initial gravimetric moisture content of the soil (w_i) was recorded before each experiment and was later used to determine the initial VWC (θ_i) (section 3.2.3, Eq 3.5). The final VWC (θ_f) after the end of each experiment was also recorded. The saturated VWC (θ_s) was calculated for each experiment using specific gravity (G) (from Chapter 7, Table 7.1) and corresponding γ_d. The measured WWRCCs from six repetitions of each soil were then fitted to the van Genuchten (vG) model (van Genuchten, 1980) (Eq. 3.27, section 3.4) to determine the measured water retention parameters, α, and n (van Genuchten, 1980). The non-linear fitting of WWRCC was carried out in excel solver, and the sum of squared error (SSE) between the measured and computed θ-h relationship was minimized during the fitting process (Sreedeep & Singh, 2006).

8.2.2. Inverse simulation of infiltration and sensor measurements (indirect evaluation of WWRCC)

The software, HYDRUS 3D (version 3.01; Simunek et al., 2018) was used for conducting the inverse modelling of MDI data using parameter optimization. The set of expressions and the details of the optimization process for the inverse simulation (IS) is provided in Chapter 3 (section 3.4). A 2-D axisymmetric domain (z = 0.25 m and r = 0.15 m) (as in Figure 6.3) was considered to analyze the flow, and the boundary conditions (BC) were kept similar to that of Chapter 7 (section 7.2.3.3). The cumulative infiltration (CI) measurements from MDI and VWC and SWP measurements from sensors were separately used as input during inverse simulation to produce the modelled outputs, by optimizing the parameters α, n, and also saturated hydraulic conductivity (K_s), in few cases. Accordingly, the objective functions (Eq. 3.31, section 3.4) were defined in terms of either CI or VWC/ SWP. Finally, the optimized values (α, n, K_s) and other modelled results from inverse analysis (namely WWRCC, CI, VWC, and SWP) were compared with the measured results. The reference/measured value for K_s were used from the falling head permeameter (PM) tests (section 3.3.4) conducted for the same soils.

Table 8.1 Different cases used to determine van Genuchten (vG) WWRCC model parameters and saturated hydraulic conductivity

Case No	Sub case	Method used	Input data for inverse simulation	Initial Condition used	Soil Depth	Optimized parameters
1- MDI measured data	C1-1	Inverse simulation	Cumulative infiltration (CI) versus time	θ_i	Not applicable	α, n
	C1-2		Cumulative infiltration (CI) versus time along with θ_f			α, n
	C1-2'					α, n, K_s
2- Measured 5TM and TEROS 21data	C2-1	vG model fitted to WWRCC data	Not applicable. WWRCC parameters obtained directly		5cm	α, n
	C2-2				10cm	
3- Measured 5TM data	C3-1	Inverse simulation	VWC vs time	ψ_i (calculated from θ_i)	5cm	α, n
	C3-2				10cm	
	C3-3			θ_i (from 5TM measurement at time = 0)	5cm	
	C3-4				10cm	
4- Measured TEROS 21 data	C4-1	Inverse simulation	SWP vs time	ψ_i (from TEROS 21 measurement)	5cm	α, n
	C4-1'					α, n, K_s
	C4-2				10cm	α, n
	C4-2'					α, n, K_s
	C4-3			θ_i (calculated from measured ψ_i)	5cm	α, n
	C4-3'					α, n, K_s
	C4-4				10cm	α, n
	C4-4'					α, n, K_s

The IS was carried out using four different approaches designated as Cases 1 to 4, and are listed in Table 8.1. Case 1 was exclusively based on CI versus time data from MDI measurements for determining α and n. The three subcases depended on whether or not the θ_f was used in the objective function for optimization. The θ_f corresponds to the tension head h_0 set in the device (Schwartz & Evett, 2003; Šimůnek et al., 1998). The (θ_f, h_0) represents a data point in the WWRCC curve and, therefore, is believed to improve the optimization process

when used along with CI versus time data (Šimůnek et al., 1999). In the subcase C1-2', K_s was also considered as an optimized parameter along with α and n. The initial condition (IC) for Case 1 was defined in terms of θ_i. The past studies (Šimůnek et al., 1998; Šimůnek & Van Genuchten, 1997) reported stable and unique solutions of CI versus time data for the inverse problem based on θ_i. Hence, this IC was chosen for Case 1. The details of the θ_i are listed in Table 8.2. The Case 2 in Table 8.1 corresponds to the direct evaluation method discussed in section 8.2.1 and provides the measured α and n. The two subcases (C2-1 and C2-2) refer to the measurements at two depths (5 cm and 10 cm below the soil surface). The mean values determined from 12 measurements at the two depths (six repetitions of each soil) were used as the reference values (α_{true}, n_{true}) for comparison.

Table 8.2 Summary of the initial volumetric water content for various cases and sub cases used in numerical simulation

Soil Type	Replicate	θ_i (m^3/m^3)				
		*C1	#C3-3	#C3-4	$C4-3 & C4-3'	$C4-4 & C4-4'
LM	1	0.031	0.068	0.047	0.004	0.004
	2	0.031	0.097	0.051	0.004	0.004
	3	0.035	0.096	0.057	0.004	0.004
	4	0.048	0.111	0.117	0.004	0.004
	5	0.051	0.102	0.093	0.004	0.004
	6	0.050	0.076	0.103	0.004	0.004
SL	1	0.008	0.024	0.023	0.018	0.017
	2	0.009	0.026	0.026	0.018	0.017
	3	0.009	0.024	0.019	0.017	0.017
	4	0.007	0.015	0.008	0.019	0.019
	5	0.007	0.035	0.028	0.019	0.020
	6	0.004	0.029	0.025	0.019	0.020

*Initial VWC calculated from gravimetric water content (w_i) for Case 1
Initial VWC measured using 5TM sensor for Case 3
$ Initial VWC calculated from the soil water potential measured using TEROS 21 and van Genuchten model for Case 4

The Cases 3 and 4 used the measured VWC versus time data and SWP versus time data, respectively, obtained from the wetting process (flow beneath MDI) for vG WWRCC parameters determination. For Case 3, the inverse estimation was performed in HYDRUS by minimizing the error between the estimated and the measured VWC from the 5TM sensor. It was divided into subcases C3-1 to C3-4 depending on whether SWP (ψ_i) or VWC (θ_i) was

used as the IC and whether 5 cm or 10 cm depth of measurements were used. For subcases C3-1 and C3-2, ψ_i (calculated from θ_i using Eq. 3.27, section 3.4) were used as the IC, and the θ_i measured using the 5TM sensor (time, t=0) was taken as the IC for subcases C3-3 and C3-4 (Table 8.2). Case 4 utilized the SWP measurements using TEROS 21 for determining the WWRCC parameters by inverse estimation. Four subcases of Case 4 (C4-1' to C4-4') optimized K_s parameter as well, in addition to α and n. Similar to Case 3, IC was considered in terms of measured ψ_i (at t = 0) from TEROS 21 and θ_i (Table 8.2) (calculated from ψ_i using Eq. 3.27, section 3.4). A total of 17 different combinations were analysed for determining WWRCC parameters and/or K_s. These cases and subcases represent the widely possible combinations of WWRCC parameter estimation.

For inverse modelling, the values of vG model parameters l and θ_r were taken, respectively as 0.5 and 0.001 m^3/m^3. The parameter θ_s was calculated from the known initial compaction state (section 8.2.1). The first initial guess values for the α and n were taken from Case 2 results (α_{true}, n_{true}) for the two soils. Following this, multiple simulations were also carried out by varying the initial values of α and n arbitrarily (nearly five different combinations) within the corresponding standard deviation (SD) calculated from Case 2 (α_{true} ± SD, n_{true} ± SD). For these simulations, the K_s values measured using laboratory PM experiments were used as input or initial guess values as applicable. In addition, a few more simulations were performed using the initial guess values of α, n, and K_s obtained from CP based on soil texture. These values are recommended in the MDI user manual and are generally preferred by common users. The primary purpose of using several initial guess values was to address the issue of parameter uniqueness by verifying whether different guess values lead to the same or nearly identical final parameter estimates (Šimůnek et al., 2012). Accordingly, a total of 180 simulations (90 per soil) for Case 1, 24 simulations for Case 2, 240 simulations for Case 3, and 480 simulations for Case 4 were considered in this study.

8.2.3. Capillary rise test (independent evaluation of WWRCC)

The independent determination of WWRCC for the soils was done using capillary rise (CR) experiments. The schematic diagram of the CR setup used in this study is shown in Figure 8.2. Fabricated cylindrical mould of height 19.5 cm and diameter 20 cm were used to conduct the CR experiments. While packing the soil inside the mould, one 5TM and one TEROS 21 sensor were placed at a suitable depth to record the VWC and SWP changes. The initial compaction conditions of the soils for the CR tests were maintained similar to that of the MDI infiltration measurements (section 8.2.1). The θ_i was kept as 0.04, and 0.007 m^3/m^3 for LM and

SL soils, respectively, and a γ_d of nearly 1.4g/cm^3 was maintained for both the soils. A water reservoir was used to continuously supply water for the capillary rise process, and a piezometer attached to the water reservoir allowed to monitor the required water height. The sensors placed at a given height (approximately 5cm from the mould's base) recorded the WWRCC as the water migrated upwards due to the CR process. Total five such experiments were conducted for each of the LM and SL soils. Each experiment was conducted for 5 to 6 days, depending on the soil type. The vG model was fitted to CR-measured WWRCC to determine the parameters α and n using the procedure described in section 8.2.1. Finally, the WWRCC and the fitted α and n from CR tests were used to compare with the results obtained from MDI measurements.

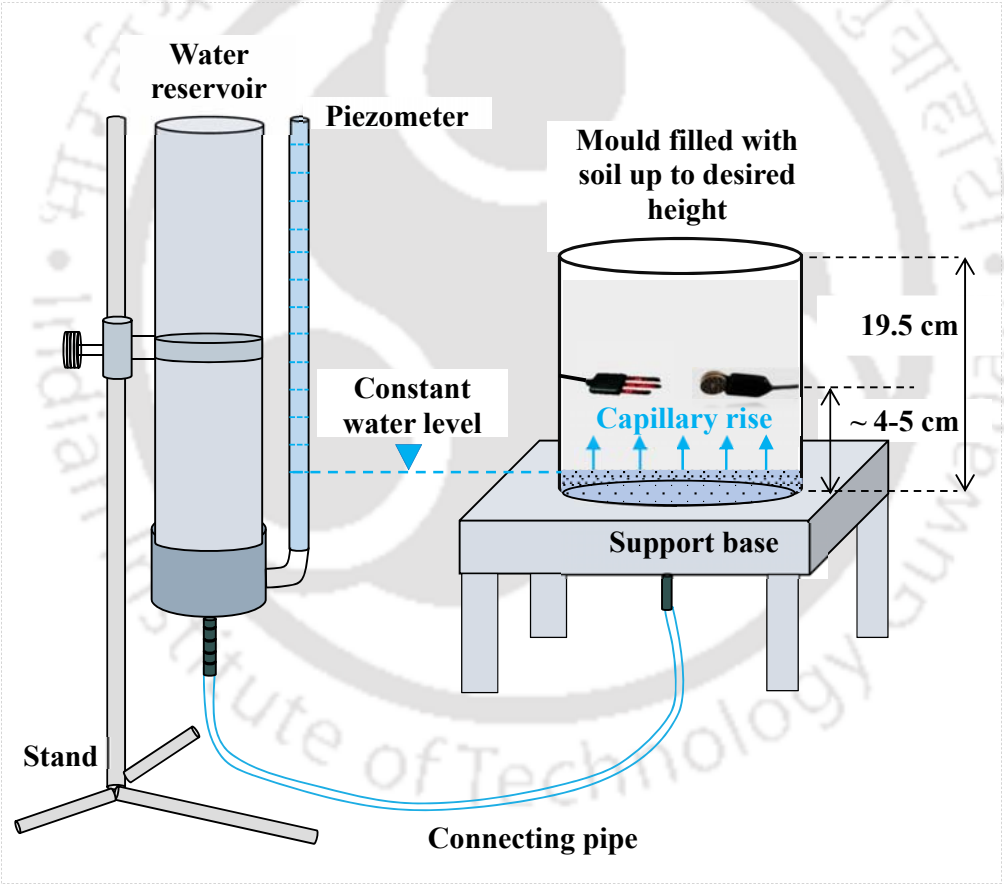

Figure 8.2 Schematic diagram of capillary rise set up in laboratory for independent water retention characteristics curve measurement

8.3. Results

In the first part, the results from the direct (Case 2 in Table 8.1) and independent (CR) evaluation methods (Figure 7.1) for the two soils are compared to check their similarity. This

step was deemed necessary for establishing the accuracy of the measured results from direct method. In the subsequent sections, the results from the indirect evaluation method are compared with the direct evaluation method to appraise its accuracy.

8.3.1. Comparison between the direct and independent evaluation methods

The WWRCC measured during infiltration measurements using sensors and the independently generated WWRCC from the CR method for the two soil textures are compared in Figure 8.3. For each soil, a total of six WWRCCs from MDI measurements (MDI_1 to MDI_6) and five from CR tests (CR_1 to CR_5) are obtained and plotted in the figure. For MDI measurements, the WWRCC obtained at the two depths (5 and 10cm) were identical (discussed in section 8.3.2.1). Hence, for clarity, only one curve from each experiment is utilized here for comparison.

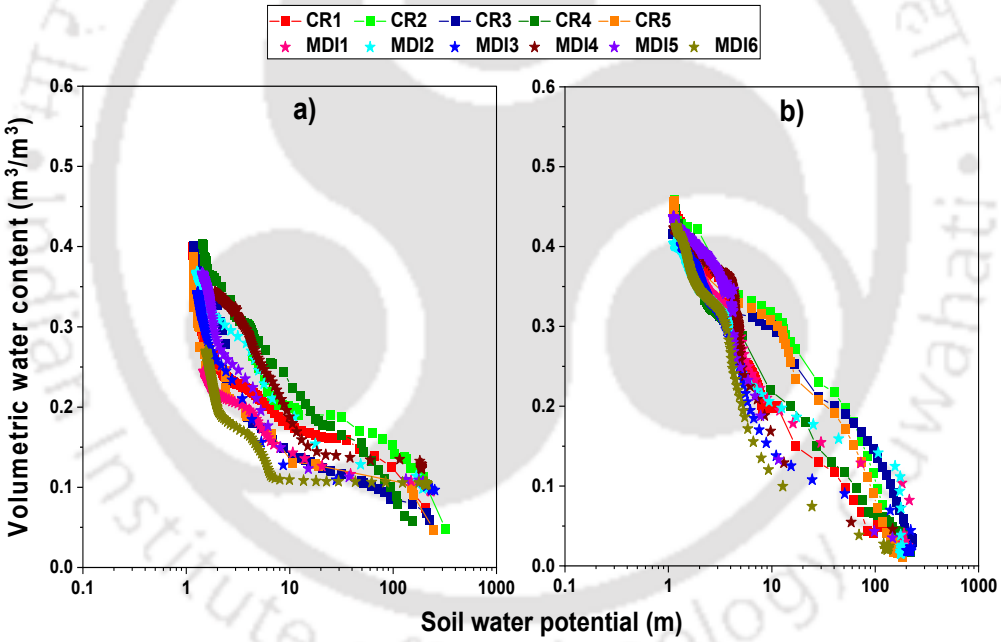

Figure 8.3: **The comparison of WWRCC obtained directly from MDI infiltration measurements using sensors with the independently measured WWRCC using the capillary rise method for a) Loam and b) Silt loam soils**
(MDI-Mini disc infiltrometer, CR-capillary rise)

As seen in the figures, for each soil, the WWRCC from the sensor measurements under MDI (MDI_1 to MDI_6) were fairly repeatable. Similarly, the CR measured WWRCCs for the five repetitions (CR_1 to CR_5) also generated nearly similar curves. It is also observed from the figure that for both the soil textures, the MDI measured retention curves were comparable

with the independently generated retention curves using the CR method. The spread of the data is expected because of the different measurement methodologies adopted. Ideally, such data need to be considered for the probabilistic determination of WWRCC, which is beyond the scope of this thesis. The same has been added to the future scope of the work (Chapter 9). The impact of such measurement variations on WWRCC parameters α and n was determined. A plot showing the comparison between the fitted parameters from the two measurement methods is depicted in Figure 8.4. The values from all the repetitions and the corresponding mean (± standard deviation, SD) values are also listed in Table 8.3, along with the α and n values from CP.

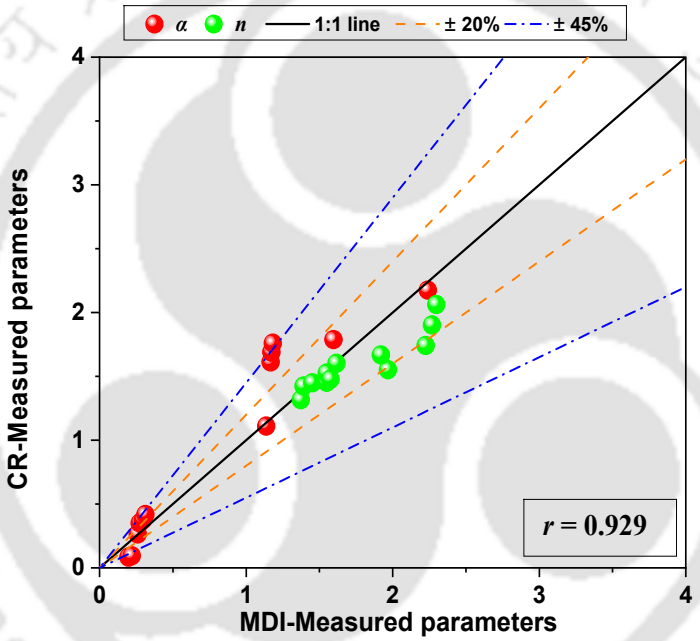

Figure 8.4: **The fitted parameters α and n (van Genuchten, 1980) determined from the measured WWRCC curves using MDI infiltration and CR tests for the two soil textures plotted using a 1:1 line for comparison (**MDI- Mini disc infiltrometer method, CR-Capillary rise method)

As observed from Figure 8.4, the marginal variations in WWRCC depicted in Figure 8.3 does not translate to a noticeable variation in the parameters considering both measurement methods and repetition. The parameters from both the methods were within a maximum deviation of ± 45% from the 1:1 line. Moreover, the two methods have shown a strong correlation with Pearson's r = 0.93. Also noted from Table 8.3, the fitted parameters from all the repetitions of MDI and CR measured curves for a given soil are comparable in magnitude. Consequently, the mean parameter values from the two measured curves are also

comparable, as listed in the table. The mean α (m^{-1}) from six repetitions of MDI measurements and five repetitions of CR tests were, respectively, 1.42 and 1.69 for LM soil, with SD of ±0.44 and ±0.38, while 0.26 and 0.27 for SL soil with corresponding SD of ±0.04 and ±0.16. Similarly, the mean n from all the repetitions of MDI measurements and CR tests were, respectively, 1.55 (±0.22) and 1.45(±0.09) for LM soil, and 1.98(±0.33) and 1.74(±0.24) for SL soil. Using the mean α and n for MDI and CR methods, the mean WWRCCs are obtained and are plotted in Figure 8.5 for comparison. In addition, for each soil, the WWRCC curve obtained using the α and n from CP is provided for comparison.

Table 8.3 WWRCC parameters α and n (van Genuchten, 1980) determined from the measured WWRCC curves (MDI infiltration) and CR tests, and the mean α and n from literature CP (Carsel and Parrish, 1988)

Fitted parameter	Loam		Silt loam	
	MDI-Measured	CR-Measured	MDI-Measured	CR-Measured
α (m^{-1})	1.18	1.61	0.26	0.35
	1.60	1.76	0.31	0.10
	2.24	1.79	0.30	0.42
	1.17	1.11	0.20	0.38
	1.17	2.18	0.22	0.08
	1.14	-	0.27	-
Mean*(±SD)	1.42 (±0.44)	1.69 (±0.38)	0.26 (±0.04)	0.27 (±0.16)
CP	3.6		2.0	
n	1.55	1.45	1.58	1.67
	1.39	1.32	1.62	1.90
	1.45	1.53	1.92	1.48
	1.37	1.42	2.22	1.60
	1.97	1.55	2.27	2.06
	1.55	-	2.30	-
Mean*(±SD)	1.55 (±0.22)	1.45 (±0.09)	1.98 (±0.33)	1.74 (±0.24)
CP	1.56		1.41	

*The values in parenthesis are the corresponding standard deviations (SD)

It is apparent from the Figure 8.5 that the WWRCCs from MDI and CR measured mean parameters (α and n) are highly comparable for both the textures. The coefficient of determination (R^2) between the two methods is 0.999, and the root means square error (RMSE) are 0.010 and 0.007 $m^3/m^{3,}$ respectively, for LM and SL soils (Table 8.4). As expected, the WWRCC from texture-based CP is different from both the measured WWRCC for the two soil textures. This discrepancy is also reported from the R^2 and RMSE values in

Table 8.4. This was due to the difference of the CP parameters from the measured retention parameters, particularly for α (Table 8.3), which resulted in the prediction of different WWRCC.

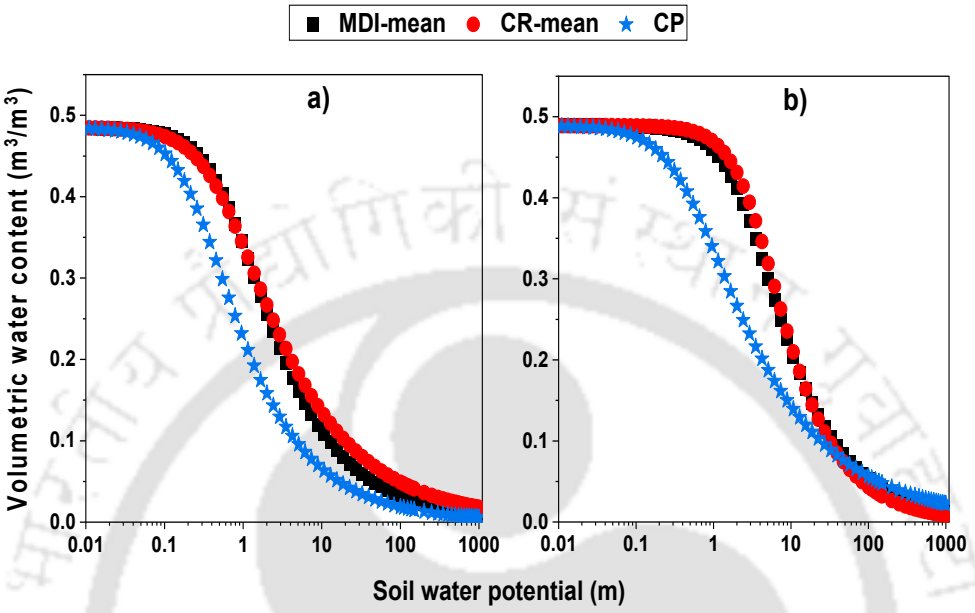

Figure 8.5 The WWRCC obtained using mean parameter values (α and n) from MDI infiltration and Capillary rise tests along with the curve obtained using CP α and n (Carsel and Parrish, 1988) for a) loam and b) silt loam soils

Table 8.4 Summary of coefficient of determination (R^2) and root mean square error (RMSE) (m^3/m^3) between mean WWRCC obtained using various methods for the two soil textures

Soil texture		MDI-Measured vs. CR-Measured	MDI-Measured vs. CP	CR-Measured vs. CP
Loam	R^2	0.999	0.977	0.975
	RMSE	0.010	0.038	0.044
Silt loam	R^2	0.999	0.953	0.940
	RMSE	0.007	0.046	0.052

MDI- Mini disc infiltrometer method, CR-Capillary rise method, CP-Carsel and Parrish (Carsel and Parrish, 1988)

Based on the above results, it is clear that the WWRCC measured for the same soils using both direct and independent evaluation methods have resulted in identical WWRCC and comparable van Genuchten parameters. This implies that the direct method employed in this study, which involves measurement of the WWRCC using sensors during MDI infiltration, is

reliable. Hence, for conducting further evaluations in this study, the results from the direct method were used as the reference.

8.3.2. Comparison between the direct and indirect evaluation methods

In the first part of this section, the WWRCC determined from MDI measured/ estimated CI, sensor measurements, optimization based on VWC, and SWP conforming to various cases and subcases listed in Table 8.1 were compared. This was followed by assessing the statistical difference in the parameters α, n, and K_s obtained from various subcases. Finally, the estimated α, n, and K_s from different subcases were compared with the reference values (Case 2 results) and the values reported in the literature for the same soil textures.

8.3.2.1. Measured and estimated results for various cases

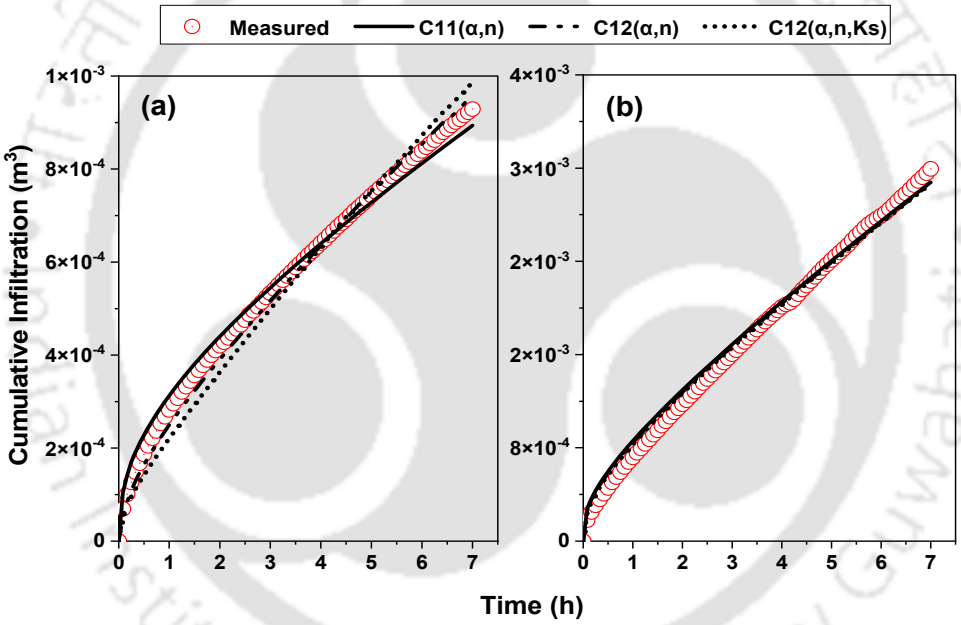

Figure 8.6 Measured and estimated (Case 1) cumulative infiltration response for (a) loam and (b) silt loam

Table 8.5 Error calculation between estimated and measured values for all the cases shown in Figures 8.6 to 8.9

Figure details		R^2	MAE	RMSE
8.6a	C11	0.976	2.10E-05	2.40E-05
	C12	0.992	1.80E-05	2.00E-05
	C12’	0.997	3.50E-05	4.00E-05
8.6b	C11	0.992	8.20E-05	9.20E-05
	C12	0.992	7.50E-05	8.40E-05
	C12’	0.992	6.90E-05	7.70E-05
8.7a	5cm depth	0.995	6.50E-03	1.28E-02
	10cm depth	0.986	7.80E-03	1.31E-02
8.7b	5cm depth	0.989	7.70E-03	1.06E-02
	10cm depth	0.975	9.30E-03	1.72E-02
8.8a	5cm depth	0.984	1.73E-01	2.12E-01
	10cm depth	0.972	2.29E-01	4.04E-01
8.8b	5cm depth	0.965	7.44E-01	9.25E-01
	10cm depth	0.961	8.20E-01	9.75E-01
8.9a	5cm depth	0.995	3.60E-03	4.70E-03
	10cm depth	0.982	1.16E-02	1.31E-02
8.9b	5cm depth	0.981	1.35E-02	1.49E-02
	10cm depth	0.985	1.14E-02	1.48E-02

Figures 8.6 (a) and (b) compare the measured and estimated cumulative infiltration with time for soils LM and SL, respectively. To quantify the difference, the R^2, the mean absolute error (MAE), and the RMSE between the measured and the estimated values for the three subcases of Case 1 (C1-1, C1-2, C1-2’) are calculated and listed in Table 8.5. It can be noted that the estimated CI versus time curve matches well with the measured MDI results with high R^2 (> 0.9) and low MAE and RMSE (both in the order of 10^{-5} m^3). For Case 3, measured and estimated VWC variation with time is compared for two depths as shown in Figure 8.7. It is seen from the figures that the estimated θ_f in both the soils (0.375 and 0.438, respectively) are lower than the calculated θ_s values (section 8.2.1) even after 7 hours of the wetting experiment. The calculated θ_s for LM soil ranged between 0.461 to 0.487 m^3/m^3, and for SL soil ranged between 0.477 to 0.489 m^3/m^3. The presence of air pockets or entrapped air can result in measured θ_s (or θ_f) generally less than the calculated θ_s (Šimůnek et al., 1999; Touma et al., 1984). Moreover, the calculated θ_s value is dependent on the geometrical volume

of the soil sample and not the pore distribution. However, the actual flow and saturation are dependent on the random distribution of pores and their connectivity. It is also observed that for both the soils, the sensor responses at 5 and 10 cm depths are identical, with an expected marginal delay in wetting at 10 cm depth. Figure 8.7 further depicts a reasonable matching between the measured and estimated results for both the soils. The calculated MAE (m^3/m^3) between measured and estimated VWC for 5 cm and 10 cm depths in Figure 8.7a are 6.5×10^{-3} and 7.8×10^{-3}, respectively. For SL soil (Figure 8.7b), these values are 7.7×10^{-3} and 9.3×10^{-3} as listed in Table 8.5. The observed R^2 values are > 0.9 in all the cases, and RMSE values are in the order of 10^{-2} m^3/m^3.

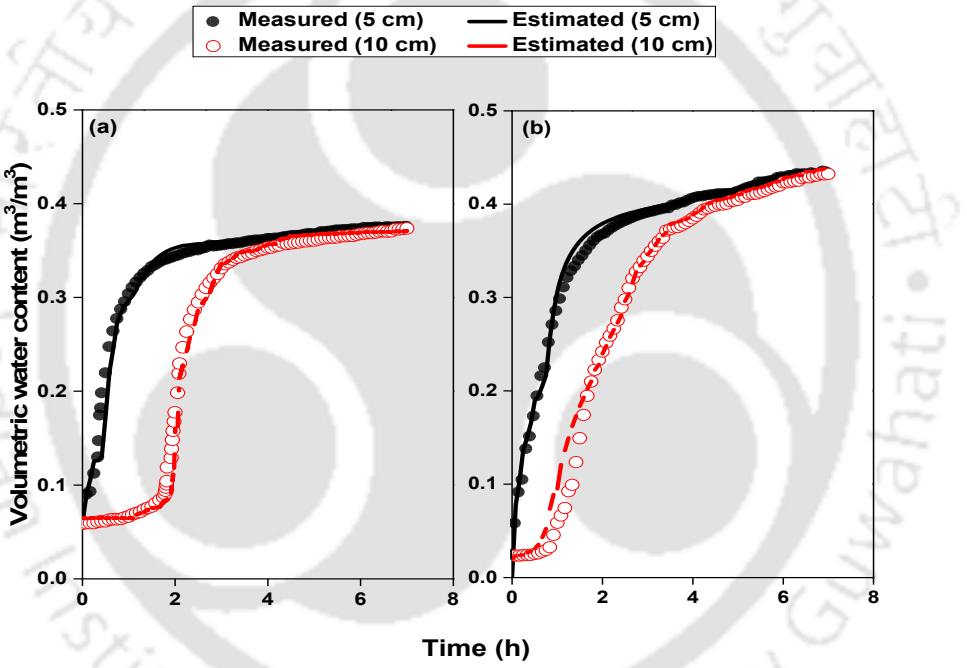

Figure 8.7 Measured and estimated volumetric water content variation with time for (a) loam and (b) silt loam

The comparison of measured and estimated SWP versus time response corresponding to Case 4 is shown in Figure 8.8. It is observed from the figures that an overall wide range of SWP value (-170 m to -1.01 m) is recorded over the entire duration of the experiment for both the soils, and a good agreement ($R^2 \geq 0.9$, MAE in the range of 0.17 to 0.82 m, and RMSE in the range of 0.21 to 0.97 m, Table 8.5) is noted between the measured and estimated results. It is also witnessed that within the starting few hours (4-5 hours) of the wetting experiment, steep changes in the SWP values were recorded, beyond which the changes in SWP values

are less significant. This is also visible in Figure 8.7, which shows a sudden change in VWC within the first few hours akin to decrease in SWP. This behavior is well anticipated given the initial dry state and progressive wetting during infiltration.

During the inverse optimization, different paths to the objective function minimum are possible depending on the initial hydraulic parameters. Simunek and van Genucthen (1996) observed that error maps from a global optimization of a CI curve present elongated valley shapes. Depending on the initial values, local optimization can stop along this valley at a local minimum at a certain distance from the absolute global minimum. To avoid this, Simunek et al. (2012) suggested re-running the simulations with different initial parameters to verify that the objective function converges to the same global minimum. Hence, this study repeated the optimization using five to six different initial guess values for each subcase (section 8.2.2) until similar final estimates were produced. The final parameter estimates (optimized) producing fair (i.e., high R^2 and low MAE and RMSE) modelled outputs (CI/VWC/SWP) were subsequently considered for further analysis.

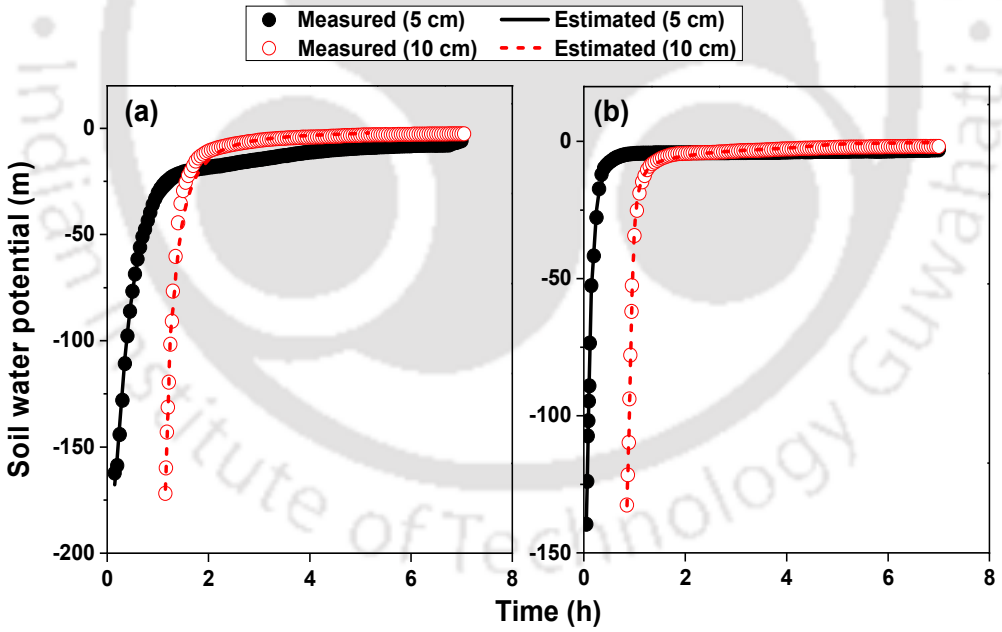

Figure 8.8 Measured and estimated soil water potential variation with time for (a) loam and (b) silt loam

For Case 2 results, Figure 8.9 (a) and (b) show the fitted curves for LM and SL, respectively at the two considered depths (note that for presenting in log scale, the absolute

values of SWP measurements are taken). It can be noted that the vG model adequately fits to the experimental observations for both the soils with $R^2 \geq 0.9$ in all cases. Also, the calculated MAE and RMSE are < 0.015 m^3/m^3 for both the soils (listed in Table 8.5). It is also worth mentioning that for each soil, the measured WWRCC at both 5 and 10 cm depths match well. Hence, as already stated (section 8.2.2), the parameters from measured WWRCC at the two depths are used to determine the mean fitted parameters (α_{true}, n_{true}) and considered as reference value (designated as Case 2_{ref}) for evaluating all other cases.

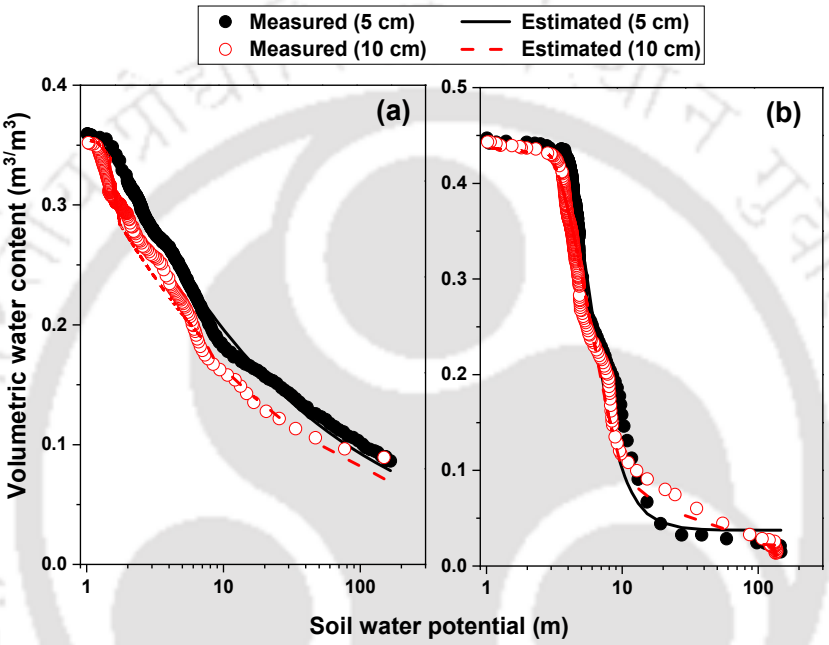

Figure 8.9 Measured and estimated (van Genuchten model) wetting water retention curve for (a) loam and (b) silt loam

8.3.2.2. Statistical analysis of the estimated WWRCC parameters

For the two soils, the estimated vG WWRCC parameters α and n from 17 subcases and K_s from 5 subcases were analysed using a one-way ANOVA test and Fisher's least significant difference (LSD) post hoc test available in SPSS Statistics software (version 25). The post hoc test results for α, n, and K_s are presented in Tables 8.6, 8.7, and 8.8, respectively. The tables list the statistical difference in mean between all the subcases and their corresponding significance value (p) (given in parenthesis). For $p > 0.05$, the mean difference is not significant, and the group means are comparable. Cells marked in * correspond to $p \leq 0.05$, and hence the difference between group means is significant. Based on p values for loam, the α from Case 1 (C1-1, C1-2, and C1-2') are comparable with results from Case 2 (C2-1,

C2-2) and 4 (C4-1 to C4-4'). The results from Case 3 (C3-1 to C3-4) are statistically different from other subcases. For silt loam, α from a majority of the subcases is comparable. The overall mean difference values for α (in m^{-1}) range between 0.006 to 0.84 for LM and 0.0002 to 0.31 for SL. For parameter n (Table 8.7), the results from all the subcases are comparable except C1-1 and C3-3 for both soils and additionally C4-1, C4-1', C4-2, and C4-2' for SL soil. The mean difference for n ranges between 0.002 to 0.50 for LM and 0.002 to 0.45 for SL. For the K_s parameter (Table 8.8), the statistical difference between all the subcases and the measured PM is insignificant. The mean difference in K_s varies in the range of 10^{-7} to 10^{-9} m/s.

A graphical representation of the mean and SD of estimated parameters for each subcase are presented in Figure 8.10a to f, along with the mean values reported by CP for the two soil textures. The mean parameters α and n from Case 2_{ref} and the mean K_s from PM are plotted as the reference value in Figure 8.10. For the soil LM, the estimated α from all the subcases except Case 3 is comparable with the reference mean. The subcases C1-2, C1-2', and C4-2' match well with the reference mean, indicating the usefulness of θ_f as input. The observation is similar for SL, with most of the Case 4 and C1-2, C1-2' comparing well with the reference mean. The observations in this study strongly advocate the use of MDI measurements along with the final VWC for the inverse estimation of WWRCC parameters. This observation is consistent with those reported in the literature (Šimůnek et al., 1999). For both the soil texture, the VWC versus time (Case 3) as input for inverse simulation did not fare well for the estimation of α and n compared to other cases. According to Šimůnek & van Genuchten (1996), the convergence to well-defined minima always does not guarantee a unique solution. A similar situation might have occurred in the Case 3 where, even though convergence was attained and use of different initial guess values have resulted in nearly similar final estimates, however, they represented the local minima only and not the global minimum. This could be possibly due to the choice of the initial parameters close to the local minima which aided in quick convergence but failed to generate unique solutions. The two different initial conditions in Cases 3 and 4 (Table 8.1) have given comparable WWRCC parameter values with an insignificant statistical difference. The mean K_s from all the subcases are comparable with the measured mean from PM regardless of the type of input variable for both the soils as shown in Figures 8.10e and f.

Table 8.6 Mean difference (m^{-1}) and significance value (in parenthesis) for van Genuchten parameter α for the two soils (LM in lower left and SL in upper right)

		Silt loam-α																
		C11	C12	C12'	**C21**	**C22**	C31	C32	C33	C34	C41	C41'	C42	C42'	C43	C43'	C44	C44'
Loam- α	C11		*	*	0.22 (0.08)	0.16 (0.21)	0.03 (0.82)	0.15 (0.23)	- 0.13 (0.32)	*	0.11 (0.36)	0.16 (0.21)	0.14 (0.26)	0.13 (0.30)	0.16 (0.21)	*	*	0.14 (0.27)
	C12	*		-0.02 (0.73)	-0.02 (0.88)	-0.08 (0.52)	-0.21 (0.09)	-0.09 (0.48)	*	0.09 (0.49)	-0.13 (0.32)	-0.08 (0.51)	-0.10 (0.44)	-0.11 (0.39)	-0.08 (0.52)	0.06 (0.62)	0.09 (0.45)	-0.10 (0.42)
	C12'	*	-0.15 (0.53)		0.01 (0.96)	-0.06 (0.65)	-0.19 (0.14)	-0.06 (0.61)	*	0.11 (0.37)	-0.10 (0.42)	-0.06 (0.64)	-0.07 (0.56)	-0.08 (0.50)	-0.06 (0.65)	0.09 (0.49)	0.12 (0.34)	-0.08 (0.50)
	C21	-0.77 (0.08)	-0.19 (0.60)	-0.04 (0.91)		-0.06 (0.70)	-0.19 (0.24)	-0.07 (0.66)	*	0.11 (0.51)	-0.11 (0.51)	-0.06 (0.69)	-0.08 (0.62)	-0.09 (0.58)	-0.06 (0.70)	0.08 (0.62)	0.11 (0.49)	-0.08 (0.61)
	C22	-0.46 (0.17)	0.12 (0.75)	0.27 (0.43)	0.31 (0.48)		-0.13 (0.42)	-0.01 (0.96)	-0.28 (0.08)	0.17 (0.30)	-0.04 (0.79)	0.002 (0.99)	-0.02 (0.92)	-0.03 (0.86)	0.00 (1.00)	0.14 (0.37)	0.18 (0.28)	-0.02 (0.91)
	C31	*	*	*	*	*		0.12 (0.45)	-0.15 (0.34)	0.30 (0.07)	0.09 (0.60)	0.13 (0.42)	0.11 (0.48)	0.10 (0.53)	0.13 (0.42)	0.27 (0.09)	0.31 (0.06)	0.11 (0.49)
	C32	*	*	*	*	*	-0.18 (0.69)		-0.28 (0.09)	0.18 (0.28)	-0.04 (0.83)	0.01 (0.96)	-0.01 (0.96)	-0.02 (0.91)	0.01 (0.95)	0.15 (0.35)	0.18 (0.26)	-0.01 (0.95)
	C33	*	*	*	*	*	-0.26 (0.55)	-0.08 (0.84)		*	0.24 (0.14)	0.28 (0.08)	0.27 (0.10)	0.26 (0.11)	0.28 (0.08)	*	*	0.27 (0.10)
	C34	*	*	*	*	*	0.13 (0.77)	0.30 (0.49)	0.39 (0.37)		-0.21 (0.19)	-0.17 (0.30)	-0.19 (0.25)	-0.20 (0.23)	-0.17 (0.30)	-0.02 (0.88)	0.01 (0.96)	-0.19 (0.25)
	C41	*	-0.38 (0.29)	-0.23 (0.50)	-0.19 (0.66)	-0.50 (0.25)	*	*	*	0.80 (0.07)		0.04 (0.80)	0.03 (0.87)	0.02 (0.92)	0.04 (0.79)	0.19 (0.25)	0.22 (0.18)	0.02 (0.88)
	C41'	-0.44 (0.19)	0.13 (0.71)	0.29 (0.40)	0.33 (0.45)	0.02 (0.97)	*	*	*	*	0.52 (0.23)		-0.01 (0.93)	-0.03 (0.88)	0.00 (0.99)	0.15 (0.37)	0.18 (0.27)	-0.02 (0.92)
	C42	-0.01 (0.99)	0.57 (0.12)	*	0.76 (0.08)	0.45 (0.30)	*	*	*	*		0.43 (0.32)		-0.01 (0.95)	0.02 (0.92)	0.16 (0.32)	0.19 (0.24)	0.00 (0.99)
	C42'	-0.54 (0.11)	0.04 (0.92)	0.19 (0.58)	0.23 (0.60)	-0.08 (0.85)	*	*	*	*	0.42 (0.33)	-0.10 (0.82)	-0.53 (0.22)		0.03 (0.87)	0.17 (0.29)	0.20 (0.21)	0.01 (0.96)
	C43	*	-0.34 (0.35)	-0.19 (0.58)	-0.15 (0.73)	-0.46 (0.29)	*	*	*	0.84 (0.05)	0.04 (0.93)	-0.48 (0.27)	*	-0.38 (0.38)		0.14 (0.37)	0.18 (0.28)	-0.02 (0.91)
	C43'	-0.04 (0.89)	0.53 (0.15)	*	0.72 (0.10)	0.41 (0.34)	*	*	*	*	*	0.40 (0.36)	-0.04 (0.93)	0.49 (0.26)	*		0.03 (0.84)	-0.16 (0.32)
	C44	*	-0.57 (0.12)	-0.41 (0.23)	-0.38 (0.39)	-0.68 (0.12)	0.74 (0.09)	*	*	0.62 (0.16)	-0.19 (0.67)	-0.70 (0.11)	*	-0.60 (0.17)	-0.23 (0.60)	*		-0.19 (0.23)
	C44'	*	-0.36 (0.32)	-0.21 (0.55)	-0.17 (0.70)	-0.48 (0.27)	*	*	*	0.82 (0.06)	0.02 (0.96)	-0.50 (0.25)	*	-0.40 (0.36)	-0.02 (0.97)	*	*	

Table 8.7 Mean difference and significance value (in parenthesis) for van Genuchten parameter *n* for the two soils (LM in lower left and SL in upper right)

		Silt loam- *n*																
Loam- *n*		C11	C12	C12'	**C21**	**C22**	C31	C32	C33	C34	C41	C41'	C42	C42'	C43	C43'	C44	C44'
	C11		*	*	-0.45 (0.05)	-0.34 (0.07)	*	*	*	-0.33 (0.07)	-0.05 (0.77)	-0.06 (0.75)	*	*	-0.16 (0.36)	-0.21 (0.26)	*	-0.32 (0.08)
	C12	-0.13 (0.34)		-0.09 (0.40)	0.02 (0.92)	0.13 (0.48)	-0.15 (0.42)	-0.18 (0.31)	*	0.13 (0.47)	*	*	-0.13 (0.48)	-0.13 (0.48)	0.30 (0.10)	0.26 (0.15)	-0.01 (0.96)	0.14 (0.43)
	C12'	-0.20 (0.10)	-0.07 (0.64)		0.11 (0.55)	0.22 (0.23)	-0.06 (0.75)	0.09 (0.60)	*	0.22 (0.23)	*	*	-0.04 (0.83)	-0.04 (0.82)	*	0.35 (0.06)	0.08 (0.66)	0.23 (0.20)
	C21	-0.13 (0.51)	0.00 (0.98)	0.07 (0.72)		0.11 (0.64)	-0.16 (0.48)	-0.20 (0.39)	*	0.11 (0.63)	0.39 (0.09)	0.39 (0.10)	-0.15 (0.53)	-0.15 (0.53)	0.28 (0.23)	0.24 (0.30)	-0.03 (0.90)	0.12 (0.60)
	C22	-0.11 (0.58)	0.02 (0.91)	0.09 (0.65)	0.02 (0.94)		-0.27 (0.24)	-0.13 (0.19)	*	0.00 (0.99)	0.28 (0.22)	0.28 (0.23)	-0.25 (0.28)	-0.26 (0.27)	0.17 (0.46)	0.13 (0.58)	-0.14 (0.56)	0.01 (0.95)
	C31	*	-0.39 (0.07)	-0.32 (0.11)	-0.39 (0.12)	-0.41 (0.11)		-0.04 (0.88)	-0.34 (0.14)	0.28 (0.24)	*	*	0.02 (0.93)	0.02 (0.94)	0.45 (0.06)	0.41 (0.08)	0.14 (0.56)	0.29 (0.22)
	C32	-0.28 (0.15)	-0.15 (0.49)	-0.08 (0.69)	-0.15 (0.55)	-0.17 (0.50)	0.24 (0.34)		-0.31 (0.19)	0.31 (0.18)	*	*	0.06 (0.81)	0.05 (0.82)	*	0.44 (0.06)	0.17 (0.46)	0.33 (0.17)
	C33	*	*	*	*	*	-0.25 (0.32)	-0.50 (0.05)		0.28 (0.23)	*	*	*	0.02 (0.94)	0.45 (0.05)	0.41 (0.08)	0.14 (0.55)	0.29 (0.21)
	C34	-0.18 (0.37)	-0.04 (0.84)	0.02 (0.90)	-0.05 (0.85)	-0.07 (0.79)	0.35 (0.18)	0.10 (0.68)	*		0.28 (0.22)	0.28 (0.23)	*	-0.26 (0.26)	0.17 (0.46)	0.13 (0.58)	-0.14 (0.54)	0.01 (0.96)
	C41	0.06 (0.77)	0.19 (0.37)	0.26 (0.20)	0.19 (0.46)	0.17 (0.51)		0.34 (0.18)	*	0.23 (0.36)		-0.01 (0.98)	*	*	-0.11 (0.63)	-0.15 (0.51)	-0.42 (0.07)	-0.27 (0.25)
	C41'	-0.18 (0.35)	-0.05 (0.82)	0.02 (0.93)	-0.05 (0.83)	-0.07 (0.77)	0.34 (0.18)	0.10 (0.70)	*	-0.01 (0.98)	-0.24 (0.34)		*	*	-0.11 (0.65)	-0.15 (0.53)	-0.42 (0.08)	-0.27 (0.26)
	C42	-0.28 (0.16)	-0.14 (0.50)	-0.07 (0.71)	-0.15 (0.56)	-0.17 (0.51)	0.25 (0.33)	0.01 (0.98)	0.50 (0.05)	-0.10 (0.70)	-0.33 (0.19)	-0.09 (0.72)		0.00 (0.99)	0.43 (0.07)	0.39 (0.10)	0.12 (0.62)	0.27 (0.25)
	C42'	-0.27 (0.17)	-0.14 (0.52)	-0.07 (0.73)	-0.14 (0.58)	-0.16 (0.53)	0.25 (0.32)	0.01 (0.97)	*	-0.09 (0.71)	-0.33 (0.20)	-0.09 (0.73)	0.01 (0.98)		0.43 (0.07)	0.39 (0.10)	0.12 (0.61)	0.27 (0.25)
	C43	-0.19 (0.35)	-0.05 (0.81)	0.02 (0.94)	-0.06 (0.82)	-0.08 (0.77)	0.34 (0.19)	0.10 (0.71)	*	-0.01 (0.97)	-0.24 (0.34)	0.00 (0.99)	0.09 (0.72)	0.08 (0.74)		-0.04 (0.86)	-0.31 (0.19)	-0.16 (0.50)
	C43'	*	-0.27 (0.21)	-0.20 (0.32)	-0.27 (0.28)	-0.29 (0.25)	0.12 (0.64)	-0.12 (0.64)	0.37 (0.14)	-0.23 (0.38)	-0.46 (0.07)	-0.22 (0.39)	-0.13 (0.62)	-0.13 (0.60)	-0.22 (0.40)		-0.27 (0.25)	-0.12 (0.62)
	C44	*	-0.27 (0.20)	-0.20 (0.31)	-0.28 (0.28)	-0.30 (0.25)	0.12 (0.65)	-0.12 (0.63)	0.37 (0.15)	-0.23 (0.37)	-0.46 (0.07)	-0.22 (0.38)	-0.13 (0.61)	-0.14 (0.60)	-0.22 (0.39)	0.00 (0.99)		0.15 (0.52)
	C44'	*	*	-0.40 (0.05)	-0.47 (0.07)	-0.49 (0.06)	-0.08 (0.77)	-0.32 (0.21)	0.18 (0.48)	-0.42 (0.10)	*	-0.41 (0.11)	-0.32 (0.21)	-0.33 (0.20)	-0.41 (0.11)	-0.20 (0.44)	-0.19 (0.45)	

Table 8.8 Mean difference (m/s) and significance value (in parenthesis) for K_s for the two soils (LM in lower left and SL in upper right)

		Silt loam-K_s					
Loam- K_s		C12'	C41'	C42'	C43'	C44'	**PM[#]**
	C12'		6.1E-08 (0.707)	-5.3E-08 (0.745)	-1.0E-07 (0.522)	2.6E-08 (0.875)	2.1E-08 (0.896)
	C41'	-1.5E-07 (0.398)		-1.1E-07 (0.582)	-1.7E-07 (0.426)	-3.6E-08 (0.864)	-4.0E-08 (0.847)
	C42'	1.1E-07 (0.527)	2.6E-07 (0.244)		-5.2E-08 (0.804)	7.9E-08 (0.705)	7.5E-08 (0.721)
	C43'	3.1E-08 (0.861)	1.8E-07 (0.420)	-8.0E-08 (0.717)		1.3E-07 (0.531)	1.3E-07 (0.545)
	C44'	-7.3E-08 (0.674)	7.5E-08 (0.735)	-1.8E-07 (0.406)	-1.0E-07 (0.638)		-4.5E-09 (0.983)
	PM[#]	-3.1E-08 (0.859)	1.2E-07 (0.596)	-1.4E-07 (0.522)	-6.1E-08 (0.781)	4.2E-08 (0.847)	

[#]Reference value from falling head permeameter (PM) measurements

It is worth noting from Figure 8.10 that the parameter values obtained from CP (based on texture) are high in all the subcases except for n of SL. The relative error (RE) (in percentage) between the CP values and the mean values from various subcases are plotted using pie charts in Figure 8.11 (a to f) for the two soil textures. The RE is high for parameter α than n. The RE for α varies between 17 to 76% for LM and 65 to 88% for SL (Fig 10a and b), while for n, it varies between 1.3 to 30% for LM and 0.3 to 56% for SL (Figure 8.11c and d). For K_s, nearly one order difference is observed with an average RE of 81% for LM and 57% for SL. The overall results show that except for n, the parameter values obtained from CP are significantly different from all the subcases and the reference mean value. Similar discrepancy of CP parameters has also been observed with the CR parameters (Table 8.3). It is explicit from the results that texture-based estimation of hydraulic parameter values is inconsistent for the two soils considered in this study. The study endorses that the non-invasive MDI measurements and inverse analysis of CI versus time data can be quite handy for estimating hydraulic parameters instead of relying on texture-based estimations. The same is also applicable in the absence of sensors for quantifying the WWRCC.

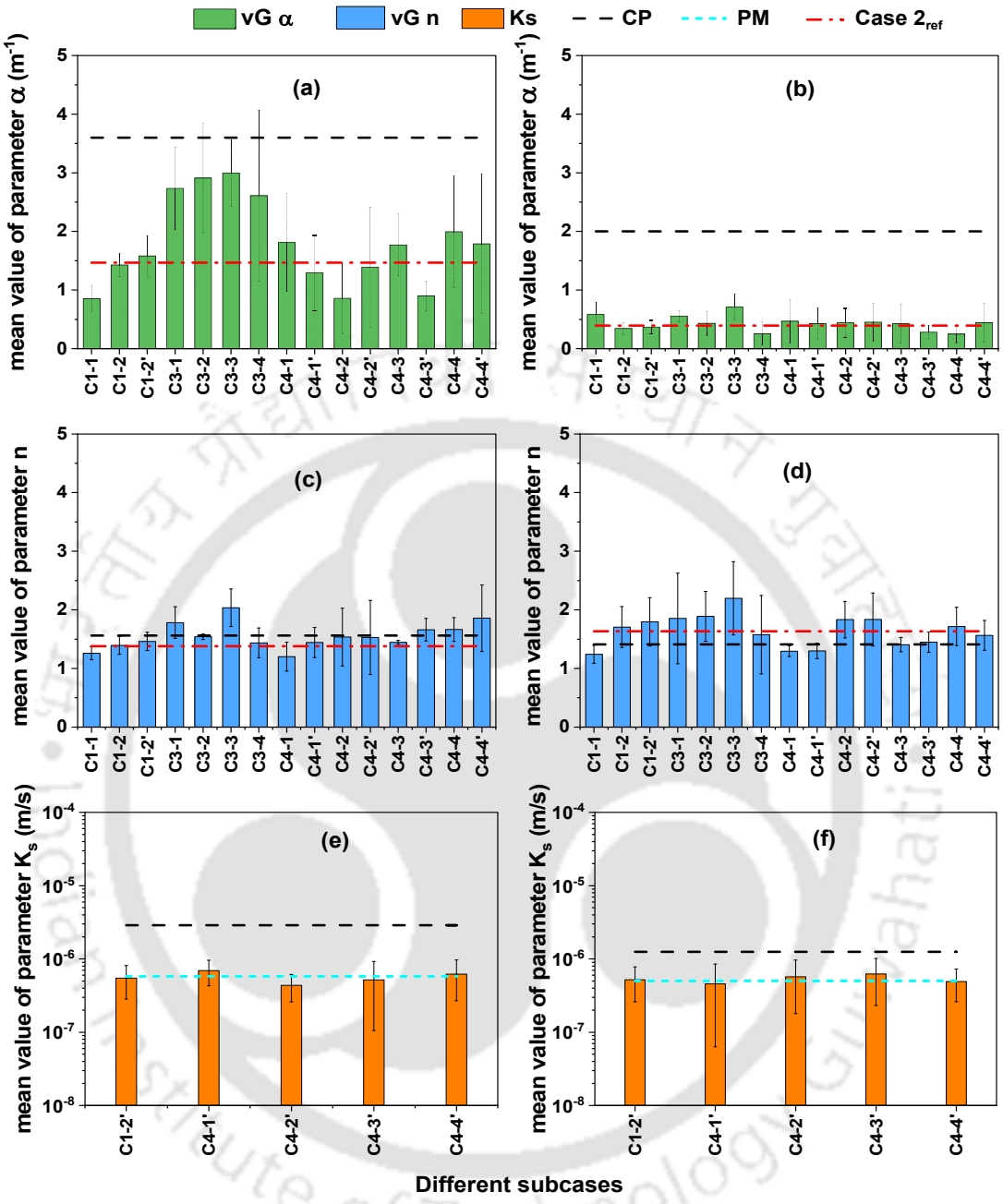

Figure 8.10 Comparison of WWRCC van Genuchten parameters (*α* and *n*) and K_s determined from different cases (Table 8.1) with reference value and Carsel and Parrish estimation for loam (a, c & e) and silt loam (b, d & f)

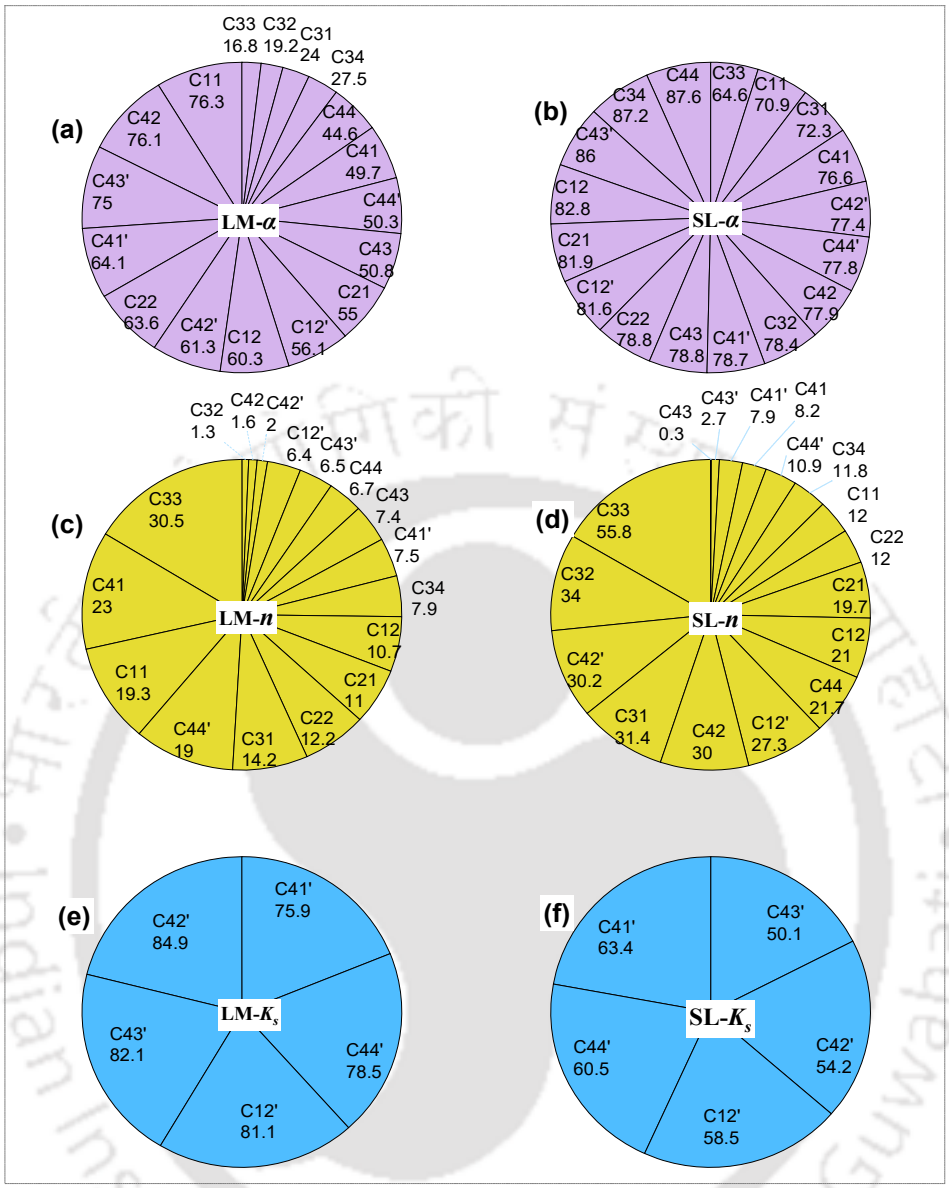

Figure 8.11 Pie-charts showing Relative error (%) between the estimated means and the Carsel and Parrish texture-based values for *α*, *n*, and K_s for loam (a, c & e) and silt loam (b, d & f)

8.3.2.3. Final mean values of α, n, and Ks

For the three estimated hydraulic parameters *α*, *n*, and K_s, the final mean and SD are calculated by discarding those values having significant differences from reference values (Tables 8.6, 8.7, and 8.8). Accordingly, the calculated final mean value for *α* (m^{-1}), *n*, and K_s (m/s) for LM soil are 1.43 (± 0.38), 1.50 (± 0.18), and 5.63×10^{-7} (± 9.89×10^{-8}), respectively.

Similarly, for SL soil the values of α, n, and, K_s are 0.41 (± 0.09), 1.61 (± 0.22), and 5.33 × 10^{-7} (± 6.57 × 10^{-8}), respectively. The final estimated mean hydraulic parameter values were used to determine the WWRCC of both soils. This is compared with the measured and CR WWRCC, and the curve obtained based on CP estimation as shown in Figures 8.12 a and b. The figures also provide error bands showing 30% and 10% deviations from the measured WWRCC for both soils. The WWRCC from the final estimated means is comparable with both the CR and measured WWRCC. The deviations are within 30% in the lower VWC region, which has further reduced to < 10% for higher VWC values.

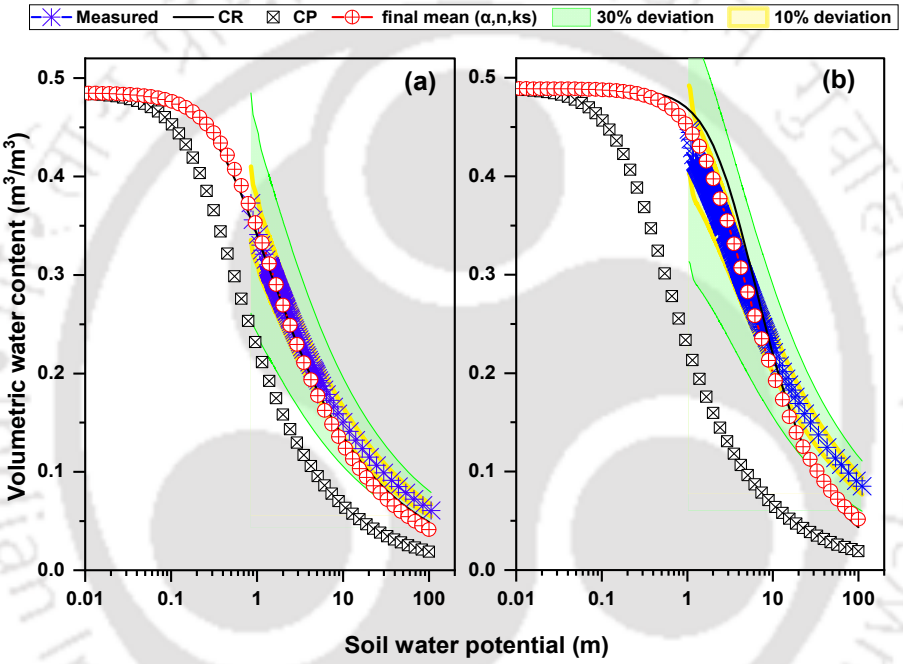

Figure 8.12 Comparison of WWRCC obtained using the estimated final means and the CP means with the measured and CR results for (a) loam and (b) silt loam soils (CR-Capillary rise method, CP-Carsel and Parrish (Carsel and Parrish, 1988))

Further, the final mean estimates of α and n were used to calculate near-saturated hydraulic conductivity (K_0) using Zhang's method (Zhang, 1997a, b) for all six repetitions and compared with the K_0 obtained from CP estimations as depicted in Figures 8.13a and b. For reference, the K_0 values calculated using the power functions recommended in the literature (Bordoloi et al., 2018, Eq. 7 and 8) are plotted for both the soils. The power functions developed by Bordoloi et al. (2018) were based on MDI infiltration measurements and considering ten different soils of varying fine contents. Additionally, the K_0 values for LM soil from literature (Šimůnek et al., 1999), calculated using Wooding's method (Ankeny et

al., 1991; Wooding, 1968), are also provided in the figure (Figures 8.13a). Their study was carried out using tension infiltrometer, and the calculated K_0 corresponded to a negative pressure head of 7.5cm (closest to 6cm). All the determined K_0 values are listed in Table 8.9. The K_0 results using final means are fairly comparable (same order of 5 to 6 in a log-transformed scale) with the reference values from the past literature (Figures. 8.13a and b). The K_0 values for the six repetitions of LM soil range between 1.72×10^{-6} to 3.23×10^{-6} m/s, while for SL soil, the values range between 4.15×10^{-6} to 6.4×10^{-6} m/s (Table 8.9). The WWRCC from CP has shown higher deviations from the measured WWRCC (Figure 8.12). Similarly, the K_0 from CP has shown difference by one order of magnitude for SL soil (Figure 8.13b). Fodor et al. (2011) also reported a significant difference in K_s values calculated using the measured WRCC retention parameters and estimated CP parameters.

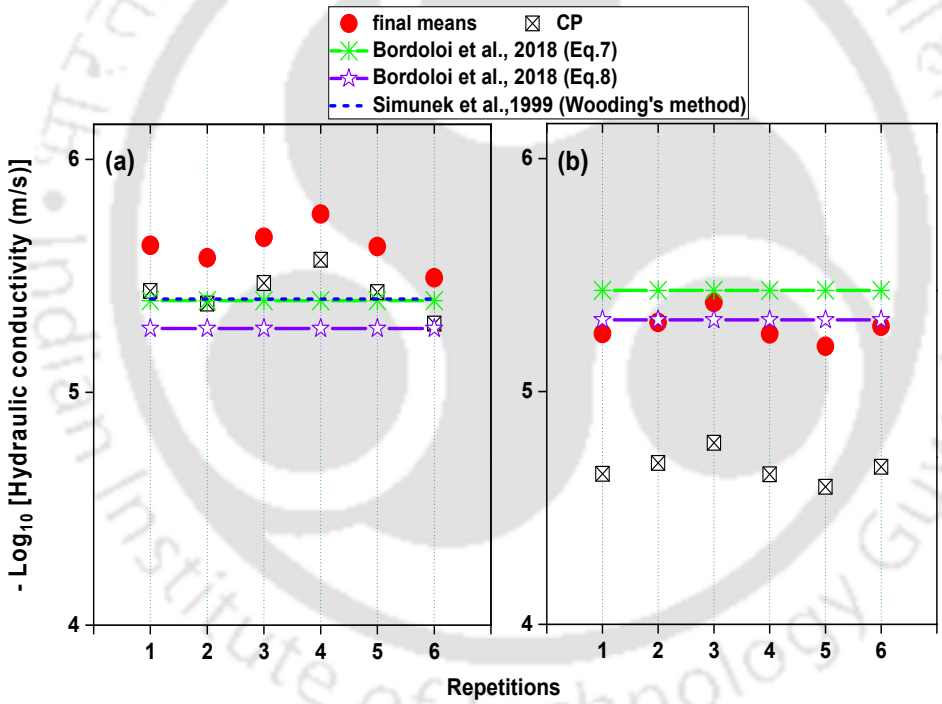

Figure 8.13 Comparison of negative log-transformed K_0 for six repetitions of (a) loam and (b) silt loam soils calculated using Zhang's method by considering estimated final mean α and n and the CP α and n along with the reference values from literature (Simunek et al., 1999 and Bordoloi et al., 2018)

Table 8.9 Summary of K_0 (m/s) using estimated final mean α and n and the CP α and n along with the reference values from literature (Bordoloi et al., 2018 and Simunek et al., 1999)

Experiment repetitions	K_0 (m/s)				
	Estimated final means	CP	Bordoloi et al., 2018 (fitted power eq.)		Simunek et al., 1999 (Woodings method)
			Eq-7	Eq-8	
Loam					
1	2.34E-06	3.68E-06	4.042E-06	5.33E-06	3.98E-06
2	2.65E-06	4.17E-06			
3	2.16E-06	3.40E-06			
4	1.72E-06	2.70E-06			
5	2.37E-06	3.72E-06			
6	3.23E-06	5.07E-06			
Average	2.41E-06	3.79E-06			
Silt loam					
1	5.65E-06	2.26E-05	3.685E-06	4.93E-06	NA
2	5.06E-06	2.03E-05			
3	4.15E-06	1.66E-05			
4	5.67E-06	2.27E-05			
5	6.40E-06	2.57E-05			
6	5.26E-06	2.11E-05			
Average	5.36E-06	2.15E-05			

(NA-Not available)

8.4. Discussion

Past studies have shown that tension infiltrometer measurements can be used to determine wetting water retention characteristic curve (WWRCC) parameters by considering a suitable combination of optimized parameters for the inverse simulation process (Schwartz & Evett, 2003; Šimůnek et al., 1999). However, the utility of handy MDI for the same purpose has not been explicitly demonstrated and validated in the past. Therefore, this study conducted experimental and numerical investigations for exclusively assessing the utility of MDI infiltration for determining WWRCC and its parameters. The WWRCC from MDI flow and sensor measurements were first validated with the help of independent capillary rise (CR) method in the laboratory. The CR method is an already established method to produce WWRCC in the laboratory (Chetia and Sekharan, 2016; Li et al., 2021), and thus, it was considered suitable for comparison in this study. A comparison of the MDI measurements with CR results (Figures 8.3 to 8.5 and Tables 8.3 and 8.4) revealed the efficiency of MDI flow monitoring using relevant sensors in producing WWRCCs for the two soil textures

considered in this study. This was followed by conducting extensive analysis with the help of inverse modelling to evaluate the vG WWRCC hydraulic parameters and saturated hydraulic conductivity from MDI infiltration measurements by accounting for the four different cases mentioned in Table 8.1.

It may be noted that the four cases considered in this study are pre-established scenarios to analyze water retention and hydraulic conductivity measurements (Šimůnek & van Genuchten, 1996). The results from this study indicated a fair agreement between the estimated and measured vG hydraulic parameters α, n, and K_s presented in Figures 8.6 to 8.10, and the statistical results presented in Tables 8.6 to 8.8. It is demonstrated from the results that, similar to other disc infiltrometers of large diameter (Ramos et al., 2006; Schwartz & Evett, 2003), the infiltration measurements from MDI is a non-invasive and non-destructive method to estimate the WWRCC parameters and hydraulic conductivity using inverse simulation. It was also noted that the adequacy of the inverse simulation is considerably improved by using the knowledge of final VWC along with the CI measurements. This result is specifically useful for field studies since the handy MDI may be used to replace the more laborious and cumbersome existing infiltrometers. Consequently, a considerable reduction can also be made in the volume of soil sample required for measurement. The evaluation of MDI for direct measurement of WWRCC was not carried out in any of the past literature till date. In most cases, the WWRCC parameters were either taken directly from literature (CP estimation) or measured separately using independent soil cores (core different from MDI measurement).

As discussed, inverse simulation in HYDRUS using CI (with and without θ_f), VWC, and SWP from MDI flow measurements were able to produce comparable vG model parameters (α, n, and K_s) with the measured ones (Table 8.6 to 8.8), except for some noted discrepancies for Case 3 results of LM- α. Among the 3 cases reported in Table 8.1, Case 1 (CI) results showed the least coefficient of variation (CV). The calculated average CV for Case 1 (from subcases C1-1, C1-2, and C1-2') was 24%, while for Cases 3 and 4 were 31% and 43%, respectively. It is evident that measuring CI during infiltration tests is easier than measuring VWC and SWP, as the latter require additional sensors and data loggers for continuous recording. Moreover, pre-installing the sensors at specific depths may not always be convenient and can disturb the soil structure, unlike the former measurement, which involves least disturbance to the soil. Based on the relative advantages offered and the least CV values calculated by Case 1 measurements in this study, the CI measurements from MDI

can be recommended as a reliable procedure for determining the vG WWRCC parameters. Additionally, if K_s also needs to be determined, then besides CI, the final VWC measurement taken immediately after the termination of an experiment is considered essential.

Using the subcases with comparable means (insignificant difference), the overall final mean values for α, n, and K_s were calculated. Table 8.10 presents the comparison for α and n with previous studies. These two parameters are considered since these are directly involved in MDI data analysis (Zhang's method) for estimating near-saturated hydraulic conductivity. In the absence of reference data for MDI for the two soils, the final estimated α and n were compared with the texture-based database from CP and other relevant literature listed in Table 8.10. The results show that the final means for both soils differed from the CP database. However, they were close to the values from the database of Schaap et al. (2001) and the measured values of (Bruckler et al., 2002). At the same time, the final mean values were different from those of Shao and Horton (1998) and Simunek et al. (1999). The quantity of fine particles (silt and clay) or texture plays a crucial role in deciding the shape parameters and hydraulic conductivity (Bordoloi et al., 2018). Simultaneously, several related factors, including porosity, compaction, inter-aggregate arrangements, and initial moisture, may also affect their estimation deciding the shape of the WWRCC (Albadri et al., 2018). To some extent, the interplay of these factors regulates the estimation of the modelled parameters, and therefore discrepancies are expected for the same soil texture. An important consequence of this can be that considering texture-based parameters from pedotransfer functions (PTFs) for evaluating soil hydraulic properties may not always be appropriate (Bordoloi et al., 2018; Fodor et al., 2011; Naik et al., 2019). There is always a chance for the errors in WWRCC parameters, which would further propagate to the subsequent estimation of hydraulic conductivity (Fodor et al., 2011) and the retention curves (Figures 8.12 and 8.13, in this study).

Addressing this issue for MDI measurements is crucial because it is preferably one of the most convenient infiltrometers at present for soil hydraulic characterization (Bordoloi et al., 2018; Dohnal et al., 2010). Its measurements using Zhang's method depend on estimates of these retention parameters (Ghosh & Pekkat, 2019a). It was noted that the WWRCC determined using the α and n from Case 1 was closest ($R^2 > 0.93$) to the measured reference WWRCC. Therefore, it is recommended to estimate the WWRCC parameters inversely based on direct infiltration measurements and using it for calculating the soil hydraulic properties by Zhang's method. It is noteworthy that the objective function in this study was defined using the most common data sets generated during an infiltration experiment. Another advantage is

that the inherent factors stated above are inclusive when MDI measurements were performed on the soil surface, which cannot be otherwise captured by the texture-based pedo transfer function (PTF) methods.

Table 8.10 van Genuchten WWRCC parameters (α and n) estimated using MDI measurements and comparison with the past literature

	Loam		Silt loam		Retention parameters taken from
	α (m^{-1})	n	α (m^{-1})	n	
Final estimated mean	1.43	1.5	0.41	1.61	Average of measured results and from inverse simulation of MDI
Carsel and Parrish, 1988	3.6	1.56	2	1.41	PTF developed on American soil database
Schaap et al., 2001	1.11	1.47	0.51	1.66	PTF developed on soil database from temperate to subtropical climate regions of North America and Europe
Shao and Horton, 1998	5.13	1.43	4.97	1.43	Integral method applied on horizontal infiltration measurements
	17.81	1.16	10.92	1.18	Measured retention curve using pressure plate method
Simunek et al., 1999	23.1	1.46	NA	NA	Inverse simulation of tension infiltrometer data
	3.47	1.46	NA	NA	Measured using evaporation experiment (Wind's method (Wind, 1968))
Bruckler et al., 2002	0.17	2.58	NA	NA	Measured using evaporation experiment (Wind's method (Wind, 1968))

8.5. Summary

This study critically analysed and established the accuracy of wetting water retention characteristic curve (WWRCC) and its parameters from mini disc infiltrometer (MDI) measurements with the help of independent measurements from capillary rise tests and indirect measurements using inverse modelling, for two different soil textures (loam, LM, and silt loam, SL). During the inverse analysis, a total of four cases, divided into seventeen subcases, were used to estimate van Genuchten (vG) WWRCC hydraulic parameters (α and n) along with the saturated hydraulic conductivity (K_s). Inputs used for inverse estimation of vG α and n were (a) Case 1 - cumulative infiltration (CI) versus time measured using MDI with and without

final measured volumetric water content (VWC) below the MDI disc, (b) Case 2 - VWC versus soil water potential (SWP) measured using sensors at a specific depth (direct measurement of WWRCC), (c) Case 3 - VWC variation with time at a specific depth, and (d) Case 4 - SWP variation with time at a specific depth. A total of 12 MDI infiltration experiments for two soils (6 repetitions for each soil) and 924 inverse simulations corresponding to different subcases using different initial conditions and initial guess values were performed for determining α, n, and K_s. The estimated results from inverse simulation were compared with the measured values using R^2, mean absolute error (MAE), and root mean square error (RMSE) for their accuracy. The estimated model parameters (α, n, and K_s) were analysed using ANOVA and LSD posthoc tests to determine the statistical difference between various subcases. The statistically comparable cases were further used to determine the overall final mean values of α, n, and K_s. Following are the major conclusions derived from this chapter.

- This study demonstrated MDI as a reliable, non-invasive, and non-destructive method for quick estimation of the WWRCC parameters (α, n) and K_s using inverse simulation of the wetting process and independent capillary rise measurement. This would translate to the fact that MDI can replace the conventional devices, which are tedious and require high water volume for their measurement. Since MDI is handy, a large number of measurements are possible to quantify spatial variability.
- The adequacy of the inverse simulation was improved by considering the final VWC as additional input if α, n, and K_s were estimated from CI versus time measurements.
- It is recommended estimating the WWRCC retention parameters inversely based on CI versus time measurements first and then using it for calculating the near-saturated hydraulic conductivity by Zhang's method. This could alleviate the disadvantages associated with using texture-based pedo transfer function (PTF) methods for estimating WWRCC parameters. The same is also applicable in the absence of sensors for measuring WWRCC.
- The two different initial conditions in terms of θ_i and h_i used in the inverse analysis (Case 3 and Case 4) gave WWRCC parameters with an insignificant statistical difference.
- Based on the statistical comparison, the VWC versus time input for inverse simulation did not fare well for the estimation of α and n compared to other cases.
- Following a successful comparison between measured and estimated parameters, the final mean values for α and n were determined for the two soils. The mean α (m^{-1})

for LM and SL was 1.43 and 0.41, and n was 1.5 and 1.61, respectively. The WWRCCs developed using the final set of values were close to the measured curves.

- The K_s values estimated from the inverse analysis of CI versus time for both the soils were comparable with reference falling head permeameter results.

The WWRCC from infiltration measurements are suitable for studying flow through the vadose zone than the retention curves obtained from traditional steady-state approaches (Šimůnek et al., 1999) and drying WRCC. Moreover, the traditional infiltration methods used to generate the WWRCCs in geotechnical laboratory studies are generally more time-intensive (several days to months). With the help of this study, it was demonstrated that MDI could be employed to overcome these limitations since it offers a relatively faster way to carry out the infiltration/wetting process in the laboratory. However, further evaluation is needed for widely varying soil textures to generalize the observations made in this study.

Chapter 9

General discussion, conclusions, and future scopes

9.1. General discussion

This study is centred around the use of a miniature version of disc infiltrometer, called mini disc infiltrometer (MDI), as a tool for effective characterization of soil hydraulic properties. It evaluates the potential of MDI infiltration measurements to accurately quantify soil hydraulic characteristics, such as near-surface near-saturated soil hydraulic conductivity (K_0) and sorptivity (S_0), wetting water retention characteristics curves (WWRCC), and soil hydraulic conductivity functions (SHCF) by employing various analytical and empirical methods and inverse modelling technique. This study compares the results obtained using MDI with those obtained using other established devices and methods, using both laboratory and field measurements, and on different soil textures. The findings highlight the influence of various factors, such as tension head, initial water content, and soil texture, on the estimated soil hydraulic parameters from MDI infiltration measurements. Additionally, this study provides insights into the time dependence of MDI measurements and suggests adequate measurement durations for different soil textures. This study conducts an extensive and rigorous evaluation to demonstrate the potential of MDI as one of the ideal infiltrometers for application in both laboratory and in-situ studies. It concludes that MDI is a useful, non-intrusive, and non-invasive tool for characterizing soil hydraulic properties, with important implications for improving our understanding of infiltration at the soil surface and redistribution, and further movement of soil water in the vadose zone.

9.2. Summary

As a part of this study, the transient flow process at the soil surface was recorded using MDI, while the flow in the subsurface beneath the disc was monitored with the help of volumetric water content and matric potential sensor measurements. The observations from various measurements were evaluated using existing mathematical models, numerical analysis, and statistical tools. This study was accomplished with the help of both laboratory and field

measurements and using a variety of soil textures ranging from coarse to fine soils. The conclusions from this study are as follows

- Based on both laboratory and field experiments, it was observed that the role of imposed tension head, h_0, on the determination of the near-surface near-saturated soil hydraulic conductivity (K_0) and sorptivity (S_0) from MDI measurements was marginal. The difference in the estimates was limited to a maximum of one order of magnitude.
- The analysis of MDI measurements using three different transient methods (Haverkamp, Zhang, and Dohnal) reported differences in the magnitudes of the estimated K_0 and S_0. This discrepancy was assigned to the difference in the formulations and the use of empirical constants in the mathematical expressions.
- Based on investigation using controlled laboratory measurements, the initial water content was found to have a more pronounced impact on the estimated parameters (S_0 than K_0) compared to other factors like dry density and h_0. Also, the impact of initial water content was relatively more on estimated S_0 than K_0. This was mainly due to the capillary forces driving the flow predominantly in the case of the dry initial state of soils.
- The adequacy of measured infiltration data from MDI can be verified using both the linearization methods; cumulative linearization (CL) and differentiated linearization (DL). A strong correlation was noted between the linearity or data adequacy times, T_{CL} and T_{DL}, obtained from the two linearization methods applied to MDI measurements for six different soil textures.
- The time fractionation method (based on Zhang's method (Zhang, 1997a, b)) adopted for the initially dry soil samples to identify the adequate MDI measurement duration (T_m) gave identical values based on both S_0 and K_0 variations.
- The calculated final measurement durations for MDI using time fractionation (T_m) and data adequacy approach (T_{DL} and T_{CL}) were highly comparable with Pearson's correlation close to 1 based on the comparison conducted for MDI tests carried out both in field and laboratory using six different soil textures.
- The impact of marginal difference among T_m, $T_{DL,}$ and T_{CL} on the determination of infiltration coefficients (C_1 and C_2) and K_0 revealed an excellent match for C_2 obtained from time fractionation and linearization methods. While the C_1 obtained from T_m and T_{DL} exhibited some deviations from the 1:1 line, the mean K_0 estimates from all the time considerations were highly comparable.

- For accurate quantification of soil hydraulic parameters, it is recommended to consider the maximum value among T_m, $T_{DL,}$ and T_{CL} as the MDI measurement duration. The recommended MDI measurement duration depended on the soil texture and varied from 45 minutes for silt to 50 minutes for loamy sand, 60 minutes for loam, 70 minutes for loamy sand, and 120 minutes for both silt loam and silty clay loam soils.
- The saturated hydraulic conductivity (K_s) measurements from MDI (head-based device) reported consistent and more repeatable measurements from inverse modelling (MDI-inv) than using the empirical analysis method (MDI-emp).
- The K_s from MDI-emp were one order higher than the K_s estimates from the other head-based (SATURO infiltrometer) and flux-based (rainfall simulator, RS) devices and also from the reference falling-head permeameter (PM) measurements.
- Based on the statistical significance tests (one-way ANOVA and posthoc) and graphical statistical assessment (Bland Altman plots), the sequence of K_s estimation followed the order RS-(analysed using Green-Ampt method) ≈ SATURO ≈ MDI-inv ≤ RS-(analysed using Philips method) < MDI-emp.
- The SATURO, RS, and MDI-inv were reported to be the reliable methods for determining K_s.
- The difference in K_s estimates among various instruments was found to be significantly dependent on the measurement footprints for the coarse-textured sand soil while, on the mathematical formulation, for the fine-textured loam.
- The instantaneous profile method (IPM) and the wetting front advancing method (WFAM), applied to the MDI flow measurements, were able to produce consistent and comparable soil hydraulic conductivity functions (SHCF) or $K(\psi)$ relationships.
- The investigations in this study endorse the suitability of MDI as a convenient handy device to generate unsaturated SHCFs in the laboratory using soil column studies.
- This study also demonstrated MDI as a reliable, non-invasive, and non-destructive method for quick estimation of the water retention characteristics (WWRCC) parameters (α, n) and K_s using inverse simulation of the wetting process and independent measurements from capillary rise tests.
- The adequacy of the inverse simulation, while optimizing α, n, and K_s from MDI measurements, was improved by considering the final volumetric water content (measured just below the MDI disc after the termination of each experiment) as additional input with the cumulative infiltration versus time measurements.

- Following a successful comparison between measured and estimated parameters, this study proposed a list of optimized α and n for two different soil textures (loam and silt loam) for improving accurate predictions of WWRCC from MDI measurements. The mean α (m^{-1}) and n for loam were 1.43 and 1.5, respectively, and for silt loam, it was 0.41 and 1.61.

9.3. Major contributions from this study

- Investigated the time dependence and adequate measurement durations for accurate characterization of the soil hydraulic parameters based on MDI measurements for six different soil textures.
- Established the utility of MDI for estimating wetting water retention characteristic curve and its parameters from inverse modelling of MDI measurements along with sensor response.
- Appraised the accuracy of the MDI measured wetting water retention characteristic curve and its parameters by employing independently determined measurements using the capillary rise method.
- Determined soil hydraulic conductivity functions from three independent procedures along with quantifying its variability.
- Investigated the dependency of estimated soil hydraulic parameters from MDI measurements on the imposed tension head from both field and laboratory measurements.
- Investigated the utility of MDI to determine saturated soil hydraulic conductivity by utilizing the numerical inversion technique as against the existing empirical method.
- Assessed the role of measurement footprint and mathematical model on saturated soil hydraulic conductivity estimates from various flux-based and head-based methods.

9.4. Future scopes of this study

- The variability in the water retention curves and soil hydraulic conductivity functions obtained from different procedures, including MDI measurements, need to be studied further to understand their inconsistency. This can be achieved through probabilistic modeling, which will help to quantify the uncertainty associated with such measurements.
- The methodology proposed in this study for identifying adequate measurement duration for MDI using different soil textures needs to be extended to cover a broader range of soil types. This will help to determine the generalizability of the findings and make the MDI technique more widely applicable.

- The soil hydraulic conductivity functions obtained from MDI infiltration using soil column studies need to be further evaluated for coarse-textured soils, such as sand. This will help to determine the effectiveness of the MDI technique for other soil types, which are often used in various applications, including construction, agriculture, and environmental management.
- The potential applications of MDI in real-world environmental problems, such as monitoring soil moisture for irrigation management and practices, evaluating soil contamination, and predicting infiltration and soil characteristics for flood or drought modelling, need to be investigated in detail. This is critical for gaining a deeper understanding of MDI's potential in various hydrological processes.

References

Adams, R., Parkin, G., Rutherford, J. C., Ibbitt, R. P., & Elliott, A. H. (2005). Using a rainfall simulator and a physically based hydrological model to investigate runoff processes in a hillslope. Hydrological Processes: An International Journal, 19(11), 2209-2223.

Aksoy, H., Unal, N. E., Cokgor, S., Gedikli, A., Yoon, J., Koca, K., ... & Eris, E. (2012). A rainfall simulator for laboratory-scale assessment of rainfall-runoff-sediment transport processes over a two-dimensional flume. Catena, 98, 63-72.

Alagna, V., Bagarello, V., Di Prima, S., & Iovino, M. (2016). Determining hydraulic properties of a loam soil by alternative infiltrometer techniques. Hydrological Processes, 30(2), 263–275. https://doi.org/10.1002/hyp.10607

Alagna, V., Bagarello, V., Di Prima, S., Giordano, G., and Iovino, M. (2013). "A simple field method to measure the hydrodynamic properties of soil surface crust." Journal of Agricultural Engineering, 44, 74–79.

Alagna, V., Bagarello, V., Di Prima, S., Guaitoli, F., Iovino, M., Keesstra, S., & Cerdà, A. (2019). Using Beerkan experiments to estimate hydraulic conductivity of a crusted loamy soil in a Mediterranean vineyard. Journal of Hydrology and Hydromechanics, 67(2), 191-200.

Alagna, V., Iovino, M., Bagarello, V., Mataix-Solera, J., & Lichner, L. (2019). Alternative analysis of transient infiltration experiment to estimate soil water repellency. Hydrological Processes, 33(4), 661–674. https://doi.org/10.1002/hyp.13352

Alaoui, A., Lipiec, J., & Gerke, H. H. (2011). A review of the changes in the soil pore system due to soil deformation: A hydrodynamic perspective. Soil and Tillage Research, 115, 1-15.

Albadri, W. M., Noor, M. J. M., & Alhani, I. J. (2018). The importance of incorporating hysteresis effect in determining shear strength of unsaturated soil. AIP Conference Proceedings, 2020. https://doi.org/10.1063/1.5062633

Angulo-Jaramillo, R., Bagarello, V., Iovino, M., & Lassabatere, L. (2016). Infiltration measurements for soil hydraulic characterization. Springer.

Angulo-Jaramillo, R., Vandervaere, J. P., Roulier, S., Thony, J. L., Gaudet, J. P., & Vauclin, M. (2000). Field measurement of soil surface hydraulic properties by disc and ring infiltrometers. A review and recent developments. In Soil and Tillage Research (Vol. 55, Issues 1–2, pp. 1–29). Elsevier. https://doi.org/10.1016/S0167-1987(00)00098-2

Ankeny, M. D., Ahmed, M., Kaspar, T. C., & Horton, R. (1991). Simple field method for determining unsaturated hydraulic conductivity. Soil Science Society of America Journal, 55(2), 467–470. https://doi.org/10.2136/sssaj1991.03615995005500020028x

Ankeny, M. D., Kaspar, T. C., & Horton, R. (1988). "Design for an automated tension infiltrometer". Soil Science Society of America Journal, 52(3), 893-896.

Askarinejad, A., Beck, A., Casini, F., & Springman, S. M. (2012). Unsaturated hydraulic conductivity of a silty sand with the instantaneous profile method. In Unsaturated Soils: Research and Applications (pp. 215-220). Springer, Berlin, Heidelberg. https://doi.org/10.1007/978-3-642-31343-1_27

Assouline, S. (2013). Infiltration into soils: Conceptual approaches and solutions. Water Resources Research, 49(4), 1755-1772.

Bagarello, V., & Iovino, M. (2003). Field testing parameter sensitivity of the two-term infiltration equation using differentiated linearization. Vadose Zone Journal, 2(3), 358–367. https://doi.org/10.2113/2.3.358

Bagarello, V., & Iovino, M. (2004). Indagine di laboratorio su una metodologia innovativa per la determinazione della conducibilità idraulica del suolo con l'infiltrometro a depressione.

Bagarello, V., Baiamonte, G., Castellini, M., Di Prima, S., and Iovino, M. (2014a). A comparison between the single ring pressure infiltrometer and simplified falling head techniques. Hydrological Processes, 28(18), 4843–4853. https://doi.org/10.1002/HYP.9980

Bagarello, V., Di Prima, S., Iovino, M., & Provenzano, G. (2014b). Estimating field-saturated soil hydraulic conductivity by a simplified Beerkan infiltration experiment. Hydrological Processes, 28(3), 1095-1103.

Bagarello, Vincenzo, Ferraris, S., & Iovino, M. (2004). An Evaluation of the Single-test Tension Infiltrometer Method for determining the Hydraulic Conductivity of Lateral Capillarity Domain Soils. Biosystems Engineering, 87(2), 247–255. https://doi.org/10.1016/j.biosystemseng.2003.11.007

Baker, F. G., Veneman, P. L., & Bouma, J. (1974). Limitations of the instantaneous profile method for field measurement of unsaturated hydraulic conductivity. Soil Science Society of America Journal, 38(6), 885-888. https://doi.org/10.2136/sssaj1974.03615995003800060017x

Bhave, S. and Pekkat, S. (2013) "Influence of initial soil condition on infiltration characteristics determined using a disk infiltrometer." ISH Journal of Hydraulic Engineering, 19 (3), 291–296, Taylor and Francis.

Bland, J. M., & Altman, D. G. (1986). Statistical methods for assessing agreement between two methods of clinical measurement. The Lancet, 327(8476), 307–310. https://doi.org/10.1016/S0140-6736(86)90837-8

Bodhinayake, W., Si, B. C., & Noborio, K. (2004). Determination of hydraulic properties in sloping landscapes from tension and double-ring infiltrometers. Vadose Zone Journal, 3(3), 964-970.

Bordoloi, S., Yamsani, S. K., Garg, A., & Sekharan, S. (2018). Critical assessment of infiltration measurements for soils with varying fine content using a mini disk infiltrometer. Journal of Testing and Evaluation, 47(2), 868–888. https://doi.org/10.1520/JTE20170328

Bordoloi, Sanandam, Shaikh, J., Horák, J., Garg, A., Sreedeep, S., & Sarmah, A. K. (2021). Role of biochar as a cover material in landfill waste disposal system: Perspective on unsaturated hydraulic properties. Advances in Chemical Pollution, Environmental Management and Protection, 7, 93–106. https://doi.org/10.1016/BS.APMP.2021.08.004

Bouwer, H. (1986). Intake rate: cylinder infiltrometer. Methods of Soil Analysis: Part 1 Physical and Mineralogical Methods, 5, 825-844.

Boxell, J., and Drohan, P. J. (2009). "Surface soil physical and hydrological characteristics in Bromus tectorum L. (cheatgrass) versus Artemisia tridentata Nutt. (big sagebrush) habitat." Geoderma, Elsevier B.V., 149(3–4), 305–311.

Brooks, R. H., & Corey, A. T. (1964). Hydraulic properties of porous media and their relation to drainage design. Transactions of the ASAE, 7(1), 26-0028.

Bruckler, L., Bertuzzi, P., Angulo-Jaramillo, R., & Ruy, S. (2002). Testing an infiltration method for estimating soil hydraulic properties in the laboratory. Soil Science Society of America Journal, 66(2), 384–395. https://doi.org/10.2136/sssaj2002.3840

Buckingham, E. (1907). Studies on the movement of soil moisture.

Cai, G., Zhou, A., & Sheng, D. (2014). Permeability function for unsaturated soils with different initial densities. Canadian Geotechnical Journal, 51(12), 1456-1467. https://doi.org/10.1139/cgj-2013-0410

Cai, W., Bordoloi, S., Ng, C. W. W., & Sarmah, A. K. (2022). Influence of pore fluid salinity on shrinkage and water retention characteristics of biochar amended kaolin for landfill liner application. Science of the Total Environment, 838. https://doi.org/10.1016/j.scitotenv.2022.156493

Carsel, R. F., & Parrish, R. S. (1988). Developing joint probability distributions of soil water retention characteristics. Water Resources Research, 24(5), 755–769. https://doi.org/10.1029/WR024i005p00755

Casey, F. X.,and Derby, N. E. (2002). "Improved design for an automated tension infiltrometer." Soil Science Society of America Journal, 66(1), 64-67.

Cauchy, A. (1847). Méthode générale pour la résolution des systemes d'équations simultanées. *Comp. Rend. Sci. Paris*, *25*(1847), 536-538.

Chetia, M., & Sekharan, S. (2016). Evaluation of different laboratory procedures for determining suction–water content relationship of cohesionless geomaterials. Journal of Materials in Civil Engineering, 28(2), 04015123. https://doi.org/10.1061/(ASCE)MT.1943-5533.0001399

Cho, C. M. (1971). Convective transport of ammonium with nitrification in soil. Canadian Journal of Soil Science, 51(3), 339-350.

Chong, S. K., & Green, R. E. (1983). "Sorptivity measurement and its application."

Chow, T. V. (1988), Applied Hydrology, McGraw-Hill Book Company, New York.

Clausnitzer, V., Hopmans, J. W., & Starr, J. L. (1998). Parameter uncertainty analysis of common infiltration models. Soil Science Society of America Journal, 62(6), 1477–1487. https://doi.org/10.2136/sssaj1998.03615995006200060002x

Clothier, B. E., & White, I. (1981). Measurement of sorptivity and soil water diffusivity in the field. Soil Science Society of America Journal, 45(2), 241-245.

Cui, Y. J., Tang, A. M., Loiseau, C., & Delage, P. (2008). Determining the unsaturated hydraulic conductivity of a compacted sand–bentonite mixture under constant-volume and free-swell conditions. Physics and Chemistry of the Earth, Parts A/B/C, 33, S462-S471. https://doi.org/10.1016/j.pce.2008.10.017

Dagadu, J. S., & Nimbalkar, P. T. (2012). Infiltration studies of different soils under different soil conditions and comparison of infiltration models with field data. *International Journal of Advanced Engineering Technology*, *3*(2), 154-157.

Darcy, Henry. Les fontaines publiques de la ville de Dijon: exposition et application... Victor Dalmont, 1856.

Di Prima, S., Concialdi, P., Lassabatere, L., Angulo-Jaramillo, R., Pirastru, M., Cerda, A., & Keesstra, S. (2018). Laboratory testing of Beerkan infiltration experiments for assessing the role of soil sealing on water infiltration. Catena, 167, 373-384.

Dirksen, C. (1974). Measurement of hydraulic conductivity by means of steady, spherically symmetric flows. Soil Science Society of America Journal, 38(1), 3-8.

Dirksen, C. (1975). "Determination of soil water diffusivity by sorptivity measurements." Soil Science Society of America Journal, 39(1), 22-27.

Dixon, R. M. (1975). Design and use of closed-top infiltrometers. Soil Science Society of America Journal, 39(4), 755-763.

Dohnal, M., Dusek, J., & Vogel, T. (2010). Improving hydraulic conductivity estimates from minidisk infiltrometer measurements for soils with wide pore-size distributions. Soil Science Society of America Journal, 74(3), 804–811. https://doi.org/10.2136/sssaj2009.0099

Ebrahimian, A., Sample-Lord, K., Wadzuk, B., & Traver, R. (2020). Temporal and spatial variation of infiltration in urban green infrastructure. Hydrological Processes, 34(4), 1016–1034. https://doi.org/10.1002/HYP.13641

Elbl, J., Plošek, L., Kintl, A., Hynšt, J., Záhora, J., and Charousová, I. (2014). "Effects of Drought on Microbial Activity in Rhizosphere , Soil Hydrophobicity and Leaching of Mineral Nitrogen from Arable Soil Depending on Method of Fertilization." 8(8), 790–796.

Elrick, D. E., Reynolds, W. D., Geering, H. R., & Tan, K. A. (1990). Estimating steady infiltration rate times for infiltrometers and permeameters. Water Resources Research, 26(4), 759-769.

Faé, G. S., Kemanian, A. R., Roth, G. W., White, C., and Watson, J. E. (2020). Soybean yield in relation to environmental and soil properties. European Journal of Agronomy, 118, 126070. https://doi.org/10.1016/J.EJA.2020.126070

Fajardo-Cantos, Á., Peña, E., de Las Heras, J., Plaza-Álvarez, P. A., González-Romero, J., Lucas-Borja, M. E., & Moya, D. (2022). Short-term recovery of soil and pine tree canopy in late prescribed burning in a semi-arid landscape. Science of The Total Environment, 159044.

Fatehnia, M., Paran, S., Kish, S., & Tawfiq, K. (2016). Automating double ring infiltrometer with an Arduino microcontroller. Geoderma, 262, 133-139.

Fatehnia, M., Tawfiq, K., and Abichou, T. (2014). "Comparison of the methods of Hydraulic Conductivity estimation from Minidisk Infiltrometer." Ejge, 19, 2756.

Ferraris, S., Iovino, M., Bagarello, V. (2003). A comparison between analytically and numerically simulated tension infiltrometer data. In P. Piccarolo (Ed.), Management and technology application to empower agriculture and agro-food system. XXX CIOSTA-CIGR V Congressproceedings, Torino, pp. 1192–1201.

Fodor, N., Sándor, R., Orfanus, T., Lichner, L., & Rajkai, K. (2011). Evaluation method dependency of measured saturated hydraulic conductivity. Geoderma, 165(1), 60–68. https://doi.org/10.1016/j.geoderma.2011.07.004

Fredlund, D. G., Xing, A., & Huang, S. (1994). Predicting the permeability function for unsaturated soils using the soil-water characteristic curve. Canadian Geotechnical Journal, 31(4), 533-546. https://doi.org/10.1139/t94-062

Gadi, V. K., Tang, Y.-R., Das, A., Monga, C., Garg, A., Berretta, C., & Sahoo, L. (2017). Spatial and temporal variation of hydraulic conductivity and vegetation growth in green infrastructures using infiltrometer and visual technique. Catena, 155, 20–29. https://doi.org/10.1016/j.catena.2017.02.024

Gardner, R. (1937). A method of measuring the capillary tension of soil moisture over a wide moisture range. *Soil Science*, *43*(4), 277-284.

Gardner, W. R. (1958), "Some steady-state solutions of the unsaturated moisture flow equation with application to evaporation from a water table", Soil Science, 85, 228-232.

Ghosh, B., & Pekkat, S. (2019a). A critical evaluation of measurement induced variability in infiltration characteristics for a river sub-catchment. Measurement: Journal of the International Measurement Confederation, 132, 47–59. https://doi.org/10.1016/j.measurement.2018.09.018

Ghosh, B., & Pekkat, S. (2019b). A critical evaluation of the variability induced by different mathematical equations on hydraulic conductivity determination using disc infiltrometer. Acta Geophysica. https://doi.org/10.1007/s11600-019-00266-6

Ghosh, B., & Pekkat, S. (2019c). Effect of Initial Compaction State on Near-Saturated Hydraulic Conductivity. Journal of Irrigation and Drainage Engineering. https://doi.org/10.1061/(ASCE)IR.1943-4774.0001428

Ghosh, B., & Pekkat, S. (2019d). An appraisal on the interpolation methods used for predicting spatial variability of field hydraulic conductivity. Water Resources Management, 33(6), 2175-2190. https://doi.org/10.1007/s11269-019-02248-1

Ghosh, B., Pekkat, S., & Yamsani, S. K. (2019). Evaluation of infiltrometers and permeameters for measuring hydraulic conductivity. Advances in Civil Engineering Materials, 8(1), 308–321. https://doi.org/10.1520/ACEM20180056

Giavarina, D. (2015). Understanding Bland Altman analysis. Biochemia Medica, 25(2), 141–151. https://doi.org/10.11613/BM.2015.015

Glenn, N. F., and Finley, C. D. (2010). "Fire and vegetation type effects on soil hydrophobicity and infiltration in the sagebrush-steppe: I. Field analysis." Journal of Arid Environments, Elsevier Ltd, 74(6), 653–659. https://doi.org/10.1016/j.jaridenv.2009.11.009

Goncalves, M. C., Šimůnek, J., Ramos, T. B., Martins, J. C., Neves, M. J., & Pires, F. P. (2006). Multicomponent solute transport in soil lysimeters irrigated with waters of different quality. Water Resources Research, 42(8). https://doi.org/10.1029/2005WR004802

González-Pelayo, O., Andreu, V., Gimeno-García, E., Campo, J., & Rubio, J. L. (2010). Effects of fire and vegetation cover on hydrological characteristics of a Mediterranean shrubland soil. Hydrological Processes, 24(11), 1504–1513. https://doi.org/10.1002/hyp.7612

Gonzalez-Sosa, E., Braud, I., Dehotin, J., Lassabatère, L., Angulo-Jaramillo, R., Lagouy, M., Branger, F., Jacqueminet, C., Kermadi, S., and Michel, K. (2010). "Impact of land use on the hydraulic properties of the topsoil in a small French catchment." Hydrological Processes, 24(17), 2382–2399.

Gordillo-Rivero, A. J., García-Moreno, J., Jordán, A., Zavala, L. M., & Granja-Martins, F. M. (2014). Fire severity and surface rock fragments cause patchy distribution of soil water repellency and infiltration rates after burning. Hydrological Processes, 28(24), 5832–5843. https://doi.org/10.1002/hyp.10072

Green, W., & Ampt, G. A. (1911). Studies on Soil Phyics. The Journal of Agricultural Science, 4(1), 1–24. https://doi.org/10.1017/S0021859600001441

Guo, L., Chen, J., & Lin, H. (2014). Subsurface lateral preferential flow network revealed by time-lapse ground-penetrating radar in a hillslope. Water Resources Research, 50(12), 9127-9147.

Gupta, R. K., Rudra, R. P., Dickinson, W. T., Patni, N. K., & Wall, G. J. (1993). Comparison of saturated hydraulic conductivity measured by various field methods. Transactions - American Society of Agricultural Engineers, 36(1), 51–55.

Gupta, R. K., Rudra, R. P., Dickinson, W. T., Wall, G. J. (1994). Spatial and seasonal variations in hydraulic conductivity in relation to four determination techniques. Canadian Water Resources Journal, 19(2), 103-113.

Haghverdi, A., Singh, A., Sapkota, A., Reiter, M., & Ghodsi, S. (2021). Developing irrigation water conservation strategies for hybrid bermudagrass using an evapotranspiration-based smart irrigation controller in inland southern California. Agricultural Water Management, 245, 106586. https://doi.org/10.1016/J.AGWAT.2020.106586

Haverkamp, R., Ross, P. J., Smettem, K. R. J., & Parlange, J. Y. (1994). Three-dimensional analysis of infiltration from the disc infiltrometer: 2. Physically based infiltration equation. Water Resources Research, 30(11), 2931–2935. https://doi.org/10.1029/94WR01788

Herrada, M. A., Gutiérrez-Martin, A., & Montanero, J. M. (2014). Modeling infiltration rates in a saturated/unsaturated soil under the free draining condition. Journal of Hydrology, 515, 10-15.

Holden, J., & Burt, T. P. (2002). Infiltration, runoff and sediment production in blanket peat catchments: implications of field rainfall simulation experiments. Hydrological Processes, 16(13), 2537–2557. https://doi.org/10.1002/HYP.1014

Homolák, M., Capuliak, J., Pichler, V., & Lichner, L. (2009). Estimating hydraulic conductivity of a sandy soil under different plant covers using minidisk infiltrometer and a dye tracer experiment. Biologia, 64(3), 600–604. https://doi.org/10.2478/s11756-009-0088-5

Horton, R. E. (1933). The role of infiltration in the hydrologic cycle. Eos, Transactions American Geophysical Union, 14(1), 446-460.

https://library.metergroup.com/Manuals/20496_SATURO_Manual.pdf

Hu, H., Cui, Y., Li, C., Su, W., & Wang, Z. (2021). Improvement of three common methods for determining hydraulic conductivity curve of unsaturated soil upon wetting. Journal of Hydrology, 594, 125947. https://doi.org/10.1016/j.jhydrol.2020.125947

Huang, L., Zhang, P., Hu, Y., & Zhao, Y. (2015). Vegetation succession and soil infiltration characteristics under different aged refuse dumps at the Heidaigou opencast coal mine. Global Ecology and Conservation, 4, 255–263. https://doi.org/10.1016/j.gecco.2015.07.006

Hunter, A. E., Chau, H. W., & Si, B. C. (2011). Impact of tension infiltrometer disc size on measured soil water repellency index. *Canadian Journal of Soil Science*, *91*(1), 77-81.

Hussain, R., & Ravi, K. (2021). Investigating unsaturated hydraulic conductivity and water retention characteristics of compacted biochar-amended soils for potential application in bioengineered structures. Journal of Hydrology, 603, 127040. https://doi.org/10.1016/j.jhydrol.2021.127040

Jahanzad, E., Holtz, B. A., Zuber, C. A., Doll, D., Brewer, K. M., Hogan, S., and Gaudin, A. C. M. (2020). Orchard recycling improves climate change adaptation and mitigation potential of almond production systems. PLOS ONE, 15(3), e0229588. https://doi.org/10.1371/JOURNAL.PONE.0229588

Jarvis, N. J., & Messing, I. (1995). Near-saturated hydraulic conductivity in soils of contrasting texture measured by tension infiltrometers. Soil Science Society of America Journal, 59(1), 27-34.

Kirkham, M. B., and Clothier, B. E. (2000). "Infiltration into a New Zealand native forest soil." ASA Special Publication, 62(62), 13–26.

Klute, A. (1965). Laboratory measurement of hydraulic conductivity of saturated soil. Methods of Soil Analysis: Part 1 Physical and Mineralogical Properties, Including Statistics of Measurement and Sampling, 9, 210-221. https://doi.org/10.2134/agronmonogr9.1.c13

Köhne, J. M., Alves Júnior, J., Köhne, S., Tiemeyer, B., Lennartz, B., & Kruse, J. (2011). Medidas de condutividade hidráulica e movimento de água no solo por anéis concêntricos e infiltrômetro de tensão. Pesquisa Agropecuária Tropical, 41(3), 336–347. https://doi.org/10.5216/pat.v41i3.11376

Kool, J. B., & Parker, J. C. (1987). Development and evaluation of closed-form expressions for hysteretic soil hydraulic properties. Water Resources Research, 23(1), 105–114. https://doi.org/10.1029/WR023i001p00105

Kool, J. B., Parker, J. C., & Van Genuchten, M. T. (1985). Determining soil hydraulic properties from one-step outflow experiments by parameter estimation: I. Theory and numerical studies. Soil Science Society of America Journal, 49(6), 1348–1354.

Kostiakov, A. N. (1932), "On the dynamics of the coefficient of water-percolation in soils and on the necessity for studying it from a dynamic point of view for purposes of amelioration", Transactions Congress International Society for Soil Science, 6th, Moscow, Part A: 17-21.

Kruk, E., Malec, M., Klatka, S., Brodzińska-Cygan, A., Kołodziej, J., Sci Pol Kruk, A. E., Malec, M., Klatka, S., Brodzińska-Cygan, A., & Kołodziej, J. (2017). Pedotransfer function for determining saturated hydraulic conductivity using artificial neural network (ANN). Acta Sci. Pol. Formatio Circumiectus, 16(4), 115–126. https://doi.org/10.15576/ASP.FC/2017.16.4.115

Kumar, S., Sekhar, M., Reddy, D. V, & Mohan Kumar, M. S. (2010). Estimation of soil hydraulic properties and their uncertainty: comparison between laboratory and field experiment. Hydrological Processes, 24(23), 3426–3435.

Kutilek, M.; Nielsen, D.R. Soil Hydrology; Catena-Verlag: Cremlingen-Destedt, Germany, 1994

Lai, J., & Ren, L. (2007). Assessing the Size Dependency of Measured Hydraulic Conductivity Using Double-Ring Infiltrometers and Numerical Simulation. Soil Science Society of America Journal, 71(6), 1667–1675. https://doi.org/10.2136/SSSAJ2006.0227

Lassabatère, L., Angulo-Jaramillo, R., Soria Ugalde, J. M., Cuenca, R., Braud, I., & Haverkamp, R. (2006). Beerkan estimation of soil transfer parameters through infiltration experiments—BEST. Soil Science Society of America Journal, 70(2), 521-532.

Lassabatere, L., Di Prima, S., Bouarafa, S., Iovino, M., Bagarello, V., & Angulo-Jaramillo, R. (2019). BEST-2K method for characterizing dual-permeability unsaturated soils with ponded and tension infiltrometers. Vadose Zone Journal, 18(1). https://doi.org/10.2136/vzj2018.06.0124

Latorre, B., & Moret-Fernández, D. (2019). Simultaneous estimation of the soil hydraulic conductivity and the van Genuchten water retention parameters from an upward infiltration experiment. Journal of Hydrology, 572, 461–469. https://doi.org/10.1016/j.jhydrol.2019.03.011

Latorre, B., Peña, C., Lassabatere, L., Angulo-Jaramillo, R., & Moret-Fernández, D. (2015). Estimate of soil hydraulic properties from disc infiltrometer three-dimensional infiltration curve. Numerical analysis and field application. Journal of Hydrology, 527, 1-12.

Leong, E. C., & Rahardjo, H. (1997). Permeability functions for unsaturated soils. Journal of geotechnical and geoenvironmental engineering, 123(12), 1118-1126.

Leung, A. K., Coo, J. L., Ng, C. W. W., & Chen, R. (2016). New transient method for determining soil hydraulic conductivity function. Canadian Geotechnical Journal, 53(8), 1332-1345. https://doi.org/10.1139/cgj-2016-0113

Lewis, S. A., Robichaud, P. R., Elliot, W. J., Frazier, B. E., and Wu, J. Q. (2004). "Hyperspectral remote sensing of postfire soil properties." Tenth Forest Service Remote Sensing Applications Conference , 9 pp.

Lewis, S. A., Wu, J. Q., & Robichaud, P. R. (2006). Assessing burn severity and comparing soil water repellency, Hayman Fire, Colorado. Hydrological Processes, 20(1), 1–16. https://doi.org/10.1002/hyp.5880

Li, B., Shi, B., Yao, Z., Kumar Shukla, M., & Du, T. (2020). Energy partitioning and microclimate of solar greenhouse under drip and furrow irrigation systems. Agricultural Water Management, 234, 106096. https://doi.org/10.1016/J.AGWAT.2020.106096

Li, X. Y., González, A., & Solé-Benet, A. (2004). "Laboratory methods for the estimation of infiltration rate of soil crusts in the Tabernas Desert badlands".Catena, 60(3), 255-266..

Li, X., Zhang, L. M., & Fredlund, D. G. (2009). Wetting front advancing column test for measuring unsaturated hydraulic conductivity. Canadian Geotechnical Journal, 46(12), 1431-1445. https://doi.org/10.1139/T09-072

Li, X., Zhang, Z., Zhang, L., Zhang, L., & Wu, L. (2021). Combining two methods for the measurement of hydraulic conductivity over a wide suction range. Computers and Geotechnics, 135. https://doi.org/10.1016/j.compgeo.2021.104178

Lichner, L., Hallett, P., Feeney, D., Ďugová, O., Šír, M., & Tesař, M. (2007). Field measurement of soil water repellency and its impact on water flow under different vegetation. Biologia, 62(5), 537–541. https://doi.org/10.2478/S11756-007-0106-4

Liu, Q., Xi, P., Miao, J., Li, X., & Wang, K. (2020). Applicability of wetting front advancing method in the sand to silty clay soils. Soils and Foundations, 60(5), 1215-1225. https://doi.org/10.1016/j.sandf.2020.07.002

Logsdon, S. D., & Jaynes, D. B. (1993). Methodology for determining hydraulic conductivity with tension infiltrometers. Soil Science Society of America Journal, 57(6), 1426-1431.

Ma, B., Liang, X., Liu, S., Jin, M., Nimmo, J. R., & Li, J. (2017). Evaluation of diffuse and preferential flow pathways of infiltrated precipitation and irrigation using oxygen and hydrogen isotopes. Hydrogeology Journal, 25(3), 675-688.

Madsen, M. D., and Chandler, D. G. (2007). "Automation and Use of Mini Disk Infiltrometers." Soil Science Society of America Journal, 71(5), 1469.

Marquardt, D. W. (1963). An algorithm for least-squares estimation of nonlinear parameters. Journal of the Society for Industrial and Applied Mathematics, 11(2), 431–441.

Mein, R. G., & Larson, C. L. (1973). Modeling infiltration during a steady rain. Water resources research, 9(2), 384-394.

METER Group, Inc. 2020, Minidisk Infiltrometer, User's Manual. www.metergroup.com/environment/products/mini-disk-infiltrometer.

Mezencev, V. J. (1948), "Theory of formation of the surface runoff", Meteorologiae Hidrologia, 3, 33-40.

Milatz, M., Törzs, T., Nikooee, E., Hassanizadeh, S. M., & Grabe, J. (2018). Theoretical and experimental investigations on the role of transient effects in the water retention behaviour of unsaturated granular soils. Geomechanics for Energy and the Environment, 15, 54–64. https://doi.org/10.1016/j.gete.2018.02.003

Minasny, B., & George, B. H. (1999). The measurement of soil hydraulic properties in the field. Science, 22, 26th.

Mohanty, B. P., Kanwar, R. S., & Everts, C. J. (1994). Comparison of Saturated Hydraulic Conductivity Measurement Methods for a Glacial-Till Soil. Soil Science Society of America Journal, 58(3), 672–677. https://doi.org/10.2136/SSSAJ1994.03615995005800030006X

Moody, J. A., Kinner, D. A., and Úbeda, X. (2009). "Linking hydraulic properties of fire-affected soils to infiltration and water repellency." Journal of Hydrology, Elsevier B.V., 379(3–4), 291–303.

Morbidelli, R., Saltalippi, C., Flammini, A., Cifrodelli, M., Picciafuoco, T., Corradini, C., & Govindaraju, R. S. (2017). In situ measurements of soil saturated hydraulic conductivity: Assessment of reliability through rainfall–runoff experiments. Hydrological Processes, 31(17), 3084–3094. https://doi.org/10.1002/hyp.11247

Moret-Fernández, D., Latorre, B., Peña-Sancho, C., & Ghezzehei, T. A. (2016). A modified multiple tension upward infiltration method to estimate the soil hydraulic properties. Hydrological Processes, 30(17), 2991–3003. https://doi.org/10.1002/hyp.10827

Mualem, Y. (1976). A new model for predicting the hydraulic conductivity of unsaturated porous media. Water Resources Research, 12(3), 513–522. https://doi.org/10.1029/WR012i003p00513

Mubarak, I., Mailhol, J. C., Angulo-Jaramillo, R., Ruelle, P., Boivin, P., & Khaledian, M. (2009). Temporal variability in soil hydraulic properties under drip irrigation. Geoderma, 150(1-2), 158-165.

Murray, C. J., Ward, A. L., and Wilson, J. L. (2007). "Influence of clastic dikes on vertical migration of contaminants at the Hanford Site." Vadose Zone J, 6(4), 959–970.

Nagpal, N. K., & VRIES, J. D. (1976). An evaluation of the instantaneous profile method for in situ determination of hydrologic properties of layered soil. Canadian Journal of Soil Science, 56(4), 453-461. https://doi.org/10.4141/cjss76-054

Naik, A. P., Ghosh, B., & Pekkat, S. (2019). Estimating soil hydraulic properties using mini disk infiltrometer. ISH Journal of Hydraulic Engineering, 25(1). https://doi.org/10.1080/09715010.2018.1471363

Nakhaei, M., & Šimůnek, J. (2014). Parameter estimation of soil hydraulic and thermal property functions for unsaturated porous media using the HYDRUS-2D code. Journal of Hydrology and Hydromechanics, 62(1), 7–15. https://doi.org/10.2478/johh-2014-0008

Narasimhan, T. N. (2007). Central ideas of Buckingham (1907): A century later. *Vadose Zone Journal*, *6*(4), 687-693.

Nestingen, R., Asleson, B. C., Gulliver, J. S., Hozalski, R. M., & Nieber, J. L. (2018). Laboratory Comparison of Field Infiltrometers. Journal of Sustainable Water in the Built Environment, 4(3). https://doi.org/10.1061/JSWBAY.0000857

Ng, C. W. W., & Leung, A. K. (2012). Measurements of drying and wetting permeability functions using a new stress-controllable soil column. Journal of Geotechnical and Geoenvironmental Engineering, 138(1), 58-68. https://doi.org/10.1061/(ASCE)GT.1943-5606.0000560

Nimmo, J. R. (2012). Preferential flow occurs in unsaturated conditions. *Hydrological Processes*, *26*(5), 786-789.

Nimmo, J. R., Schmidt, K. M., Perkins, K. S., & Stock, J. D. (2009). Rapid measurement of field-saturated hydraulic conductivity for areal characterization. Vadose Zone Journal, 8(1), 142–149. https://doi.org/10.2136/vzj2007.0159

Norambuena, M., Neaman, A., Schiappacasse, M. C., and Salgado, E. (2014). "Effect of liquid humus and calcium sulphate on soil aggregation." Journal of Soil Science and Plant Nutrition, 14(3), 701–709.

Norris, C. E., Bean, G. Mac, Cappellazzi, S. B., Cope, M., Greub, K. L. H., Liptzin, D., Rieke, E. L., Tracy, P. W., Morgan, C. L. S., and Honeycutt, C. W. (2020). Introducing the North American project to evaluate soil health measurements. Agronomy Journal, 112(4), 3195–3215. https://doi.org/10.1002/AGJ2.20234

Ogawa, S., Kishi, Y., and Yamada, A. (1992), "Studies on the infiltration-discharge of rain water and translation phenomena in soil," Journal of Hydrology, 132, 1992. pp. 1-23.

Paige, G. B., and Hillel, D. (1993). Comparison of three methods for assessing soil hydraulic properties. Soil Science, 155(3), 175-189.

Patra, S., Julich, S., Feger, K. H., Jat, M. L., Jat, H., Sharma, P. C., & Schwärzel, K. (2019). Soil hydraulic response to conservation agriculture under irrigated intensive cereal-based cropping systems in a semiarid climate. Soil and Tillage Research, 192, 151-163.

Pérez-Latorre, F. J., de Castro, L., & Delgado, A. (2010). A comparison of two variable intensity rainfall simulators for runoff studies. Soil and Tillage Research, 107(1), 11-16.

Perroux, K.M., and White, I. (1988), "Design for disc parameters", Soil Science Society of America Journal, 52, 1205-1215.

Philip, J. R. (1957). The theory of infiltration: 1. The infiltration equation and its solution. Soil science, 83(5), 345-358.

Philip, J. R. (1957). The theory of infiltration: 4. Sorptivity and algebraic infiltration equations. Soil Science, 84(3), 257–264. https://doi.org/10.1097/00010694-195709000-00010

Philip, J.R. (1969), "Theory of infiltration", Advances in Hydro science, 5, 215-305.

Provenzano, G. (2007). "Using HYDRUS-2D simulation model to evaluate wetted soil volume in subsurface drip irrigation systems." Journal of irrigation and drainage engineering, 133(4), 342-349.

Radinja, M., Vidmar, I., Atanasova, N., Mikoš, M., & Šraj, M. (2019). Determination of spatial and temporal variability of soil hydraulic conductivity for urban runoff modelling. Water (Switzerland), 11(5). https://doi.org/10.3390/w11050941

Rahimi, A., Rahardjo, H., Leong, E.C., 2015. Effect of range of soil–water characteristic curve measurements on estimation of permeability function. Eng. Geol. 185, 96–104. https://doi.org/10.1016/j.enggeo.2014.11.017

Ramos, T. B., Gonçalves, M. C., Martins, J. C., Van Genuchten, M. T., & Pires, F. P. (2006). Estimation of soil hydraulic properties from numerical inversion of tension disk infiltrometer data. Vadose Zone Journal, 5(2), 684–696. https://doi.org/10.2136/vzj2005.0076

Ramos, T. B., Simunek, J., Goncalves, M. C., Martins, J. C., Prazeres, A., Castanheira, N. L., and Pereira, L. S. (2011). "Field evaluation of a multicomponent solute transport model in soils irrigated with saline waters." Journal of Hydrology, 407, 129–144.

Rashid, N. S. A., Askari, M., Tanaka, T., Simunek, J., & van Genuchten, M. T. (2015). Inverse estimation of soil hydraulic properties under oil palm trees. Geoderma, 241–242, 306–312. https://doi.org/10.1016/j.geoderma.2014.12.003

Ravi, S., D'Odorico, P., and Okin, G. S. (2007). "Hydrologic and aeolian controls on vegetation patterns in arid landscapes." Geophysical Research Letters, 34(24), 1–5.

Ravi, S., Wang, L., Kaseke, K. F., Buynevich, I. V., and Marais, E. (2017). Ecohydrological interactions within "fairy circles" in the Namib Desert: Revisiting the self-organization hypothesis. Journal of Geophysical Research: Biogeosciences, 122(2), 405–414. https://doi.org/10.1002/2016JG003604

Reynolds, W. D., & Elrick, D. E. (1990). Ponded Infiltration From a Single Ring: I. Analysis of Steady Flow. Soil Science Society of America Journal, 54(5), 1233. https://doi.org/10.2136/sssaj1990.03615995005400050006x

Reynolds, W. D., & Elrick, D. E. (1991). Determination of hydraulic conductivity using a tension infiltrometer. Soil Science Society of America Journal, 55(3), 633-639.

Reynolds, W. D., Bowman, B. T., Brunke, R. R., Drury, C. F., and Tan, C. S. (2000). Comparison of Tension Infiltrometer, Pressure Infiltrometer, and Soil Core Estimates of Saturated Hydraulic Conductivity. Soil Science Society of America Journal, 64(2), 478–484. https://doi.org/10.2136/SSSAJ2000.642478X

Rice, E., and Grismer, M. (2010). "Dry-season soil water repellency affects Tahoe Basin infiltration rates." California agriculture, 64(3), 141-148.

Richards, L. A. (1931), "Capillary conduction through porous mediums", Physics 1: 313-318.

Ritter, A., Hupet, F., Muñoz-Carpena, R., Lambot, S., & Vanclooster, M. (2003). Using inverse methods for estimating soil hydraulic properties from field data as an alternative to direct methods. Agricultural Water Management, 59(2), 77–96. https://doi.org/10.1016/S0378-3774(02)00160-9

Robichaud, P. R., Jordan, P., Lewis, S. A., Ashmun, L. E., Covert, S. A., and Brown, R. E. (2013). "Evaluating the effectiveness of wood shred and agricultural straw mulches as a treatment to reduce post-wildfire hillslope erosion in southern British Columbia, Canada." Geomorphology, Elsevier B.V., 197, 21–33.

Robichaud, P. R., Lewis, S. a, and Ashmun, L. E. (2008). "New Procedure for Sampling Infiltration to Assess Post-fire Soil Water Repellency." Res Note RMRSRN33, 16.

Romano, N., Brunone, B., & Santini, A. (1998). Numerical analysis of one-dimensional unsaturated flow in layered soils. Advances in Water Resources, 21(4), 315-324.

Ronayne, M. J., Houghton, T. B., & Stednick, J. D. (2012). Field characterization of hydraulic conductivity in a heterogeneous alpine glacial till. Journal of Hydrology, 458–459, 103–109. https://doi.org/10.1016/j.jhydrol.2012.06.036

Russo, D. (1988). "Determining soil hydraulic properties by parameter estimation: On the selection of a model for the hydraulic properties." Water Resour. Res, 24(3), 453-459.

Ruwanza, S. (2017). "Invasion of Abandoned Agricultural Fields By Acacia Mearnsii Affect Soil Properties in Eastern Cape, South Africa." Applied Ecology and Environmental Research, 15(1), 127–139.

Saha, A., Sekharan, S., & Manna, U. (2020). Evaluation of Capacitance Sensor for Suction Measurement in Silty Clay Loam. Geotechnical and Geological Engineering, 38(4), 4319–4331. https://doi.org/10.1007/s10706-020-01297-3

Schaap, M. G., Leij, F. J., & Van Genuchten, M. T. (2001). Rosetta: A computer program for estimating soil hydraulic parameters with hierarchical pedotransfer functions. Journal of hydrology, 251(3-4), 163-176. https://doi.org/10.1016/S0022-1694(01)00466-8

Schacht, K., and Marschner, B. (2015). "Treated wastewater irrigation effects on soil hydraulic conductivity and aggregate stability of loamy soils in Israel." Journal of Hydrology and Hydromechanics, 63(1), 47–54.

Schacht, K., Chen, Y., Tarchitzky, J., Lichner, L., and Marschner, B. (2014). "Impact of treated wastewater irrigation on water repellency of Mediterranean soils." Irrigation Science, 369–378.

Schiesser, W. E. (2012). The numerical method of lines: integration of partial differential equations. Elsevier.

Schwartz, R. C., & Evett, S. R. (2003). Conjunctive use of tension infiltrometry and time-domain reflectometry for inverse estimation of soil hydraulic properties. Vadose Zone Journal, 2(4), 530–538. https://doi.org/10.2113/2.4.530

Schwärzel, K., Šimůnek, J., Stoffregen, H., Wessolek, G., and Van Genuchten, M. T. (2006). "Estimation of the unsaturated hydraulic conductivity of peat soils." Vadose Zone Journal, 5(2), 628-640.

Shaikh, J., Bordoloi, S., Yamsani, S. K., Sekharan, S., Rakesh, R. R., & Sarmah, A. K. (2019). Long-term hydraulic performance of landfill cover system in extreme humid region: Field monitoring and numerical approach. Science of The Total Environment, 688, 409–423. https://doi.org/10.1016/J.SCITOTENV.2019.06.213

Shao, M., & Horton, R. (1998). Integral method for estimating soil hydraulic properties. Soil Science Society of America Journal, 62(3), 585–592. https://doi.org/10.2136/sssaj1998.03615995006200030005x

Sihag, P., 2018. Prediction of unsaturated hydraulic conductivity using fuzzy logic and artificial neural network. Modeling Earth Syst. Environ. 4 (1), 189–198. https://doi.org/10.1007/s40808-018-0434-0

Šimůnek, J., & van Genuchten, M. T. (1996). Estimating Unsaturated Soil Hydraulic Properties from Tension Disc Infiltrometer Data by Numerical Inversion. Water Resources Research, 32(9), 2683–2696. https://doi.org/10.1029/96WR01525

Šimůnek, J., & Van Genuchten, M. T. (1997). Estimating unsaturated soil hydraulic properties from multiple tension disc infiltrometer data. Soil Science, 162(6), 383–398. https://doi.org/10.1097/00010694-199706000-00001

Šimůnek, J., Angulo-Jaramillo, R., Schaap, M. G., Vandervaere, J.-P., & Van Genuchten, M. T. (1998). Using an inverse method to estimate the hydraulic properties of crusted soils from tension-disc infiltrometer data. Geoderma, 86(1–2), 61–81. https://doi.org/10.1016/S0016-7061(98)00035-4

Šimůnek, J., Šejna, M., & Van Genuchten, M. T. (2018). New features of version 3 of the HYDRUS (2D/3D) computer software package. Journal of Hydrology and Hydromechanics, 66(2), 133-142.

Šimunek, J., Van Genuchten, M. T., & Šejna, M. (2012). HYDRUS: Model use, calibration, and validation. Transactions of the ASABE, 55(4), 1263-1274.

Šimůnek, J., Van Genuchten, M. T., & Šejna, M. (2012). The HYDRUS software package for simulating the two-and three-dimensional movement of water, heat, and multiple solutes in variably-saturated porous media. Technical Manual.

Šimůnek, J., van Genuchten, M. T., Gribb, M. M., and Hopmans, J. W. (1998). "Parameter estimation of unsaturated soil hydraulic properties from transient flow processes." Soil and Tillage Research, 47(1), 27-36.

Šimůnek, J., Wendroth, O., & Van Genuchten, M. T. (1999). Estimating unsaturated soil hydraulic properties from laboratory tension disc infiltrometer experiments. Water Resources Research, 35(10), 2965–2979. https://doi.org/10.1029/1999WR900179

Skaggs, T. H., Trout, T. J., Šimunek, J., & Shouse, P. J. (2004). "Comparison of HYDRUS-2D simulations of drip irrigation with experimental observations." Journal of irrigation and drainage engineering, 130(4), 304-310.

Smettem, K. R. J., & Clothier, B. E. (1989). Measuring unsaturated sorptivity and hydraulic conductivity using multiple disc permeameters. Journal of Soil Science, 40(3), 563-568.

Smettem, K. R. J., & Ross, P. J. (1992). Measurement and prediction of water movement in a field soil: The matrix-macropore dichotomy. *Hydrological processes*, *6*(1), 1-10.

Smettem, K. R. J., Parlange, J. Y., Ross, P. J., & Haverkamp, R. (1994). Three-dimensional analysis of infiltration from the disc infiltrometer: 1. A capillary-based theory. Water Resources Research, 30(11), 2925–2929. https://doi.org/10.1029/94WR01787

Smiles, D. E., & Knight, J. H. (1976). A note on the use of the philip infiltration equation. Australian Journal of Soil Research, 14(1), 103–108. https://doi.org/10.1071/SR9760103

Song, L., Li, J. H., Zhou, T., & Fredlund, D. G. (2017). Experimental study on unsaturated hydraulic properties of vegetated soil. Ecological Engineering, 103, 207-216. https://doi.org/10.1016/j.ecoleng.2017.04.013

Sprenger, M., Volkmann, T. H., Blume, T., & Weiler, M. (2015). Estimating flow and transport parameters in the unsaturated zone with pore water stable isotopes. Hydrology and Earth System Sciences, 19(6), 2617.

Sreedeep, S., & Singh, D. (2006). Nonlinear Curve-Fitting Procedures for Developing Soil-Water Characteristic Curves. Geotechnical Testing Journal, 29(5), 409–418. https://doi.org/10.1520/GTJ14104

Sreedeep, S., & Singh, D. (2006). Nonlinear Curve-Fitting Procedures for Developing Soil-Water Characteristic Curves. Geotechnical Testing Journal, 29(5), 409–418. https://doi.org/10.1520/GTJ14104

Subramanya, K. (2013). Engineering hydrology, 4e. Tata McGraw-Hill Education.

Taiwo, A. A., Olufayo, A. A., Fasinmirin, J. T., and Olorunfemi, I. E. (2016). "Spatial analysis of soil hydraulic properties of an alfisol in Akure, Southwestern Nigeria." 18(1), 19–41.

Talsma, T. (1969). "In situ measurement of sorptivity." Soil Rese

arch, 7(3), 269-276.

Thomas, M. A., Mirus, B. B., Collins, B. D., Lu, N., and Godt, J. W. (2018). Variability in soil-water retention properties and implications for physics-based simulation of landslide early warning criteria. Landslides, 15(7), 1265–1277. https://doi.org/10.1007/s10346-018-0950-z

Topp, G. C., & Zebchuk, W. D. (1985). "A closed adjustable head infiltrometer." Canadian Agricultural Engineering, 27, 99-104.

Touma, J., Vachaud, G., & Parlange, J.-Y. (1984). Air and water flow in a sealed, ponded vertical soil column: Experiment and model. Soil Science, 137(3), 181–187. https://doi.org/10.1097/00010694-198403000-00008

van Genuchten, M. T. (1980). A Closed-form Equation for Predicting the Hydraulic Conductivity of Unsaturated Soils1. Soil Science Society of America Journal, 44(5), 892. https://doi.org/10.2136/sssaj1980.03615995004400050002x

Vanderlinden, K., Gabriels, D., and Giráldez, J. V. (1998). Evaluation of infiltration measurements under olive trees in Córdoba. Soil and Tillage Research, 48(4), 303–315. https://doi.org/10.1016/S0167-1987(98)00137-8

Vandervaere, J.-P., Vauclin, M., & Elrick, D. E. (2000a). Transient flow from tension infiltrometers: I. The two-parameter equation. Soil Science Society of America Journal, 64(4), 1263–1272. https://doi.org/10.2136/sssaj2000.6441263x

Vandervaere, J.-P., Vauclin, M., & Elrick, D. E. (2000b). Transient flow from tension infiltrometers: II. Four methods to determine sorptivity and conductivity. Soil Science Society of America Journal, 64(4), 1272–1284. https://doi.org/10.2136/sssaj2000.6441272x

Vasudeo, A. D., & Srivastava, R. (2005). increase in groundwater level due to artificial recharge. ish Journal of Hydraulic Engineering, 11(3), 24-31.

Ventrella, D., Losavio, N., Vonella, A. V., & Leij, F. J. (2005). Estimating hydraulic conductivity of a fine-textured soil using tension infiltrometry. Geoderma, 124(3–4), 267–277. https://doi.org/10.1016/j.geoderma.2004.05.005

Verbist, K. M. J., Cornelis, W. M., Torfs, S., & Gabriels, D. (2013). Comparing methods to determine hydraulic conductivities on stony soils. Soil Science Society of America Journal, 77(1), 25–42. https://doi.org/10.2136/sssaj2012.0025

Wagenet, R. J., Biggar, J. W., & Nielsen, D. R. (1976). Analytical solutions of miscible displacement equations describing the sequential microbiological transformations of urea, ammonium and nitrate. Department of Water Science and Engineering, University of California.

Wallage, Z. E., and Holden, J. (2011). "Near-surface macropore flow and saturated hydraulic conductivity in drained and restored blanket peatlands." Soil Use and Management, 27(2), 247–254.

Wang, D., Yates, S. R., & Ernst, F. F. (1998). Determining Soil Hydraulic Properties using Tension Infiltrometers, Time Domain Reflectometry, and Tensiometers. Soil Science Society of America Journal, 62(2), 318–325. https://doi.org/10.2136/SSSAJ1998.03615995006200020004X

Wang, J., Gao, X., Zhou, Y., Wu, P., & Zhao, X. (2020). Impact of conservation practices on soil hydrothermal properties and crop water use efficiency in a dry agricultural region of the tibetan plateau. Soil and Tillage Research, 200, 104619. https://doi.org/10.1016/J.STILL.2020.104619

Wang, Q., Cui, Y. J., Tang, A. M., Barnichon, J. D., Saba, S., & Ye, W. M. (2013). Hydraulic conductivity and microstructure changes of compacted bentonite/sand mixture during hydration. Engineering Geology, 164, 67-76. https://doi.org/10.1016/j.enggeo.2013.06.013

Warrick, A. W. (1992). Models for disc infiltrometers. Water Resources Research, 28(5), 1319–1327. https://doi.org/10.1029/92WR00149

Warrick, A. W., & Broadbridge, P. (1992). Sorptivity and macroscopic capillary length relationships. Water Resources Research, 28(2), 427–431. https://doi.org/10.1029/91WR02599

Watson, K. K. (1966). An instantaneous profile method for determining the hydraulic conductivity of unsaturated porous materials. Water Resources Research, 2(4), 709-715. https://doi.org/10.1029/WR002i004p00709

Weir, G. J. (1987). Steady infiltration from small shallow circular ponds. Water Resources Research, 23(4), 733-736.

White, I., Sully, M. J., & Perroux, K. M. (1992). Measurement of surface-soil hydraulic properties: Disk permeameters, tension infiltrometers, and other techniques. Advances in measurement of soil physical properties: Bringing theory into practice, 30, 69-103.

Wind, G. P. (1968). Capillary conductivity data estimated by a simple method. In Water In The Unsaturated Zone Proc Wageningen Symp.

Wooding, R. A. (1968). Steady Infiltration from a Shallow Circular Pond. Water Resources Research, 4(6), 1259–1273. https://doi.org/10.1029/WR004i006p01259

Yilmaz, D., Lassabatere, L., Angulo-Jaramillo, R., Deneele, D., & Legret, M. (2010). Hydrodynamic characterization of basic oxygen furnace slag through an adapted BEST method. Vadose Zone Journal, 9(1), 107-116.

Young, M. H., Karagunduz, A., Šimůnek, J., & Pennell, K. D. (2002). A modified upward infiltration method for characterizing soil hydraulic properties. Soil Science Society of America Journal, 66(1), 57–64. https://doi.org/10.2136/sssaj2002.5700

Youngs, E. G. (1968). An estimation of sorptivity for infiltration studies from moisture moment considerations. Soil Science, 106(3), 157–163. https://doi.org/10.1097/00010694-196809000-00001

Zeng, Z., Cui, Y. J., & Talandier, J. (2022). Investigation of the hydraulic conductivity of an unsaturated compacted bentonite/claystone mixture. Géotechnique, 72(10), 911-921. https://doi.org/10.1680/jgeot.20.P.321

Zhang, R. (1997a). Infiltration Models for the Disk Infiltrometer. Soil Science Society of America Journal, 61(6), 1597. https://doi.org/10.2136/sssaj1997.03615995006100060008x

Zhang, R. (1997b). Determination of Soil Sorptivity and Hydraulic Conductivity from the Disk Infiltrometer; In Soil Science Society of America Journal (Vol. 61, Issue 4). John Wiley & Sons, Ltd. https://doi.org/10.2136/sssaj1997.03615995006100040005x

Zhang, S. Y., Hopkins, I., Guo, L., & Lin, H. (2019). Dynamics of Infiltration Rate and Field-Saturated Soil Hydraulic Conductivity in a Wastewater-Irrigated Cropland. Water 2019, Vol. 11, Page 1632, 11(8), 1632. https://doi.org/10.3390/W11081632

Zhang, Y. L., Chen, R., Li, J. H., & Xu, J. (2011). Evaluating the accuracy of unsaturated hydraulic conductivity determined by instantaneous profile method. In Proceedings of the 5th Asia-Pacific Conference on Unsaturated Soils, Kasetsart University, Pattaya, Thailand. Edited by Jotisankasa, Sawangsuriya, Soralump, and Mairaing (pp. 403-407).

Publications

Journals

Published

1. Naik, A. P., and Pekkat, S. (2022). "Time dependence of hydraulic parameters estimation from transient analysis of mini disc infiltrometer measurements". *European Journal of Soil Science*, Wiley, 73(2), e13228. https://doi.org/10.1111/ejss.13228
2. Naik, A. P., Ghosh, B., and Pekkat, S. (2019). "Estimating soil hydraulic properties using mini disk infiltrometer". *ISH Journal of Hydraulic Engineering*, 25(1), 62-70. https://doi.org/10.1080/09715010.2018.1471363
3. Naik, A. P., and Pekkat, S. (2022) "An appraisal on the soil wetting water retention characteristic curve determined from mini disk infiltrometer and sensor measurements". *Acta Geophysica*, 1-22. https://doi.org/10.1007/s11600-022-00932-2

Submitted

4. Naik, A. P., Norbu, T., and Pekkat, S. "Comparison of flux-based and head-based methods for near-surface saturated hydraulic conductivity determination". *Water Resources Management*, Springer.
5. Naik, A. P., and Pekkat, S. "Critical evaluation on the feasibility of mini disc infiltrometer for determining unsaturated soil hydraulic conductivity function". *Soil Science Society of America Journal*, Wiley.

Under preparation

6. Naik, A. P., and Pekkat, S. Probability modelling of wetting water retention characteristics curve measured from mini disc infiltrometer measurements.

Book Chapter

1. Naik, A. P., & Pekkat, S. (2022). "Discrepancy in Infiltration Equation Parameters While Using Ponded and Tension Boundary Pressure Head Conditions". In Hydrological Modeling (pp. 287-297). Springer, Cham. http://dx.doi.org/10.1007/978-3-030-81358-1_22

Conferences

Published

1. Naik, A. P., Ghosh, B., & Pekkat, S. (2016) "Estimating soil hydraulic properties using mini disc infiltrometer", HYDRO 2016 INTERNATIONAL, CWPRS, Pune, India.
2. Naik, A. P., & Pekkat, S. (2018) "Discrepancy in infiltration equation parameters while using ponded and tension boundary pressure head conditions", HYDRO 2018 INTERNATIONAL, NIT Patna, Bihar, India.
3. Naik, A. P., & Pekkat, S. (2019) "Soil Hydraulic Characterization using mini disc infiltrometer", Research Conclave, IIT Guwahati, Assam, India.
4. Naik, A. P., & Pekkat, S. (2019), "A comparative assessment of infiltration characteristics obtained using two disc infiltrometers", 16th Annual Meeting, Asia Oceania Geosciences Society (AOGS) 2019, Suntec, Singapore
5. Naik, A. P., & Pekkat, S. (2020) "Influence of time on hydraulic conductivity estimation using Mini Disc Infiltrometer", ASCE India Conference, Kolkata, India.
6. Naik, A. P., & Pekkat, S. (2021) "A Comparative assessment of estimated soil hydraulic conductivity from rainfall simulator and infiltrometer using laboratory repacked soil samples", EGU General Assembly 2021. https://doi.org/10.5194/egusphere-egu21-7099
7. Naik, A. P., & Pekkat, S. (2021 December) "Assessing soil water retention parameters obtained from two different databases using inverse modeling", AGU Fall Meeting 2021, AGU, New Orleans, USA.
8. Naik, A. P., & Pekkat, S. (2022, December) "Analysing unsaturated flow using retention curves from field and laboratory infiltration measurements", AGU Fall Meeting 2022, AGU, Chicago, USA.

Accepted

9. Naik, A. P., & Pekkat, S. (2023, May) "Determination of wetting soil water characteristics curve from disk infiltrometer measurements", 8th International Conference on Unsaturated Soils (UNSAT) 2023, Milos Island, Greece.